University of Bath

PHD

Temperature measurement planning for thermal compensation of dimensional measurement in assembly environments

Ross-Pinnock, David

Award date:
2021

Awarding institution:
University of Bath

Link to publication

Alternative formats
If you require this document in an alternative format, please contact:
openaccess@bath.ac.uk

Copyright of this thesis rests with the author. Access is subject to the above licence, if given. If no licence is specified above, original content in this thesis is licensed under the terms of the Creative Commons Attribution-NonCommercial 4.0 International (CC BY-NC-ND 4.0) Licence (https://creativecommons.org/licenses/by-nc-nd/4.0/). Any third-party copyright material present remains the property of its respective owner(s) and is licensed under its existing terms.

Take down policy
If you consider content within Bath's Research Portal to be in breach of UK law, please contact: openaccess@bath.ac.uk with the details. Your claim will be investigated and, where appropriate, the item will be removed from public view as soon as possible.

Download date: 05. May. 2023

Temperature measurement planning for thermal compensation of dimensional measurement in assembly environments

David Ross-Pinnock

A thesis submitted for the degree of Doctor of Philosophy

University of Bath

Department of Mechanical Engineering

February 2021

COPYRIGHT

Attention is drawn to the fact that copyright of this thesis rests with the author. A copy of this thesis has been supplied on condition that anyone who consults it is understood to recognise that its copyright rests with the author and that they must not copy it or use material from it except as permitted by law or with the consent of the author.

Abstract

As more is demanded from dimensional measurement capability, more is demanded from the understanding of its main sources of uncertainty. At the large volume scale, thermal effects contribute significantly to dimensional uncertainty, particularly through thermal expansion and contraction of parts, tooling, and instruments. The problem was highlighted in aerospace assembly, while marine, and automotive assembly are other sectors affected by complex thermal environments.

This thesis focuses on the problem of thermal expansion compensation of objects being measured. Most of the current understanding of thermal expansion compensation has been gained at the instrument level, in which manufacturers have modelled the effects of ambient temperature on measurement error and provided a calibrated correction. Simulation based thermal-structural modelling is well established for several applications. A lot of temperature measurement research and standards have focused on sensors, and not as much on the practicalities of using the sensors to produce the best outcomes.

Experimentation on structures at the laboratory scale provided insights into how simulation could be used to compensate for thermal expansion. It became evident that the position of the sensors plays a significant role in accurately reproducing temperature distributions. Industrial measurements showed spatial and temporal thermal variation of several degrees, further highlighting the need for a tool to integrate dimensional and temperature measurement planning.

A computational tool was built to test the task specific performance of temperature sensor networks in the context of thermal expansion. The tool allows for temperature distributions to be generated and FEA simulations to be run to test specified sensor networks. Results for temperature measurement capability were calculated, and its ultimate impact on the simulation's ability to determine thermal expansion can be assessed. The approach was first applied to the case of a large beam to develop the tool, and to understand how different factors affected the ability to reconstruct temperature distributions. Sensor positioning and models for reconstruction had a more significant impact on temperature distribution reproduction than individual sensor uncertainties for this task.

The final case study focused on a more complex assembly structure. Random search optimisation and sensor removal sensitivity studies of the network positions revealed most impactful sensors. Simulation of daily temperature variation using the tool demonstrated its ability to determine performance over time with varying temperature distributions. A polynomial interpolation model using a 16-sensor network with 0.1 °C (confidence interval, k = 2) uncertainty sensors could produce a consistent temperature reconstruction error of ~0.04 °C RMS, corresponding to a thermal expansion error of ~1.5 µm in aluminium over the 1.6 m-tall structure. Results such as this could impact how temperature measurement planning is valued and how resources are allocated to measurement activities.

The creation of this tool demonstrates a computational, low-risk approach to temperature measurement planning and uncertainty quantification for dimensional. It is anticipated that in the future this tool can be used for increasingly complex cases and further validated through detailed uncertainty studies at large scales.

Acknowledgements

I would like to first acknowledge the support of EPSRC, grant EP/K018124/1, “The Light Controlled Factory” and the European Metrology Research Programme (EMRP) Project IND53 – Large Volume Unified Metrology for Industry, Novel Applications & Research (LUMINAR). The EMRP is funded by the EMRP-participating countries within the European Association of National Metrology Institutes (EURAMET), and the European Union.

My supervisors have been a great source of support and are gratefully acknowledged. Prof. Paul Maropoulos gave me the opportunity to study towards a PhD part-time, whilst working on the Light Controlled Factory project to begin my research career. The Laboratory for Integrated Metrology Applications (LIMA) team, and the Department of Mechanical Engineering at the University of Bath were incredibly supportive throughout my time there. Many thanks go to the Metrology and Non-destructive Testing team at the Manufacturing Technology Centre (MTC), who helped to broaden my horizons as a digital engineer, working more closely with industry. Many thanks go to my supervisor Prof. Patrick Keogh, who has been a great source of support over the years. Special thanks to Prof. Glen Mullineux who has supervised since the beginning, patiently providing helpful guidance and good company even into his retirement.

Thank you to my friends for helping me to keep on trucking, keep my feet on the ground, and occasionally enjoy myself. Thank you to Bingru for being there to share the journey.

I’d like to break perspective to bring perspective and say thank you to myself as a reminder of all of the life changes that happened over the PhD years. Despite it all, you consistently became a better person to get this done and looked after yourself when no one else was around – thank you.

I’m ever grateful to my family, who have always been hugely supportive – I told you it was nearly done! Thank you all, near and far. Thank you to my mum most of all, who through everything was always at the end of the phone if I wasn’t nearby, helping wherever she could. Finally, I would like to dedicate this thesis in loving memory of my dad who didn’t get to see the end, but I appreciate everything he did at the beginning.

Contents

Figures

Tables

Nomenclature

Abbreviation	Definition
AIT	Assembly, integration and test
BIM	Building information modelling
BIPM	Bureau International des Poids et Mesures (International Bureau of Weights and Measures)
BSI	British Standards Institution
C	Celsius
CAD	Computer-aided design
CAIP	Computer-aided inspection planning
CFD	Computational fluid dynamics
CMM	Coordinate measuring machine
CTE	Coefficient of thermal expansion
DfM	Design for manufacturing
DfV	Design for verification
DfX	Design for X
DMSC	Dimensional Metrology Standards Consortium
FDS	Fibreoptic distributed sensing
FEA	Finite element analysis
FEM	Finite element method
GUM	Guide to the Expression of Uncertainty in Measurement
IPRT	Industrial platinum resistance thermometer
IR	Infrared
ISO	International Standards Organisation
ITS-90	International Temperature Scale of 1990
K	Kelvin
LVM	Large volume metrology
MAA	Measurement assisted assembly
MSA	Measurement systems analysis
NIST	National Institute of Standards and Technology (US NMI)
NMI	National measurement institute
NPL	National Physical Laboratory (UK NMI)
NTC	Negative temperature coefficient thermistor
PLM	Product lifecycle management
PMI	Product manufacturing information
PRT	Platinum resistance thermometer
Pt100	Platinum resistance thermometer referenced to 100-ohm resistor
QIF	Quality information framework
RTD	Resistance temperature detector
SMR	Spherically mounted retroreflector
SPRT	Standard platinum resistance thermometer
T	Temperature
TC	Thermocouple
TLC	Thermochromic liquid crystal
U	Uncertainty

Thermal Effects in Dimensional Measurement

1.1 Introduction

Temperature measurement provides a quantitative description of how hot or cold a body is. This corresponds to the amount of energy there is present in such a body. At absolute zero (-273.13 K), atoms do not have the energy to move. This temperature cannot be fully realised by humans on earth and would not make for ideal conditions in which to carry out assembly operations. At common working temperatures in manufacturing, atoms are moving around a great deal more.

Different materials exhibit different behaviour at different temperatures. Each material within the solid state, will experience a change in length corresponding to a change in temperature. For most solid materials, this is a proportional relationship. The coefficient of thermal expansion (CTE) for each material is used to describe the specific relationship for that material. Most commonly the linear coefficient of thermal expansion is used as this pertains to length. Similarly, the areal and volume coefficients exist to describe changes in area and volume. Linear CTE is given in units of microns per metre, per degree. That is to say: if a body of length 1 metre is raised uniformly by 1 °C then it will increase in length according to its CTE.

Thermal expansion then poses a problem for dimensional measurement. Measurement is a means of communication. We have units of measure so that others may understand the quantities we seek to describe – a sentiment expressed by Robert Boyle in 1662 in calling for a standard temperature scale [1]. If everyone is trying to communicate length measurement, they necessarily need to be speaking the same language by measuring at the same temperature. After some debate, 20 °C was agreed as the standard temperature for dimensional measurement as specified by ISO 1:2016 [2]. Metrology laboratories all around the world can now control temperature to around 20 °C, which makes the quantitative description of objects more straightforward.

Unfortunately, it is not always possible to control temperature in every scenario where a dimensional measurement is required. Not every part and assembly can be taken to a metrology laboratory for inspection. Not every part and assembly would fit into a metrology laboratory.

Although the problem with these environments is clear, there are several important drivers exist for wanting to carry out measurements at non-standard temperatures:

- Costs – cost of temperature control, cost of moving a part to a controlled facility;
- Practicality – large scale environments make control difficult, outdoor environments, risk of damage in transport;
- Scale – large scale products cannot be easily moved and may not even fit into a metrology laboratory;
- Time – time taken to take a product to a laboratory;
- Energy – temperature control takes a lot of energy which adds to costs and impacts sustainability metrics.

If there is not the opportunity to measure in a temperature-controlled environment, then what could be done? Below is a suggestion for a solution:

'With the knowledge of the CTE for different materials, it makes sense to measure the temperature and scale the dimensions accordingly.'

For many applications where manufacturing tolerances are not too challenging, this sentence describes a completely acceptable solution. Four portions of this sentence when viewed in further detail for higher specification products start to raise some questions:

1) "Knowledge of the CTE" – How well do you know the CTE for the material present in the workpiece and how much does this vary?
2) "Different materials" – What if I'm using more than one material in the same assembly?
3) "Measure the temperature" – With what do I measure? How? When? And where do I measure it?
4) "Scale the dimensions" – How best do I scale them back to standard temperature?

The first question regarding the knowledge of the CTE can be difficult to answer. Dilatometry is used to measure the CTE of various material samples and are published in tables. This is a very helpful resource, but materials can and do vary – it has been anecdotally reported by those in the field of metrology that CTE can vary up to ±10% in some cases.

The second question implies that more than one CTE could be present in an assembly, which is often the case. This needs to be dealt with appropriately when a method for determining the thermal expansion is selected. Materials with different CTE will have far more complex interactions under expansion than homogeneous materials.

The third question is perhaps the deepest (and most interesting) one here. Selection of temperature sensor and how it should be used is an important consideration that will depend entirely on the requirements and constraints of each individual application. More accurate sensors will provide a more accurate reading, meaning a potentially more accurate dimensional scaling. Potentially is the key here, as there were other questions asked of: how, when, and where. Temperature distributions, particularly in large volume metrology (LVM) scenarios are unlikely to be completely spatially uniform, or temporally invariant.

Finally, the fourth question asks how the dimensions can be scaled. In the most basic case, a straightforward calculation can be carried out in a case where we can assume that temperature distribution is uniform. In cases where there are thermal gradients, this becomes more difficult. In cases where the thermal gradients are non-linear, this becomes more complex. Multiple interacting materials also adds complexity.

The seemingly innocuous sentence is now left with not much more than punctuation and conjunctions, but it has prompted a new discussion. Looking at these four points, they can be categorised into three groups of problems: CTE; temperature measurement; and scaling.

Solving the CTE problem would involve the creation of a suitable technique for carrying out an in-situ CTE measurement. Solving the scaling problem is best achieved with more sophisticated methods that allow for non-linear scaling and/or mechanical interactions.

Solving the temperature measurement problem is perhaps the most significant of them all. The method of scaling is only as accurate as the temperature measurement data that is being used. In-situ CTE measurement would be useful but may not always be practical and would

add a level of complexity into manufacturing processes. Temperature is one of the most widely measured quantities [3] and there are several ways to approach it. Thinking of measurement as communication, it could be argued that measurement traceability would be better achieved through agreement in how to plan temperature measurement to support dimensional measurement.

1.2 Problem Summary

The problem can be summarised as follows:

- Thermal expansion can have significant effects upon dimensional measurement;
- Temperature cannot always be controlled in environments in which dimensional measurement is required;
- Temperature is not routinely measured as part of dimensional measurement;
- There is no agreed methodology for temperature measurement planning.
- There is no process or tool available for testing and comparing temperature sensor network configurations for thermal expansion compensation.

1.3 Research Question

How can a temperature measurement planning process be created to produce better outcomes for thermal compensation of large assembly-scale measurements?

1.4 Aims

The aim of this work was to create a process for temperature measurement to support thermal expansion compensation of dimensional measurement.

1.5 Objectives

Initially, a review needed to be carried out to determine the state of the art and associated opportunities for research. Some experimentation had to be done to determine how thermal compensation could work in practice, as well as gaining more intimate understanding of the challenges faced by industry. Considerations for how temperature measurement should be planned and carried out had to be made, to determine how best to approach the problem. A method for comparing different temperature sensor networks had to be defined and tested for different cases. This method for testing and comparison needed to be used to optimise temperature sensor networks so that they are better adapted to the challenges of their environment. The objectives of this thesis are listed in Table 1, which shows which chapter(s) fulfil each of the objectives, for ease of reference.

Table 1. Thesis objectives and location of associated content.

Objective Number	Objective Description	Fulfilled By
1.	Review the academic literature, industrial standards and published measurement guidelines;	Chapter 2 - Literature Review
2.	Experiment with thermal expansion and simulate thermal effects;	Chapter 3 - Experimentation in Temperature Measurement and Thermal Compensation
3.	Create and digitally validate a high-level framework for temperature measurement strategy for dimensional measurement;	Chapter 4 - Temperature Measurement Planning
4.	Create and digitally validate a method for establishing sensor positions of interest based upon environmental temperature distributions;	Chapter 5 - Sensor Network Performance Testing Chapter 6 - Case Study: Barrel Section Assembly
5.	Determine temperature sensor network performance;	Chapter 5 - Sensor Network Performance Testing Chapter 6 - Case Study: Barrel Section Assembly
6.	Consider the implications for optimising temperature sensor networks for thermal compensation.	Chapter 6 - Case Study: Barrel Section Assembly

1.6 Chapter 1 – Summary

Chapter 1 provided:

- An introduction to the problem of thermal expansion in assembly environments.
- Variables affecting thermal compensation capability.
- A list of aims and objectives for the thesis and where these are addressed.

Contributions:

- Posed a research question that has not yet been answered about how best to plan for temperature measurement in assembly environments.

Measured dimensions are temperature-dependent, so there is a clear need to understand how best to measure temperature.

---

2 Literature Review

2.1 Approaches to Scaling in Spatiothermal Metrology

The problem of thermal effects is well established, so the literature was reviewed to see how this was being solved and consider how it might otherwise be solved. It was apparent that scaling could be carried out in a few different ways, so that seemed like a sensible place to start. Looking at the variables required would provide an indication of where the errors might start to build up.

Various approaches to scaling dimensional measurements for thermal expansion using measured temperatures exist. These approaches generally fall into one of the following categories:

- Uniform scaling;
- Analytical linear gradient scaling;
- Analytical non-linear spatiothermal scaling;

This list of potential scaling methods are all analytical. It should be noted that after observation from working in metrology with various companies, multiple temperature measurements are rarely taken, and if they are, are often not used beyond the instrument level thermal compensation. Similarly, only uniform scaling has readily available, published guidance for its use by a national measurement institute. The methods described in this section are limited to those that deal with thermal expansion in dimensional measurement – more sophisticated methods are used for different thermal compensation applications, which will be discussed later.

The selection of the most appropriate method ultimately depends upon the:

- Dimensional tolerances from design specification;
- Access to temperature measurement instrumentation;
- Complexity of the environmental temperature distribution.

2.1.1.1 Uniform Scaling

Thermal expansion compensation is usually achieved by applying a uniform scale factor to a set of measured coordinate measurements. Compensation using a uniform scale factor is somewhat limited, but it is widely practiced and is taught in the National Physical Laboratory's dimensional measurement training [4].

The uniform scale factor is based upon the average temperature difference ΔT from the standard metrology temperature of 20 ºC, and the linear coefficient of thermal expansion α of the material, where L is the original length, and ΔL is the change in length. The new length of an object can be found using Equation 1.

Equation 1

$$L + \Delta L = L(1 + \alpha \Delta T)$$

In large volume metrology applications where the temperature distribution shows a large amount of variation, the use of a uniform scale factor becomes a limiting factor to compensation accuracy in reflecting true thermal expansion at different points on the artefact.

2.1.1.2 Analytical Linear Gradient Scaling

A more sophisticated approach to scaling than uniform scaling is used in environments where the spatial variation of temperature is more significant, and assuming uniform expansion is not acceptable. The measurement of the gradient can be arrived at by measuring temperature at the extremities of the measurement volume, often the top and the bottom in the absence of any additional heat sources. The application of this correction for points within the volume can be achieved using linear interpolation.

2.1.1.3 Analytical Non-linear Scaling

Real temperature distributions are likely to be non-linear in nature. The distribution curve of the temperature is an important aspect to consider as it is not just the maximum temperature difference over a length, but the amount of material that is subjected to each temperature.

The distribution of non-standard temperatures is the principle driver of thermal expansion, which can be described as a polynomial function of temperature. Integration of the temperature function then would yield the total thermal expansion, considering the full temperature distribution.

In one dimension, the compensated length can be given as:

Equation 2

$$L + \Delta L = L[1 + \alpha \int T(x)dx]$$

Where:

L is the length of material between positions x_0 and x_1, $(x_1 - x_0)$;

ΔL is the change in length;

α is the linear coefficient of thermal expansion of the material;

$T(x)$ is temperature of the material as a function of position, x.

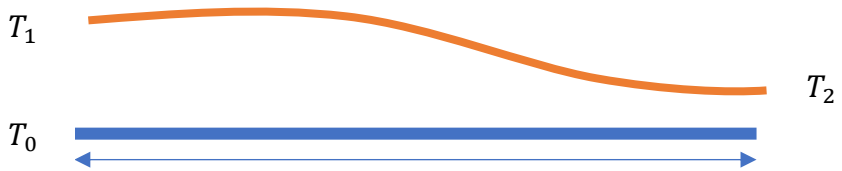

Figure 1. Diagram showing a non-linear temperature distribution in one dimension in which T_0 represents standard temperature.

Consider the example illustrated in Figure 1, in which a non-linear thermal gradient is applied across a one-dimensional length L in the x axis, or L. T_0 represents the standard metrology temperature of 20 ºC that we are trying to scale the length dimension against. At x_1, there is a new temperature T_1 and at L_{x1} , a new temperature of T_2. Along L is the temperature distribution function defining the curve.

The compensated length can be given as:

Equation 3

$$L + \Delta L = L[1 + \alpha \int_{x_0}^{x_1} T(x)dx\ ]$$

There are two main options of how to apply this to dimensional measurement data and the decision-making process is illustrated in Figure 2. Provided the temperature has been measured on a known structure, the following courses of action can be taken to transform the dimensions measurement data to compensate for thermal expansion:

a) Use a function to scale measured coordinates as in the traditional method in place of uniform scale factor;

b) Use the distribution functions as boundary conditions in subsequent finite element analyses, in which there are:

   i) Confounding mechanical interactions in an assembly which limit compensation accuracy;

   ii) Parts of significant scale made from different materials causing complex interactions (e.g. bimetallic effect) in an assembly.

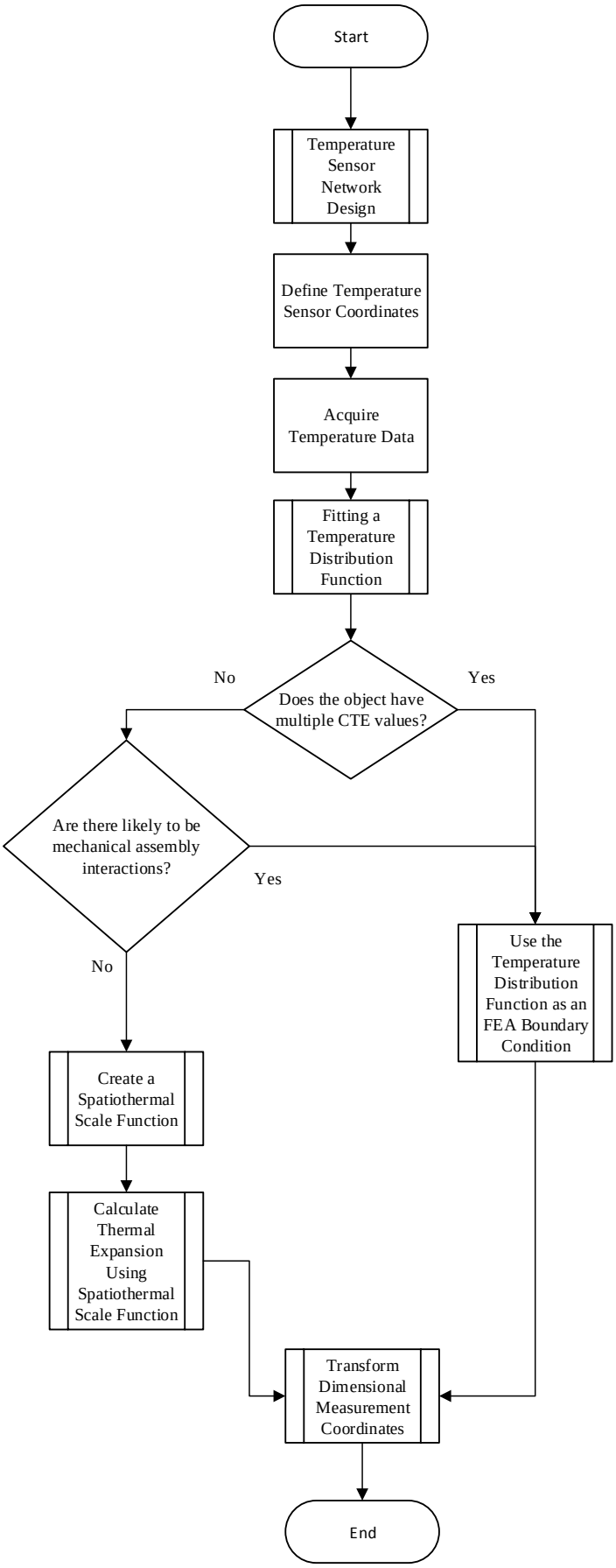
Start
Temperature Sensor Network Design
Define Temperature Sensor Coordinates
Acquire Temperature Data
Fitting a Temperature Distribution Function
Does the object have multiple CTE values?
No
Yes
Are there likely to be mechanical assembly interactions?
Yes
No
Use the Temperature Distribution Function as an FEA Boundary Condition
Create a Spatiothermal Scale Function
Calculate Thermal Expansion Using Spatiothermal Scale Function
Transform Dimensional Measurement Coordinates
End

Figure 2. A proposed decision-making process for how to perform spatiothermal scaling.

2.2 Metrology Standards and Guidelines

Standards and measurement guidelines are outlined and discussed here to provide background to the problem of temperature measurement in the context of dimensional measurement in industry. This is not intended as an exhaustive reference, and some individual companies will have their own internal practices driven by the needs of their customers and sectors. With some understanding of how scaling could be achieved, it would be useful to determine what the accepted and agreed methods are at present.

2.2.1 Industrial Standards

Industrial standards for measurement have been agreed and published. Standards in metrology are regularly updated and reviewed to better serve the needs of industry and reflect the state of the art as far as possible. Mature and widely adopted measurement technologies will often have their own standards. Some sectors publish more specific standards, with the aerospace sector being a notable example.

The ISO standard specifying the standard reference temperature for all geometric dimensions on an object to be 20 °C is ISO 1:2016 [2]. ISO 10360-2 defines the acceptance and reverification tests for CMMs [5]. To reduce error arising from thermal effects, manufacturers are required to specify environmental conditions to determine the acceptance of installations. Periodic interim checks can be carried out on a CMM to ensure that the measurement system is still working as expected. Such interim checks can be carried out using specific artefacts, and it is recommended that the artefacts used closely match the CTE of commonly measured objects.

Further guidance on the use of calibrated workpieces can be found in BS EN ISO 15530-3:2011 [6]. This standard also provides a calculation for the uncertainty contribution attributable to thermal expansion based upon uniform scaling. Design of an artefact of similar material and dimensions is likely to be use in the development of systems to further develop thermal expansion for industry. Similarity requirements are specified in this standard, and dimensions of artefacts should be within 10% for calibrated workpieces larger than 250 mm.

2.2.2 Guide to Uncertainty of Measurement (GUM)

Measurement guidelines are generated primarily through national measurement institutes, committees and working groups in the metrology community. These are generally freely accessible and are often considered to be the authority in the absence of a relevant industrial standard. These guidelines are updated every few years to better reflect the state of the art.

The Guide to Uncertainty of Measurement (GUM), is a document that was published as a means of providing guidance to those carrying out measurements and calibrations. GUM is

not technically a standard but can be said to be considered a de facto standard in cases that are not covered by international, or national standards.

Two major points are made in the GUM [7] that highlight the importance of working towards the integration of thermal and dimensional measurement:

"7.1.3 Numerous measurements are made every day in industry and commerce without any explicit report of uncertainty."

"3.3.2 In practice, there are many possible sources of uncertainty in a measurement, including: … d) inadequate knowledge of the effects of environmental conditions on the measurement or imperfect measurement of environmental conditions"

The first point illustrates how uncertainty evaluation is often neglected, meaning that many measurements recorded do not give an indication of how close that measurement is likely to be to the True Value. Following this, it is stipulated that the instrument uncertainty can be inferred from the traceability of the calibration. The second point is particularly pertinent to this thesis, as part of that uncertainty evaluation must include some characterisation of the environment in which the measurement is taken. In terms of uncertainty evaluation, this shows that relying on the calibrated instrument alone does not give a complete indication of the uncertainty of all measurements taken outside of the standard environment.

2.3 Thermal Compensation in Manufacturing

Thermal compensation has been studied in many forms in manufacturing, as thermal effects have long been known to create challenges beyond metrology applications. Thermal compensation is most extensively and successfully applied for specific instruments and tools. Measurement instruments often have their own form of thermal compensation. Often this is a case of characterisation of errors at given temperatures and applying an offset to measured dimensions. Regression methods are commonly used as a straightforward means of characterising an instrument's response to temperature changes.

The ISO 230-3:230 standard defines a procedure for the determination of thermal effects on a machine tool [8]. Example diagrams in this standard provide some guidance as to where to position temperature sensors during the test procedure with the requirement of recording their actual positions alongside the results. The test also makes use of linear displacement sensors on the structure and provides guidance for testing their stability under thermal load. This is one of the more useful standards on thermal effects as there is more discussion of the problem and impact in the body and annexes of the document. In the literature, most of the attention in thermal compensation research has been focused upon conventional CNC machine tools that are used for milling, drilling, and turning operations [9, 10]. One of the observations from reviewing the literature is that the work on thermal compensation is very specific in scope, hence the focus on machine compensation. Comparatively, there are few papers that are concerned with product, or tooling thermal compensation, for example, although low or negative expansion materials continue to be of great interest [11]. The use of FEA to predict and compensate for thermal errors is well-established in CNC machining but continues to yield useful knowledge when combined with other methods [12, 13]. Increasing interest in additive manufacturing processes has driven a lot of research in spatiothermal modelling - much of this is FEA and CFD based [14, 15].

2.4 Temperature Measurement Technologies

The review of temperature measurement technologies in this section was previously published as part of a technology comparison for presentation at a conference, which was later extended into a review paper to highlight research opportunities [16, 17].

Common to all scaling approaches is a measure of length and temperature. Despite having some idea of the technologies available for dimensional measurement to cover length, there was a need to get a clearer idea of how temperature was measured. Understanding their mode of operation as well as their strengths and weaknesses offered some insight as to what the challenges are for thermal compensation – the compensation can be only as good as the temperature measurement.

Reviewing the literature revealed tens of technologies, and many of them were unsuitable for this type of temperature measurement. Whilst each measurement task is different, on the scale of thousands of degrees that represents the ITS-90, the ones found in assembly environments span a relatively short range. The temperature measurement technologies that are the focus of this review were selected since they would be best suited to industrial temperature measurement, particularly in the range 0-50 ˚C, within an assembly environment. A truncated classification diagram based upon Childs' definitions [18] can be seen in Figure 3. Their primary classification is based upon how invasive the sensor is – contact, non-contact, or somewhere in between.

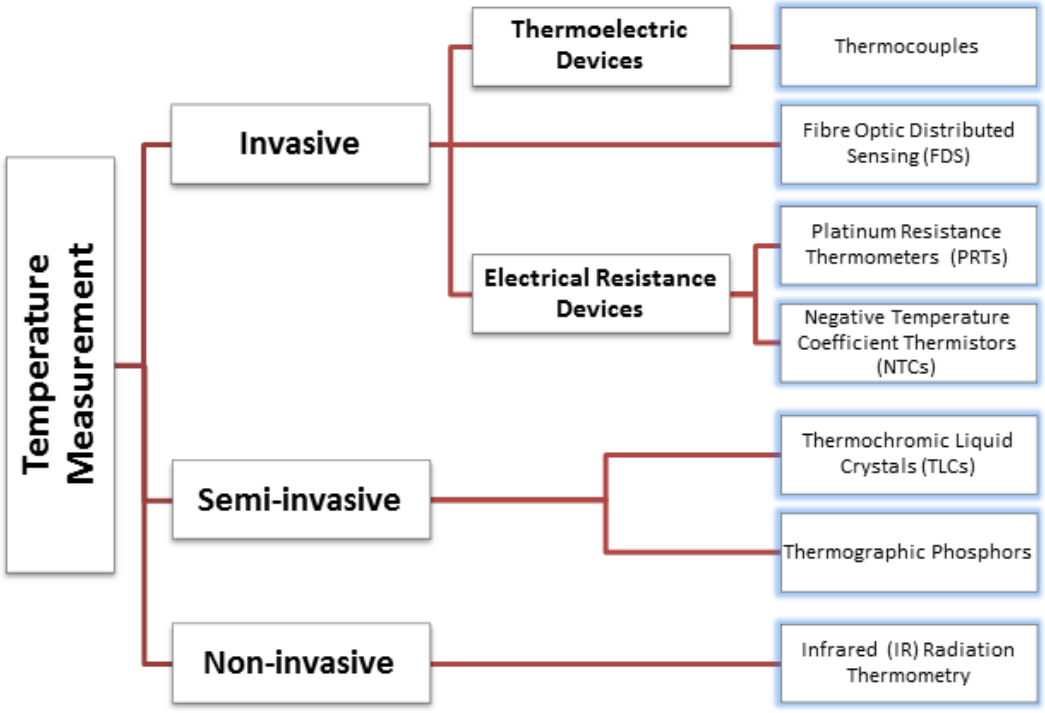

Figure 3 – Classification diagram showing seven key temperature measurement technologies for use in assembly environments [16]

2.4.1 Invasive Temperature Measurement

Invasive sensors require physical thermal contact with the measurand in order to function. Thermal contact can be achieved either through surface adhesion of the sensor head to the surface of the object, or preferably: inserted into the object.

2.4.1.1 Thermocouples

Thermocouples are the most widely used temperature measurement type in industry, which is reflected in the body of literature published on the subject in general. Contributing to their popularity are the accepted standards for use, their relative accuracy over an extended measurement range and the comparatively low cost of the sensors. Over wide ranges, accuracies between of ±0.5 ˚C and ±2 ˚C are comfortably achievable while narrower measurement ranges can manage closer to 0.1 ˚C [18].

These thermoelectric devices employ the Seebeck Effect in dissimilar metal wires. A temperature difference from a reference junction can be calculated as long as the Seebeck coefficients of the wire materials are known [19]. This temperature gradient creates within the wires a net electromotive force between T_0 and T_1 expressed as voltage of the order of microvolts, which can be measured at the terminus connections T_0 to determine the temperature. As a temperature gradient needs to be established to create a net voltage output signal, cold junctions are often used in the form of a fixed physical temperature or simulated electronically using cold junction compensation (CJC).

As the largest contributor of thermocouple uncertainty, studies have focused on the inhomogeneity of specific material wires [20-24] as well as methods for its evaluation [20, 25-27]. New quantitative methods for determining the contribution of inhomogeneity of thermocouples have been studied over a wide range of thermal gradients likely to be experienced in use and shown to be an improvement upon traditional depth immersion tests at fixed points for elemental thermocouples [28].

The self-validation of thermocouples has been studied for control applications in order to detect unusual sensor readings resulting from loss of power, open circuit and loss of contact faults [29]. This intelligent sensor then proceeds to give a best estimate reading. Individual sensors can be characterised and exhibit enhanced performance and fault detection through the use of internal memory and software [30].

Various types of thermocouples have been evaluated and compared in terms of their stability [31]. Comparisons between the stability and sensitivity of base and noble metal thermocouples have also been made [32]. Pure element thermocouples are more homogenous than alloyed thermocouples. The best base metal thermocouple over the -40-1200 °C range is the Nicrosil-Nisil or Type N while the best noble metal is the Pt/Pd thermocouple for measurements up to 1500 °C. Type S thermocouples from different manufacturers have been shown to exhibit slightly different thermoelectric characteristics, with a maximum difference at the Cu fixed-point of 1.95 °C [33].

A system has been developed for use in strong EM fields at ITER with 0.5 °C global accuracy [34]. Magnetic fields in particular also influence thermocouple sensors and studies have been carried out to establish the sensitivity of the sensor to these fields to account for this in uncertainty estimations [35].

Improvements have been made in spatial resolution of surface temperature measurement compared to standard soldered Type K thermocouple using an electrochemically etched microtip [36]. Thin film thermocouples can also be deposited onto a surface and has been used in the measurement of heat generated in the friction between sliding surfaces [37].

Non-linearity of sensors can be an issue although one study showed it to be possible to correct for this using a neural network approach in Type K thermocouples [38]. Through the improvement of high temperature alloys and more intelligent electronics, industrial thermocouple measurements can be further enhanced [39].

2.4.1.2 Industrial Platinum Resistance Thermometers (IPRTs)

Industrial platinum resistance thermometers (IPRTs) are resistance-based temperature sensors. Temperature can be measured extremely accurately by applying a small current to a length of platinum wire of known resistance. Temperature on the sensor will alter the resistance of the wire which can be compared against a reference resistor. Platinum is used due to the stability of the material and linear relationship between temperature and resistivity.

IPRTs are the rugged cousins of the standard platinum resistance thermometers (SPRTs) used to define fixed points on the International Temperature Scale. SPRTs are capable of uncertainties of the order of milliKelvins [40], however are delicate instruments. IPRTs are designed to withstand the shock, vibration and contamination found in industry and can comfortably achieve ±0.01 - 0.2 °C [18]. Shortly after the introduction and adoption of the ITS-90, a capability assessment of IPRTs was carried out at a range of temperatures [41].

IPRTs embody two main forms: wire wound and thin film. Wire wound IPRTs consist of a platinum wire wrapped around a ceramic core, whereas thin film IPRTs consist of a thin film of platinum deposited onto a ceramic substrate. Both types are typically encapsulated inside an insulating layer [42]. Thin film IPRTs can be lower cost devices as their construction lends itself readily to mass production, whilst being useful for surface measurements. Wire wound IPRTs tend to be more expensive for accurate probing.

IPRTs are starting to find applications with low cost thin film devices where previously thermocouples would have been utilised and in 2013 one paper described an IPRT adaptation to measure stagnation temperature in gas turbines [43].

Hysteresis can form a significant contribution to the uncertainty of IPRTs, caused by the construction of the sensor, with thin films exhibiting higher levels than wire wound IPRTs due to thermally induced expansion and contraction [44] . Further confirmation that sensor hysteresis was construction-dependent was provided in another 2010 study [45]. The best Pt100 sensors exhibit hysteresis of the order of milliKelvins, whilst the worst were around 20 mK [46]. IPRTs have been found to be sensitive to electromagnetic fluctuations [47].

For precise measurements at a small scale, IPRTs have been identified with performance characteristics comparable to that of the ITS-90 standard [48]. Investigations have been underway to develop a device, which can turn the IPRT into an intelligent sensor that contains calibration and sensor characteristics. This potentially offers reduced measurement uncertainty whilst being less expensive than resistance bridges used in laboratories [49].

Thermal contact and sensor protection is important and work has been carried out in order to determine the best use of thermal insulation filler although this needs to be tested in a range of conditions for further validation [50].

Methods have been developed for accurate, semi-automatic calibration on-site, resulting in reduced slow temperature drift and a reduction in calibration time [51]. The possibility of having self-testable IPRT sensors for improved long-term stability has been explored with the use of miniature fixed-point cells so the sensor can remain fixed without having to be removed for calibration. This approach was found to be good enough to monitor long-term sensor stability to 0.1 °C [52].

2.4.1.3 Negative Temperature Coefficient Thermistors (NTCs)

Thermistors are made from semiconductor materials and their temperature-resistance relationship is characteristically non-linear [40], placing greater emphasis on the importance of calibration. Use of semiconductor materials means they can provide a far higher level of sensitivity [53] than other sensor types although regular calibration is necessary to avoid the effects of sensor drift.

Schweiger argued in 2007 that a fast multichannel precision thermometer could be developed to rival PRTs using thermistors, provided there is adequate sensor selection and calibration [54]. In tests carried out in the range from -50–10 °C, deviations of less than 30 mK were observed.

Apart from a bridge resistance circuit, a voltage divider can be used to resolve temperatures. Faced with non-linearity, this can be problematic however one solution is to determine the resistance of the voltage divider itself to capitalise on the thermistor's innate sensitivity to produce a high resolution thermometer [55].

An artificial neural network approach to sensor non-linearity was investigated in 2001 by Khan et al., which appeared to be an improvement upon linear regression methods [56]. In 2008, it was suggested by Keskin, in reference to the 2001 article, that it needed to be repeated to reflect the correct form of the NTC characteristic equation to prove efficacy [57].

A promising new development allows for a thin film of graphene to be inkjet-printed onto a flexible polymer substrate and used as an NTC sensor; the response time of this thin film was shown to be an order of magnitude better than conventional NTCs [58].

2.4.1.4 Fibre-optic Distributed Temperature Sensing (FDS or DTS)

Fibre-optic Distributed Temperature Sensing (DTS) systems operate using the change in refractive index of an optical fibre at different temperatures and its resultant effect upon the collimated, monochromatic light that propagates along its path. DTS also finds application in the monitoring of power cables up to 30 km in length [59] and in pipeline monitoring for the oil and gas industry [60]. Around 0.1 °C resolution and less than ±1-2 °C can be achieved using DTS, however spatial resolution can suffer over long distances with 10 mm spatial resolution over 70 m being attainable [61].

Fully distributed systems allow measurements to be taken at discrete spatial intervals along the fibre. Fully distributed systems encompass linear-backscattering, non-linear backscattering and non-linear forward scattering [62]. Attempts have been made to use the Rayleigh backscatter to correct for background effects in Raman based systems, with limited success. This is more a concern for harsh environments and over distances of 2 km so should be of less consequence in a factory context [63].

It was argued that Brillouin scattering theoretically offered a larger measurement range than an equivalent Raman system [64]. Over long distances up to 100 km, remote Raman amplification has proved useful in improving the performance of Brillouin based DTS by boosting the signal to noise ratio [65].

Other variables can influence the propagation of the optical wave in the fibre, which means that these systems can also measure strain, pressure, electrical and magnetic fields. Combining Raman-Brillouin scattering and multiwavelength Fabry-Perot lasers allows simultaneous strain and temperature measurements to be taken. A hybrid Raman-Brillouin approach delivered significant improvements in performance [65]. In 2011, one study reported that using Allan deviation analysis on a sophisticated Raman backscatter system resulted in noise and drift improvements with a resolution of around 0.05 °C [66].

For the factories of the future, strain measurement combined with temperature measurement would be particularly useful for monitoring tooling structures subject to thermal and gravitational loading.

2.4.2 Semi-Invasive Temperature Measurement

Semi-invasive sensor types are technically invasive types whose measurements can be interpreted non-invasively from a distance. Semi-invasive sensor types are often thermally active coatings that can be applied to the surface of the object to be measured.

2.4.2.1 Thermochromic Liquid Crystals (TLCs)

Thermochromic Liquid Crystals (TLCs) are liquid crystals whose optical properties change when subjected to different temperatures. Outside of the measurement range, the sensor will appear transparent, as the crystals are in an amorphous state. Within the measurement range, the sensor will display a range of colours known as the colour play, where the crystals will become more structured and reflect different wavelengths of light according to the temperature [67]. Each TLC typically operates over a narrow bandwidth however a variety of TLCs with overlapping measurement ranges can be used in concert. A review of TLCs was published in 2011 [68].

TLCs are especially useful for heat transfer studies, providing relatively economical temperature distributions. Solving the fin temperature equation is commonly carried out and it is also possible to include natural convection in the estimation of the heat transfer coefficient [69]. Turbulent heat transfer studies such as those applied to turbine blades that were carried out using TLCs were reviewed in 1995 [70].

Image analysis techniques have been used in conjunction with TLCs in order to measure the temperature distributions as well as heat transfer and thermal polarisation coefficients found in spacer-filled channels for membrane distillation with promising results [71].

Spin-crossover (SCO) materials have been successfully used to develop a TLC for use around room temperature, which could allow for sensing in different temperature regimes [72].

In 2011 it was shown that a TLC could be used in the calibration and verification of ultra-fast scanning calorimeters, with the suggested material for this application being 80CB [73].

2.4.2.2 Thermographic Phosphors

Phosphor thermometry relies on the luminescence exhibited in phosphors when subjected to different temperatures over a sizeable range. Methods for phosphor thermometry vary. Time resolved phosphor thermometry measures the time for the phosphor to reach a critical intensity; frequency domain finds application in those measurements where the excitation is continuous and periodic. Time-integrated methods measure one absolute intensity or the ratio of a pair of intensities emitted from the phosphor [74].

Material properties are fundamental to thermographic phosphors. Seven ceramics were characterised at once to contribute to and encourage further material studies [75]. Depending on the doping materials used, it is possible to create thermographic phosphors that can give an intensity ratio at two distinct wavelengths when illuminated by ultra-violet light, allowing for improved temperature distribution measurement [76].

As coatings, measurements can be taken on curved surfaces, where the intensity ratio strategy is preferred to minimise possible viewing angle error [77].

Imaging of the wall temperature inside an optical engine can be achieved using lifetime analysis, which uses the intensity decay over time to resolve the temperature to produce "reasonable temperature maps" [78].

Transient temperature measurements for combustion applications are common and a theoretical study of heat transfer by Atakan and Roskosch was carried out to inform experimentalists of practical measurement considerations [79]. For high frequency measurements, traditional models can present challenges to the experimenter and in 2007 a new, more effective model for transient measurement was published [80]. The use of thermographic phosphors in combustion applications was reviewed in 2010 [81].

The selection of a measurement strategy should include a comparison for specific coatings. The lifetime and intensity ratio approaches were compared for one phosphor: Mg_4FGeO_6:Mn, where the former was found to be the preferred choice in accuracy and precision [74].

Thermal barrier coatings can incorporate thermographic phosphors to allow for embedded temperature sensing although further development is required to allow optical access to the surfaces [82].

A comprehensive review of thermographic phosphors for surface temperature measurement including film preparation, measurement strategies and associated uncertainties was published by Brübach in 2013 [83].

2.4.3 Non-Invasive Temperature Measurement

Non-invasive temperature measurement sensors make no physical thermal contact with the measurand.

2.4.3.1 Infrared Radiation Thermometry

Infrared Radiation thermometry measures the energy radiated from the surface of the measurand. The energy radiated from the surface depends upon the emissivity of the surface to be measured. Emissivity is a dimensionless ratio that is used to describe the amount of radiation absorbed by, and reflected from, the surface of a body. Due to the number of variables, emissivity is the largest source of uncertainty in this type of measurement but can be managed to some extent using a uniform coating of a known emissivity. Commercially available devices generally take one of three forms: single point sensors, line scanners and thermal imaging cameras. Single point sensors can be calibrated to achieve around ±1-2 °C accuracy, whereas the line scanners [84] and cameras will deliver around ±2-3 °C.

The emissivity of a surface can change as the temperature is being monitored as temperature is another variable of emissivity. A promising development is a system that can measure emissivity and temperature simultaneously to correct for emissivity changes [85].

Various emissivity models based on surface roughness have been classified. One study compared emissivity modelling approaches and validated experimentally using various surface roughness values of Al 7075 aluminium alloys [86].

The Traceability in Radiation Thermometry (TRIRAT) project was undertaken to improve industrial temperature measurement. This project resulted in a new robust instrument with the performance of a standard thermometer, measuring in the range from -50 °C up to 1000 °C [87].

IR temperature measurement is particularly useful for non-invasive measurement of higher temperature processes. Welding has benefitted from the use of this technology, and it is possible to combine IR with thermocouples to better model weld pool thermal cycles during laser welding, for example [88]. Temperature distributions during chip formation in the machining of titanium have also been measured in this way [89].

The building sector spawned a handheld system for the creation of 3D thermal models for use in the energy auditing of buildings [90]. Using two or more mounted IR cameras, 3D temperature maps can be created [91].

Wireless IR thermometers with a narrow field of view appear promising for outdoor measurements where large ambient temperature fluctuations are present [92, 93].

2.4.4 Temperature Measurement Comparison

The data presented in Table 2 [16] compares the temperature sensing capability of each of the temperature measurement technologies reviewed in terms of their characteristics. Specifications of temperature measurement technologies will vary, so this table provides more of a general guide to their relative merits.

Table 2. Table comparing the six temperature measurement technologies.

Technology	Sensor Type	Uncertainty (± °C unless percentage of reading given)	Resolution (°C)	Source	Possible Applications
Thermocouples	Invasive	0.1-0.5	0.01-0.1	[18]	Model development; embedded into tooling; air temperature; product monitoring
IPRTs	Invasive	0.01	0.001	[94]	Model development; embedded into tooling; air temperature; product monitoring
NTCs	Invasive	0.01	0.01	[53]	Model development; embedded into tooling; air temperature
FDS	Invasive	1	0.1	[61]	Model development; embedded into tooling; integrated into product
TLCs	Semi-invasive	0.1-2	1	[70]	Model development; applied to tooling
Thermographic Phosphors	Semi-invasive	1%	1	[83]	Model development; applied to tooling
IR Radiation Thermometry	Non-invasive	1-3	0.1	[18, 84]	Model development; tooling monitoring; product monitoring

2.5 Measurement Planning

Literature pertaining to measurement planning is reviewed in this section for both dimensional measurement and temperature measurement. Including dimensional measurement planning in this section this provides background to the problem, provides a basis for contrast to the state of the art in temperature measurement planning, and because it will have to be used to produce spatiothermal measurement plans. Temperature measurement planning is included as a separate section from sensor network design. Many of the learning from sensor network design is transferable to temperature measurement specifically but is not necessarily limited to the measurement of only temperature.

2.5.1 Dimensional Measurement Planning

Dimensional measurement planning is relatively mature compared to temperature measurement planning. The method used to measure the dimensions of an object has a significant impact upon the resulting measurement uncertainty. Measurement processes are in addition heavily dependent upon measurement planning for both reproducibility and traceability to international measurement standards.

Computer aided inspection planning (CAIP) is a research area that has grown significantly as more demands are placed upon quality and speed of production. Initially, the majority of CAIP focused on the application to CMM inspection as this is commonly used in industry. CMM inspection can be a source of bottlenecks depending on the production environment. Planning and programming of CMM inspection is a highly skilled job that takes time and expertise. Computational optimisation of inspection continues to be a major area of research to support metrologists. Looking at inspection from a quality perspective, a lot of work has been done to optimise for quality throughout production [95].

Computational methods are increasingly being used in the planning of measurement using optical systems such as laser tracker networks [96-98]. This approach usually considers an uncertainty model, and photogrammetry and structured light projection are other technologies that have used uncertainty modelling to facilitate traceable inspection planning [99].

Inspection planning can be carried out automatically, and several software packages exist to generate measurement plans and programs. Model based definition (MBD) is often used as one of the enabling technologies for this, as the MBD contains CAD geometry, as well as other technical information required for production such as geometric dimensioning and tolerancing (GD&T). The extra data in the MBD is machine readable, so with knowledge of the design specification as well as the geometry, software can make use of rules to generate probing strategies and output inspection plans. MBD driven CAIP has a number of associated challenges to overcome such as in interoperability and standardisation, and work has been done to address some of these issues for the Model Based Enterprise (MBE) [100, 101]. This is potentially a supporting technology that could be applied to temperature measurement planning, but this does not appear to have been done as yet.

Due to the distances covered in some large-scale applications, autonomous inspection systems are increasingly being developed to carry out inspections. CAIP provides a means to quickly plan inspection and remove some of the time-consuming path-planning required to inspect large structures [102]. Large volume metrology has typically focused on the dimensional aspects of measurement planning, and not so much on the thermal error contributions, so there is an opportunity to expand on the existing work in this area.

2.5.2 Temperature Measurement Planning and Sensor Network Design

"Temperature measurement planning" is a term that is relatively difficult to find in the literature, but research has been carried out in this area using different terminology. Temperature measurement planning as a term is used throughout this thesis as there are clear parallels in the preparation required before both types of measurement.

The objective of temperature measurement that is of most interest to this thesis is ultimately the temperature of structures so that thermal expansion can be inferred. This could be acquired from embedded or surface sensors, depending on the object being measured – this could also be invasive or non-invasive.

Measurement of ambient air temperature is very common in general [103]. Ambient air temperature measurements are useful in optical metrology for the prediction of error due to refractive index changes. The temperature of air and other fluids are often studied because they have an impact upon living things that are sensitive to changes such as crops in agriculture [104]. These measurements often contribute to the building of thermal models, and validation of CFD simulations [105]. Oceanography is another field that has a significant interest in spatial temperature distributions in a challenging environment [106].

Research in the field of heating, ventilation, and air conditioning (HVAC) has studied the temperature distribution of a range of environments and applications. Thermal stratification describes an environment in which temperature gradients operate vertically, meaning temperature increases with height. Often, work has focused on understanding thermal comfort for people working in these environments [3, 107], or for improving energy efficiency [108], for example. It has been found that large spaces with high ceilings suffer from a high degree of thermal stratification, with guidebooks advising that large halls are likely to exhibit a thermal gradient of around 1 °C/m [109].

The aerospace, marine, and automotive sectors are particularly affected as this is often where large products are assembled. Thermal expansion error frequently affects measurements in assembly due to the temperature distributions and variations in these large spaces [110].

Nath et al looked specifically at Bayesian calibration for spatially varying parameters and optimisation of sensor positions to support this calibration [111]. It is important to note that the primary motivation for this research was for the structural health monitoring of concrete structures. One of the interesting aspects of this paper is that is addresses inhomogeneity in concrete, so is necessarily complex and stochastic, as opposed to deterministic. This was applied to temperature distributions in concrete. Reproduction of the temperature field performed well computationally, and these results were validated to some extent in experimental trials. Optimised sensor locations were compared to uniform grid, with randomly positioned configurations serving as experimental controls. Using this method for spatial analysis showed promise, however the only optimisation was on position, not the number of sensors required. Solving the optimisation was also found to be computationally expensive, although this point can be overlooked to some extent at this stage of development. Time variance wasn't included in the optimisation, and there is the suggestion that extending this method to include time could be more complex than this may initially sound, at which point computing efficiency would become more of a concern.

The requirements for measuring structural temperature in solids and measuring ambient air temperature are quite different, with some similarities. The temperature in a structure placed

in an environment with stable air temperature will be stable. As air temperature becomes more variable, the structure's temperature will be quite different as not all of the heat will be transferred between the air and the structure. The NPL Good Practice Guide, Introduction to Temperature Measurement considers surface measurement, where embedding a sensor is not possible. Maximising the surface contact to increase heat transfer is key to reducing the error of surface temperature measurements [103].

2.6 Spatial Interpolation Methods

Reconstruction of temperature fields from sparse temperature sensor data requires some method of interpolation. Interpolation is a subset of the wider area of the study known as Approximation Theory, in which simplified functions can be used in lieu of more complicated functions. Approximate functions naturally produce residual errors as they do not perfectly match the original function. These errors are calculated to measure the performance, compare, and establish the limitations of a resulting approximate function [112].

Interpolation can be defined as, "The computation of points or values between ones that are known or tabulated using the surrounding points or values" [113]. Various methods exist for filling these gaps in datasets, and such methods have found application in various fields. In particular, the interest is on spatial interpolation methods that produce simplified functions in scalar fields. This section presents a brief overview of spatial interpolation methods, and a coarse selection of useful methods, some of which are discussed in more detail.

Several review papers have been published on spatial interpolation methods in different disciplines [114]. Comparative studies have been carried out on spatial interpolation methods using sample data sets to determine which methods would be preferred. These comparisons are to some extent application-specific - it would be difficult to use specifically applied methods as evidence to make general statements about interpolation methods. Looking at these comparisons with some perspective, and context as to how close each application is to the problem, it becomes easier to get a feel for which methods might work. Care is taken to avoid declaring or referencing the existence of a 'best' method. Several methods could produce an acceptable result for a specific application, but the optimal method may be different depending upon the dataset.

Li attempted to review comparative studies for spatial interpolation in the environmental sciences [115]. This provides a useful perspective of the landscape of spatial interpolation methods, and highlights more commonly used methods. There does appear to be a bias towards these common methods, meaning they are subsequently overrepresented in comparative studies. This is useful, as it shows these methods are de facto standards - it betrays a consensus that any novel method should be compared to them. In the case of novel methods, these do sometimes outperform the more popular methods, but are less widely used and therefore rarely represented in comparative studies. Over a long period of time this effect would hopefully converge towards generally better performing methods, but this is a limitation of this type of study. Many of the methods appear to be variations of some core methods.

The context of the problem is important to consider in the selection of the most appropriate interpolation method. The reconstruction of temperature fields could be posed as a 1D, 2D, or 3D problem. Ideally, the 3D scalar field case is the one that is of most interest, but useful results could come from lower dimensional approximations in many cases. As dimensionality increases, the number of options available for interpolation decrease. Another consideration is computational expense, as higher dimensional solutions will usually take more time than lower dimensional solutions.

2.6.1 Linear Interpolation

Linear interpolation involves the fitting of a continuous straight line through two or more discrete data points. The fitted line then allows values to be predicted within the limits of the first and final points. Linear interpolation is the most straightforward of interpolation methods and is widely used. In some cases, a linear interpolation can provide a good approximation of a temperature distribution.

Linear interpolation forms the basis of the finite element method. Between any two nodes on a finite element mesh, a linear interpolation is carried out in order to produce continuous results from a solution.

2.6.2 Polynomial Interpolation

Polynomial interpolation introduces curve fitting, allowing the approximation to potentially outperform straight lines using a polynomial function. Polynomial functions are described in terms of their degree, or order, which is determined by the largest power in the polynomial.

To some extent, higher order polynomial functions can produce approximations with relatively low residuals, however there can be problems with over fitting of the model to the data points. High order polynomials can produce some extremely large and unhelpful values if not properly applied - examples of this can be seen in section 4.4.4.

2.6.3 Kriging

Kriging is one of the more commonly used interpolation methods. It is a statistical interpolation method and can be used to address various types of problem [116]. Kriging allows unknown data points using known data points, distributed in space, to be estimated. Known points do not need to be regularly distributed for this to work, although density and local point distances influence usefulness of estimation.

Bohling's Kriging material [117] points to Goovaerts' explanation [118], in which he pointed out that Kriging is usually some flavour of the basic linear estimator, with different assumptions. The basic linear estimator is described by Equation 4.

Equation 4

$$Z^*(\boldsymbol{u}) - \mu(\boldsymbol{u}) = \sum_{\alpha=1}^{n(\boldsymbol{u})} \lambda_\alpha [Z(\boldsymbol{u}_\alpha) - \mu(\boldsymbol{u}_\alpha)]$$

Where:

$Z(\boldsymbol{u})$ is the variable of interest, the random field;

$\mu(\boldsymbol{u})$ is the trend component, the expected mean of $Z(u)$;

$\boldsymbol{u}$ is the location vector for the estimation point;

$n(\boldsymbol{u})$ is the number of local data points used to estimate;

$z(u_\alpha)$ is the datum for estimation location u;

$\lambda_\alpha(\boldsymbol{u})$ is the kriging weight assigned to datum.

In this case, the function Z(u) could be a temperature distribution, in which the temperature, here Z, varies with position, u. The main spatial difference is that the position is described using a Euclidian vector relative to a datum, $z(u_\alpha)$, instead of a Cartesian coordinate relative to the origin.

In ordinary kriging (OK), the assumption is that the mean is only locally constant, rather than globally constant as in simple kriging. The result is a simplified model [119] :

Equation 5

$$Z(\boldsymbol{u}) = \mu(\boldsymbol{u}) + R(\boldsymbol{u})$$

Where: $R(\boldsymbol{u})$ is the residual error component.

Cokriging is kriging with additional variables, in which the estimation is embodied in multiple models. Ordinary cokriging (OCK) makes the same assumption about local rather than global means, but instead for the two variables. Two-variable cokriging models could be expressed as:

Equation 6

$$Z(\boldsymbol{u})_1 = \mu_1(\boldsymbol{u}) + R_1(\boldsymbol{u})$$

$$Z(\boldsymbol{u})_2 = \mu_2(\boldsymbol{u}) + R_2(\boldsymbol{u})$$

As there are additional variables to consider, there is a greater degree of estimation required. More estimation can mean that the computation required is greater but can increase the uncertainty of the estimation. There may be occasions where the extra variable confers less of a benefit than expected due to this added uncertainty.

2.7 Research Gaps and Opportunities

Reviewing the literature showed that there were some opportunities for work to be done in temperature measurement to support thermal compensation of dimensional measurements.

Much new work on temperature measurement sensor development appears to be focused on the extreme ends of the temperature scale, and less on more everyday temperatures as there are significant traceability challenges [120]. Invention is required in order to engineer a sensor that can survive such extremes, but also to carry out measurements with an acceptable level of uncertainty. The temperature measurement technologies available can comfortably be used to measure within the temperature range of an assembly environment, however, which is much less hostile. The key difference is that the temperature differences are more subtle, so more sensitive temperature sensors can reduce the sensor contribution to uncertainty.

Dimensional measurement planning and computer aided inspection and planning (CAIP) are well-established areas of research, in which a lot has been done to improve the execution of dimensional measurement. When the term "temperature measurement planning" is used, it becomes more challenging to find examples of research in this area. Most of the work on temperature measurement planning is carried out outside of manufacturing engineering research, and subsequently has a different set of terminology that is used. Geospatial climate research [121] and oceanography are two examples in which temperature sensor network design is applied.

The comparison of dimensional and temperature measurement as entities should be fair to make, just as the comparison of any of the SI units. What was interesting to observe was the very different approach of the two communities, or at least, how the two communities could be perceived when looking at the literature. It is possible that the differences between dimensional measurement and temperature measurement are driven by the relative influence of end users in industry and academia.

In manufacturing, for example, if the thermal history of a part could be measured upon receipt from a supplier there might be a marked difference in the approach to temperature measurement to be more closely aligned to dimensional measurement. Product conformances are defined by geometry and dimensions, so dimensional measurement is necessarily highlighted. Products are built by processes, within which temperature is a parameter. Many processes are proprietary, so accessibility of this learning is made difficult.

The difference in the approaches warrants further work, as going forward the trend in manufacturing is towards the use of significantly more sensors to monitor a variety of quantities. In many ways, if temperature measurement is to be deployed with the same level of maturity as dimensional measurement, then much of the work that is found in CAIP needs to be repositioned. Care was deliberately taken to not say repeated: many studies have been carried out for temperature sensor networks and sensor networks in general. It appears that there are comprehensive standards for common sensor types to be manufactured, but very little guidance can be found on how to use these sensors. What is missing is a planning tool that can be used in manufacturing, and a metrological framework that supports the symbiotic measurement of interacting quantities.

In the next chapter, the results of experimental work are presented. These experiments provided valuable experience in learning more about the problem of thermal expansion in the laboratory and in the factory. Experimentation with real structures required that they be made to expand in the otherwise relatively stable conditions of the laboratory. How would thermal

compensation work in practice? What kinds of temperature variation can be observed in an assembly environment? And how significant a role should temperature measurement planning play in real world applications?

2.8 Chapter 2 – Summary

Chapter 2 provided:

- An overview of the approaches to scaling for thermal expansion and when they are likely to be used.
- Discussion of relevant guides and standards – none of which currently provide information to answer the question of how best to measure temperature for thermal compensation.
- Examples of thermal compensation research applied to manufacturing.
- A review of temperature measurement technologies.
- Examples of measurement planning and comparison between temperature and dimensional metrology.
- An overview of methods for the interpolation of temperature distributions.

Contributions:

The contributions to knowledge from this chapter are:

- Identification of gaps in the research relating to the planning of temperature measurement.
    - Work has been done to develop sensor technology.
    - Work has been done to plan for temperature measurement in individual scenarios.
    - Work has not been done to define a set method for temperature measurement planning.

The sensors are available to measure temperature to a high standard, but currently there is no agreement or guidance on how best to use them in practice, particularly for thermal compensation.

---

3 Experimentation in Temperature Measurement and Thermal Compensation

This section summarises the results of experimentation that has taken place in laboratory and industrial settings. Experimental work is presented to provide background to the problem and see the role of temperature measurement planning. The experiments presented provided key learning in the following areas which can be used to create a temperature measurement planning strategy:

- Practical experience in the measurement of dimensions and temperature;
- Methods for CAD simplification;
- Computational modelling of thermal expansion;
- Data acquisition;
- Analysis of simulation data and methods for its comparison to measured data;
- Temperature characterisation of loosely controlled and uncontrolled industrial environments.

Testing of thermal expansion and the development of a workflow for its compensation was aided by the introduction of heating in order to create more extreme, localised effects so they could be easily measured beyond the uncertainty of measurement as much as possible. Taking this approach meant that within the laboratory environment, thermal gradients could be introduced synthetically in an environment that is ordinarily much less variable. Methods for introducing heating to structures are presented in this section, with brief notes on their advantages and limitations.

As a rough guide: the ambient temperature of the laboratory in which some of these experiments have been executed was often close to standard (approximately 20 ±1 °C). More extreme periods occurred where the temperature was casually observed to exhibit around 18 °C in cold, wintry weather, to up to around 22 °C in hot, summer weather. Lessons were also learned about the relative comfort level experienced within this small range of ambient temperatures.

The work presented in this section was previously presented at the Digital Enterprise Technology 2016 conference, and later published as a special edition journal article [122].

3.1 Experimental Measurement Scenario

3.1.1 Frame structure

The experimental measurand took the form of a cuboidal frame structure. Each of the 12 beam members were made from aluminium 6063 45 mm extruded profile by MiniTec and were fastened with proprietary PowerLock fasters. The frame was 2 m in length, and 1 m height and depth. These dimensions and material choice allowed for experiments to be carried out at the lab scale whilst providing maximum thermal expansion.

Supporting this frame were 4 ball transfer units, which sat at the four bottom corners of the frame. Each of the ball transfer units rested upon flat plates adhered to the floor, which allowed the frame to expand more smoothly. One ball transfer unit was nested in a hole drilled into one of the plates in order to provide a translational constraint. To reset the frame position repeatably, and to provide constraint for yaw rotation of the frame, a fiducial post

was fixed to the floor for the frame to rest against. A photograph of the frame from the photogrammetry can be seen in Figure 4.

3.1.2 Heating method

At normal ambient temperature the laboratory environment was relatively stable, varying less than a degree at various positions on the frame. Heating of the structure was performed using a DeLonghi HVA3222 fan heater. Convective heating is the primary heat source in industrial environments and the fan heater allowed for exaggerated heating in order to significantly observe thermal expansion beyond the uncertainty of the measurement technique. The heater was placed outside of the frame next to the bottom corner, facing inwards. The heater had two heating power levels providing 1 kW and 2.2 kW [123].

3.1.3 Measurement

3.1.3.1 Photogrammetry

An Aicon DPA photogrammetry system [124] was used for these measurements. a modified Nikon 3dx digital single lens reflex (DSLR) camera equipped with a 28 mm Nikkor prime lens. Image transfer was achieved quickly using a local Wi-Fi connection to a laptop computer. Proprietary software called Aicon 3D Studio is used for these measurements and some analysis of measurement data. 14-bit ANCO coded targets were fixed to the surface of the structure.

An example of the output of deformation analysis in Aicon 3D Studio can be seen in Figure 4. The photogrammetry scale bars, data acquisition system and the heater can be seen around the frame structure.

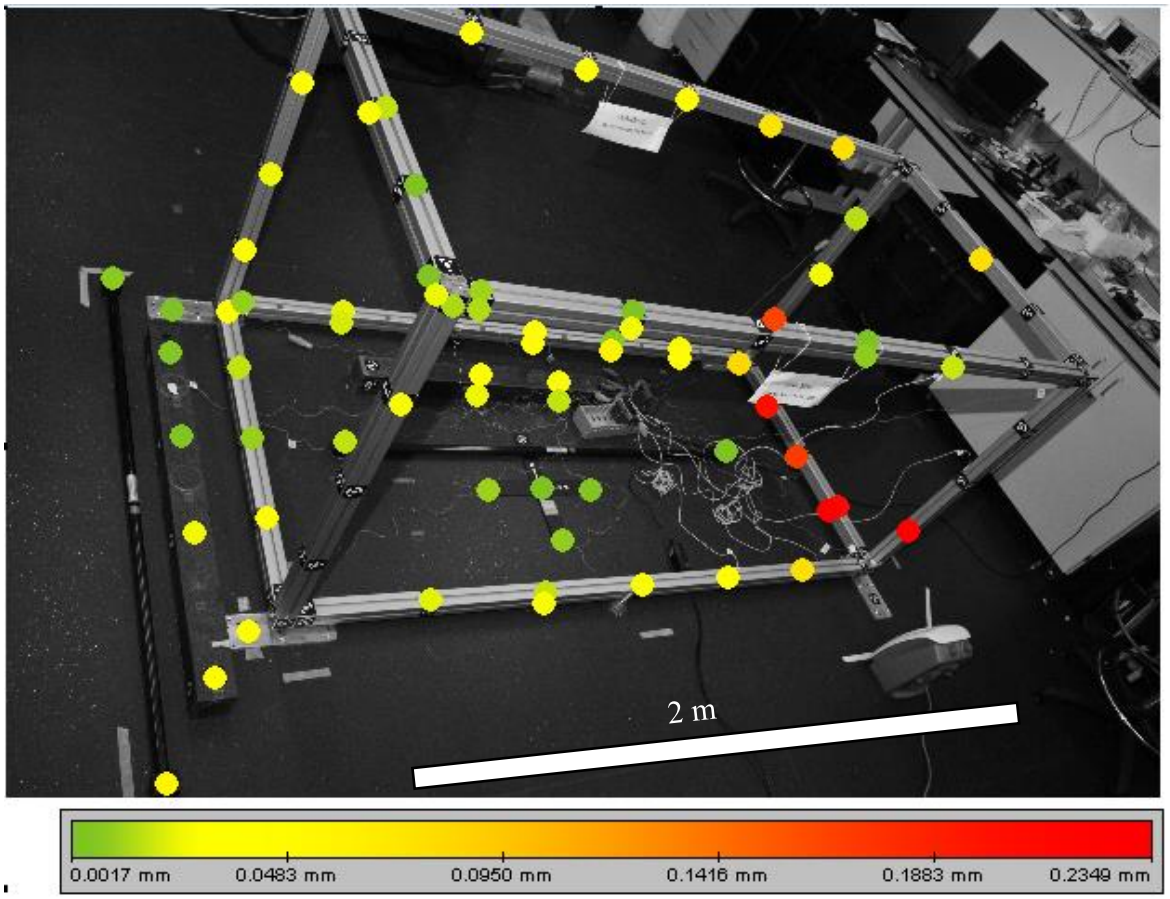

Figure 4. An example image showing deformation analysis of coded targets in Aicon Studio superimposed onto the greyscale photograph of the frame structure.

200 to 250 images were captured at a range of elevations and orientations around the structure per measurement. Roughly 10 vantage points were used in standing and crouching positions, with 8 ladder positions allowing for improved vertical vantage points. The photogrammetry is captured in Figure 5 and Figure 6. Each of the green dots in the images represent a coded target, white lines are scale bars, and the white boxes represent camera positions. It took 15-20 minutes to capture all of the required photographs.

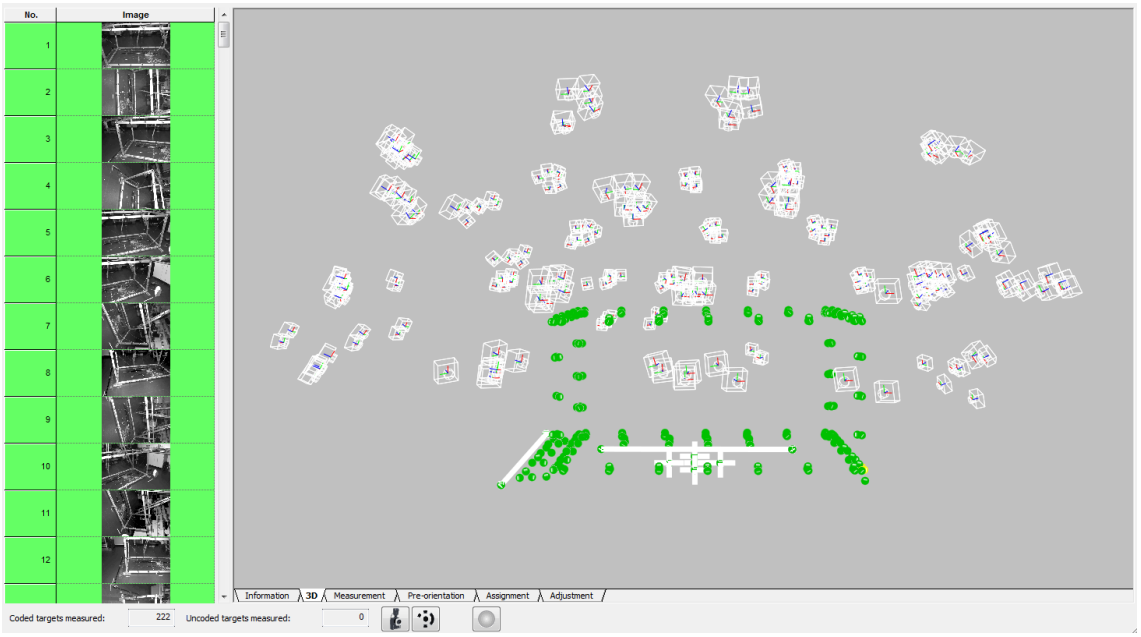

Figure 5. Screenshot from Aicon 3D Studio showing the side view of the frame structure photogrammetry.

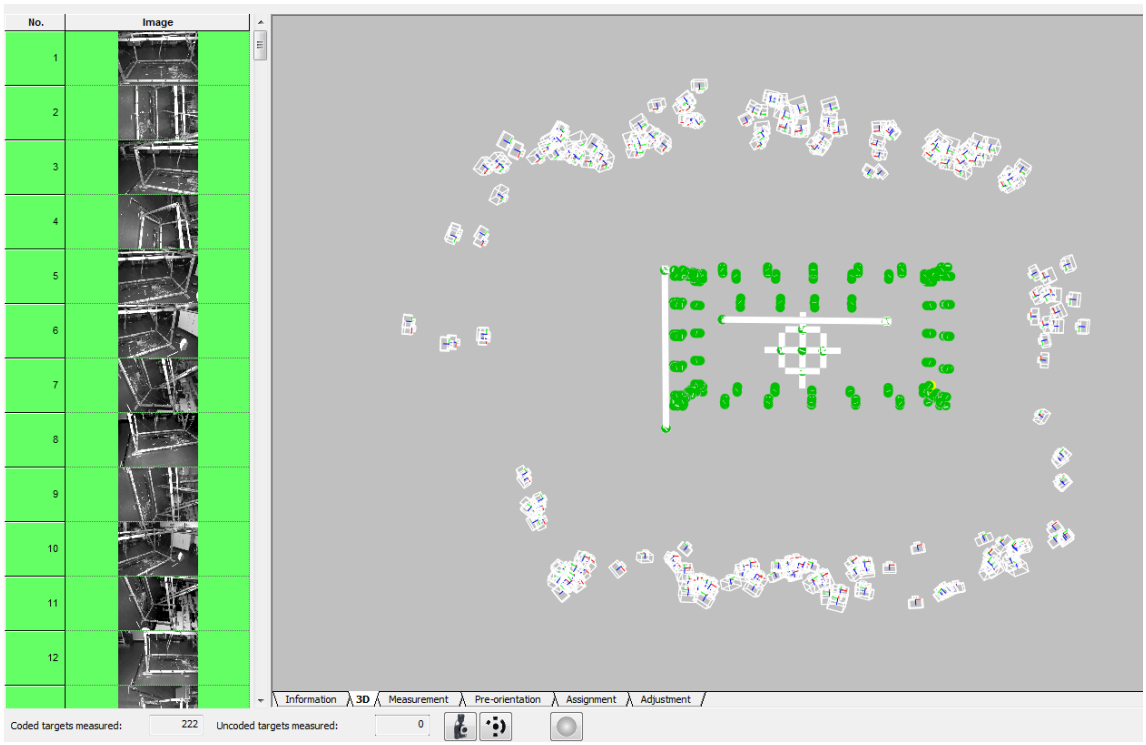

Figure 6. Screenshot from Aicon 3D Studio showing the top view of the frame structure photogrammetry.

Temperature Measurement

Type T thermocouples and class A platinum resistance temperature detectors (RTDs) were used throughout the experiments to measure surface temperature on the frame. Thermal imaging was also carried out to characterise the temperature distribution of the frame when heated by the fan heater, which can be seen in Figure. 7 showing the magnitude, and highly localized nature of the heating.

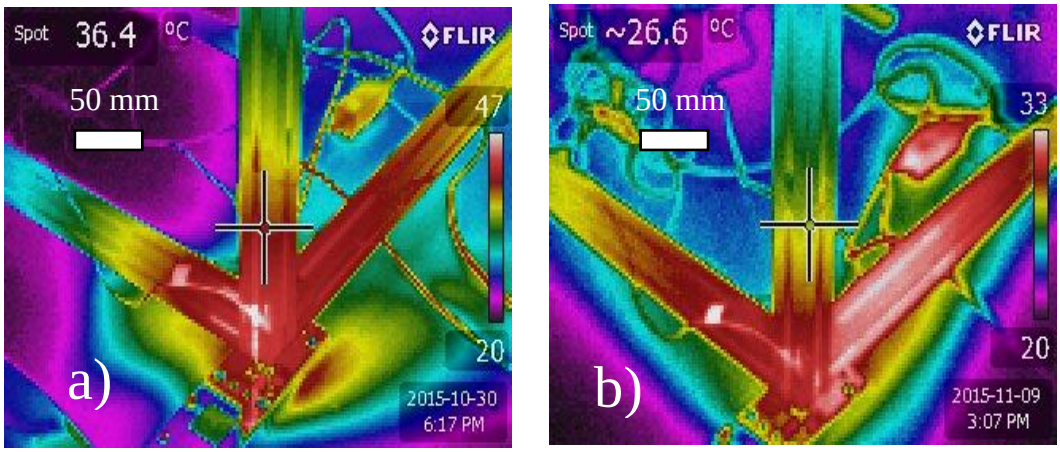

Figure. 7 - Example thermal images of a) H2P1 and b) H1P2

An FLIR handheld infrared (IR) thermal imaging camera with an absolute accuracy claimed by the manufacturer to be ± 2 °C [125] was used. The sensitivity of the camera is stated as <0.045 °C meaning that the camera is particularly useful in a qualitative capacity for sensor positioning.

The colour in the image is automatically scaled to be between 20 and the maximum temperature in the scene. On the higher heater setting, the spot temperature at the crosshair was ~36 °C, significantly higher than the value measured for the lower setting of ~27 °C. The absolute quantities are less useful than the relative quantities observed.

Invasive sensor positions were assigned and can be seen in Figure. 9. Sensor density around the heated corner was increased to capture some of the complexity of the localized temperature distribution. Ambient temperature was recorded using a thermocouple (TC0). RTD sensors are more accurate than thermocouples and therefore were used around the heated corner to increase the density in this area. A further twelve thermocouples covered the frame. The temperature sensors were attached to the surface of the structure using self-adhesive, insulating contact pads as shown in Figure 8 to ensure temperature is measured from the surface and not the air. Thermal paste was applied to the surface in preparation to improve thermal contact between the surface and the sensor. An extra layer of tape was applied to secure the sesnors throughout the experiments.

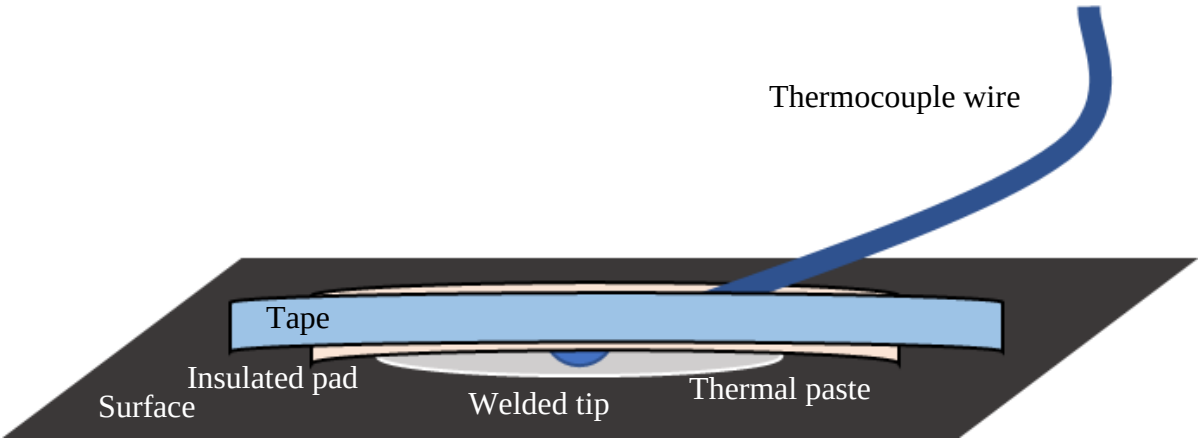

Figure 8. Diagram showing the adhesion of a welded tip thermocouple to a surface.

3.1.4 Computational Thermal Compensation

3.1.4.1 Geometry

Simplified CAD geometry was created for the frame to allow for the simulation to run quickly. Chamfers, fillets and other small details were removed from the geometry. Performing this simplification in the geometry more than halved the simulation run time. Speed of simulation would be important for metrology processes in manufacturing. Figure. 9 shows a rendering of the frame and temperature sensor positions are labelled, where TC0-12 are thermocouples and RTD0-3 are thin film platinum resistance thermometers.

3.1.4.2 Simulation – Finite Element Analysis (FEA)

FEA was used to simulate the thermal expansion under heating. A one-way coupled system was used here in which a thermal analysis is performed to find the full temperature distribution. The results are then passed to the structural analysis, which produces displacement results for each node on the geometry. Relatively coarse meshing is used for both phases of the FEA simulation, again to improve the simulation processing time.

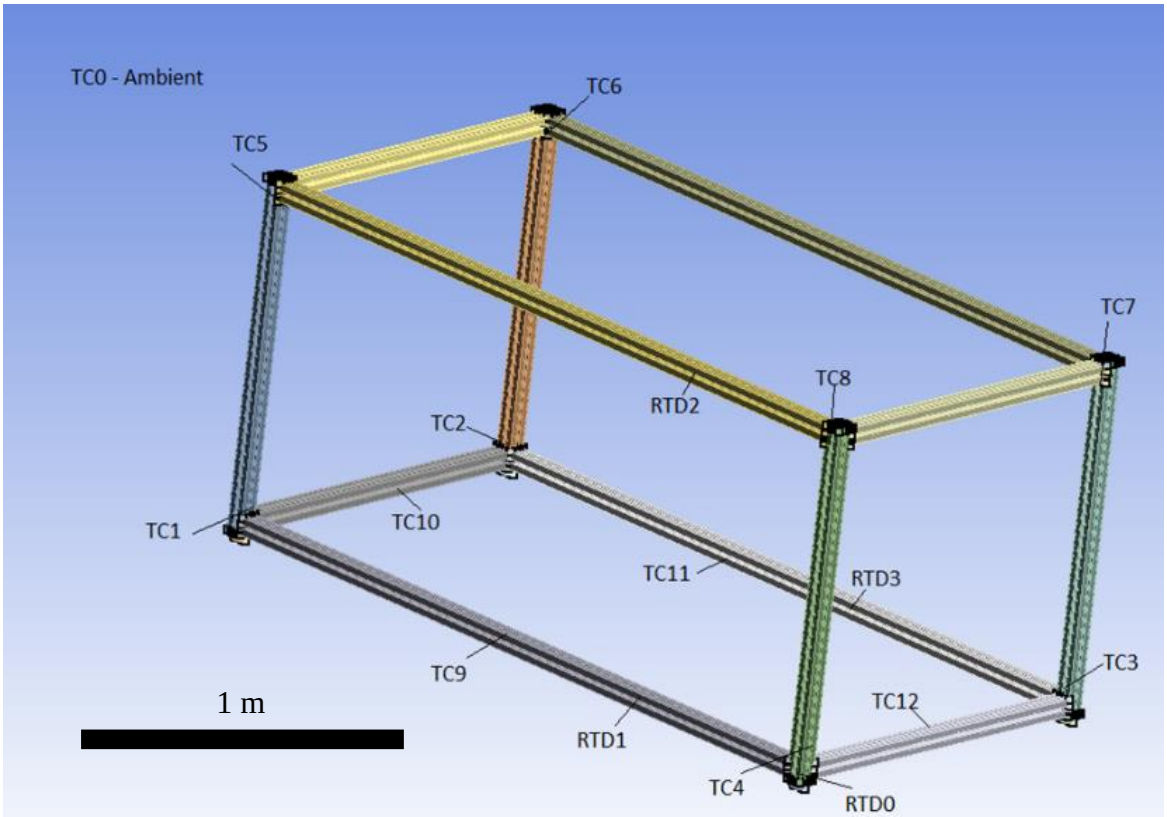

Figure. 9 - Schematic of sensor positions on frame, where TC1 is the fixed corner and RTD0 is the heated corner

3.1.4.3 FEA Thermal Analysis

Over the maximum measurement period the temperature varied by less than 0.1ºC. As the temperature variation over this period was relatively small, a steady state thermal analysis was carried out. Average temperature for the period of the dimensional measurement were applied from each sensor at the corresponding FEA coordinates. The initial temperature parameter was set to be the average ambient measurement. Thermal analysis used only a conduction model to calculate temperature at unspecified nodes.

3.1.4.4 FEA Structural Analysis

Using the thermal analysis solution, a static structural analysis was performed. Movement of the frame was constrained to match the experiment. The frame is supported using a displacement constraint in the vertical direction, with the horizontal movement unconstrained

for three of the points of contact. The ball transfer unit that was constrained in the experiment was similarly constrained in all directions. Displacement solutions along the X, Y and Z axes were calculated for each node in the simulation.

3.1.4.5 Target-node Matching

Closely matching the coordinate systems of the measurement and the simulation allowed the nearest nodes from the FE mesh to be matched to each photogrammetry target. Measured coordinates were used in a Euclidean nearest neighbour search of the mesh node location data. The corresponding displacement results for the nearest node were used for each photogrammetry target.

3.1.5 Comparison of Scaling Methods

In addition to simulation, there is also extensive use of temperature measurement in this methodology. Temperature is usually only measured using instrument weather stations unless there is a specific need for enhanced capability, or if the environment is particularly challenging.

Traditional scaling takes a single scaling factor calculated by multiplying the difference from standard temperature by the CTE and adding 1 as shown in equation 1. Multiplying this scaling factor by the original length, L_0, produces the new length, L_1.

Equation 7

$$Scaling\ Factor = 1 + (dT \times CTE)$$

Equation 8

$$\boldsymbol{L_1 = Scaling\ Factor\ \times L_0}$$

To separate the benefits of temperature measurement and simulation, the thermal expansion should be calculated for the following:

1) Traditional scaling - minimal temperature measurement, uniform scaling
   a) Mean ambient temperature at the instrument
   b) Mean temperature between maximum and minimum
   c) Worst case scenario using maximum temperature

2) Traditional scaling - full temperature measurement, uniform scaling
   a) Mean temperature of all sensors
   b) Median temperature of all sensors

3) Hybrid Metrology - all sensor temperatures and positions used, with nodal displacements from finite element analysis used to predict localised expansion.

3.1.6 Results and Discussion

Measurement of the structure was performed using the photogrammetry system and deformation analysis was carried out using the Aicon 3D studio software. The reference measurement H0Px was compared to its heated counterpart HxPx. Both sets of measurement data were initially aligned using a best fit of the measured targets. All of the data was aligned to the coordinate system using targets around and relative to the fixed corner, as this was the most mechanically and thermally stable part of the structure. The software then performed a deformation analysis, which calculates the displacement of the targets in the X, Y and Z directions. Figure. 10 shows the regions of interest, with the points measured in each region as well as the heater positions.

The RMS error was given by Aicon 3D Studio for each of the points to be roughly 20 µm on average. The analysis showed the mean total deformation (X, Y, and Z combined) observed on the targets across the whole structure was of the order of hundreds of micrometres, which was to be expected as there was significant heating on the structure by design. This meant that the deformation was an order greater than the RMS of the measured points, so there was confidence that the deformation could be separated from the measurement error.

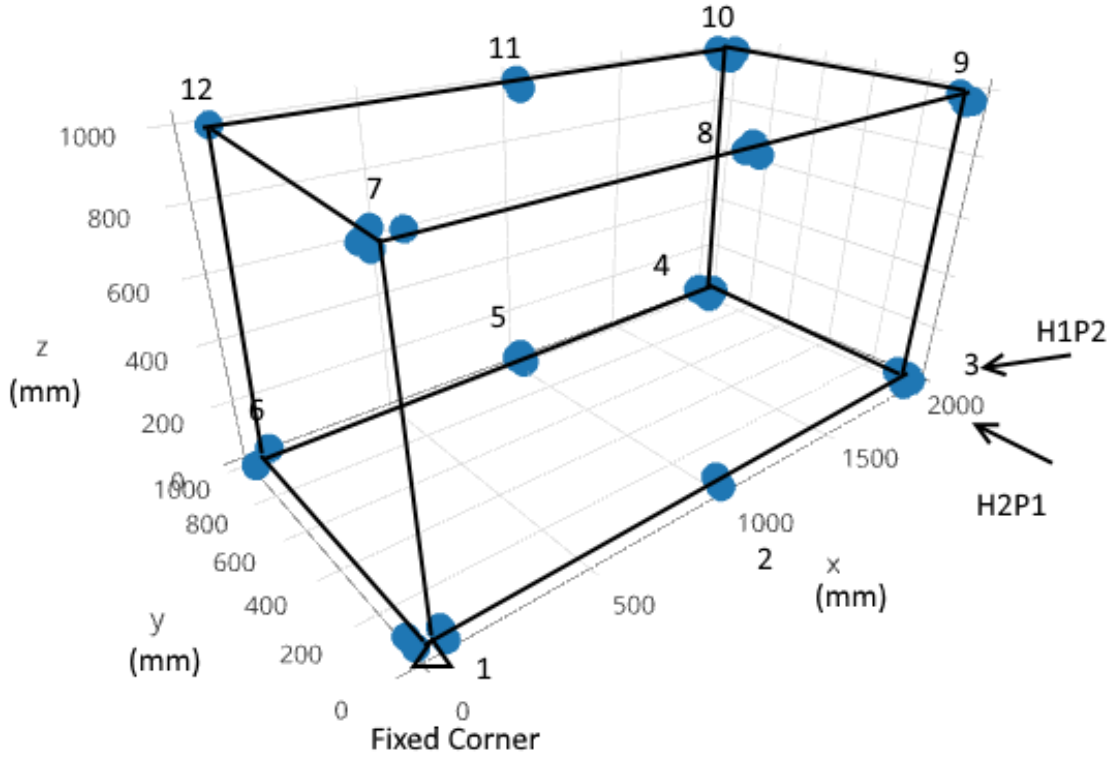

Figure. 10 - Illustration of the points measured at the numbered regions of interest with fixed point and heater positions

3.1.6.1 Scenario 1 – H2P1

Temperatures in this scenario around the frame are shown in Table 3. Maximum temperature was more than 26 °C above standard temperature.

Table 3. Temperatures measured around frame from thermocouples and RTDs.

Sensor ID	Temperature (°C)
TC0	20.56
TC1	20.73
TC2	20.74
TC3	31.78
TC4	40.45
TC5	21.3
TC6	21.34
TC7	22.52
TC8	23.23
TC9	21.31
TC10	21.43
TC11	21.56
TC12	36.74
RTD0	46.78
RTD1	26.23
RTD2	22.47
RTD3	27.37

For the traditional scaling techniques, the temperatures used can be seen in Table 4.

Table 4. Temperatures and scale factors used for each scaling method.

Method ID	Method	Temperature (°C)	ΔT from standard (°C)	Scale Factor
1a	Ambient	20.56	0.56	1.000013
1b	Mean Max-Min	33.67	13.67	1.000320
1c	Max	46.78	26.78	1.000627
2a	Mean All	26.27	6.27	1.000147
2b	Median All	22.47	2.47	1.000058

For clarity, the results have been presented for the four 2m long beams (Figure. 11) and 1m inter-regional distances for the whole frame (Figure. 12). Using methods 1a, 1b and 1c results in low agreement to the measured results.

Figure. 12 shows the ability of method 3 to scale for localised expansion is generally advantageous. Table 5 shows that the Hybrid method has a marginally lower mean difference to the measurement results over the various distances compared to other methods.

Table 5 - Absolute mean differences from the heated measurement for each method for 1 m and 2 m distances in H2P1.

Method ID	Method	1m mean difference (mm)	2m mean difference (mm)
1a	Ambient	0.128	0.198
1b	Mean Max-Min	0.242	0.515
1c	Max	0.515	1.109
2a	Mean All	0.127	0.202
2b	Median All	0.122	0.198
3	Hybrid	0.082	0.179

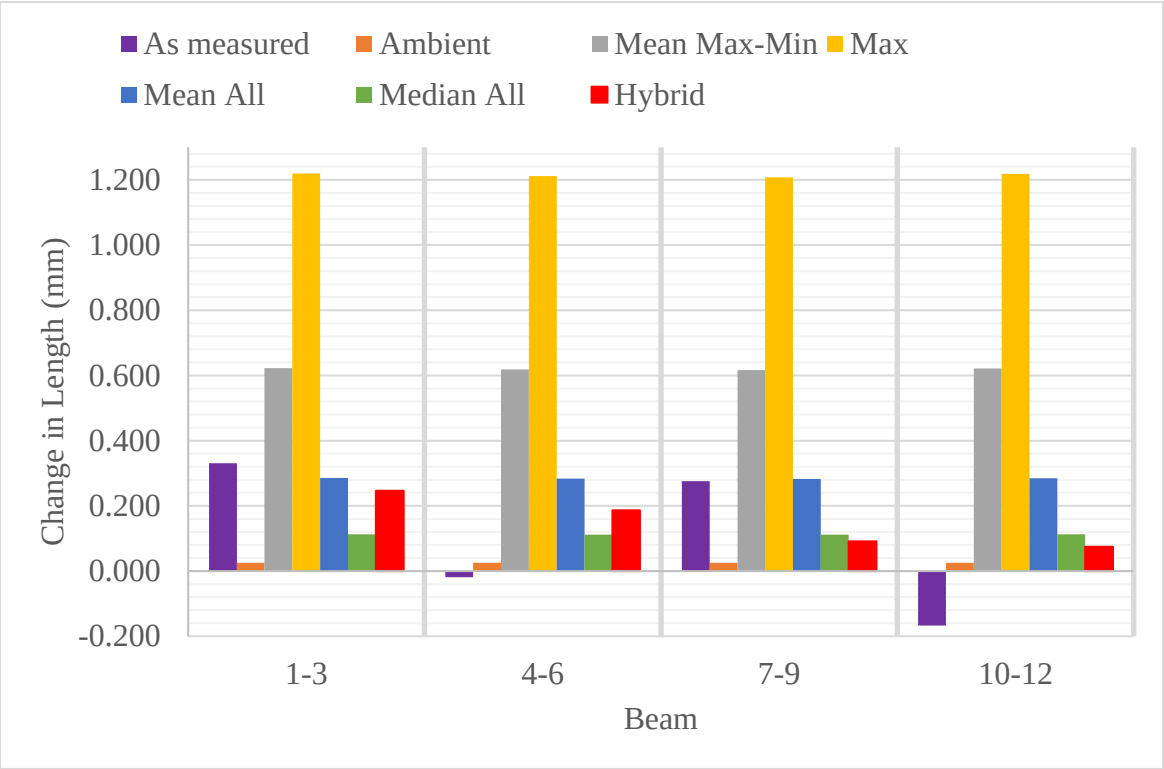

Figure. 11- Column chart showing thermal expansion in 2 m beams for all methods compared to the measured value

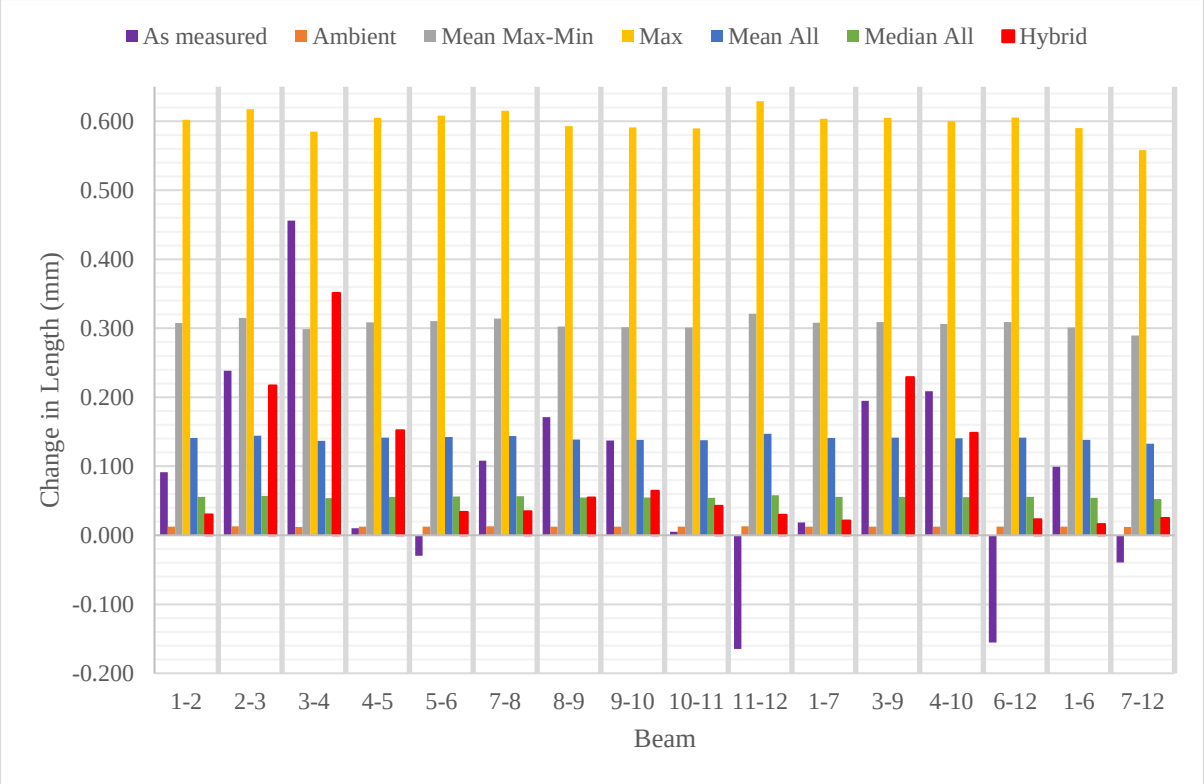

Figure. 12- Column chart showing thermal expansion between numbered regions for all methods compared to the measured value in purple.

3.1.6.2 Scenario 2 – H1P2

Temperatures in this scenario around the frame are shown in Table 6 and are less extreme than the first scenario. Maximum temperature was in excess of 12 °C above standard temperature.

Table 6. Temperatures measured in H1P2 from thermocouples and RTDs.

Sensor ID	Max Temperature (°C)
TC0	22.51
TC1	20.2
TC2	20.84
TC3	23.65
TC4	30
TC5	20.56
TC6	21.57
TC7	20.87
TC8	21.31
TC9	21.55
TC10	20.8
TC11	24.06
TC12	29.14
RTD0	32.34

RTD1	27.3
RTD2	21.53
RTD3	23.68

Scaling factors for this scenario can be seen in Table 7. Once again there are a wide range of possible scaling factors due to the localised heating.

Table 7. Temperatures and scale factors used for each of the traditional scaling methods.

Method ID	Method	Temperature (°C)	ΔT from standard (°C)	Scaling Factor
1a	Ambient	22.51	2.51	1.000059
1b	Mean Max-Min	26.27	6.27	1.000147
1c	Max	32.34	12.34	1.000289
2a	Mean All	23.64	3.64	1.000085
2b	Median All	21.57	1.57	1.000037

In Figure. 13 and Figure. 14, we can again see that the Hybrid metrology method appears to agree a little more closely with the heated measurements.

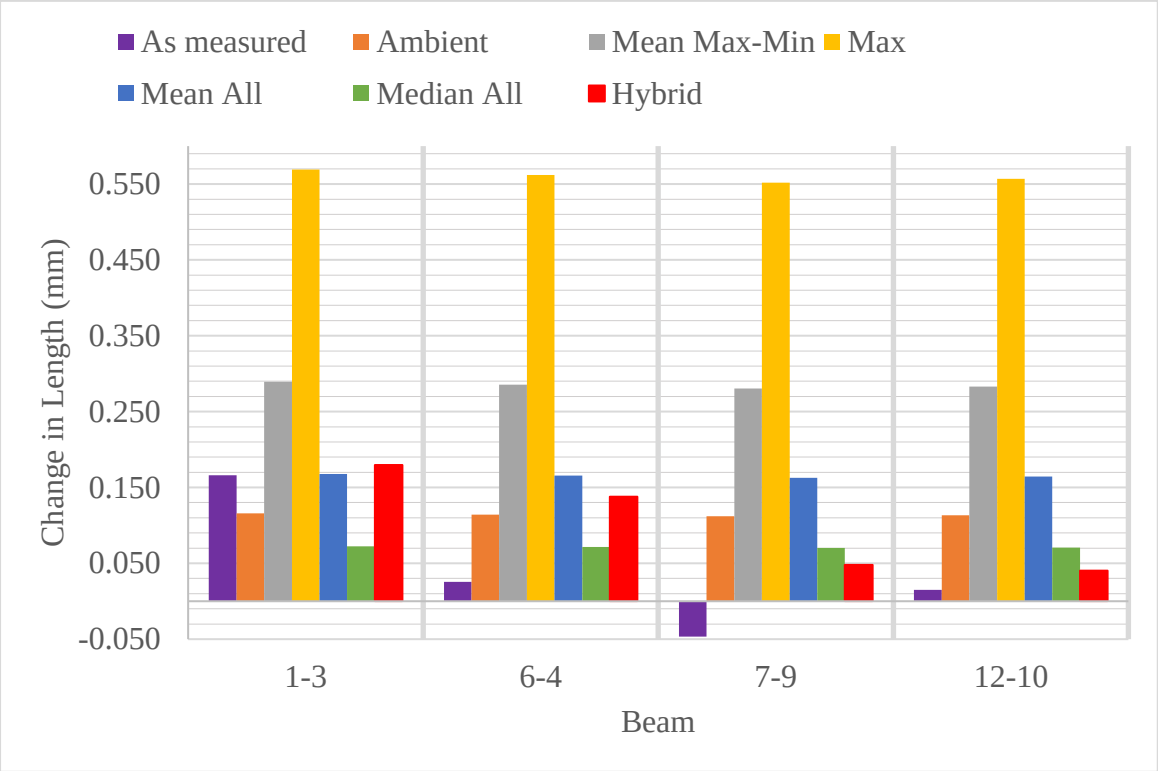

Figure. 13 - Column chart showing thermal expansion of all methods compared to measured value

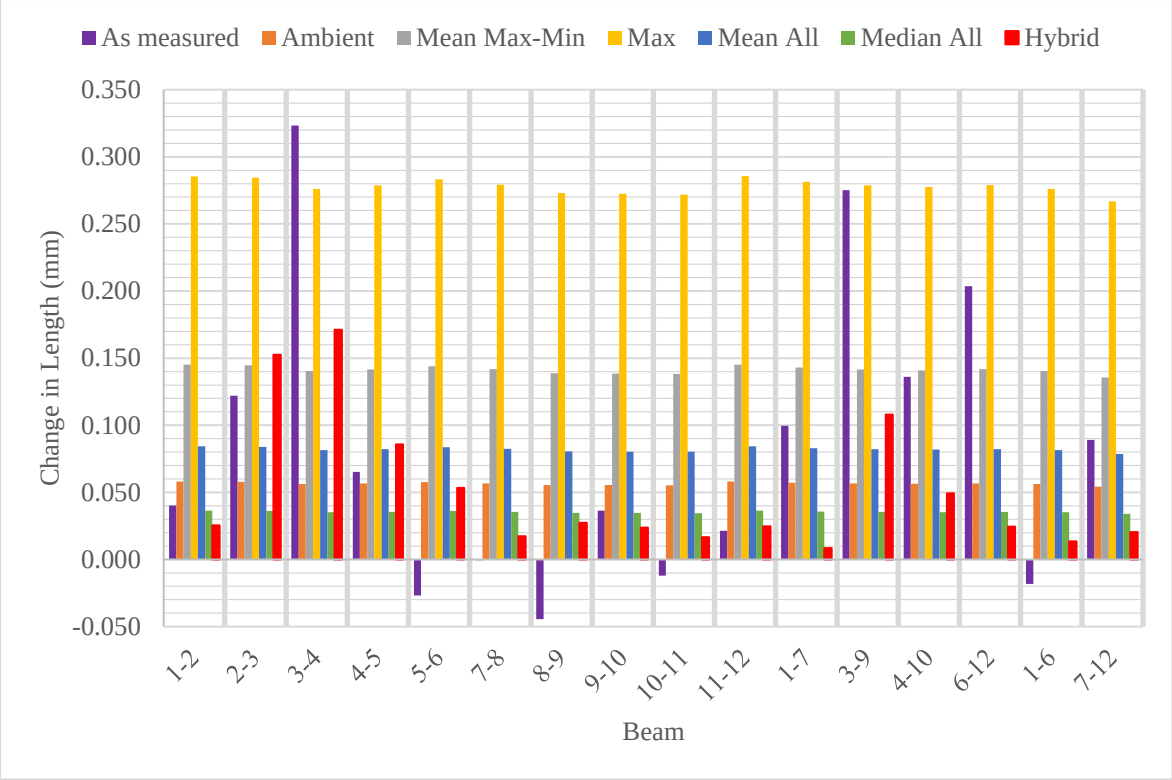

Figure. 14 - Column chart showing thermal expansion in 1m beams for all methods compared to the measured value

The mean magnitude of difference between the measured results for each of the scaling methods is given in Table 8. Ideal scaling would represent a mean difference tending towards zero, and in this case, the Hybrid method generally outperforms than the traditional scaling methods with a mean value of 0.066 mm.

Table 8. Mean absolute difference in thermal expansion of all methods from the measured value.

Method ID	Method	1 m mean difference (mm)	2 m mean difference (mm)
1a	Ambient	0.082	0.099
1b	Mean (Max-Min)	0.107	0.244
1c	Max	0.202	0.520
2a	Mean (All)	0.085	0.125
2b	Median (All)	0.083	0.078
3	Hybrid	0.066	0.061

The Hybrid method can be said to have produced marginally better results than the uniform scaling methods. As the FEA carried out was highly simplified, these results although modest are promising. Various factors can be improved from this initial study within the simulation to make a far more significant impact to the results. A contraction appeared to be observed between regions, but in reality, this was regions getting closer together due to bending of the structure. The buckling of the beams can be better characterised to provide a more accurate view of the displacements.

Finer, more tailored meshing can also be used on more complex geometry. A transient analysis can be used rather than steady state. The contacts between the beams can also be refined as these are modelled as being more stiff connections than is necessary. Similarly, the stiffness of the beams themselves can be characterised experimentally. Once the finite element model is fully calibrated in this way, the results will become a function of the time spent in setting up the FEA. This is acceptable due to the modular nature of the Hybrid metrology approach, where specialists in CAD, FEA and metrology can contribute separately in the initial setup. Ultimately, the major significant finding was the importance of temperature measurement as a far more pronounced difference can be seen from using a full complement of temperature measurement as opposed to one or two sensors.

3.1.6.3 Major Findings

This study has outlined and shown the application of a straightforward methodology for two things, the first being temperature measurement for dimensional metrology, which is currently often only carried out on the ambient temperature at the instrument. Finite element simulation of displacement allows for compensation of coordinates that would not be possible using current linear scaling methods, due to the presence of highly localized heating.

Two challenging measurement scenarios have experimentally showed that even a highly simplified FEA was able to modestly outperform the traditional scaling methods with both minimal and full temperature measurement.

Thermal compensation is only as effective as the measurement of temperature. Sparsely measured temperature is limited in value and important thermal effects can easily be missed. Temperature measurement is a major contributor to improvement in thermal compensation and can be further improved with simulation.

3.2 Chapter 3 – Summary

Chapter 3 provided:

- Results of initial laboratory-based experiments in which thermal expansion was observed in a simplified structure.
- Results that suggest using FEA based simulation using multiple sensors can provide more realistic thermal expansion than assuming a uniform temperature distribution as is currently often done in practice.

Contributions:

- Experimental work to show method of FEA driven thermal compensation.
- Discussion of challenges in thermal compensation efforts.

Measured dimensions are temperature-dependent, so there is a clear need to understand and agree upon how best to measure temperature - it could be measured in a variety of ways.

---

4 Temperature Measurement Planning

Experiments had revealed more information about thermal compensation could work in the laboratory, but how does this look in industry? How would a metrologist go from having a specific measurement challenge through to a temperature measurement plan? And then, how would people use this in operations?

4.1 Industrial Assembly Jig Temperature Measurement

This thermal study focuses upon an industrial assembly, integration and test (AIT) environment in which the temperature was controlled to within 5 °C in order to improve the measurement uncertainty, and subsequently improve the quality of assembled products.

Two ambient temperature sensors were in operation at either end of the AIT environment, and a thermostat controlled the heating and cooling of the environment.

The aims were to:

- Verify the localised performance of the temperature control;
- Characterise the periodic variation that is existent within the AIT environment;
- Measure thermal gradients between the bottom and top of large jig tooling structures used in assembly.

4.1.1 The Assembly, Integration and Test (AIT) Environment

The jig tooling structures used to assemble the products are numbered from 1-6. Jig 2 was the main jig structure that was measured dimensionally, using photogrammetry and will have much more comprehensive temperature measurement than the other jigs.

4.1.2 Temperature Measurement

4.1.2.1 Thermocouple and RTD Acquisition - Jig 2

Most of the dimensional and thermal measurement was carried out on Jig 2. This jig was not being used for assembly at the time of the study, which meant many more sensors could be placed around the structure without impeding assembly operations. Details of the jig could not be shared, but a highly simplified diagram is provided in Figure 15 to give some idea of their shape.

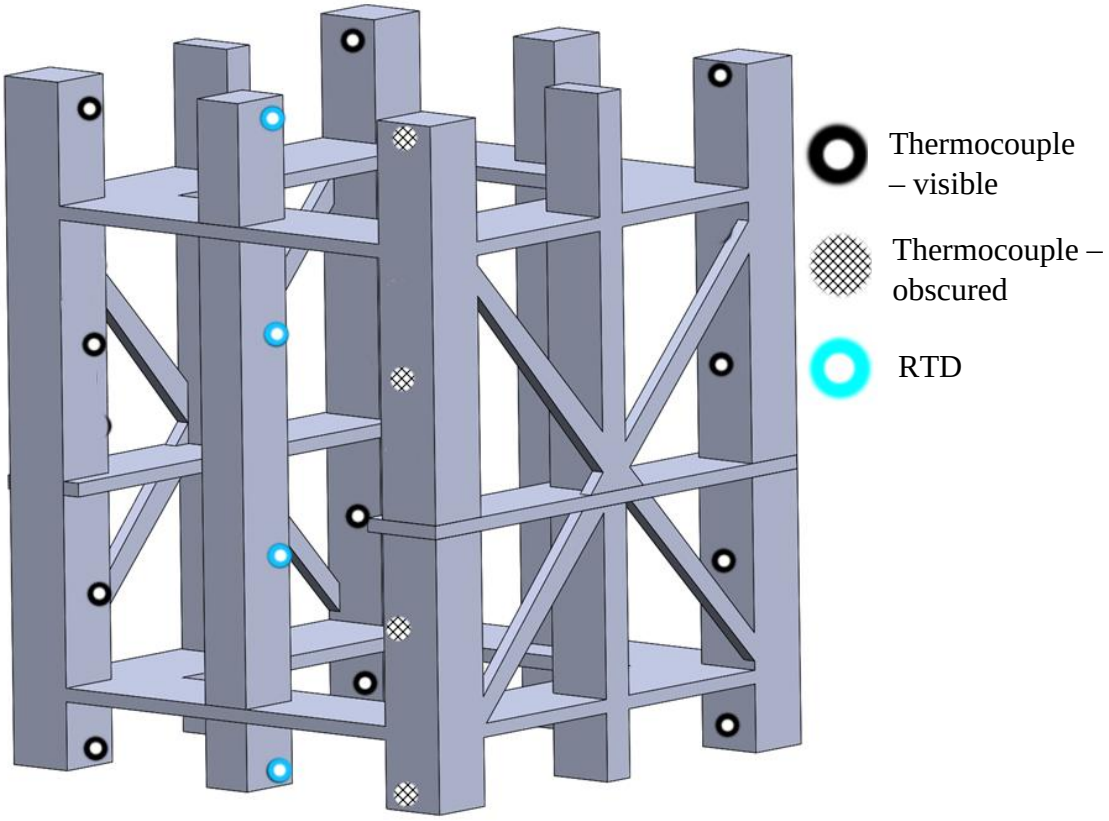

Figure 15. Simplified CAD representation of the assembly jigs with approximate sensor positions.

As the jig structure was very large at over 4 °m tall meaning many sensors were ideally required to characterise the temperature profile of the structure. 20 sensors were available in total, however due to the practical difficulties of setting up wired sensors around a large structure, one of the thermocouple sensors was damaged and therefore could not be used. In total, 19 channels of temperature data were acquired via an 8-slot National Instrument Compact DAQ chassis, which was connected to a laptop running Windows 7 and Signal Express via USB.

Of the 19 sensors, 4 channels were 3 metre thin film platinum resistance temperature detectors (RTDs), which have a measurement uncertainty of better than ±0.1 °C. The RTDs were connected to the DAQ using a National Instruments 100Ω RTD, 24-bit analogue input module (NI-9217).

The remaining 15 sensors were 5 °m T-type thermocouples (TCs) with a measurement uncertainty of around ±0.5 °C. The thermocouples were connected to a National Instruments high-accuracy, 16 channel isothermal thermocouple input module (NI-9214). The 24-bit analogue to digital converter allows for 0.02 °C measurement sensitivity. The isothermal terminal block allows for electronic cold-junction compensation for each of the thermocouples.

As can be seen in Figure 15, the approach to temperature sensor positioning was to spread the sensors evenly, and have the more accurate Pt100 sensors distributed vertically to give a good representation of the temperature gradient at the front.

4.1.2.2 Wireless Thermocouple Data Loggers

Jigs 1, 3, 4, 5 and 6 were all monitored using wireless data loggers placed at the top and at bottom of each jig. This measurement was designed to give a general idea of the temperature change over time in the AIT environment and to discover the thermal gradient from the bottom to the top of each jig.

The wireless data loggers were each equipped with two K-Type thermocouple sensors, positioned 1 m apart at the same height. The K-type thermocouples used with the wireless data loggers are generally of a lower cost than the T-type thermocouples used with the DAQ. These K-type thermocouples have a measurement uncertainty of around ±1 °C at the room temperature range. The measurement resolution of the sensors and the data logger is ±0.1 °C.

For practicality, surface temperature measurements were made of the jig structures. A more accurate reading of the jig structure could be obtained through embedding the sensors, although this was not possible in this case. As a result, the air flow within the AIT environment is likely to have influenced the measurements taken using this method. Using adhesive insulating pads to cover the sensors was one way in which this effect was mitigated and to improve thermal contact between the structure and the sensor. Extra tape was used to secure the sensors over the top of the insulating pads for added security as the AIT area was still fully operational.

4.1.3 Main Assembly Jig 2 Temperature Profile

Measurements were taken on Jig 2 throughout the course of the week, which can be seen in Figure 16 and Figure 17. These graphs show the temperature measurements over time from the four RTD sensors which served as a more accurate reference.

Over the course of the working week, particularly in Figure 16 it would appear that the temperature profile follows a fairly regular pattern. It would be advantageous to collect more data over a longer time period to better characterise the environment. This information can then be used predict the most stable times when dimensional measurements could be taken.

Figure 16 shows there is a clear and predictable thermal gradient present on the jig of circa 1 °C which appears to reduce slightly in the cooler periods. Whilst a thermal gradient of this magnitude is relatively good, this will nonetheless have a slight impact on the uncertainty of dimensional measurements taken of the whole structure.

Some temperature spikes can be seen in the data, which have arisen as a result of a person making contact or working closely to the sensor at the time. This highlights the need for temperature sensors to be well insulated and protected from extraneous disturbances. In, Figure 17, the yellow trace of TC1 shows excessive noise during a period of several hours. The spikes bounding the noise suggests that the thermocouple had been knocked loose at some point where the first temperature spike is and later replaced where the second spike is.

Again, this shows the need for the development for more practical methods of temperature measurement in working jigs.

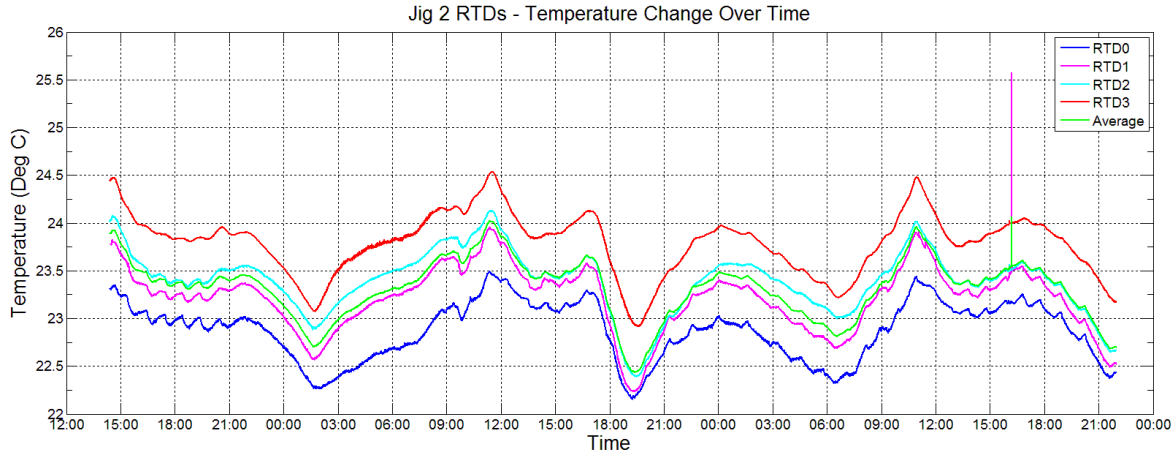

Figure 16 - Graph showing the temperature on Jig 2 over time showing measurements from 4 RTD sensors and the average temperature

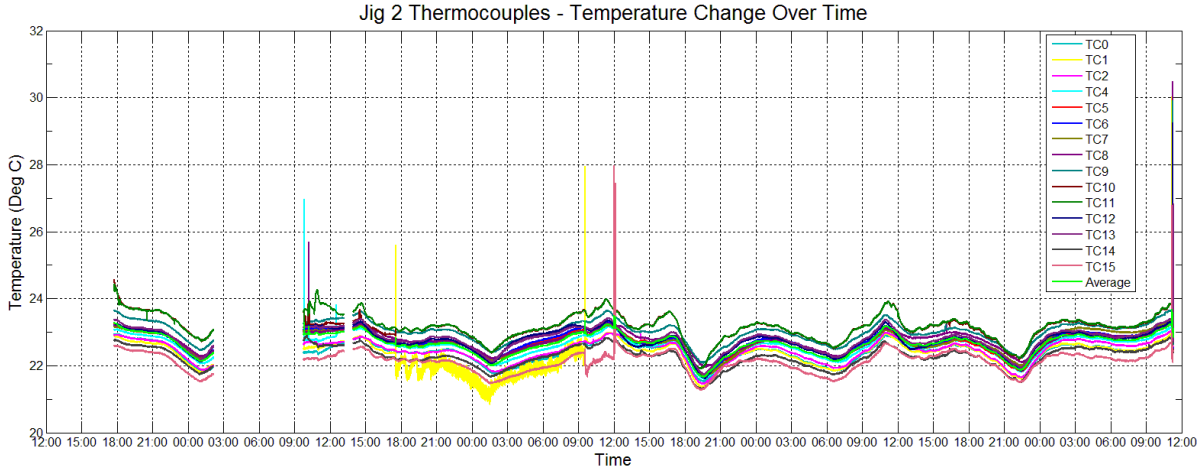

Figure 17 - Graph showing the temperature on Jig 2 over time showing measurements from 15 thermocouple (T type) sensors and the mean temperature

4.1.4 AIT Temperature Profile

Each of the jigs around the AIT environment where also measured at the top and bottom. Figure 79 to Figure 93 show the temperature change over time, and summarised in Figure 18. The agreement between TC1 and TC2 in each case is generally quite close, usually 0.1 to 0.2 °C.

At the top of the jig, the temperature generally seems to be up to 1 °C higher and can be seen to fluctuate more than the bottom of the jig. This is likely to be due to the AIT environment as there are several ventilation units mounted on the ceiling that help to regulate the air flow and temperature.

Looking at all of the jigs, the lowest mean temperatures recorded were on jig 6 (Bottom), with the highest temperatures recorded being Jig 1 (Top). The disparity in temperatures between these two extremes appears to reach a maximum of circa 1.5 °C.

As with Jig 2, the other jigs appear to follow a predictable pattern, which again will be useful to study with dimensional metrology planning in mind.

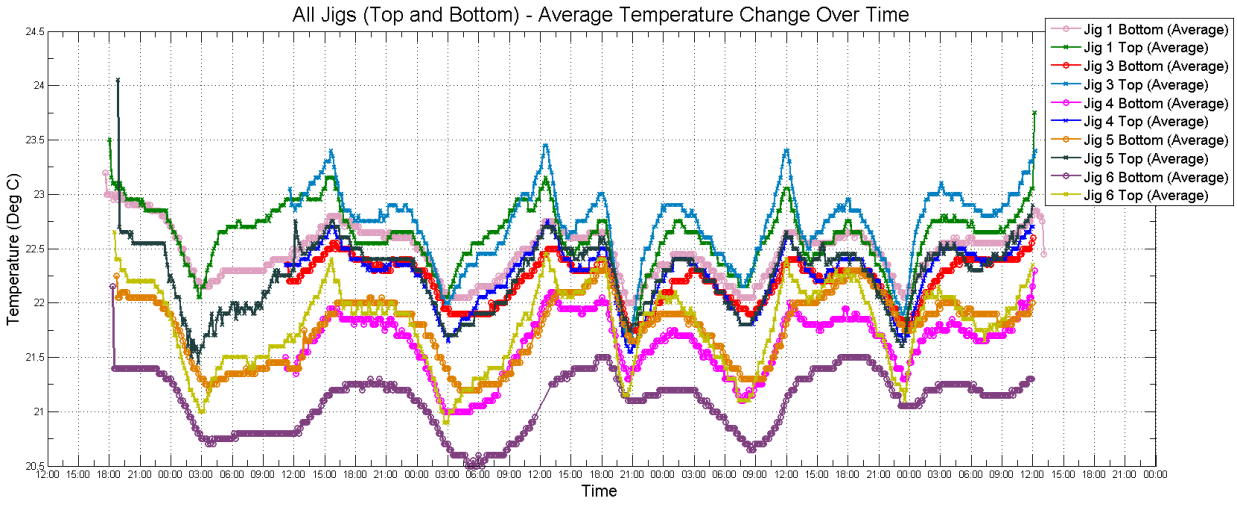

Figure 18 - Graph showing the mean temperature on all jigs over time at the bottom and top of the jigs

4.2 Temperature Measurement Planning Strategy

This section proposes a general temperature measurement strategy, from a high-level perspective. The various steps of this strategy are illustrated in Figure 19, and the succeeding sections add further detail on how each of the steps can be realised.

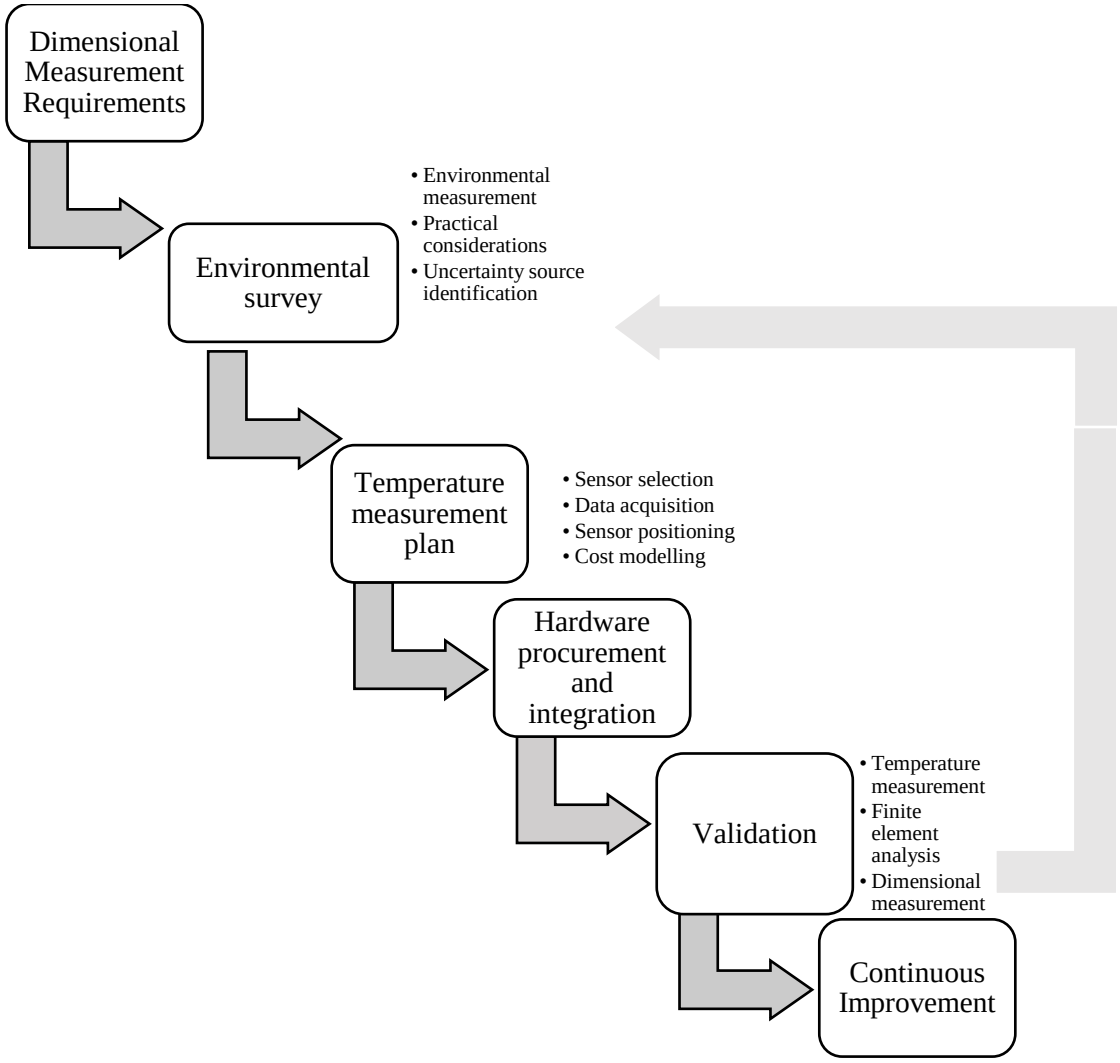

Figure 19. Diagram defining an overall strategy for temperature measurement planning.

Dimensional measurement requirements should be the starting point for producing any such temperature measurement plan. This could be conceivably be extended to any form of requirements arising from the application: in this case, dimensional measurement, but could just as easily be process requirements. The environment in which the temperature would need to be measured should first undergo some form of characterisation. Characterisation at this stage would be concerned with general trends in temperature, practical constraints imposed by the physical environment, and any sources of uncertainty likely to confound measurement in this space. Based on this survey, a first attempt at a temperature measurement plan can be made.

The temperature measurement plan must capture sensor selection, how they will be deployed, and how they will be used to acquire data. Costs of the temperature measurement instrumentation and the maintenance thereof should be estimated as well as possible at this stage. These costs can be optimised according to the requirements, and budgetary constraints.

Following the plan, the necessary equipment must then be procured and integrated into its working environment. With the necessary hardware in place, there should be a practical setup phase. In this phase the temperature sensor network and subsequent interpolations and simulations are validated for use. Dimensional measurements can be taken with a higher-than-normal frequency at this stage, to which thermal expansion simulation can be compared. Agreement between dimensional measurement and simulation results are the performance metric for this validation. Adjustments can be made to the temperature measurement plan to improve its capability for accurately measuring temperature distributions and ultimate computational prediction of thermal expansion.

Subject to observation of adequate performance, the temperature measurement plan can be approved and enacted. Continuous improvement activities can support the now live temperature measurement plan.

4.3 Environmental Survey

The environmental survey is intended to be carried out as part of the set-up of the temperature sensor network and to serve as the foundation of the temperature measurement plan. This is intended to be a characterisation of the environment. At this stage the number of sensors used will be far higher than the number of sensors that are normally used. The methodology for the environmental survey is not discussed in detail in this work, as the main interest is in what happens after this stage.

Positioning of sensors for the environmental survey will be in the form of a naïve sensor network in which no a priori knowledge of the environment in used. It is envisaged that invasive sensors be numerous and positioned with equal spacing. A less dense version of this is later used to provide a control against which the performance of the optimised temperature sensor network can be compared.

Non-invasive and semi-invasive technologies can also be used at this stage. Thermography using IR radiation and coatings can provide qualitative descriptions of the temperature distribution. Depending upon uncertainty constraints, quantitative thermography can be carried out. Where there is doubt about the uncertainty of a technology acting in this capacity, this can be corrected using invasive sensors being used within the image to provide a correction.

4.4 Methodology

This section describes how the computational testing of the temperature measurement sensor networks was carried out using a Python script. ANSYS software has been used for FEA in order to produce results for thermal expansion to form a basis for comparison. Description of the functionality of many of these scripts has been included in this section. The focus for this work is to test a range of sensor networks quickly for a range of scenarios. Automation of the simulation was important for repeatable and efficient running of experiments. Python was identified as one of the programming languages that facilitates this type of automation, as well as being a good language for prototyping. Some experimentation with MATLAB, LabVIEW, and R was carried out which was ultimately translated and absorbed into the Python script that came to be known as *Therminator*.

The overall methodology for how the temperature measurement plan is generated can be seen in Figure 20. A virtual temperature distribution is created and applied to a CAD model. FEA is then used for this case to determine the reference thermal expansion, which serves as the 'goal' for future reproductions. An initial temperature sensor network is defined by the number and type of sensors, their uncertainty, and their respective coordinate positions. This sensor network is used to take virtual measurements of the spatiothermal artefact, with or without uncertainty. Uncertainty in this case is artificially generated using normally distributed pseudo-random values defined by a given standard deviation and mean.

With a set of virtual measurements, a reconstruction of the temperature distribution can be made. Reconstruction uses virtual sensor data alongside some form of interpolation, and FEA produces a final calculation of thermal expansion as measured. Comparing the thermal expansion results from both the reference and reproduced temperature distributions can provide a measure of how well the sensor network positions have performed. Optimisation of these positions can be iteratively carried out to produce a temperature distribution that is closer to the reference. Users can then use learning from testing different sensor network configurations to specify a temperature measurement plan. The temperature measurement plan is not created using this script as this would ultimately be the generation of a technical document authored according to the needs of industry.

This methodology is the core contribution of this thesis as there isn't a tool that has yet been created to fully address this problem from beginning to end. In particular, the virtual measurement, reproduction, and optimisation steps are the most challenging, and provide the most opportunity for impact. Beyond the creation of the tool, there is a lot of learning that can be generated around specific temperature measurement strategies. Use of the tool can help those in manufacturing better understand uncertainty of dimensional measurement, temperature measurement, and how they interact. Having an understanding of how conditions change over time can provide further flexibility to adapt to new environments, whilst still maintaining a consistent, reproducible, and traceable approach to measurement.

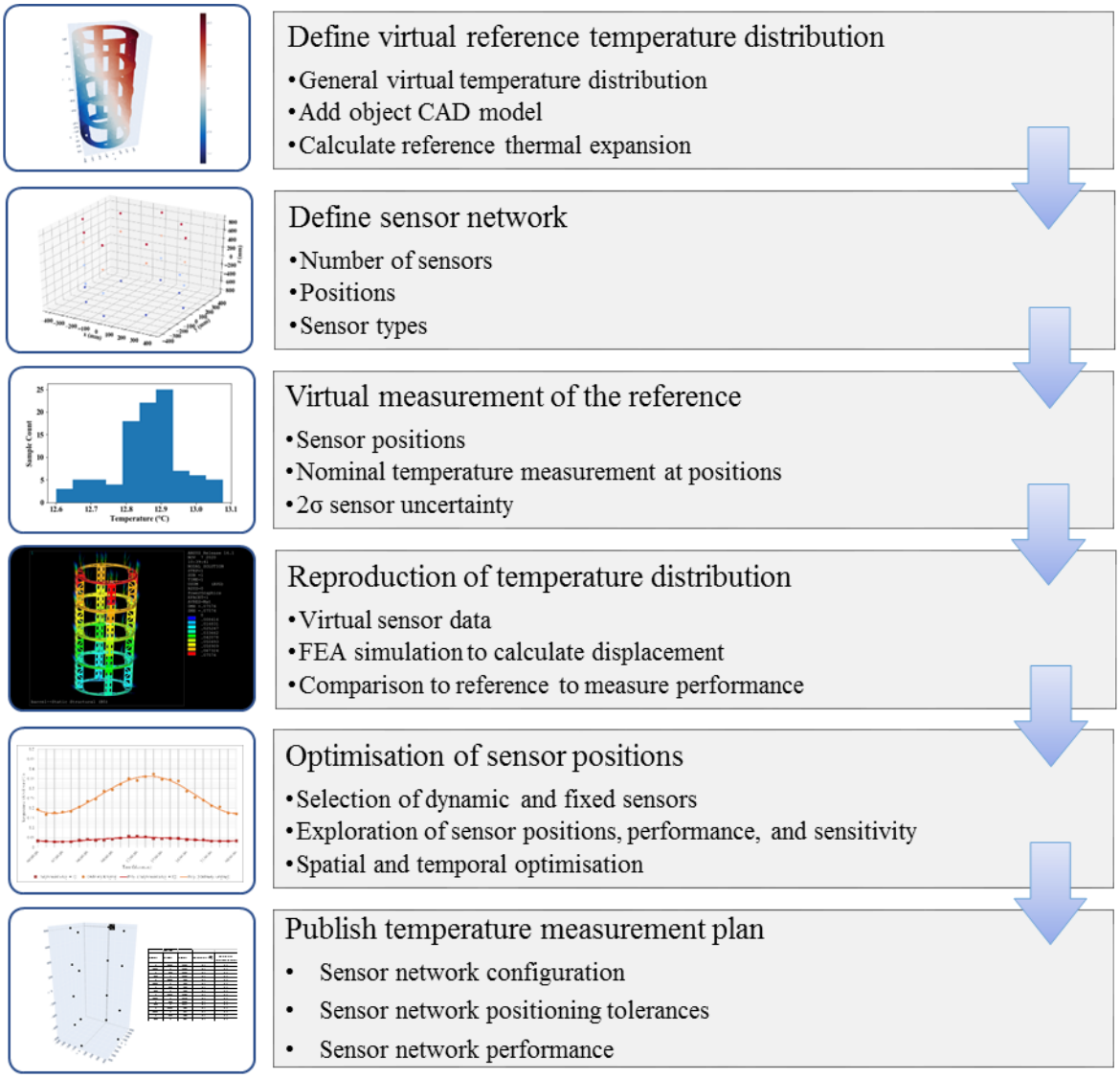

Figure 20. Diagram showing the methodology for creating a temperature measurement plan.

4.4.1 Test Script Functionality

Table 9 provides a description of each of the classes used in script forming the temperature measurement planning tool in order to provide an overview of the functionality. Each of the classes contains methods (functions defined within classes) that carry out each of the required operations.

Table 9. Table describing the classes used in the Python script used for testing temperature sensor networks.

Class Name	Description
Experiment	Initialises experiment run by setting up folders and reading the parameter file.
SpatialGrid	Defines the grid of points used to generate the temperature distribution for a given volume to bound the CAD model of the part or assembly.
TempDistFunction	Generates a temperature distribution from the parameter file, which can be used as a nominal 'true value' temperature distribution, against which reconstructions from sparse measurements can be compared.
Figures	Plots figures in both 2D and 3D, which can be used to visualise temperature distributions (generated, and reconstructed) as well as errors within the volume at each point on the grid.
ThermalBypass	Makes use of analytical means of interpolation to circumvent the need to perform thermal FEA.
FEThermal	Edits a template input file for thermal FEA and runs the simulation automatically in batch mode.
FEStructural	Edits a template input file for structural FEA and runs the simulation automatically in batch mode
SensorNetwork	Defines fixed 'naïve' temperature sensor networks which can be used as a basis for comparison to bespoke and optimised temperature sensor networks.
SensorNetworkInfo	Reads temperature sensor network information from file for use in virtual measurements.
VirtualMeasurement	Performs a virtual measurement based upon coordinates and uncertainties of temperature sensors within the network.
Reconstruction	Reconstructs the full temperature distribution from sparse points given by the virtual measurement using the defined sensor network. Methods include polynomial regression and ordinary kriging.
Results	Calculates error in reconstruction of temperature distribution and error in simulated displacement from FEA. Produces a final table of results for comparison of sensor networks.

4.4.2 Virtual Spatiothermal Environment

Testing temperature measurement plans can be achieved through the creation of a virtual spatiothermal environment. A virtual spatiothermal environment in this case is defined as a volume with a defined temperature distribution, in which a CAD model can be positioned. The distribution as it is applied to the CAD model can then define a nominal reference temperature distribution on the object. This reference temperature distribution then serves as a virtual ‘true value’ representation. Creation of a virtual reference enables two things:

1. Reference values for thermal expansion can be calculated, to which the reconstructions from virtual measurements can be compared;
2. Potential sensor positions can be used to take virtual temperature measurements. These virtual temperature measurements can be used to try to reproduce the reference temperature distribution.

4.4.3 Generation of Virtual Temperature Distributions

A script for generating virtual temperature distributions was written using the Python programming language. The process for using the script is illustrated in the flowchart presented in Figure 21.

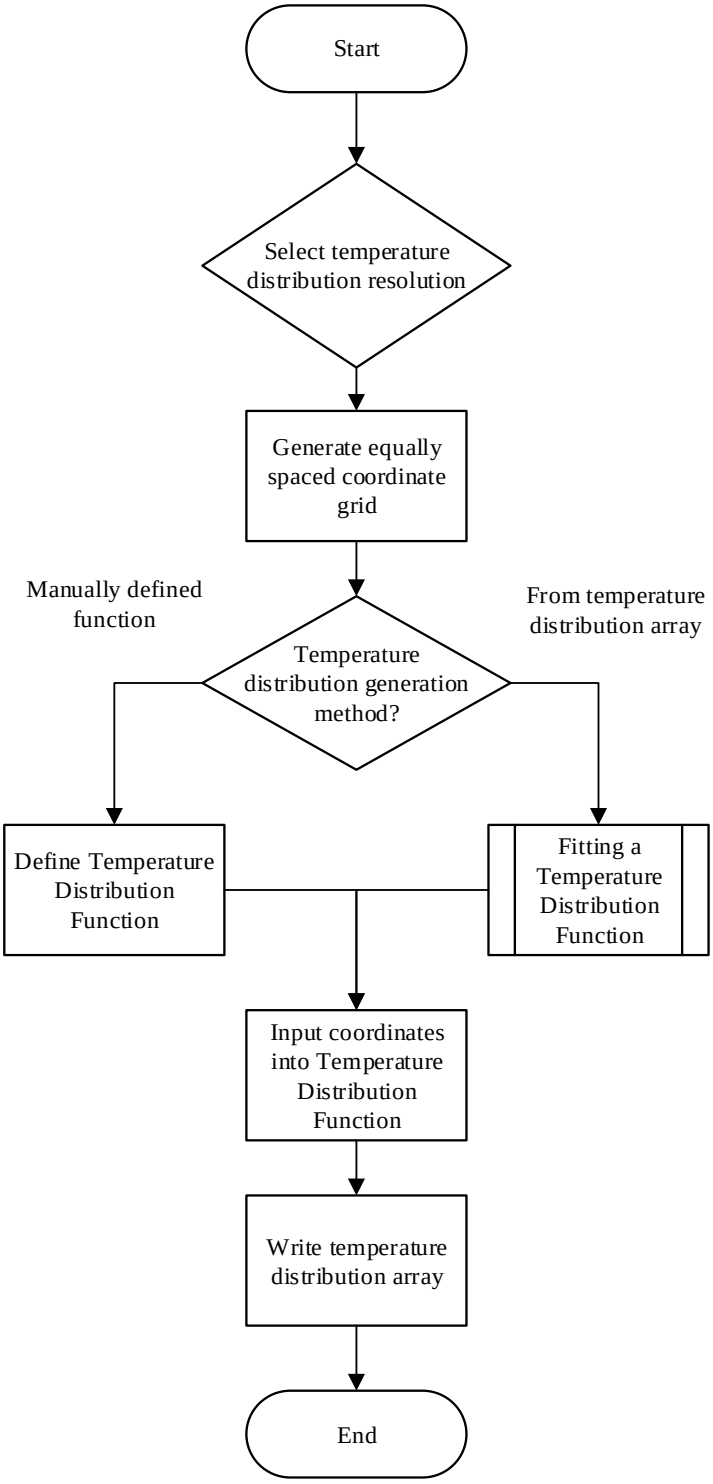

Figure 21. Flowchart of the process for generating a temperature distribution.

The beginning of this script defines the size of the volume to be described by the virtual temperature distribution in terms of minimum and maximum values in the x, y, and z axes. A grid of equidistant points in space can be generated with the number of points required. Two examples of grids have been created using coarse (5x5x5 points), and fine grids (50x50x50 points) in Figure 22 and Figure 23 respectively. It is possible to control the point spacing in x, y, and z individually, so a finer grid in just the vertical z direction could

be specified, for example.

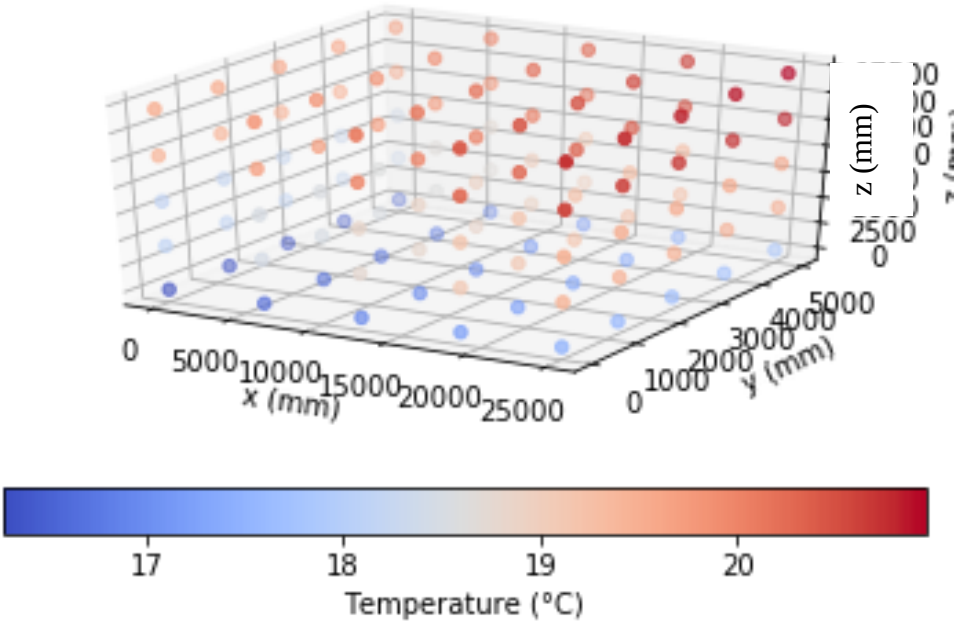

Figure 23. Temperature distribution generated using a 5x5x5 grid.

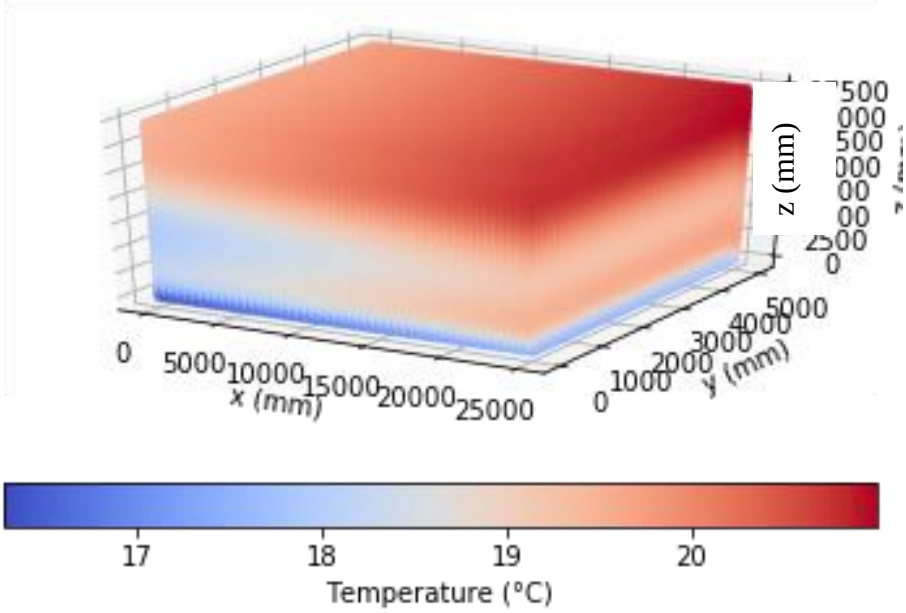

Figure 22. Temperature distribution generated using a 50x50x50 grid.

A temperature distribution function is required to find the temperature at each of the 3D points. The user can manually define a temperature distribution function, as will be done for

the testing of sensor positions. Similarly, this can be achieved by applying a function derived from a curve fitting exercise, for which another script has been written. The temperature distribution function can simply use the z direction as a variable, for example, or for more complex distributions all three axes can be included. The resulting 4D array is reshaped for use as a 2D array, which can be used for further actions including defining boundary conditions. A colour mapped plot like that shown in Figure 23 can also be generated for visualisation purposes, in which colours are used to describe relative temperature at each point. The distribution was generated using the deliberately complicated polynomial temperature function:

Equation 9

$$T = (7.489 \times 10^{-20})\, z^5 - (3.816 \times 10^{-15})\, z^4 + (6.973 \times 10^{-11})\, z^3 - (5.426 \times 10^{-7}) z^2 + (0.001754) z + 16.27 + (5 \times 10^{-5}) x + (2.5 \times 10^{-5}) y + (4 \times 10^{-9}) y^2$$

4.4.4 Reconstruction of Temperature Distributions

One-dimensional temperature distribution functions can be created through the curve fitting of temperature measurement data. Curve fitting can be carried out in Python from a .csv file of temperature and position data. A flowchart of the script used can be seen in Figure 24.

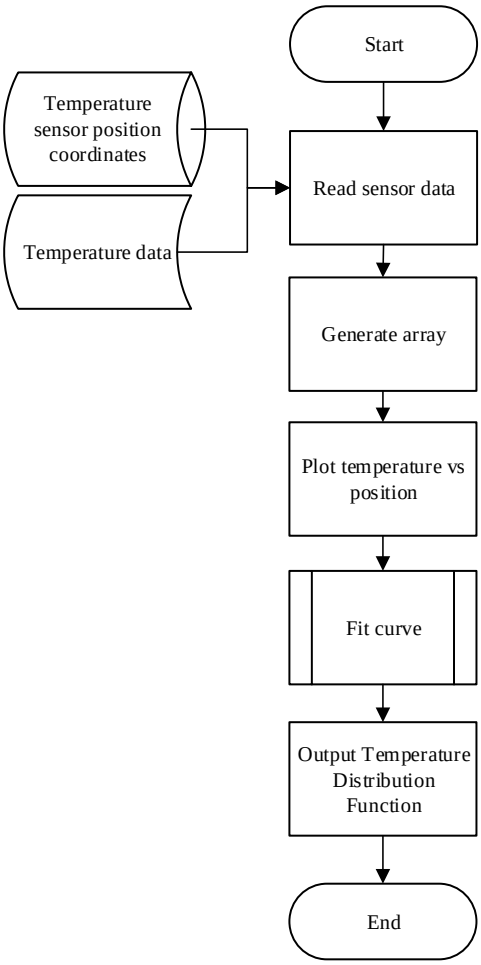

Figure 24. Flowchart of the process for creating a temperature distribution function from sensor data.

Temperature gradients in assembly environments are often most pronounced with change in height, so a non-linear temperature gradient is used here as an example. Table 10 contains temperatures at different heights in mm to give an example of a measured temperature distribution on a large structure.

Table 10. Table showing examples of temperature at different heights measured on a large, 17 m tall structure.

Height (mm)	Temperature (°C)
0	16.1
500	17.3
1000	17.6
1500	17.8
2000	18
5000	18.1
9000	18.3
13000	19.4

17000	19.5

Using the script, the data was plotted using a scatter plot, and a curve fitted to the points. Figure 25, Figure 26 and Figure 27 show how the data was described as a function using 1st, 3rd and 5th degree polynomials respectively. Adjusting the curve fitting method to reduce the value of the residuals. As shown in the fitting, there are larger residuals for the 1st and 3rd degree polynomials. Using a quintic provides the lowest residuals, but the decrease in temperature is an example of overfitting. Adding a 6th term results in a maximum temperature within these limits at around 15 m of almost 23 °C, before returning down to 19.5 °C at 17 m. A 7th term produces an even more erroneous temperature at 15 m where it plummets below -30 °C. Higher order polynomials can undoubtedly cause problems and other methods for modelling temperature distributions were considered due to this limitation.

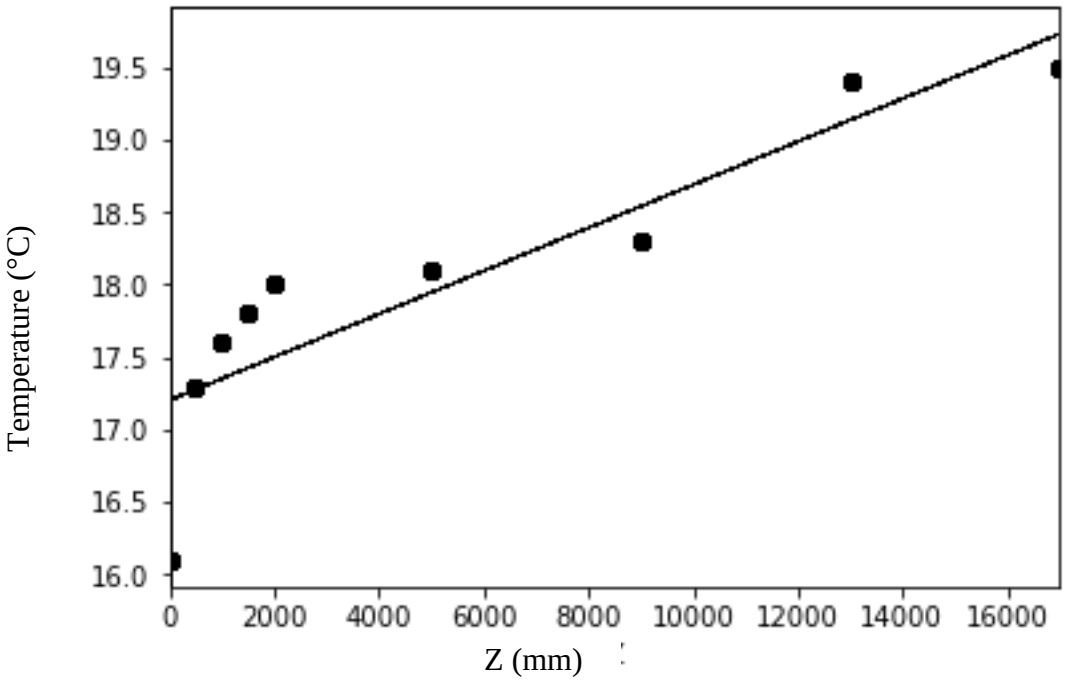

Figure 25. Graph showing the temperature distribution function using a line of best fit.

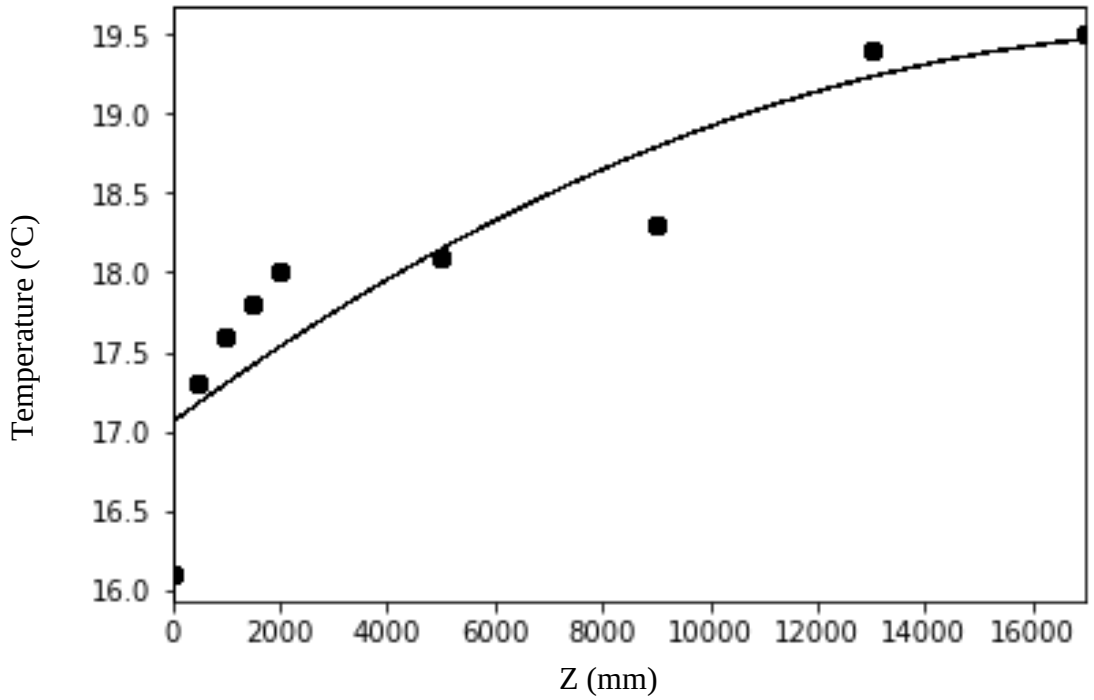

Figure 26. Graph showing the temperature distribution function using a cubic fit.

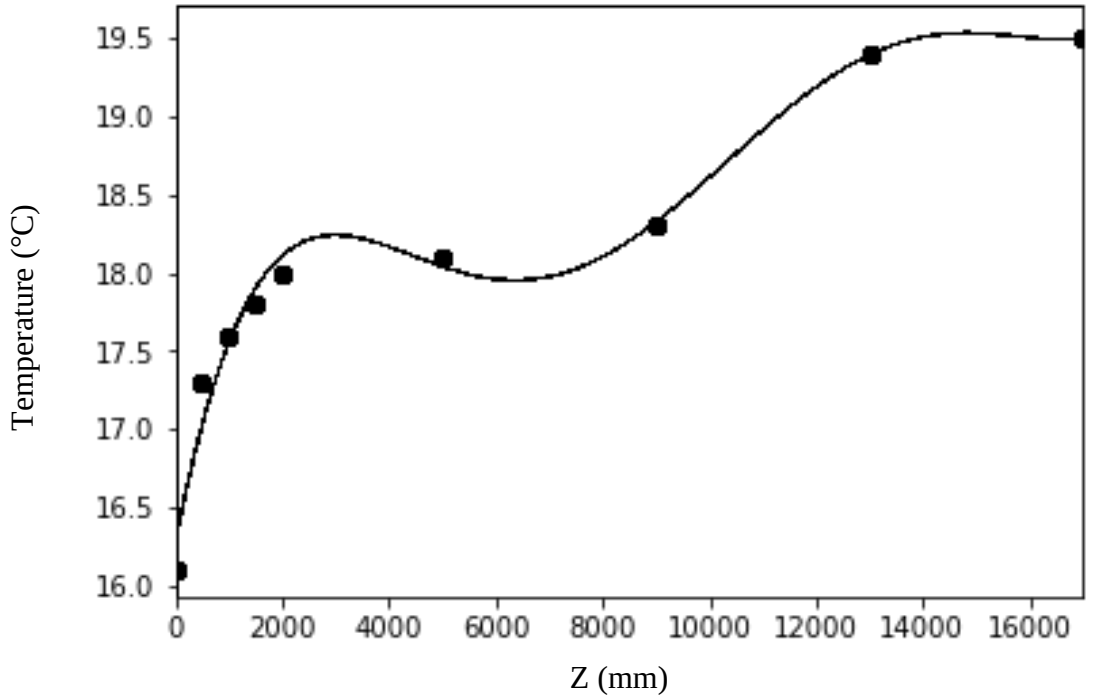

Figure 27. Graph showing the temperature distribution function using a quintic fit, and the apparent overfitting observed when using higher order polynomials.

4.4.5 Using a Temperature Distribution as FEA Boundary Condition

The flowchart in Figure 28 shows how the virtual temperature distribution can be used as part of FEA in order to produce a spatiothermal artefact.

FEA input file templates are generated which can be edited or rather reproduced including the new boundary conditions. The template input file can be written manually or can be generated through the ANSYS software. ANSYS Workbench was used to create the input file in this case due to its more intuitive user interface compared to the ANSYS APDL interface.

Temperatures from the virtual temperature distribution are used to write a series of commands, in which the nodal coordinates are used to define temperatures. The Python script reads the input file template and creates a new file. The beginning of the template up to a set point is read and copied to the new file. At the point at which the commands need to be inserted, these are copied to the new file. Then the end of the file is read and subsequently copied. Finally, an adjustment is made to the resulting input file to remove any blank lines as ANSYS interprets blank lines as being a break point. The same actions are repeated for the structural input file. ANSYS has a product launcher, which can generate a command line for batch execution of simulations. The Python script has included this so that the FEA simulation can be run automatically from a specific input file.

Results are generated by ANSYS itself using post processing commands that are present within the initially generated input file templates. Resulting output files come in the form of CSV files in the working directory, which subsequent Python scripts can then read into NumPy arrays for further operations.

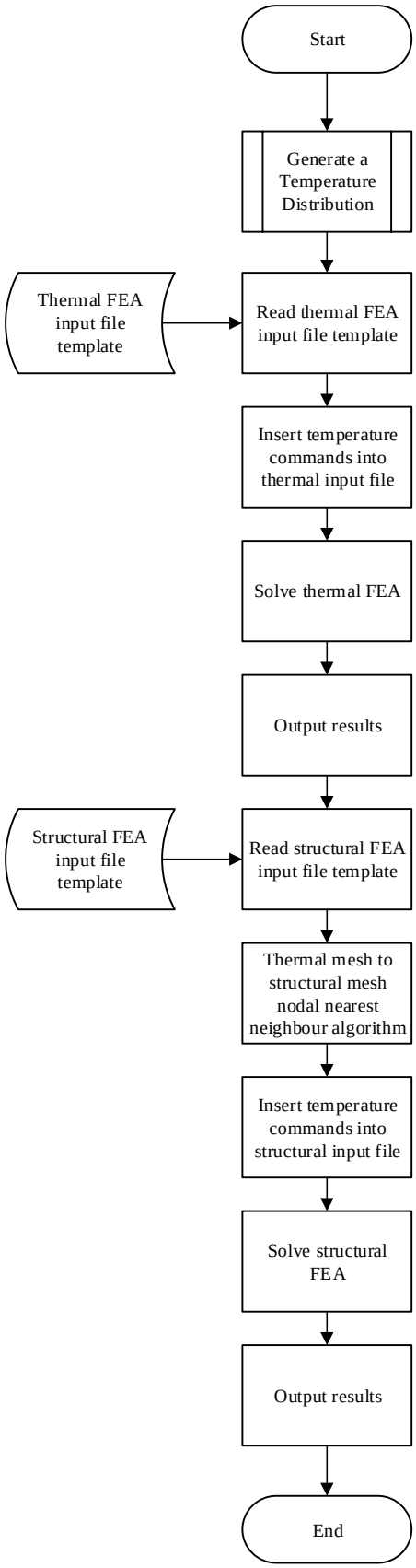

Figure 28. Flowchart showing the use of the script to produce structural displacement results when thermal FEA is included.

The thermal analysis can alternatively be avoided entirely, which is the method of experimentation presented here. As the temperature distribution is generated from a function to provide a nominal reference, the thermal analysis adds little extra value. The method for the use of thermal analysis is presented in order to describe how this might be used in cases where more sophisticated thermal models have been created. The modular design of the script and the methodology means that specialists can be engaged at each stage, as would be the case in industry.

In cases in which CFD has been used to create a spatiothermal model of temperature distribution, the points can be directly imported in place of the generated temperature distribution as an array. The script can then avoid thermal FEA or interpolation entirely, and structural FEA will become the primary focus.

4.4.6 Analytical Interpolation of Temperature Distributions

Reconstruction of temperature distributions has been carried out using the following methods:

1. Polynomial regression;
2. Ordinary Kriging.

The polynomial regression method is performed using separate curve fitting in the X, Y, and Z axes. This separation is useful in cases in which the temperature is being measured along one of the axes due to known variation, which is typically the Z (vertical) axis.

Ordinary Kriging has been described in section 2.6.3, and has been used to provide an alternative approach to polynomial regression. The inclusion of Kriging means that not only is a temperature distribution interpolated in 3D, but a variogram is produced. The variogram provides a statistical measure of confidence in the prediction of the interpolation for each of the points. Having a variogram means that these confidence levels can potentially be used as the basis for temperature sensor positioning optimisation.

4.4.7 Sensor Network Definition

Definition of sensor networks has been achieved in the script using hard coded sensor networks, and there is also a method to import designed sensor networks from CSV files. The CSV contains information on:

- Sensor ID number;
- X, Y, and Z coordinate positions;
- Type of sensor;
- Sensor calibrated uncertainty;
- Dynamic or fixed - whether they can change coordinate position for optimisation purposes.

Definition of uncertainty has been given based upon reasonable values for sensor types. For the purposes of the experiments, thermocouples have been used in all cases as these sensors are widely used in industry, standardised, and low cost.

4.4.8 Spatiothermal Scenarios

Representation of a range of spatiothermal scenarios is another important aspect of properly testing the algorithm. To make the tests useful and representative without being exhaustive, it was decided that the main variables that needed to be included were:

- Maximum temperature differential;
- Type of distribution;
- Number of varying dimensions.

The maximum temperature differential will determine the net thermal expansion. As has been discussed in the literature, and observed in measurements, realistic thermal gradients are likely to be several degrees at any given time. The magnitude of the distributions becomes important when temperature sensor uncertainty is included in the simulations. Reproduction of temperature distributions with smaller temperature differentials would be more sensitive to temperature sensor uncertainty than larger ones.

The type of temperature distribution is the most important variable to include as this will have the largest effect on the optimal sensor positions. Type of distribution and number of varying dimensions are closely related. Linear and non-linear thermal gradients certainly need to be tested but could yield quite different temperature distributions.

More complex distributions could be included but at this stage would not be useful. Temperature distributions in assembly environments generally are not likely to have such a high degree of complexity. Some manufacturing environments will have far more complex temperature distributions due to the range of active heat sources present. A similar temperature measurement planning approach could be applied to more complex cases in future work.

To test the generation of temperature distributions using the tool, some different types of spatiothermal scenarios were generated. This showed some of the ways in which the tool could be used for experimentation and provided some concept of the magnitude of the coefficients that need to be used to produce temperature distributions that look realistic. Some examples of linear and non-linear thermal gradients, alongside the coefficients used to generate them.

Linear thermal gradients represent the most straightforward cases, so they are useful in developing the planning tool and to illustrate the methodology. Figure 29 and Figure 30 illustrate a temperature distribution designed to produce thermal expansion and contraction varying linearly with height between 19.4 °C to 20.9 °C from a 1.2 °C per metre gradient. In these figures, light blue shading denotes the area between the temperature and standard temperature, representing contribution to thermal contraction. Conversely, the areas shaded in light pink denote the portion of the temperature field that is above standard, which contributes to thermal expansion.

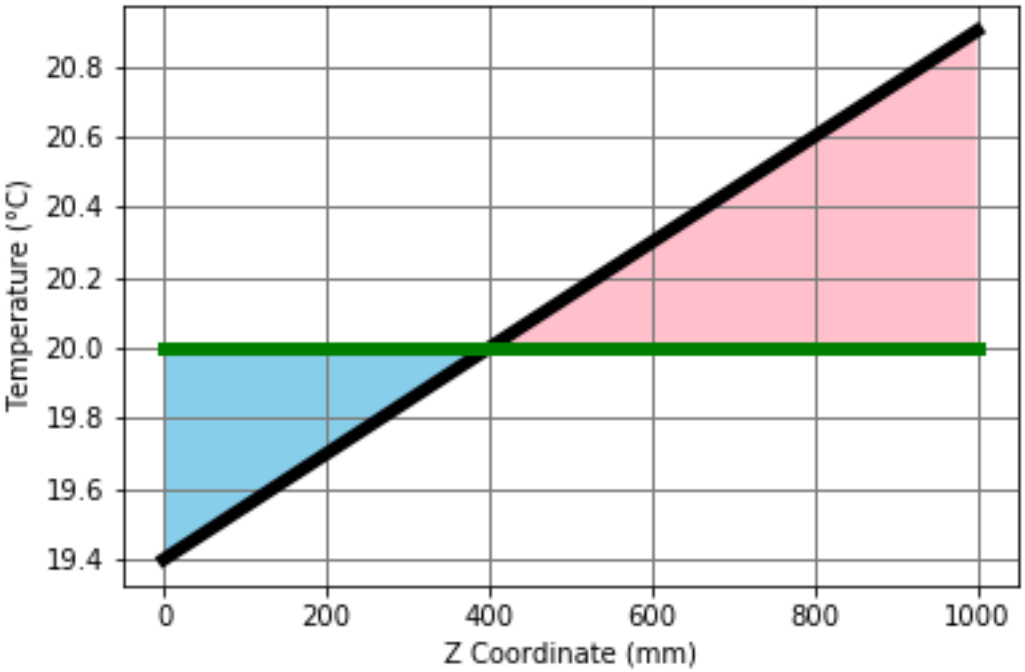

Figure 29. Graph showing 1-dimensional linear temperature variation along the Z axis.

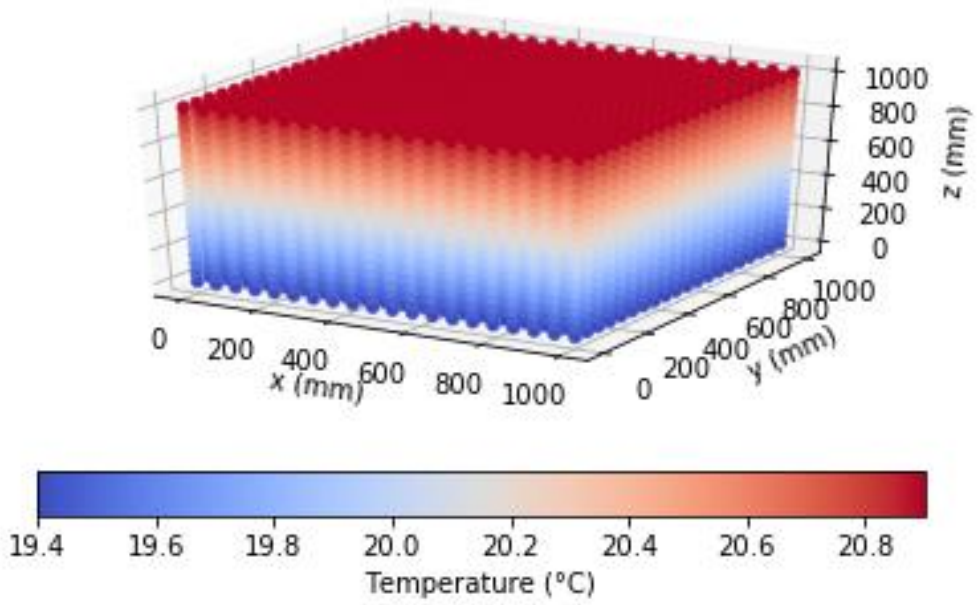

Figure 30. 3D colour plot showing the linear 1-dimensional temperature distribution within a volume of 1 cubic metre.

4.4.8.1 Non-linear Thermal Gradients

Non-linear thermal gradients are of greater interest in this work as they are arguably more realistic than a perfectly linear temperature gradient. There is also more sensitivity to positioning of sensors in order to reproduce the temperature distribution. Some examples are presented here, although the exact magnitude of these gradients is tailored to accommodate the range of sizes of CAD models. Scenarios in which temperature varies only according to height in the Z axis are considered first, before progressing to non-linear variation with both vertical and horizontal positions.

Figure 31 shows an example of a temperature distribution below standard temperature to create thermal contraction in which temperature varies non-linearly as height increases. A starting temperature of 15 °C was used to generate this temperature distribution and increased using the fractional exponent $c_{ry}\ Z^{0.5}$, where $c_r = 100$. Figure 32 shows the associated 3D colour plot of this temperature distribution. This type of distribution has been observed in large volume environments during colder months in which the ground is cold, but heating keeps the space at a more comfortable operating temperature. This means that the thermal gradient is more pronounced closer to the ground.

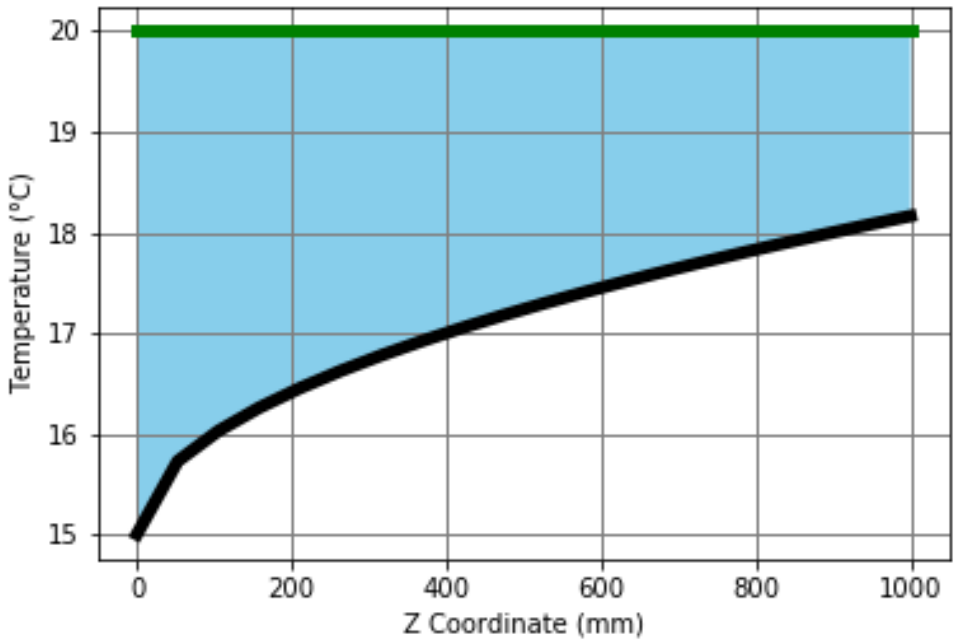

Figure 31. Graph showing 1-dimensional non-linear temperature variation along the Z axis, below standard temperature.

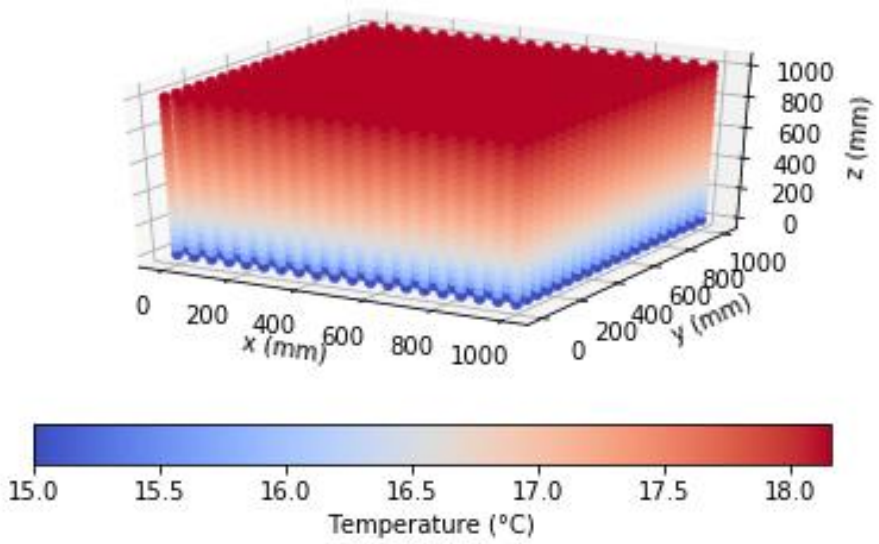

Figure 32. 3D colour plot showing the associated non-linear 1-dimensional temperature distribution around a volume of 1 cubic metre.

In Figure 33 and Figure 34 the graphs show the same idea was applied in two dimensions. Here three coefficients were defined to produce the final generated temperature distribution pictured in Figure 35. The starting temperature was 18.9 °C, and varied as a quadratic with coefficient 0.002 in X. In Z, the temperature varied with a fractional exponent as in the previous example, $c_r Z^{0.5}$, where $c_r = 110$.

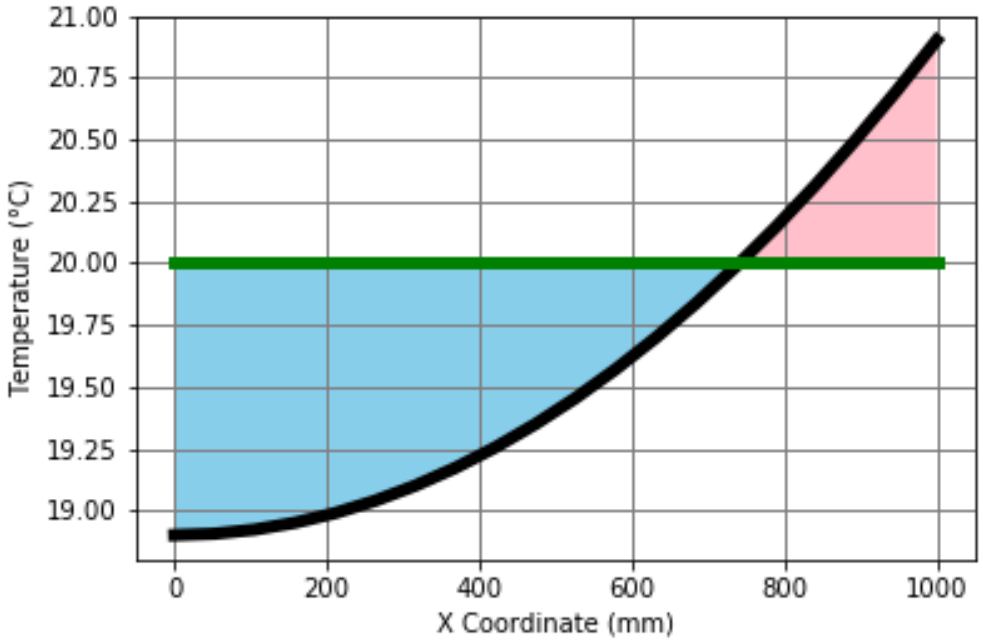

Figure 33. Graph showing non-linear temperature variation along the X axis with regions of contraction and expansion relative to standard temperature (green).

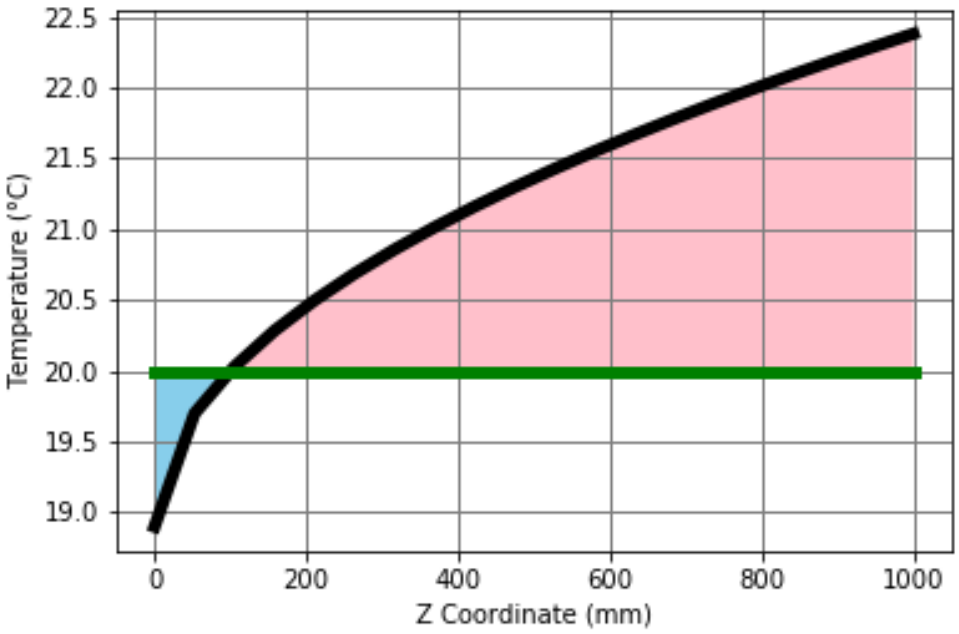

Figure 34. Graph showing non-linear temperature variation along the Z axis regions of contraction and expansion relative to standard (green).

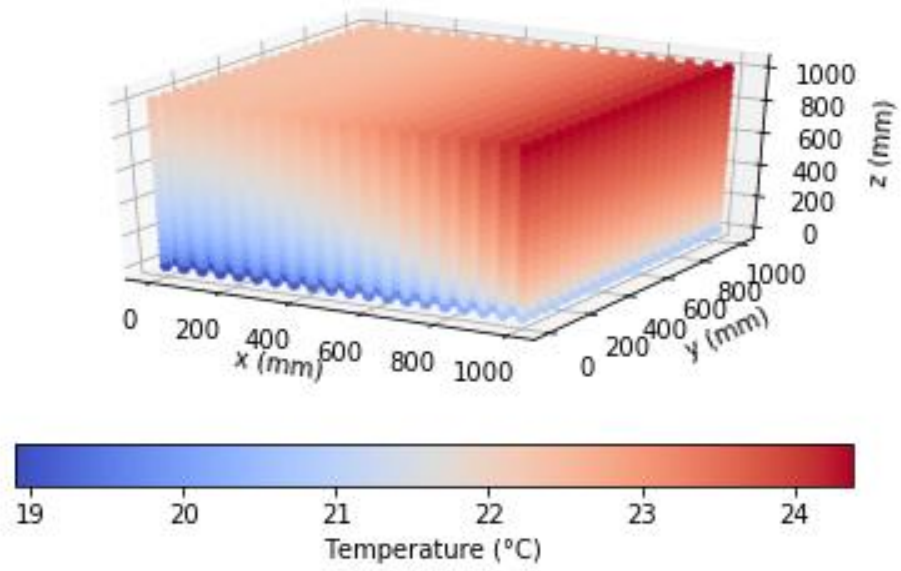

Figure 35. 3D colour plot showing the associated non-linear 2-dimensional temperature distribution around a volume of 1 cubic metre.

4.5 Ideas for Identifying Sensor Positions

Non-standard temperature distributions need to be approached from two perspectives in the steady state case. First of these is the temperature distribution function i.e. how the point-wise temperature is different around the volume described as a function. The second is to get a useful picture of the entire artefact. The temperature will not be measured at all positions, so the question of how coverage can be maximised for geometry becomes important.

In the linear and non-linear gradient cases operating principally along one axis (e.g. a vertical gradient with approximate uniformity with change in height, $T \propto \Delta h$), the impact of limited coverage will be less significant than in more complex temperature distributions. In more complex temperature fields, the coverage of temperature sensor networks becomes more important.

From what is known of ambient temperature distributions, it appears that the more common case is that temperature distributions are most likely to show a vertical temperature gradient, which is often non-linear but can in some cases be approximately linear. Indeed, applying a linear approximation will still yield a more realistic result than scaling a non-uniformly expanding artefact uniformly. On this basis, the measurement of a characteristic temperature distribution should take priority over sensor network coverage. This is allowable because the naive environmental survey should have provided sufficient coverage to capture as much of the artefact and measurement envelope as possible to identify points of interest. Coverage will be discussed in more depth later - whilst being considered the secondary process of sensor allocation, it is nonetheless still very important.

If the starting point is to characterise temperature distribution reproducibly, let us revisit the notion of measurement as communication. From previous experiments in thermal expansion prediction, capturing the full range of the temperatures is important. The additional information provides further detail about the function, which is useful for non-linear distributions where the distribution forms a curve.

How can this be put into practice? The virtual spatiothermal artefact contains a nominal temperature distribution derived from the naive environmental survey. Exporting this temperature distribution, we can then run a straightforward statistical analysis to find the temperature values for each of the summary points. The spatiothermal artefact also contains coordinate data. Using the summary points, the positions of interest can be found by searching for the nearest values and indexing the coordinates associated against these temperature values. The resulting coordinates represent a reduced set of the positions at which temperature is to be measured. This process lends itself to reproducibility whilst still allowing for a modicum of flexibility in practice. One of the other advantages to this approach is that any outliers are identified, meaning that expansion is not calculated based upon very extreme values. In some cases where erroneous extreme values occur during finite element analysis, this approach should act as a filter.

Consider the example of a familiar object: a table. In this example, it is known that there is a non-linear vertical temperature gradient driving thermal expansion in the four stainless steel legs. Having found the box-plot summary points, all of the temperature sensors could be lined up one leg of the four-legged table. This may be a tempting way to approach this measurement because the temperature distribution is quite uniform at a specific height and having only one leg covered by sensors is more practical. On the other hand, this is only

theoretically the case and leans too heavily on having an accurate model of the table in its environment. From a metrology standpoint it would be preferable to maximise the coverage; if the same number of sensors is used the sensor network would be more effective if they were spread around the four legs of the table. Coverage is also extremely important in transient cases. Although an environmental survey has been carried out, the confidence in this survey data as an accurate reflection of the environment will deteriorate with time. This means that even in a static model, time (with the temperature variance it brings) cannot be wholly neglected. In a sense, it could be argued that the box-plot summary as opposed to a basic maximum-minimum approach confers better coverage to the network; not just owing to the fact that it represents a network with more sensors, but because the sensor positions are chosen as being representative of the distribution it aims to describe.

This leads to the discussion of how temperature sensor coverage optimisation is achieved. Sensor network design studies have focused on sensor network coverage optimisation. The coverage problem that is being solved here is quite different to many others because it has more than one quantity operating. Thermal expansion is driven by temperature, but also by length itself. A beam of 10 m in length will expand ten times more than a beam of 1 m in length. If they are both present in the same assembly, this will be significant to the ability to predict expansion for the entire artefact. Given this disparity of scale, it would make sense to allocate sensors so that the number of sensors is proportional to length. Tolerances are similarly likely to be proportionally larger at this scale, depending on the application.

Ideas have been outlined here about the positioning of temperature sensors. These ideas were generated based upon measurements and experiments. Communication of temperature distributions was also considered in order to foster reproducibility. These ideas must be tested on the virtual spatiothermal artefact using finite element analysis to see if these discrete sensor positions can be used to recreate the original temperature distribution. This simulation-based testing needs to be broken down into phases for the various types of distribution and compared. As with many ideas generated up-front, they could be incorrect. There is an argument for carrying out experiments in a less prescriptive manner to determine whether some of these ideas will naturally come to the fore through iterative optimisation.

Each method needs to be defined and resulting temperature distributions from each test can then be used in a static structural analysis. The deformation resulting from the nominal spatiothermal artefact will serve as a benchmark against which each method is measured. To ensure that these are not isolated cases, the spatiothermal artefact will need to be altered numerically, insomuch as it will retain the same type of distribution but the actual temperatures within that distribution will be altered. An initial proof of concept example is provided to illustrate the process before moving to different virtual spatiothermal artefacts.

4.6 Considerations for Specifying Sensor Networks

This section discusses the requirements of the sensor positioning algorithm and asks key questions about where sensors are likely to be placed based on knowledge of the problem. General approaches to answering these questions, and the means of testing the solution are proposed, with the results of these tests presented in section 5.

In defining the sensor network positions, there are to be both fixed and optimised points. Fixed spatial positions will represent points that can be defined without knowledge of the temperature distribution. Spatial positions of interest can be derived from knowledge of best

practice for dimensional measurement. Similarly, fixed thermal positions are informed by knowledge of the temperature distribution to define the working temperature range through measurement of extreme regions.

Optimisation of sensor positions will aim to increase spatial coverage and increase thermal distribution coverage. Thermal optimisation will be determined through the characterisation of the temperature distribution, so that non-linearities can be reproduced with acceptable accuracy, with a minimal number of sensors. This makes temperature measurement planning more straightforward in the sense that only a subset of the positions needs to be optimised.

Full automation is not necessary for the sensor positioning process. For the fixed points to be measured for example, depending upon the geometry and accessibility it would be useful to have human input. Automation is useful, however, in optimising and in the testing of optimised positions.

Fixed spatial positions can be informed by the position of the following spatial characteristics, for example:

- Instrument;
- Scale bars;
- Measurement envelope extremities;
- Datum features;

Many instruments have their own temperature sensors as discussed previously, so these can be easily included. Scale bars are calibrated to a known length, but are not immune to thermal expansion, meaning the temperature should be measured. Capturing the extremities of the measurement envelope such as the vertices of a cuboidal structure will allow for thermal gradients to be identified. Datum features are used to define datum systems, which other dimensions are defined in reference to. Measuring temperature of the datum features can give a clearer idea of the thermal stability of the datum system.

Instrument temperatures are not of interest for computational experiments as they are usually acquired but will form part of the wider temperature measurement plan.

Fixed thermal positions are informed by the position of the following temperature distribution characteristics:

- Maximum and minimum absolute temperature region;
- Maximum and minimum temperature variation region (transient).

These fixed thermal positions inform the absolute temperature range. Knowledge of the full range of temperatures is useful as this allows for an evaluation of the maximum uncertainty due to thermal expansion within the measurement envelope. Unlike the spatial fixed points, these points should be checked periodically to ensure that they are representative of the maximum and minimum temperatures. The variation of temperature should also be measured, by identifying regions that are most variable, and most stable.

Thinking more practically, using the absolute maxima and minima could increase uncertainty arising from poor thermal contact. Consider for example a 1 m bar that is vertically supported. The maximum temperature might be at the very top, and the minimum might be at the very bottom. Placing temperature sensors at these edges would likely mean that the measurement being taken is less indicative of the part temperature and reflects more closely the ambient temperature at those edges. All types of surface temperature measurement suffer from these issues, in the best of circumstance. It may in some cases be more useful to specify

positions that are near to the maximum or minimum, within a spatial range. For the 1 m bar, this could be the maximum position multiplied by 0.9, for example, as a means of filtering out these edge effects.

One of the more interesting questions to answer for these fixed thermal points is: in a varying temperature field, how are the maximum and minimum temperatures selected, given that the positions at which these occur could change over time?

Optimised positions can appear anywhere within defined regions and otherwise constrained by practical limitations. These measurements are taken to better characterise the temperature distribution, particularly in the case of more complex temperature fields. A more faithful reproduction of the temperature distribution means a more accurate simulation of thermal expansion.

1) Establish fixed spatial positions;
2) Establish fixed thermal positions;
3) Calculate optimised static thermal positions;
4) Calculate optimised transient thermal positions;

At each stage, the temperature sensor network design needed to be tested in order to provide some level of evidence that the ds used in the algorithm regarding sensor positioning are valid.

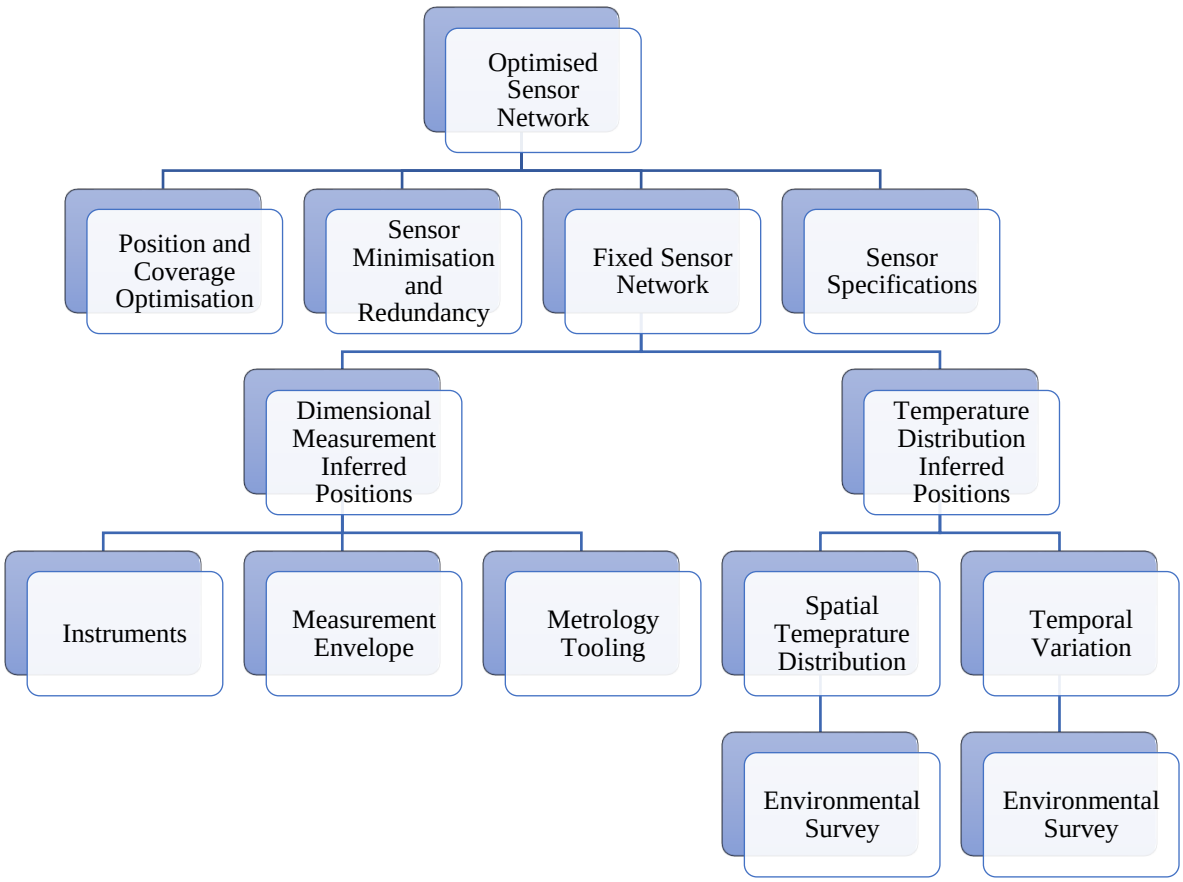

Figure 36. Diagram showing various contributing factors to planning an optimal sensor network.

The positions of the sensor network, defined for dimensionally inferred and temperature distribution inferred positions, need to be integrated into a single sensor network specification. Dimensional measurement plans for tactile CMM inspection, for example, contain points that need to be probed on the part. Similarly, the sensor network needs to contain enough information that the sensor network can be integrated into the assembly environment to be as close as possible to the planned network. In cases where practical issues arise, such as the accessibility of a feature by a temperature sensor, the plan may contain instructions for successful integration.

Final sensor network specifications should also contain some traceability of the temperature measurement planning process. Parameter files, simulation information and results of error mapping can be included to improve the communication of the temperature measurement plan. The approach has been discussed, but will still contain a level of human judgement, so the traceability and communication of sensor network design rationale is imperative.

Now that some functionality is in place, a formal methodology for testing the performance of sensor networks needs to be defined and used for a range of scenarios. At this point a lot of ideas have been offered, but so too has a tool, and it is in using the tool that the real learning will be done.

4.7 Chapter 4 – Summary

Chapter 4 provided:

- A proposed overall strategy for organisations to plan temperature measurement.
- A description of the temperature measurement planning tool and its functionality.
- Suggestions for types of temperature distribution to consider in computational experiments.
- General discussion for how sensor positions may be identified and specified in the context of an assembly environment.

Contributions:

- Measurement of temperature distribution complexity in industry.
- Creation of a novel computer-aided temperature measurement planning test bed supported by FEA.

There are many considerations for temperature measurement planning, so a tool has been created to test and compare sensor network designs.

---

5 Sensor Network Performance Testing

What makes a good sensor network and more importantly, how can this be virtually validated? Referring to the methodology defined in Chapter 4, Chapter 5 aims to run through each of the functional steps to ensure the planning tool can test a given temperature sensor network. The optimisation step repeats the first four steps, so can be added later, once some experience has been gained in using the tool.

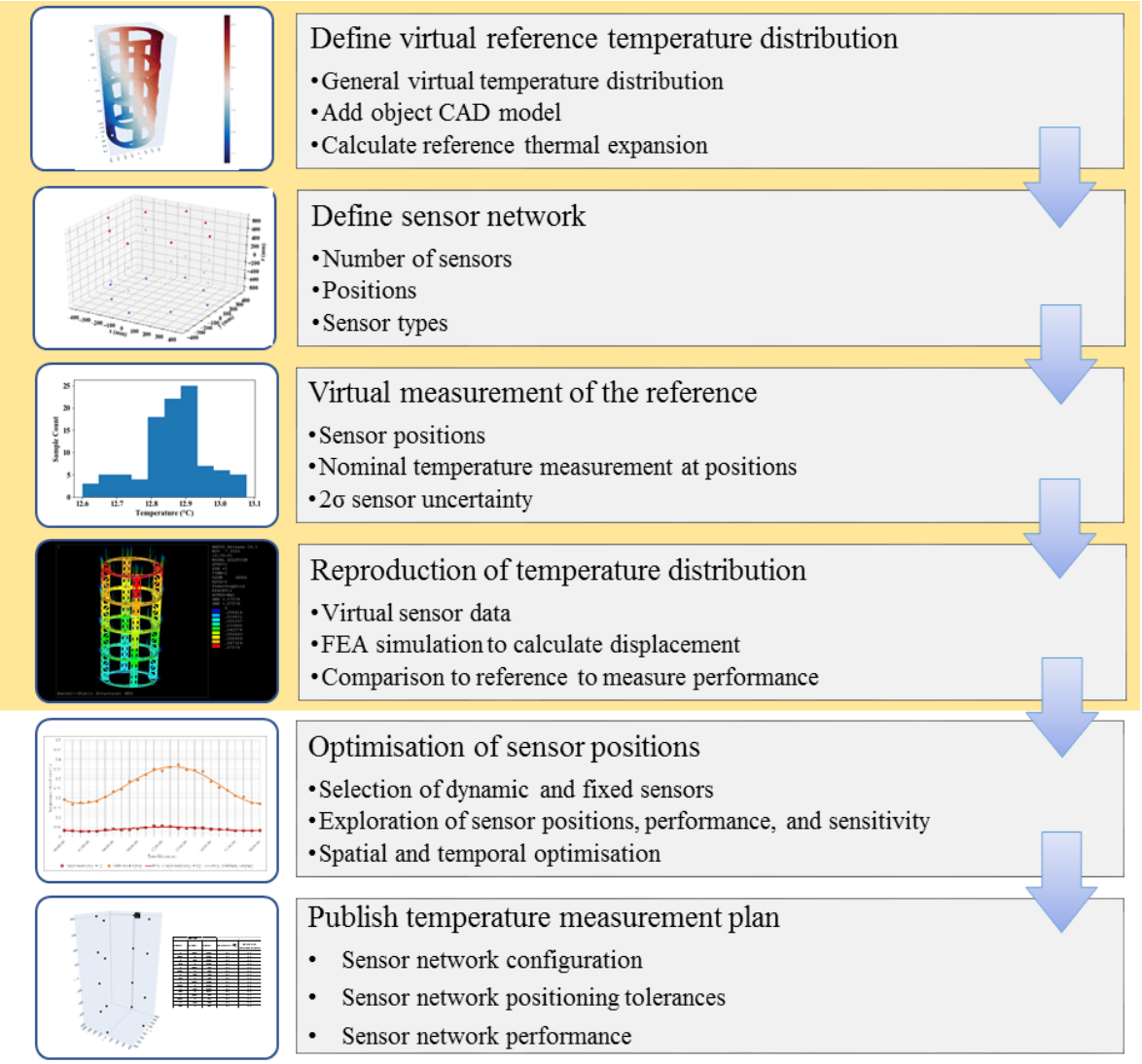

Figure 37. Temperature measurement planning methodology, highlighting the key activities in Chapter 5.

Before moving to more complex geometry, a straightforward cuboidal geometry is used for performance testing, which is depicted in Figure 38. The better the methodology and results can be understood by removing object complexity, the more confidence and understanding can be had about the most significant variables.

Many of the results presented in this chapter have been published as a conference paper [126].

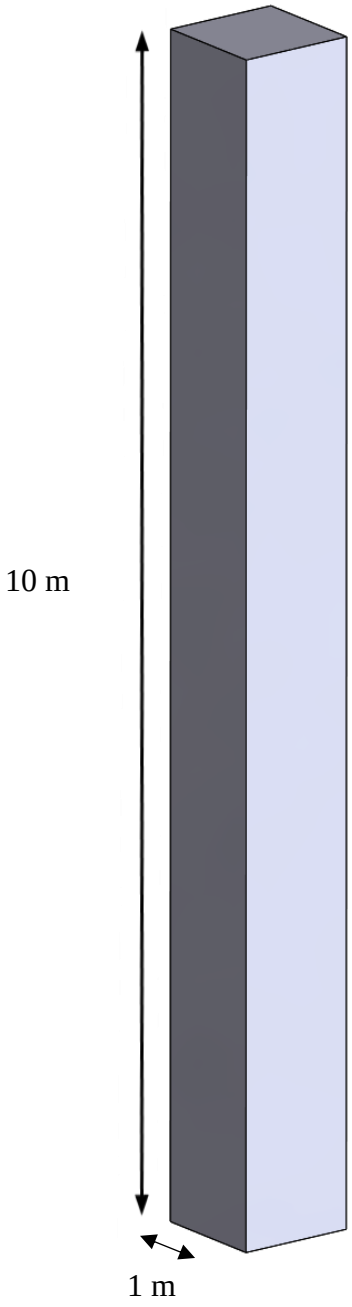

Figure 38. Rendering of the cuboidal beam geometry.

5.1 Naïve Sensor Network Experimental Controls

The immediate reaction for a rational person when presented with a document in excess of 100 pages on temperature measurement planning should probably be to procure a lot of sensors and distribute them evenly. Such pragmatism serves as a useful experimental control in evaluating the performance of an optimised temperature sensor network. Naïve so-called, as this type of network assumes no prior knowledge of the spatial or thermal character of the environment.

The number of sensors in the naïve sensor network experimental controls vary according to base 2. $2^0 = 1$ represents a single temperature sensor, as is often the case where temperature is measured in dimensional measurement. 2 sensors can describe a 1D linear thermal gradient; 4 can describe a 2D thermal gradient; 8 can be positioned at each of the 8 vertices of the measurement envelope bounding box; 16 can provide vertices as well as midpoint temperature measurements; and 32 provides further coverage. Data acquisition devices usually also have a base 2 number of temperature sensor channels, as with other electronic devices.

The positions used for these sensors can also be used as points that are used to give nodal displacement results for each simulation. Solutions are given graphically to supplement the sparse control point results.

5.2 Generated Temperature Distribution Parameters

To test how well the naïve networks performed, a battery of tests was needed. Some temperature distributions were thought to be easier to measure and reproduce than others, so there needed to be a range of levels of complexity. The assumption was made that linear temperature distributions are less complex than non-linear temperature distributions. While thermal gradients are often most pronounced vertically (Z Axis), having thermal gradients in more than one dimension would also add complexity. Table 11 shows the coefficients used to generate each of the 21 reference temperature distributions for testing. Images showing each of these temperature distributions can be found in Appendix B – Naïve Network Test Temperature Distributions.

Table 11. Coefficients used to generate 21 distinct temperature distributions used for testing with varying degrees of complexity.

ID	Coefficients									
	X Axis			Y Axis			Z Axis			
	a1	a2	a3	b1	b2	b3	c0	c1	c2	c3
1	0	0	0	0	0	0	18	0.5	0	0
2	0.5	0	0	0	0	0	18	0.5	0	0
3	0	0.005	0	0	0	0	18	0.5	0	0
4	0	0	0.000005	0	0	0	18	0.5	0	0
5	0	0	0	0.5	0	0	18	0.5	0	0
6	0	0	0	0	0.005	0	18	0.5	0	0
7	0	0	0	0	0	0.000005	18	0.5	0	0
8	0	0	0	0	0	0	18	0.5	0.00001	0
9	0.5	0	0	0	0	0	18	0.5	0.00001	0
10	0	0.005	0	0	0	0	18	0.5	0.00001	0
11	0	0	0.000005	0	0	0	18	0.5	0.00001	0
12	0	0	0	0.5	0	0	18	0.5	0.00001	0
13	0	0	0	0	0.005	0	18	0.5	0.00001	0
14	0	0	0	0	0	0.000005	18	0.5	0.00001	0
15	0	0	0	0	0	0	18	0.5	0.00001	0.00000001
16	0.5	0	0	0	0	0	18	0.5	0.00001	0.00000001
17	0	0.005	0	0	0	0	18	0.5	0.00001	0.00000001
18	0	0	0.000005	0	0	0	18	0.5	0.00001	0.00000001
19	0	0	0	0.5	0	0	18	0.5	0.00001	0.00000001
20	0	0	0	0	0.005	0	18	0.5	0.00001	0.00000001
21	0	0	0	0	0	0.000005	18	0.5	0.00001	0.00000001

5.3 Virtual Measurement without Uncertainty

Despite being a significant contributor to dimensional measurement uncertainty, the business case for integrating and maintaining many sensors must be considered. Each enterprise has a limited number of resources and at some point, the addition of sensors exhibits diminishing returns. If a metrologist needs to measure temperature to improve the uncertainty of their dimensional measurement, how can they do as much as possible with what is available to them?

In order to provide a basis for comparison, the naïve networks were tested to determine their capability in reconstructing the nominal temperature distributions (see section 5.1). Four naïve networks have been trialled with different numbers of sensors, using two reconstruction methods: polynomial regression and kriging.

Table 12 gives the mean standard deviation in X, Y, and Z for each of the naïve networks, which comprise 4, 8, 16, and 32 sensors. A linear (1^{st} order) polynomial regression fitting

was carried out to interpolate between the measured temperatures. In this case, no randomisation was added to provide uncertainty in the sensor readings. As the dimensions in X and Y were similar, so too were the results. In general, the results appeared to improve most dramatically between 4 and 8 sensors. The standard deviation in this case was larger for 32 sensors, however this is likely due to overfitting. 16 sensors produced the lowest standard deviation in Z, and this again is likely due to fitting. The improvements in X and Y were observed to be much the same for 8-32 sensors. A higher order polynomial would be preferable in many cases, and such reconstructions would need to be tailored to the environment.

Table 12. Results of naïve sensor network performance without uncertainty using 1^{st} order polynomial reconstruction.

			Standard Deviation of Reconstruction Error (mm)			Temperature (°C)	
Number of Sensors	Reconstruction Method	Order	X	Y	Z	Standard Deviation Error	RMS Error
32	Polynomial	1^{st}	0.012	0.012	0.158	1.02	6.67
16	Polynomial	1^{st}	0.013	0.013	0.087	1.02	8.10
8	Polynomial	1^{st}	0.015	0.015	0.108	1.03	12.30
4	Polynomial	1^{st}	0.070	0.058	0.431	8.14	212.52

Kriging was used as an alternative method of reconstruction. Recalling Equation 4,

Equation 10

$$Z^*(\boldsymbol{u}) - \mu(\boldsymbol{u}) = \sum_{\alpha=1}^{n(\boldsymbol{u})} \lambda_\alpha [Z(\boldsymbol{u}_\alpha) - \mu(\boldsymbol{u}_\alpha)]$$

Where:

$Z(\boldsymbol{u})$ is the variable of interest, the random field;

$\mu(\boldsymbol{u})$ is the trend component, the expected mean of $Z(u)$;

$\boldsymbol{u}$ is the location vector for the estimation point;

$n(\boldsymbol{u})$ is the number of local data points used to estimate;

$z(u_\alpha)$ is the datum for estimation location u;

$\lambda_\alpha(\boldsymbol{u})$ is the kriging weight assigned to datum.

Tthe function Z(u) describes temperature distribution, in which the temperature, here Z, varies with position, u, relative to a datum, $z(u_\alpha)$. The mean, $\mu(\boldsymbol{u})$, is the mean temperature of the temperature distribution – the usefulness of this trend component may be more appropriate for some distributions than others and so should be tested for specific applications.

Using Kriging as a means of interpolation in this case gave improved results relative to the use of a 1st order polynomial regression. The Kriging in X produced a mean standard deviation roughly twice that of Y. The Kriging results were noticeably more consistent and can be seen in Table 13. In general, an order of magnitude improvement could be seen in the mean standard deviation in Z for Kriging, compared to the 1st order polynomial regression. The results for Kriging for 4 sensors significantly outperformed regression for 32 sensors and improved with further sensors. In cases in which there would be a preference for fewer sensors and a confidence that the environment was relatively stable, 8 sensors would perform adequately.

Table 13. Results of naive sensor network performance using Kriging reconstruction.

		Standard Deviation of Reconstruction Error (mm)			Temperature (°C)	
Number of Sensors	Reconstruction Method	X	Y	Z	Standard Deviation Error	RMS Error
32	Kriging	0.017	0.008	0.035	1.20	3.42
16	Kriging	0.017	0.008	0.032	1.24	3.13
8	Kriging	0.016	0.006	0.029	1.17	2.05
4	Kriging	0.018	0.009	0.047	1.40	4.77

5.4 Polynomial Reconstruction – 1st to 5th Order

To provide a more comprehensive comparison of polynomial regression-based reconstruction to Kriging, the naïve networks have been tested from 1st order to 5th order polynomials. The results of these tests are summarised in Table 14. 32 sensors have been used for each of the polynomial reconstructions for this test, to control the number of variables. In general, the performance of the reconstruction appears to peak at 3rd order polynomials. Higher order polynomials tend to create predictions that are improbable. Notable are the results for the 4th and 5th order polynomial reconstructions, as these appear to generate significantly higher errors, particularly in the X direction. Many of the generated temperature distributions are non-linear, so it makes sense that orders beyond the 1st are explored. With all of these results comes the reminder that more than one temperature reading is usually taken in practice at present. Any readings taken are often not used for part compensation, but instead for instrument compensation (if used at all).

Table 14. Results of naive sensor network performance comparing 1st to 5th order polynomial reconstruction.

			Standard Deviation of Reconstruction Error (mm)			Temperature (°C)	
Number of Sensors	Reconstruction Method	Order	X	Y	Z	Standard Deviation Error	RMS Error
32	Polynomial	1st	0.012	0.012	0.079	1.02	6.67
32	Polynomial	2nd	0.010	0.008	0.050	0.73	3.82
32	Polynomial	3rd	0.008	0.007	0.048	0.42	3.06
32	Polynomial	4th	0.037	0.009	0.052	0.91	4.14
32	Polynomial	5th	0.046	0.009	0.052	0.99	4.24

5.5 Single Sample Measurement with Pseudo-random Uncertainty

The tests were repeated, this time with normally distributed pseudo-random uncertainties. A single sample measurement was taken, which served as a worst-case scenario that simulated a static snapshot of the temperature distribution on the sensor network.

A 1st order polynomial regression was used to reconstruct the distribution from the sensor network measurements, and the results can be seen in Table 15. The most notable result is that significant changes in individual sensor uncertainty made a less impactful difference to the standard deviations in X, Y, and Z than might be expected. This adds to the argument that broader coverage of temperature measurement from multiple sensors in dimensional measurement tasks is likely to lead to improvements. The difference in the cost of sensors can be significant across this uncertainty range, and the provision of expensive low uncertainty sensors appears to be less important than how the measurement data is subsequently used.

Table 15. Results of naive sensor network performance using 1st order polynomial reconstruction, based upon single sample virtual measurement including uncertainty.

				Standard Deviation of Reconstruction Error (mm)		
Number of Sensors	Reconstruction Method	Order	Uncertainty	X	Y	Z
4	Polynomial	1	2	0.075	0.063	0.465
4	Polynomial	1	1	0.072	0.060	0.442
4	Polynomial	1	0.5	0.070	0.058	0.428
4	Polynomial	1	0.1	0.070	0.058	0.431
8	Polynomial	1	2	0.018	0.017	0.126
8	Polynomial	1	1	0.017	0.016	0.119
8	Polynomial	1	0.5	0.016	0.015	0.111
8	Polynomial	1	0.1	0.015	0.015	0.108
16	Polynomial	1	2	0.015	0.015	0.104
16	Polynomial	1	1	0.013	0.013	0.088
16	Polynomial	1	0.5	0.013	0.012	0.085
16	Polynomial	1	0.1	0.013	0.012	0.085
32	Polynomial	1	2	0.012	0.011	0.080
32	Polynomial	1	1	0.013	0.013	0.087
32	Polynomial	1	0.5	0.012	0.012	0.079
32	Polynomial	1	0.1	0.012	0.012	0.079
			Mean	0.028	0.025	0.182

The Kriging method created greater impact, and again was more consistent across the networks (see Table 16). It appears that the network improves more significantly with lower uncertainty sensors than for the first order polynomial. This is to be expected, since the results of the first order polynomial is likely to be dominated by fitting error. In some cases, the standard deviation in Z approximately halved from U = 2 °C to U = 0.1 °C.

Table 16. Results of naive sensor network performance with Kriging reconstruction, based upon single sample virtual measurement including uncertainty.

			Standard Deviation of Reconstruction Error (mm)		
Number of Sensors	Reconstruction Method	Uncertainty	X	Y	Z
4	Kriging	2	0.020	0.012	0.066
4	Kriging	1	0.019	0.009	0.051
4	Kriging	0.5	0.019	0.009	0.049
4	Kriging	0.1	0.018	0.009	0.047
8	Kriging	2	0.019	0.012	0.072
8	Kriging	1	0.017	0.008	0.039
8	Kriging	0.5	0.017	0.007	0.037
8	Kriging	0.1	0.016	0.006	0.028
16	Kriging	2	0.020	0.012	0.068
16	Kriging	1	0.018	0.009	0.037
16	Kriging	0.5	0.018	0.009	0.042
16	Kriging	0.1	0.017	0.008	0.034
32	Kriging	2	0.020	0.011	0.066
32	Kriging	1	0.018	0.009	0.048
32	Kriging	0.5	0.018	0.009	0.043
32	Kriging	0.1	0.017	0.008	0.037
		Mean	0.018	0.009	0.048

5.6 10 Sample Measurement with Pseudo-random Uncertainty

10 samples with pseudo-random uncertainty were then used in place of single sample 'instantaneous' measurements across each of the naïve networks. The mean of the ten generated samples were subsequently used in the reconstruction using both polynomial regression and Kriging.

Table 17 shows the polynomial regression results. The majority are first order polynomials, with one 32 sensor 3rd order polynomial regression and U = 0.1 °C for reference: in theory the best naïve network settings from previous sections. The main result from these tests was that the use of 10 samples served to further reduce the effect of reducing individual sensor uncertainty. The benefit from using U = 2 °C to U = 0.1 °C sensors appeared to be very slight, further raising questions about the value of investing in low uncertainty sensors, without first considering their spatial positioning, and subsequent spatiothermal reconstruction.

Table 17. Results of naive sensor network performance with polynomial reconstruction, based upon 10 sample virtual measurement including uncertainty. The equivalent values for the 3rd order polynomial is provided at end bottom for reference.

				Standard Deviation of Reconstruction Error (mm)		
Number of Sensors	Reconstruction Method	Order	Uncertainty	X	Y	Z
4	Polynomial	1	2	0.085	0.058	0.431
4	Polynomial	1	1	0.075	0.059	0.434
4	Polynomial	1	0.5	0.072	0.058	0.432
4	Polynomial	1	0.1	0.070	0.058	0.431
8	Polynomial	1	2	0.025	0.015	0.110
8	Polynomial	1	1	0.018	0.015	0.107
8	Polynomial	1	0.5	0.017	0.015	0.109
8	Polynomial	1	0.1	0.015	0.015	0.108
16	Polynomial	1	2	0.020	0.013	0.086
16	Polynomial	1	1	0.015	0.013	0.087
16	Polynomial	1	0.5	0.014	0.013	0.087
16	Polynomial	1	0.1	0.013	0.013	0.087
32	Polynomial	1	2	0.016	0.012	0.081
32	Polynomial	1	1	0.014	0.012	0.078
32	Polynomial	1	0.5	0.013	0.012	0.079
32	Polynomial	1	0.1	0.012	0.012	0.079
			Mean	0.031	0.024	0.177
32	Polynomial	3	0.1	0.009	0.008	0.050

The same test was carried out using the Kriging reconstruction method, and the results are presented in Table 18. Mean standard deviation across each of the temperature distributions was most improved with uncertainty in the X direction, as in the polynomial reconstructions. The standard deviation in Y and Z did not improve appreciably with sensor uncertainty. Reconstruction through Kriging in general outperforms the 3rd order polynomial regression with lowest uncertainty.

Table 18. Results of naive sensor network performance with Kriging reconstruction, based upon 10 sample virtual measurement including uncertainty.

			Standard Deviation of Reconstruction Error (mm)		
Number of Sensors	Reconstruction Method	Uncertainty	X	Y	Z
4	Kriging	2	0.037	0.009	0.047
4	Kriging	1	0.025	0.009	0.046
4	Kriging	0.5	0.019	0.009	0.048
4	Kriging	0.1	0.018	0.009	0.048
8	Kriging	2	0.025	0.007	0.030
8	Kriging	1	0.018	0.006	0.028
8	Kriging	0.5	0.017	0.007	0.029
8	Kriging	0.1	0.016	0.006	0.029
16	Kriging	2	0.023	0.009	0.035
16	Kriging	1	0.020	0.008	0.032
16	Kriging	0.5	0.018	0.008	0.033
16	Kriging	0.1	0.017	0.008	0.032
32	Kriging	2	0.025	0.009	0.035
32	Kriging	1	0.022	0.008	0.036
32	Kriging	0.5	0.019	0.008	0.036
32	Kriging	0.1	0.017	0.008	0.036
		Mean	0.021	0.008	0.036

5.7 Vertical Positioning Error Monte Carlo Simulation

How can the dimensional measurement error due to sensor positioning error be calculated?

For each temperature sensor network that is generated, the sensitivity of temperature sensor position can be calculated statistically. In this case, what is meant by sensor position sensitivity is to what extent the positioning of temperature sensors away from their nominally prescribed position have on overall temperature distribution reproduction. Definition of this can help in the definition of tolerances for how precisely temperature sensors need to be positioned during set up and integration. Positioning a temperature sensor a millimetre away from its nominal position is unlikely to make an impact in measurement of ambient temperature. If, however, a temperature sensor was positioned a millimetre away from its

nominal position during the measurement of a weld melt pool then sensitivity to this variation would be much higher.

Assigning variation to sensors in a sensor network and running a Monte Carlo simulation can provide an estimate of how sensitive the temperature field reproduction is to positional variation of sensors. This method would require the selection of a range of suitable values for how much each of the temperature sensor positions is likely to vary. A reasonable starting point over several metres, for example, might be for a sensor to be positioned against a flat surface within ± 50 mm (at a confidence interval of 2 standard deviations, k=2) of the vertical position in the Z axis by a human operator. This informs the parameters of the Monte Carlo simulation. The Monte Carlo simulation uses the given variation to produce a distribution of simulated points around the nominal sensor position. For each case, the temperature distribution can be reproduced, and the error between the nominal and the Monte Carlo simulation can be calculated. After multiple iterations, it is possible to build the distribution of errors between the nominal and the Monte Carlo reproduction of the temperature field to provide the uncertainty due to temperature sensor position, which represents how sensitive the network is to positional variation. The same method can be used for both temperature and dimensional measurement uncertainty due to temperature sensor positioning.

A Monte Carlo simulation was carried out in which each of the vertical (Z) positions was varied by a pseudorandom number. The sensor network had 32 sensors, and both third order polynomial and Kriging were used as reconstruction methods. In this test, 100 iterations were carried out and a full set of results produced for the 100 unique temperature sensor networks. Each of the positioning errors (1 mm, 10 mm, 25 mm, 50 mm, and 100 mm) were entered as a normal distribution with the nominal position as the mean, and the positioning error as the standard deviation.

In order to make sure the sensor positions were valid and not positioned beyond the bounding box of the part, the boundaries were used as limits, and the half of the distributions that would have otherwise been invalid were, in effect, layered on top of the valid half of the distribution. Temperature sensor positions that were nominally beyond the boundary could fluctuate in both positive and negative directions.

Results of the Monte Carlo Simulation are presented in Table 19 and Table 20, with a graph of the results in Z given in Figure 39. The mean of the 100 values for standard deviation of the error in Z were taken and used to provide a general comparison of each of the sensor network specifications. The effect of the positioning error was negligible in the polynomial case, in which the reconstruction was likely dominated by fitting error. The effect of positioning error was most noticeable in the Kriging Reconstruction. The difference between 1 mm, 10 mm appears to be small on the graph, but in effect would be difficult to achieve in practice over this distance. This would also make the ratio of the sensor positioning tolerance to the actual footprint of the sensor be quite large. At 25 mm there was a slight increase in the effect of the positioning error, and there was a more marked increase at 50 mm. The worst result was 100 mm, which gave a comparable result to the polynomial reconstruction.

One of the aspects of the reconstruction method that differs, is the effect of the positioning error in X and Y. The polynomial reconstruction is far less sensitive to effects occurring in X and Y, and these remain stable throughout. For the Kriging reconstruction at larger

positioning errors (i.e. 50 mm and 100 mm), the positioning error has a larger effect on X and Y reconstruction error.

An allowable positioning error of between 10 mm and 25 mm would be ideal, as 1 mm is unlikely to provide benefits relative to the time taken to carefully position. It seems that positioning error does in fact make a difference, and its effect can be calculated using the temperature measurement planning tool. This can then be used to provide clear specifications on a temperature measurement plan. In practice, an experiment could be carried out testing the repeatability of sensor placement to ensure that this is achievable. Having some way to enable measurement of sensor coordinates would be beneficial to reducing sensor positioning error.

Table 19. Results of naive sensor network performance Monte Carlo simulation with vertical positioning error, and polynomial reconstruction.

				Mean of Standard Deviation of Reconstruction Error (mm)		
Number of Sensors	Iterations	Positioning Error in Z (mm)	Reconstruction Method	X	Y	Z
32	100	1	Polynomial	0.028	0.025	0.164
32	100	10	Polynomial	0.028	0.025	0.164
32	100	25	Polynomial	0.028	0.025	0.164
32	100	50	Polynomial	0.028	0.025	0.164
32	100	100	Polynomial	0.028	0.025	0.165

Table 20. Results of naive sensor network performance Monte Carlo simulation with vertical positioning error, and Kriging reconstruction.

				Mean of Standard Deviation of Reconstruction Error (mm)		
Number of Sensors	Iterations	Positioning Error in Z (mm)	Reconstruction Method	X	Y	Z
32	100	1	Kriging	0.024	0.028	0.119
32	100	10	Kriging	0.024	0.028	0.119
32	100	25	Kriging	0.025	0.028	0.122
32	100	50	Kriging	0.029	0.031	0.142
32	100	100	Kriging	0.039	0.034	0.162

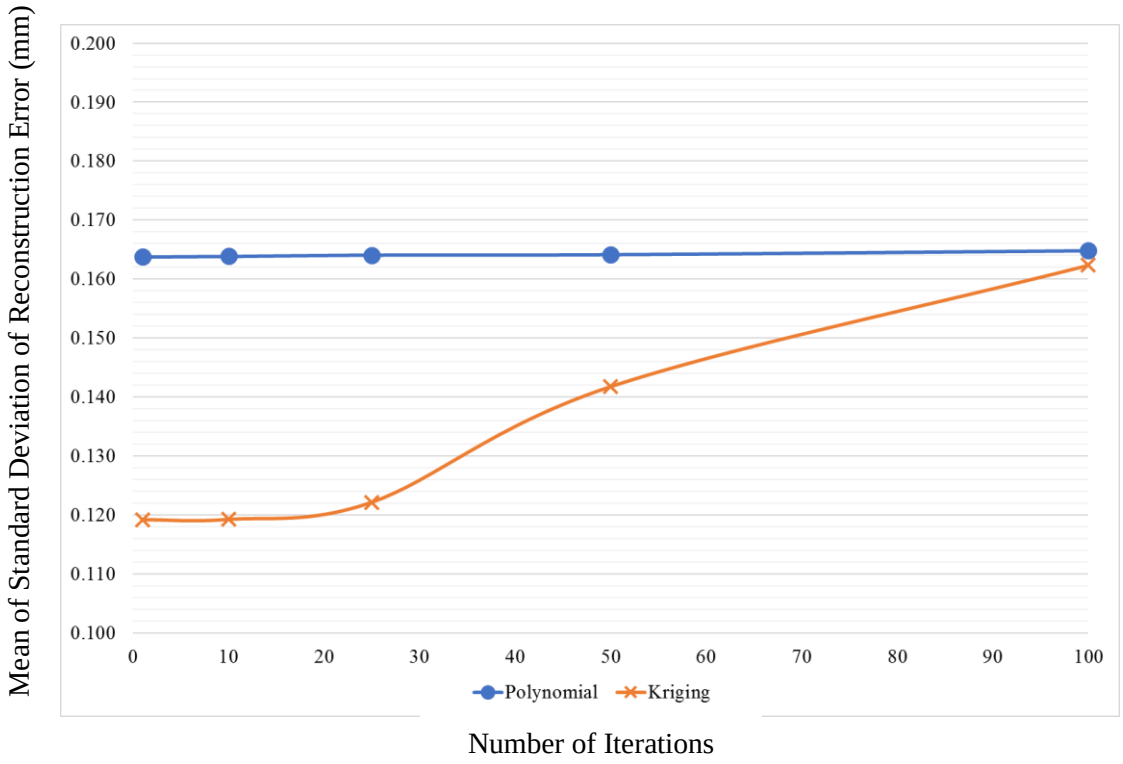

Figure 39. Comparison of results of naive sensor network performance Monte Carlo simulation with vertical positioning error for Polynomial and Kriging reconstruction.

5.8 Sequential Sensor Removal

One method to test the sensitivity of the sensors in a network is to define an 'ideal' temperature sensor network, and iteratively remove sensors from the network to see how the performance alters. Sensitivity in this case is defined as the contribution of an individual sensor to the performance of a specific sensor network, as opposed to the physical sensitivity of the individual sensor to small variations in temperature.

- Define sensor network;
- Remove sensor 1;
- Determine sensor network performance;
- Replace sensor 1;
- Remove sensor 2;
- Repeat for n sensors.

The performance of networks with a single removed sensor was compared to the baseline performance of the full sensor network. This was carried out with both the polynomial and Kriging methods of reconstruction. The third order polynomial case was used, and the sensors measured nominal temperatures at given positions. Three naïve networks were tested of 8, 16, and 32 sensors.

5.8.1 Naïve 8-Sensor Network with Sequential Removal

Results of the sensor removal performance test for 8 sensors can be seen in Figure 40 and Figure 41. As there are fewer sensors in total, it was expected that each sensor removed would have a large effect on the network performance as a whole – in this case the standard deviation of the error in Z was used. On reflection, using displacement was useful in the sense that it gives the results some context and shows the full workflow in action for completeness. On the other hand, having to do FEA for every single run meant that these experiments took a lot longer than needed compared to focusing on temperature reconstruction error, which ultimately is what is driving the displacement error.

The full network baseline is somewhere near the middle, and resembles a line of best fit when presented in this way, which shows that whilst the performance of the network often gets worse as sensors are removed, there are some cases in which the performance is improved when individual sensors are removed.

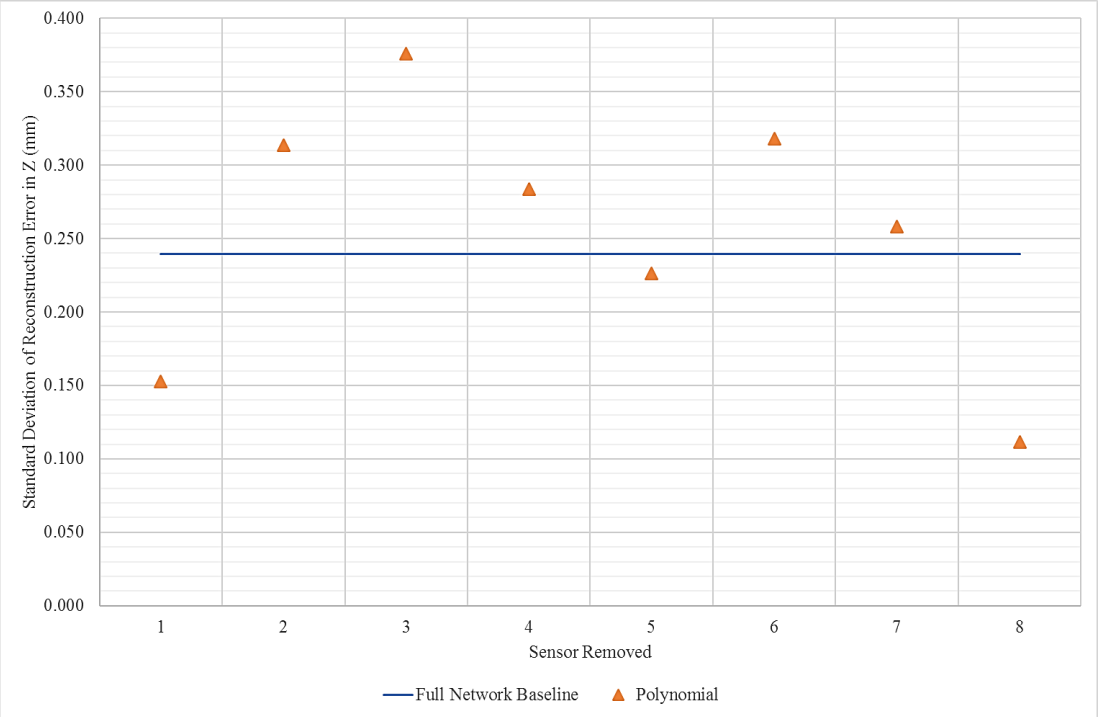

Figure 40. Results of naïve 8-sensor network performance as sensors removed with polynomial reconstruction.

Comparing both reconstruction methods in Figure 40 and Figure 41, polynomial reconstruction is significantly more sensitive to the removal of individual sensors than Kriging. Kriging also performs significantly better when using this metric. In cases where the temperature distribution varies a lot spatially over time, it would be best to use Kriging to reconstruct the temperature distribution. Similarly, it would be useful to use Kriging as a reconstruction method if there are fewer regions that temperature sensors can safely and practicably be positioned.

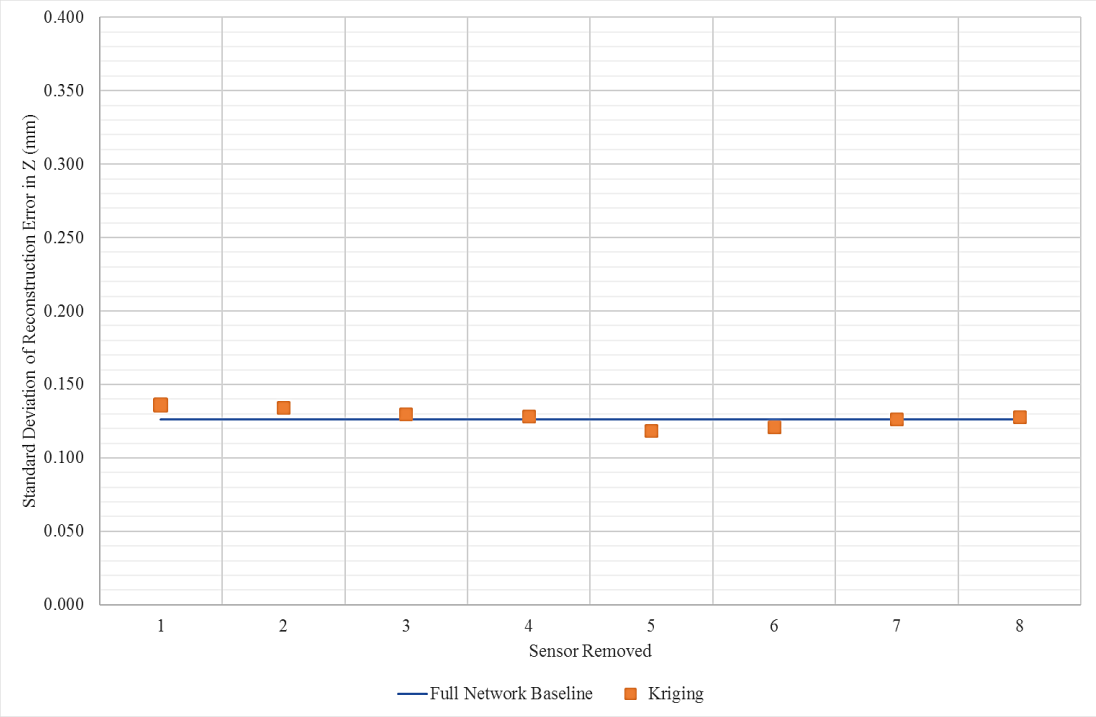

Figure 41. Results of naïve 8-sensor network performance as sensors removed with Kriging reconstruction.

5.8.2 Naïve 16-Sensor Network with Sequential Removal

At 16 sensors, the performance of the full sensor network improves for both reconstruction methods when compared to 8 sensors, as can be seen in Figure 42 and Figure 43. Sensitivity to sensor removal shows a marked decline compared to 8 sensors for both reconstruction methods. In all cases, it seems that the removal of Sensor 8 appears to improve the reconstruction of the temperature distribution – Sensor 1 also seems to create problems. It may suggest that the sensor network positions need to be further optimised.

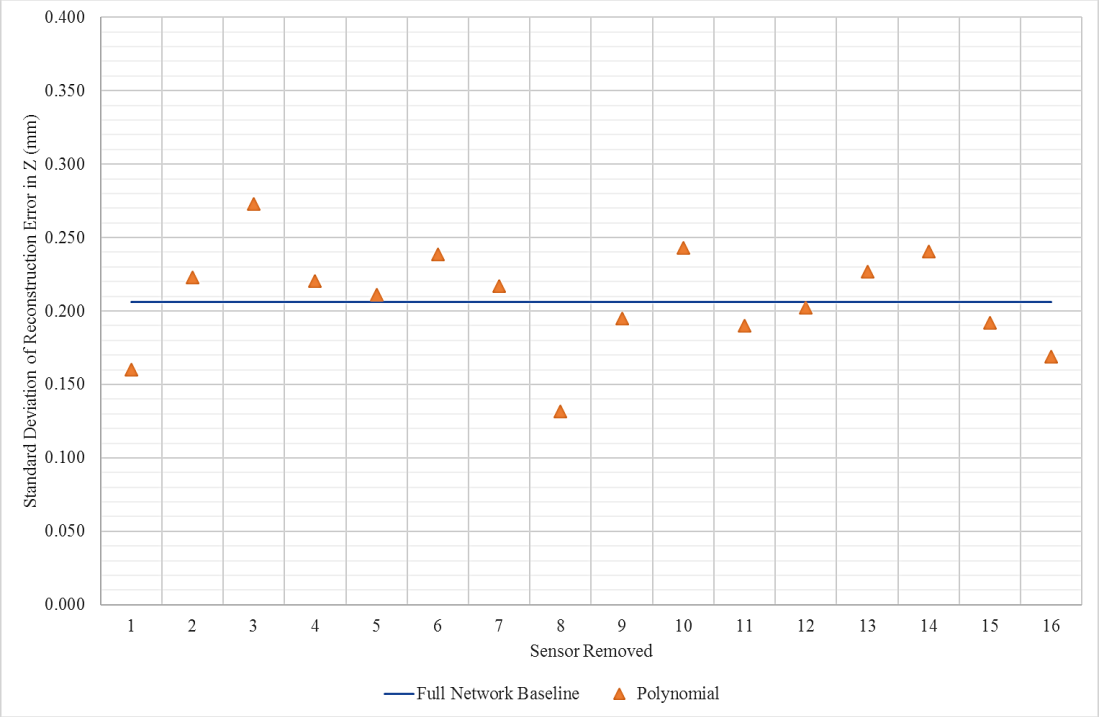

Figure 42. Results of naïve 16-sensor network performance as sensors removed with polynomial reconstruction.

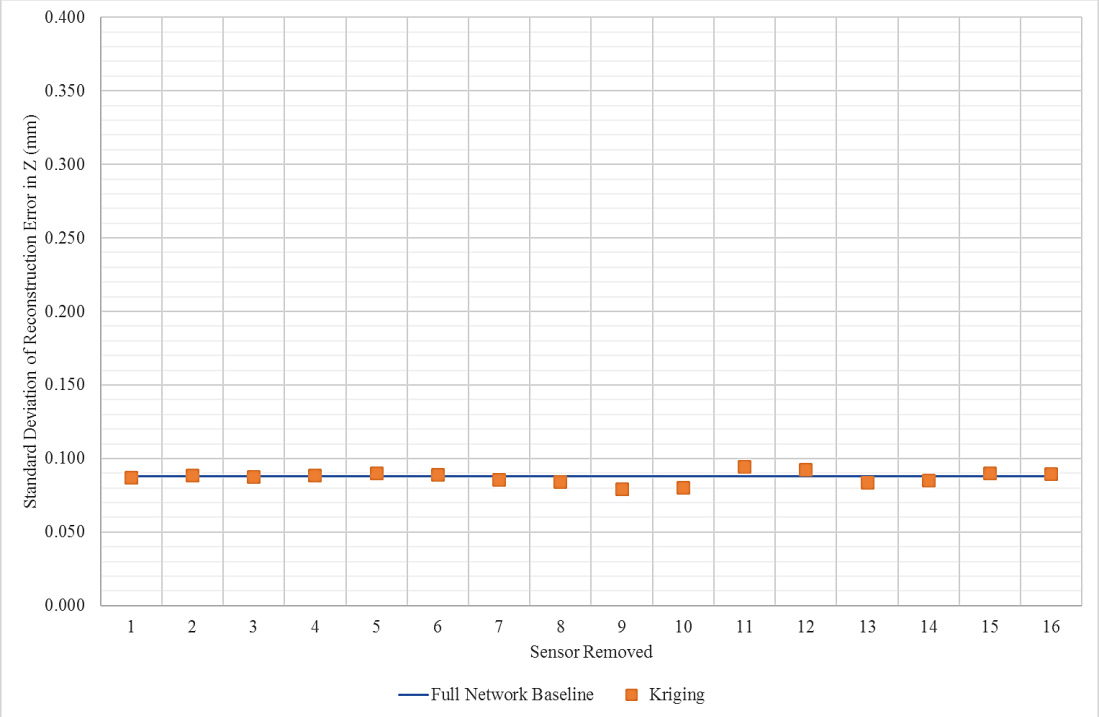

Figure 43. Results of naïve 16-sensor network performance as sensors removed with Kriging reconstruction.

5.8.3 Naïve 32 Sensor Network with Sequential Removal

Removing sensors from the 32-sensor network revealed similar trends for both the polynomial and Kriging reconstruction methods, as shown in Figure 44 and Figure 45. With polynomial reconstruction, there was again a significant improvement over the 16-sensor network. For Kriging, however, the overall performance of the sensor network got worse when 32 sensors were used rather than 16.

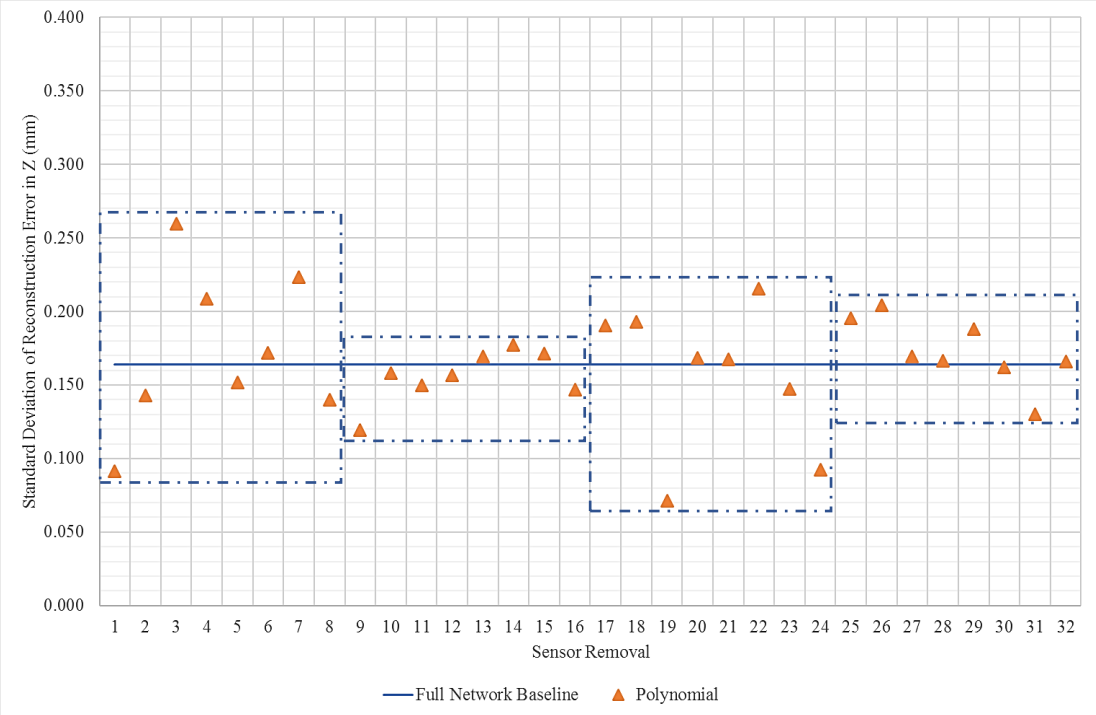

Figure 44. Results of naïve 32 sensor network performance as sensors removed with polynomial reconstruction

The way that sensors have been added to the network in the case means that there are discernible ‘clusters’ in the results. The first 8 sensors, for example, defined sensors at each of the vertices of the measurement volume, while the second group of 8 sensors added sensors at intermediate mid points in the Z-axis. Looking at the sensor network in terms of these ‘clusters’ as annotated with dash-dot boxes, it appears that the first and third sensor clusters added are more impactful than the second and fourth clusters. The third sensor cluster is in fact related to the first cluster, in the sense that they occupy positions at the top and bottom of the measurement volume, but instead are positioned at the mid-points rather than the vertices.

The Kriging sensitivity to removal has reduced further, to the point where removal of a sensor makes very little difference. Now that clusters have been identified in the polynomial reconstruction results, it is clear now that the same clusters exist in the Kriging network. The final 8 sensors added to the network appear to deliver the most impact to the network, as

shown in Figure 45. It seems there is a limit to the performance of the Kriging reconstruction method when using this magnitude of number of sensors.

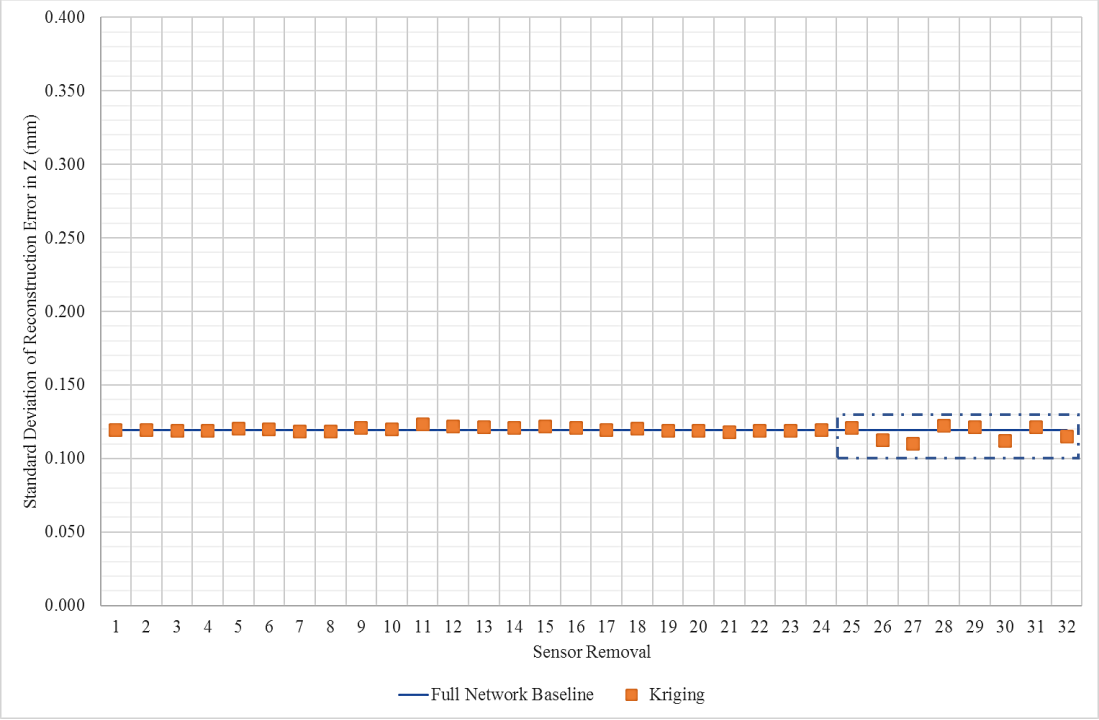

Figure 45. Results of naïve 32 sensor network performance as sensors removed with Kriging reconstruction.

5.9 Chapter 5 – Summary

Chapter 5 provided:

- Generation of naive temperature sensor networks to compare against, which are based upon arbitrary spacing.
- Description of the different temperature distributions used with increasing complexity.
- Computational experiments that show how temperature sensor network performance can be estimated and compared.
- Comparison of:
    - Number of sensors;
    - Reconstruction methods;
    - Effect of sensor uncertainty;
    - Effect of removal of individual sensors.

Contributions:

- Estimation of temperature sensor network performance;
- Estimation of thermal expansion contribution to measurement error;

The temperature measurement planning tool can be used to estimate temperature sensor network performance for a range of defined scenarios, including consideration of sensor uncertainty.

---

6 Case Study: Barrel Section Assembly

Assembly: the final challenge. Now that the tool can run a battery of tests to determine sensor network performance, do the tests hold up to more complex representative geometry? And what can we learn from their application? This chapter seeks to answer these questions and get more in-depth learning about how the tool can be used for industrial applications for planning temperature sensor networks.

In addition to the tests done in the previous chapter, optimisation has been included in Chapter 6 to iteratively compare different types of sensor network and go beyond manual definitions. The main activities in this chapter from the methodology can be seen in Figure 46. The previous results also focused on variations on the steady state case, but a lot could be learned by generating a temperature distribution and varying this over time. Each new case brings new lessons, which challenges the up-front approach to defining sensor networks based upon rules. Are there any rules or are all measurement tasks completely unique? It was decided that it would be more beneficial to explore, rather than prescribe.

The majority of this chapter has been submitted to be published in a journal article at the time of writing [127].

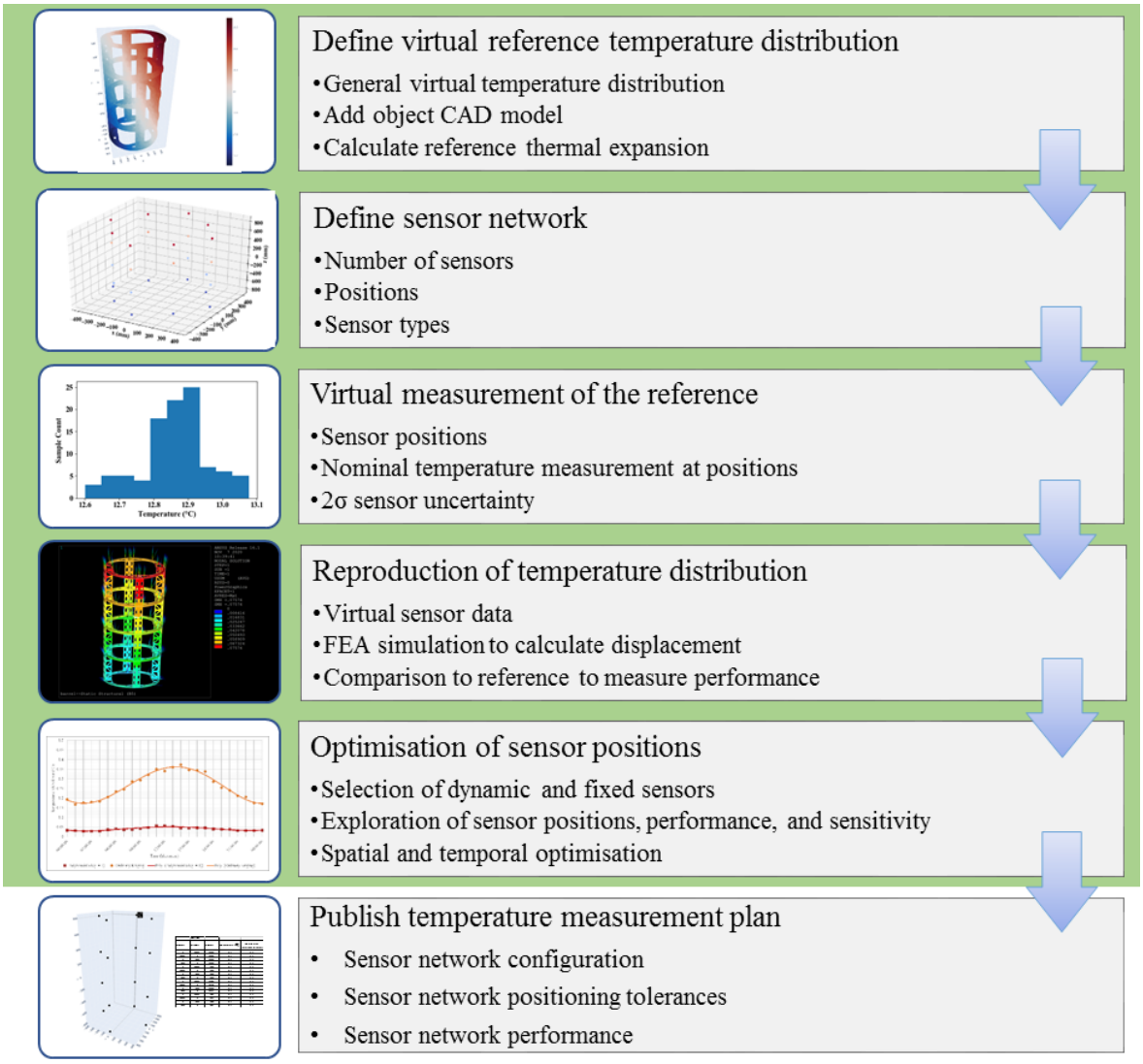

Figure 46. Temperature measurement planning methodology, highlighting activities in Chapter 6 to introduce optimisation.

6.1 Generated Temperature Distribution

A specific measurement scenario has been selected as a case study, using far more complex geometry but at a smaller scale. The assembly of barrel sections is a 1.6 m tall structure made of aluminium 6061 alloy is comprised of 40 parts. The temperature distribution was fixed to illustrate how the temperature sensor network planning tool could be used for a given scenario.

The following function was used to generate the temperature distribution from -400 to 400 mm in x and y, and -800 to 800 mm in the z axis.

Equation 11

$$T = 18 + (3 \times 10^{-7})x^3 + 0.5y + (3 \times 10^{13})y^4 + 1.3z - (3 \times 10^{-13})z^5$$

As can be seen in **Error! Reference source not found.**, the thermal gradient is particularly e vident in the Z axis, followed by the Y and X axes respectively. The temperature differences are subtle, but in line with what might be observed in a factory environment. The average

temperature of the structure in this scenario is below standard 20°C, so there is a net contraction.

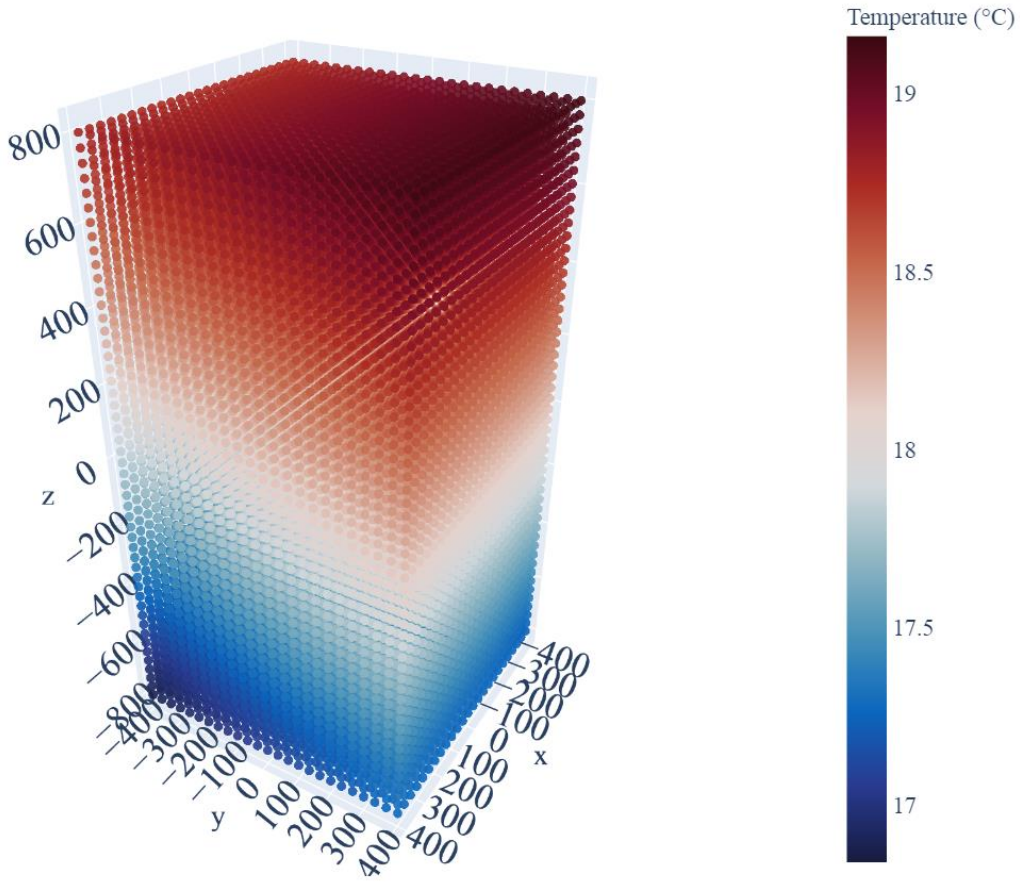

Figure 47. Colour plot of the generated temperature distribution for the case study.

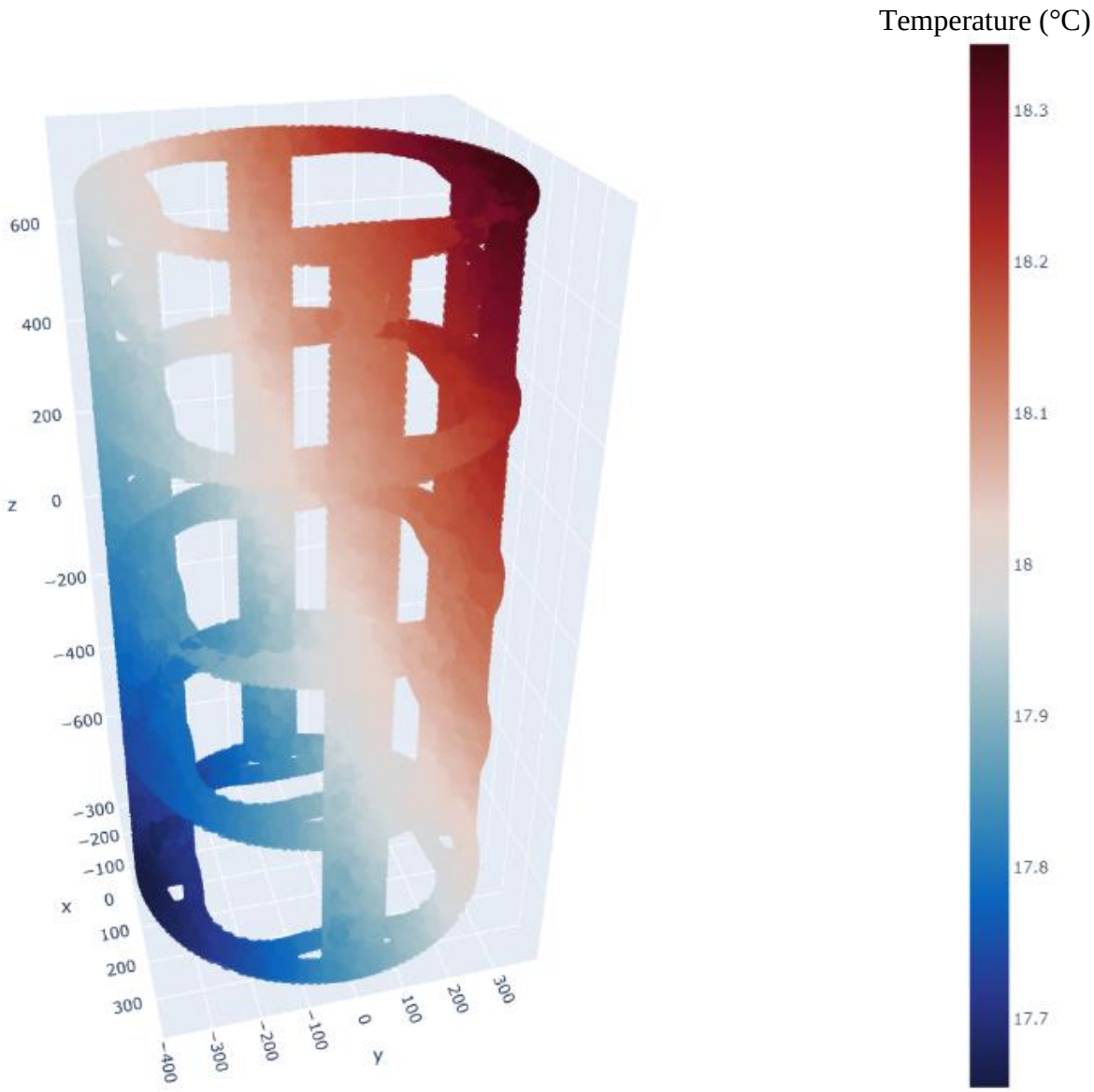

Figure 48. Generated temperature distribution as applied to the barrel section assembly as boundary conditions.

6.2 Finite Element Model

The finite element analysis performed on the structure was rudimentary to provide a very rapid calculation of thermal expansion over the structure. A static structural analysis was set up, and the temperature boundary conditions were updated automatically using the planning tool, based upon the generated temperature distribution. 135411 nodes were used in the model, and the structure was supported at the base. Gravity was not applied in this case so as not to dominate the effects of thermal deformation. All the displacements appear relative to the global coordinate system whose origin is in the centre of the structure as illustrated in Figure 49. Figure 50 shows the simulated contraction of the structure under the applied, temperature distribution below standard temperature.

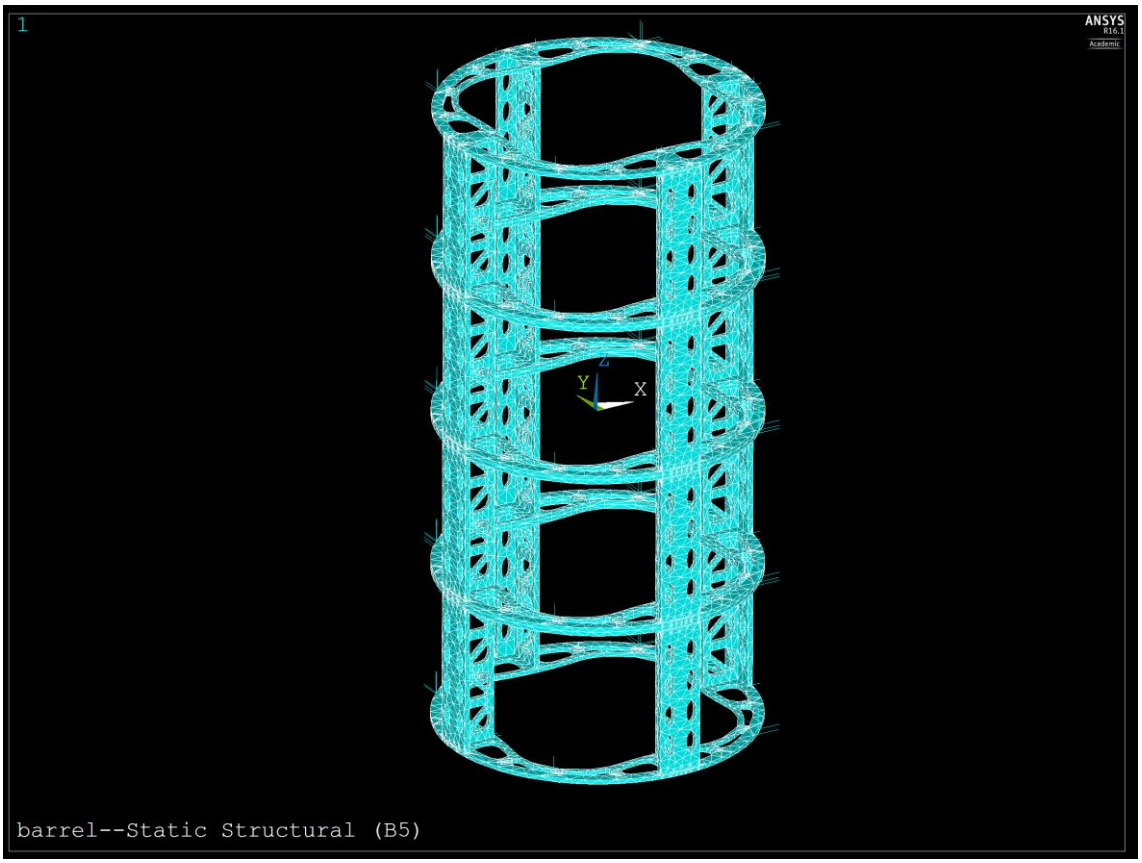

Figure 49. Screenshot showing the undeformed barrel section assembly in ANSYS APDL FEA environment

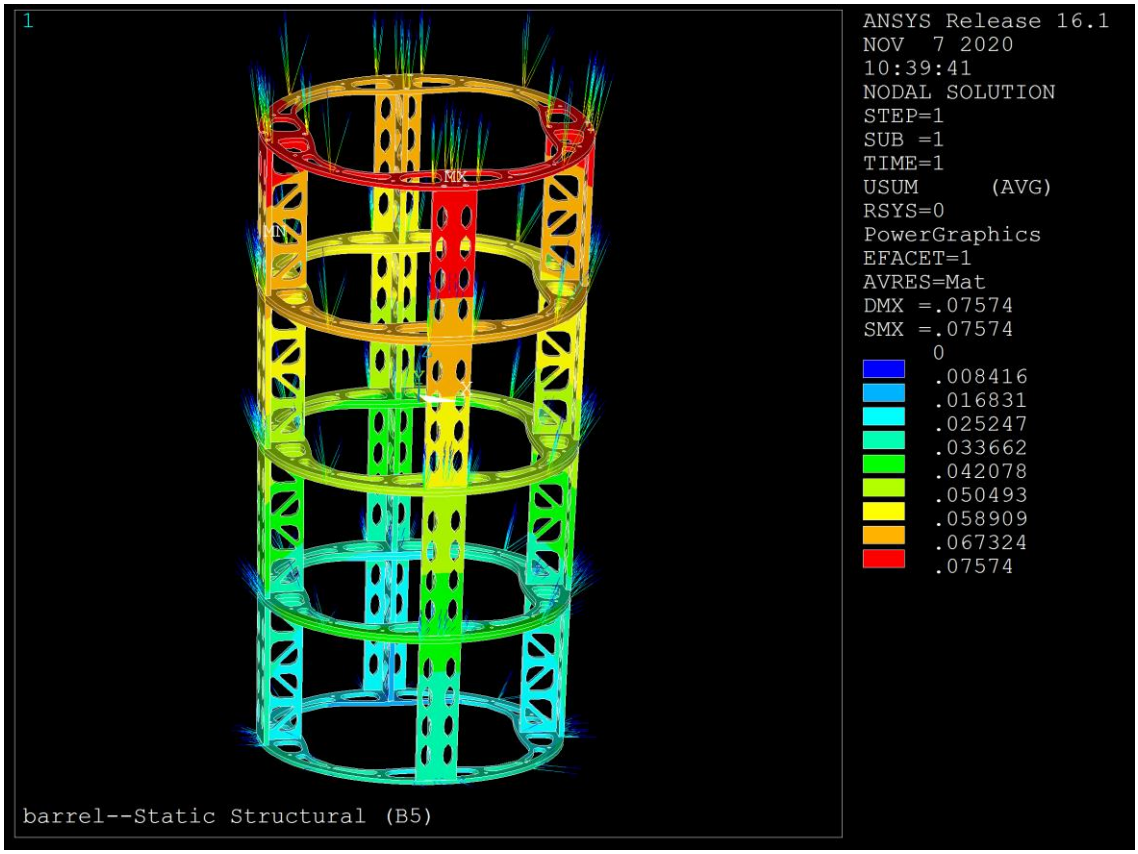

Figure 50. Colour plot showing static structural results and thermal contraction in mm after the generated temperature distribution is applied.

6.3 Number of Sensors

Determination of the optimal number of sensors was carried out initially as more sensors are not necessarily better for performance and have a cost implication. Each of the sensor networks was a subset of the 32-sensor naïve network shown in Figure 52.

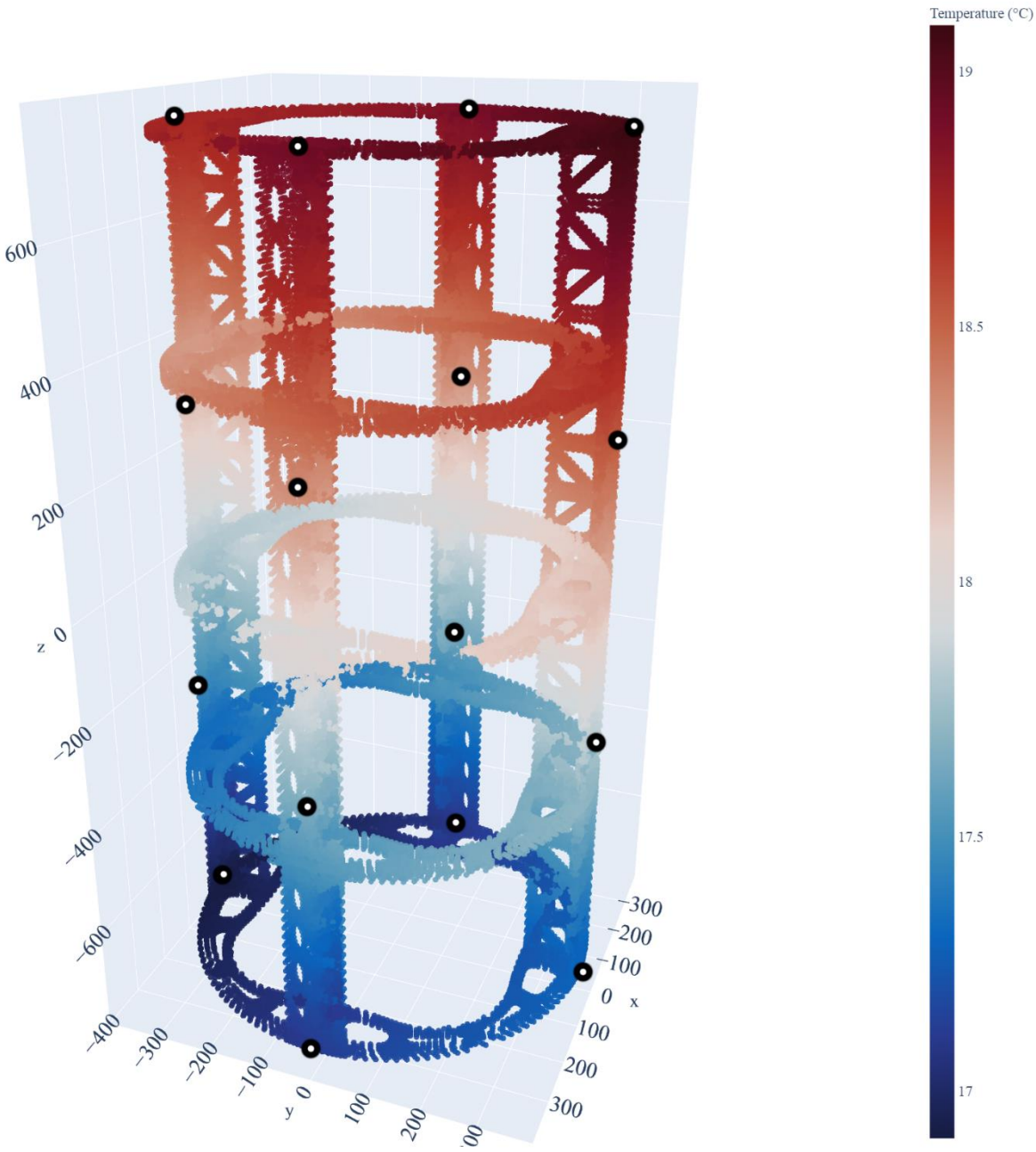

Figure 51. Plot showing 16 sensor naïve network positions in context of the temperature distribution as applied to the structure.

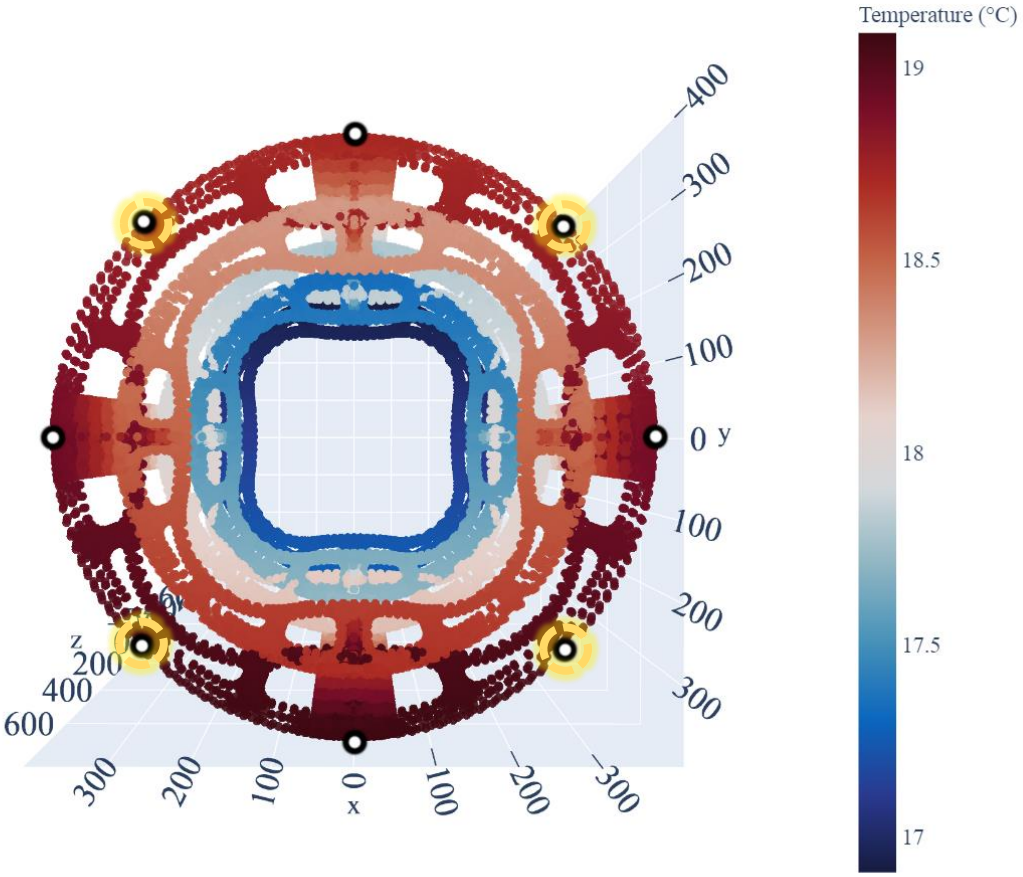

Figure 52. Plot showing additional positions used in the 32-sensor network in X and Y from the top view of the structure.

During these tests the same reconstruction methods of polynomial and Kriging were used. In this case, Kriging was outperformed by polynomial fitting for all cases except 4 sensors. For 8, 16, and 32 sensors, polynomial reconstruction was comparatively good. The best results appeared to come in general from 16 sensors, but as can be seen in Figure 53 and Figure 54 the results showed diminishing returns after 8 sensors. At this stage, the 16-sensor network was selected for further testing and optimisation.

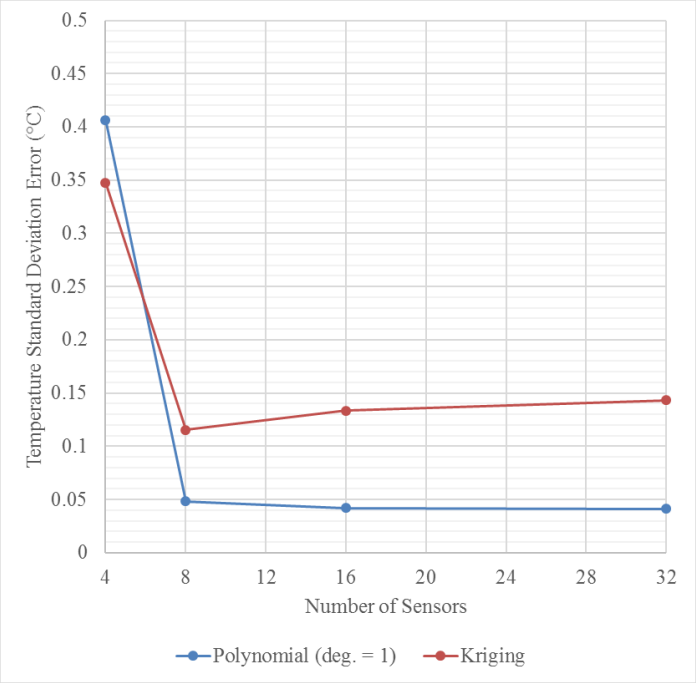

Figure 53. Comparison of temperature distribution reconstruction using different numbers of sensors

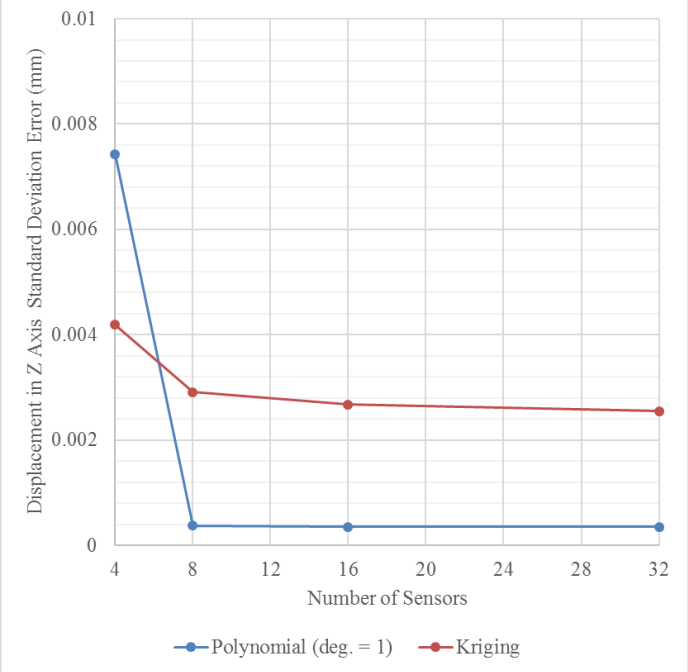

Figure 54. Comparison of vertical displacement when using different numbers of sensors for reconstruction

6.4 Sensors with Simulated Uncertainty

There is no such thing as a perfect measurement and all measurements have inherent uncertainty. To simulate this, pseudo-randomness was introduced to the virtual measurements using a normal distribution. Uncertainties were applied to individual sensors of 0, 0.5, 1, and

2 °C during the virtual measurements. As it is good practice to repeat measurements several times to reduce the effects of random error, the simulation generated 10 virtual measurement samples and the mean average was taken to be used for reconstruction. The objective was to compare the individual uncertainty to the standard deviation of the error in the reconstructed temperature distribution. In this case, this produced the results that can be seen in Figure 55. The results for the higher uncertainty sensors was not as proportional as might be expected. An uncertainty of 0.1 °C was shown to produce the lowest reconstruction error as expected, but the different between the 0.1 °C and the 0.5 °C or 1 °C is not that large – in some cases other factors such as cost may be able to inform this decision, depending upon the requirements of the product and the required thermal compensation performance. To achieve the best results going forward the 0.1 °C uncertainty sensors were selected for further optimisation.

In each scenario the first-degree polynomial reconstruction outperformed the Kriging reconstruction. In Figure 55 and Figure 56, the reconstruction methods track fairly closely when 8 and 16 sensors are used. In Figure 57, the difference between the two reconstruction methods diverges as sensor uncertainty increases. It is thought that the tendency of Kriging towards local autocorrelation is contributing to this effect. In Kriging, measurements taken near to each other are more likely to agree. In this case this could be described using the analogy of a group of people taking measurements of a bolt diameter using a micrometer. Instead of totally trusting their own measurement, they're being influenced by their neighbours' measurements. The more this happens as nearby sensors are added, the more the error propagates through the group, further increasing the overall sensor network error. Once the pseudo-random sensor error is increased, this effect amplifies even further so that when one measurement sample has a lot of error, the error compounds.

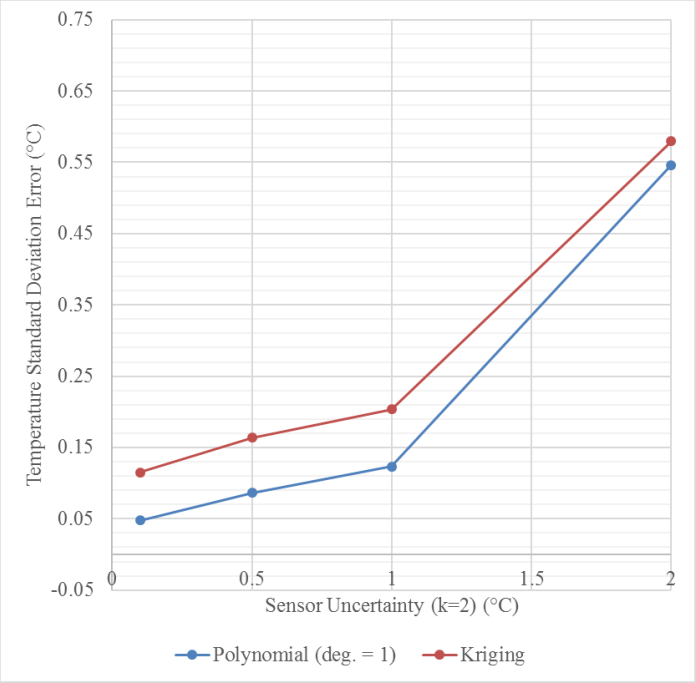

Figure 55. Comparison of temperature distribution reconstruction methods using repeated measurements from the 8-sensor naïve network with pseudo-random uncertainty applied.

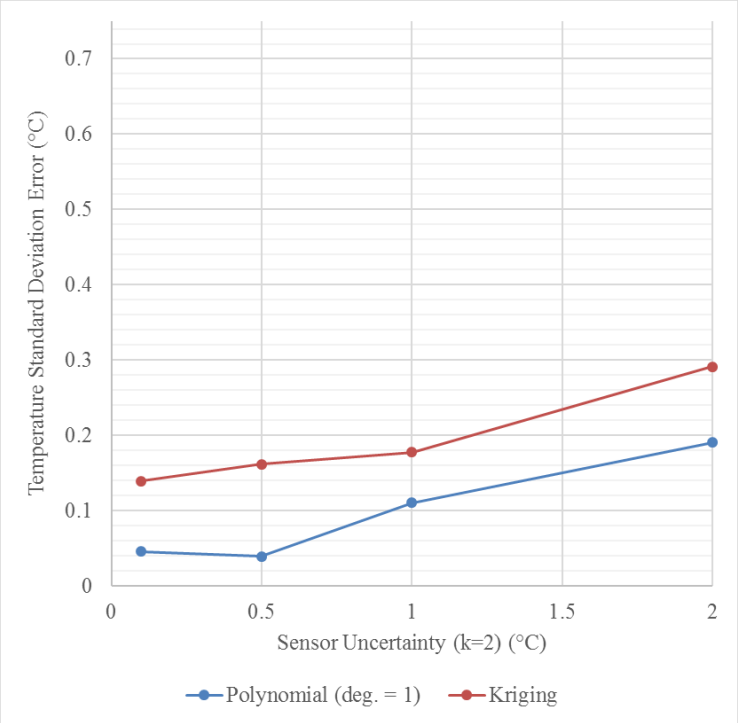

Figure 56. Comparison of temperature distribution reconstruction methods using repeated measurements from 16-sensor naïve network with pseudo-random uncertainty applied.

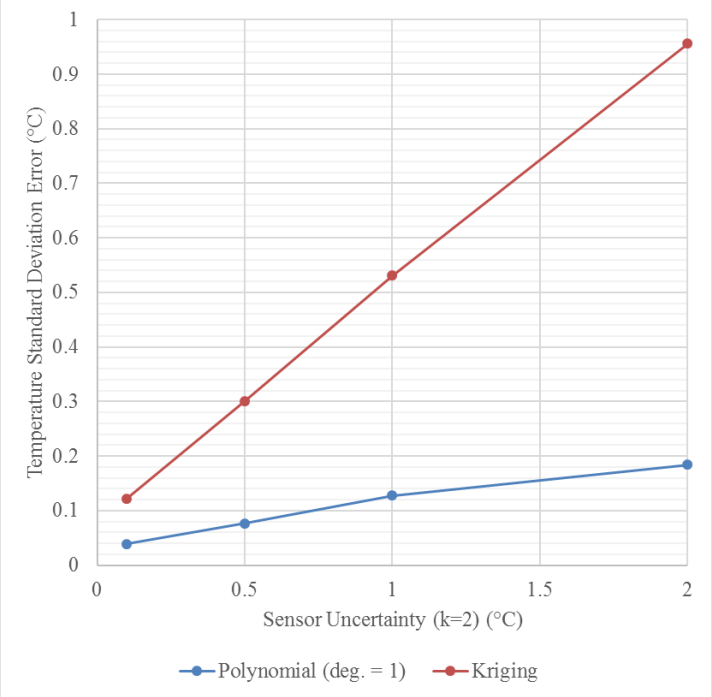

Figure 57. Comparison of temperature distribution reconstruction methods using repeated measurements from 32 sensor naïve network with pseudo-random uncertainty applied.

6.5 Position Optimisation

6.5.1 Random Search

Optimising the position of the sensor networks was carried out using the random search method. At this point, the exploratory approach was favoured to provide more learning as there weren't any heuristics that had been generated and proven to work. Each iteration of the optimisation represented a different configuration, so as the number of iterations increased, the greater the number of possible configurations can be explored.

The 16-sensor naïve network is based on the only heuristics that have so far been used, which are to: optimise coverage at the boundaries of the assembly; and to spread them at regular intervals. Knowing the temperature at the boundaries of the assembly is a reasonable heuristic to keep based upon interpolation being preferable to extrapolation. Regularly spaced sensors however should be challenged since the temperature distribution may not be regular, and different geometries will have different coverage requirements.

Eight of the positions that measure the temperature at the boundaries at the top and bottom were retained as fixed points. For the optimisation, the other 8 points were designated as dynamic points, that can change position after each iteration. To better understand the dominating vertical thermal gradient, the 8 dynamic sensors were constrained to move up and down in a uniform distribution ±125 mm from their initial position as defined in the 16-sensor naïve network: 4 sensors at 266.67 mm and 4 sensors at -266.67 mm. A diagram showing the initial positions of the sensors on the structure with the temperature distribution can be seen in Figure 58. Over the random search of 250 iterations, the positions occupied by the dynamic sensors can be seen in Figure 59. At each iteration, standard deviation error and RMS metrics were captured. The error in reconstruction is used to show how accurately the temperature sensor configuration measures the temperature distribution compared to the reference distribution. At this stage no FEA was carried out as the FEA provides the structural displacements, and the optimisation focused on the temperature distribution.

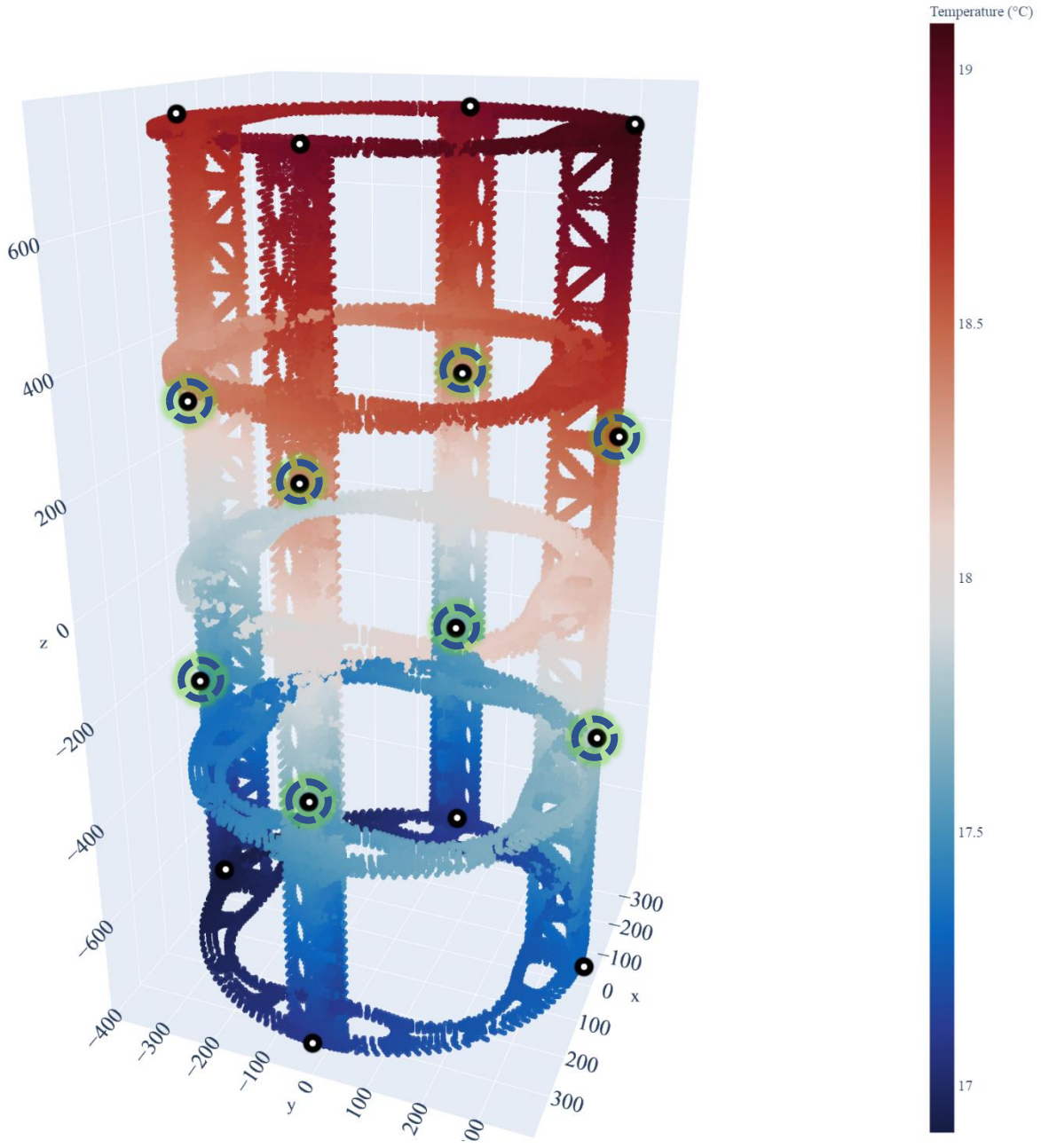

Figure 58. Diagram showing the positions of sensors in the 16-sensor network and highlighting the 8 dynamic sensors in the middle that were used in the optimisation.

6.5.2 Reference Optimisation – No Uncertainty

Running the optimisation without uncertainty provided some insights about which positions are most likely to produce more favourable results without the element of good fortune. A top ten sensor configurations list can be seen in Figure 60, which runs left to right in order of best to worst performance. From this figure it is clear that having the sensors at different heights is favourable. The separation distance between the top set of sensors also appears to be more consistent than the bottom sensors, which appear to be more variable and more able to tolerate a larger sensor spread. One way to compare the sensors was to see whether their position

correlates to any of the performance metrics, as shown in Figure 61. Weak correlation can be observed between the polynomial reconstruction, most notably on four of the sensors (9, 11, 13, and 15), which may mean these are the sensors driving the results most. Kriging reconstruction appears to have no, or extremely weak correlation to sensor height, which could be useful for certain applications.

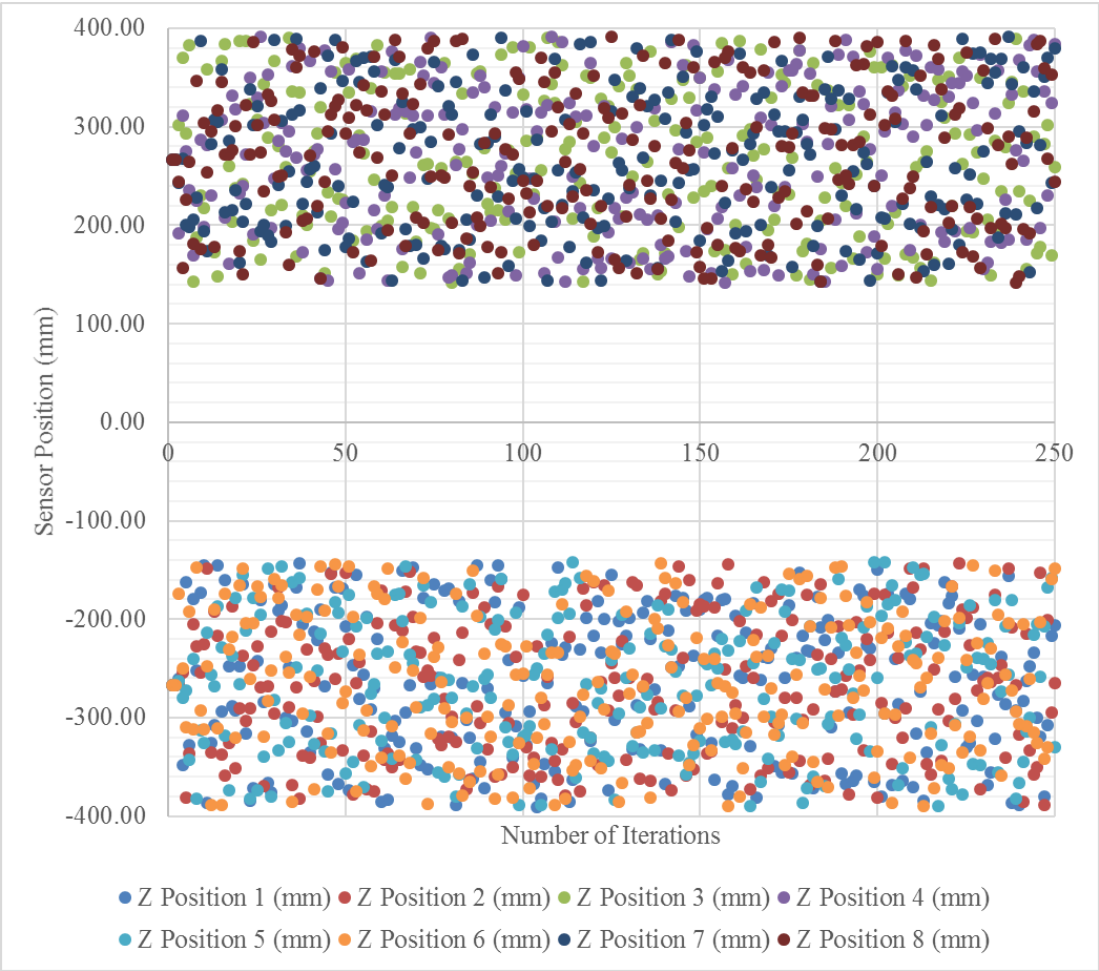

Figure 59. Scatter plot showing the random search positions of the 8 dynamic sensors over 250 iterations.

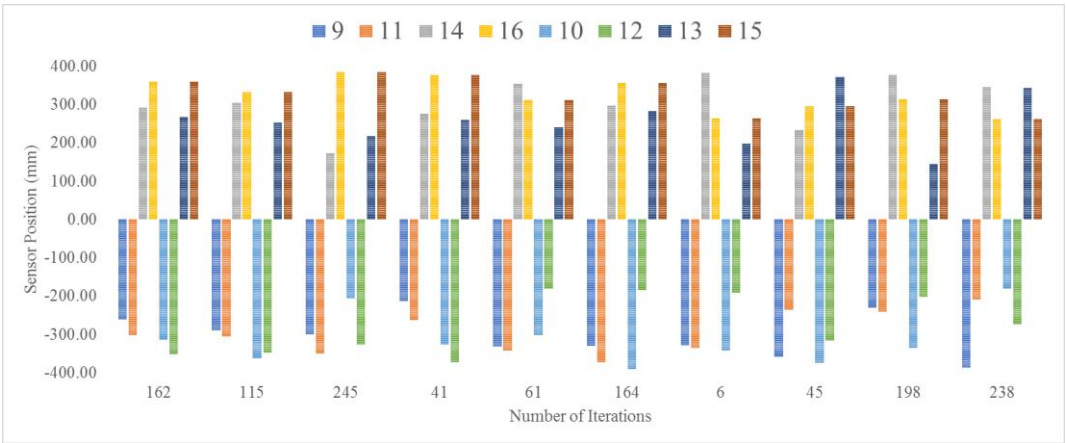

Figure 60. Column chart showing the positions that produced the top 10 results in the random search optimisation.

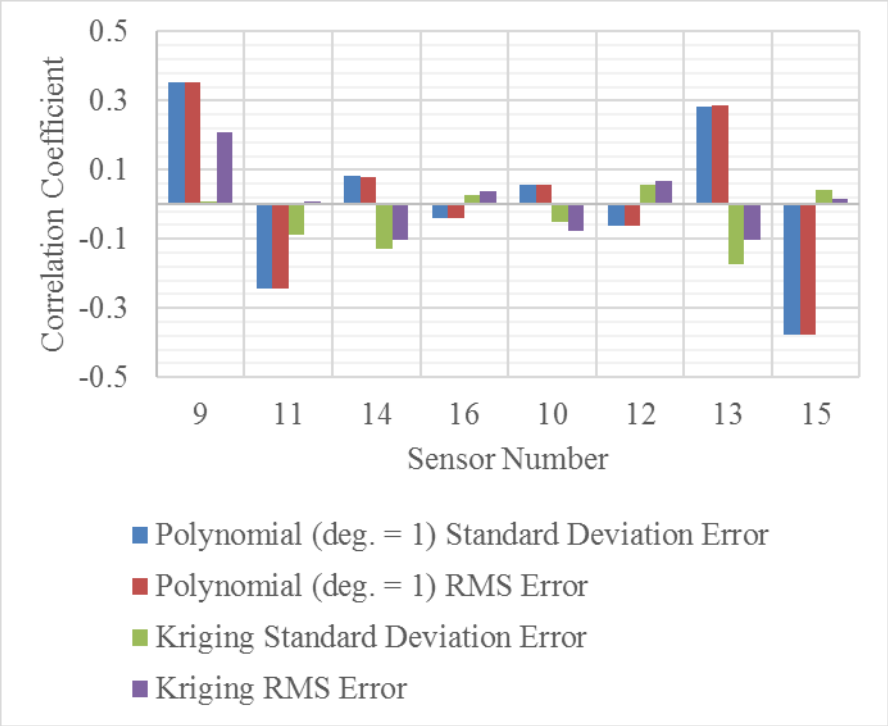

Figure 61. Comparison of sensor position correlation to sensor network performance metrics. The standard deviation error and the RMS error of the reconstructed temperature distribution are relative to the reference.

6.5.3 Reconstruction Comparison

The results up to this point have presented the first-degree polynomial and the OK reconstruction methods, but the other degree polynomial reconstructions have also been tested. Comparing the reconstructions reveals that the most consistent results in this case come from the first-degree polynomial reconstruction. This is also the most straightforward to implement for measurement operators as it can easily be checked, so is preferable and should be the reconstruction method of choice. OK leads to larger and more variable errors in this application.

The performance of OK was somewhat disappointing, as on the battery of tests carried out in Chapter 5, OK performed better than polynomial fitting in general. The geometry in question is an important factor. The cuboidal beam used in Chapter 5 had a 1:10 aspect ratio, compared to ~ 1:4 for the barrel sections. Kriging has some characteristics that may explain its limitations here. Kriging's tendency towards spatial autocorrelation assumes that near points are like points, which means that temperature gradients could be smoothed out more than in reality. Equation 5 (Section 2.6.3) describes OK and shows one of the terms, $\mu(u)$, represents the mean value, which is used as part of the estimate. In some distributions the average temperature will be useful and misleading in others. On the other hand, as can be seen in this Chapter, is that polynomial reconstruction is more sensitive to sensor positioning, but in Chapter 5, only fixed naïve networks were tested.

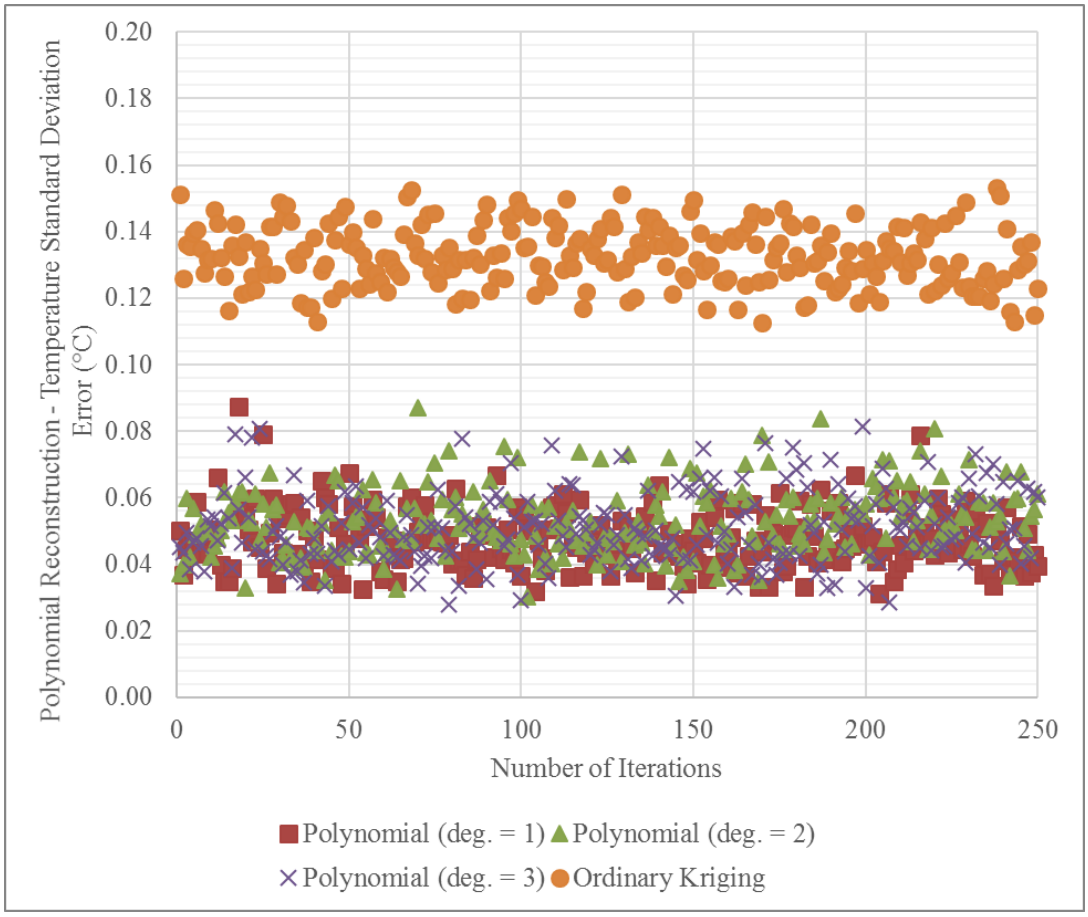

Figure 62. Scatter plot comparing reconstruction methods over 250 iterations

6.5.4 Optimal Network Performance

After determining the optimal sensor network for 16 0.1 °C sensors using a first-degree polynomial reconstruction, the positions were recorded and used for further performance testing. The optimal sensor positions can be found in Table 21.

Table 21. Optimal sensor heights

Sensor ID	Z Position (mm)
9	-259.76
10	-314.15
11	-300.39
12	-351.40
13	266.78
14	291.09
15	359.99
16	341.46

The sensor network should exhibit low error, repeatably. The RMS error was captured over 250 iterations and can be seen in the histogram in Figure 63.

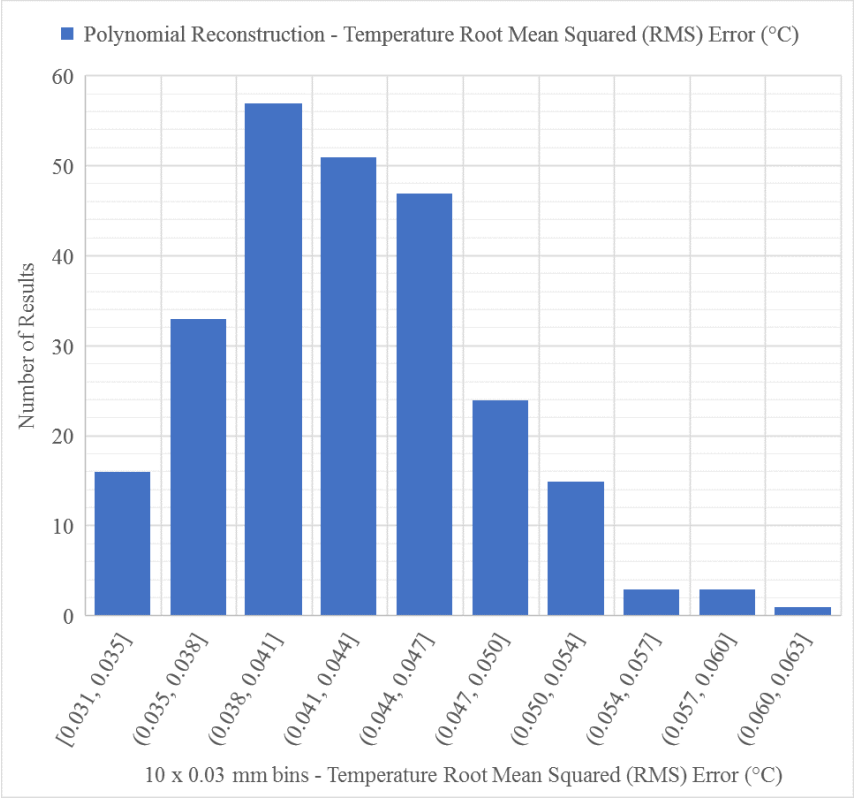

Figure 63. Histogram of optimal sensor network performance over 250 repeats

When the temperature distribution is reconstructed using this sensor network, the resulting errors on the barrel section assembly's temperature distribution can be seen in Figure 64. The errors on the interactive plot appear to be within ±0.08 C.

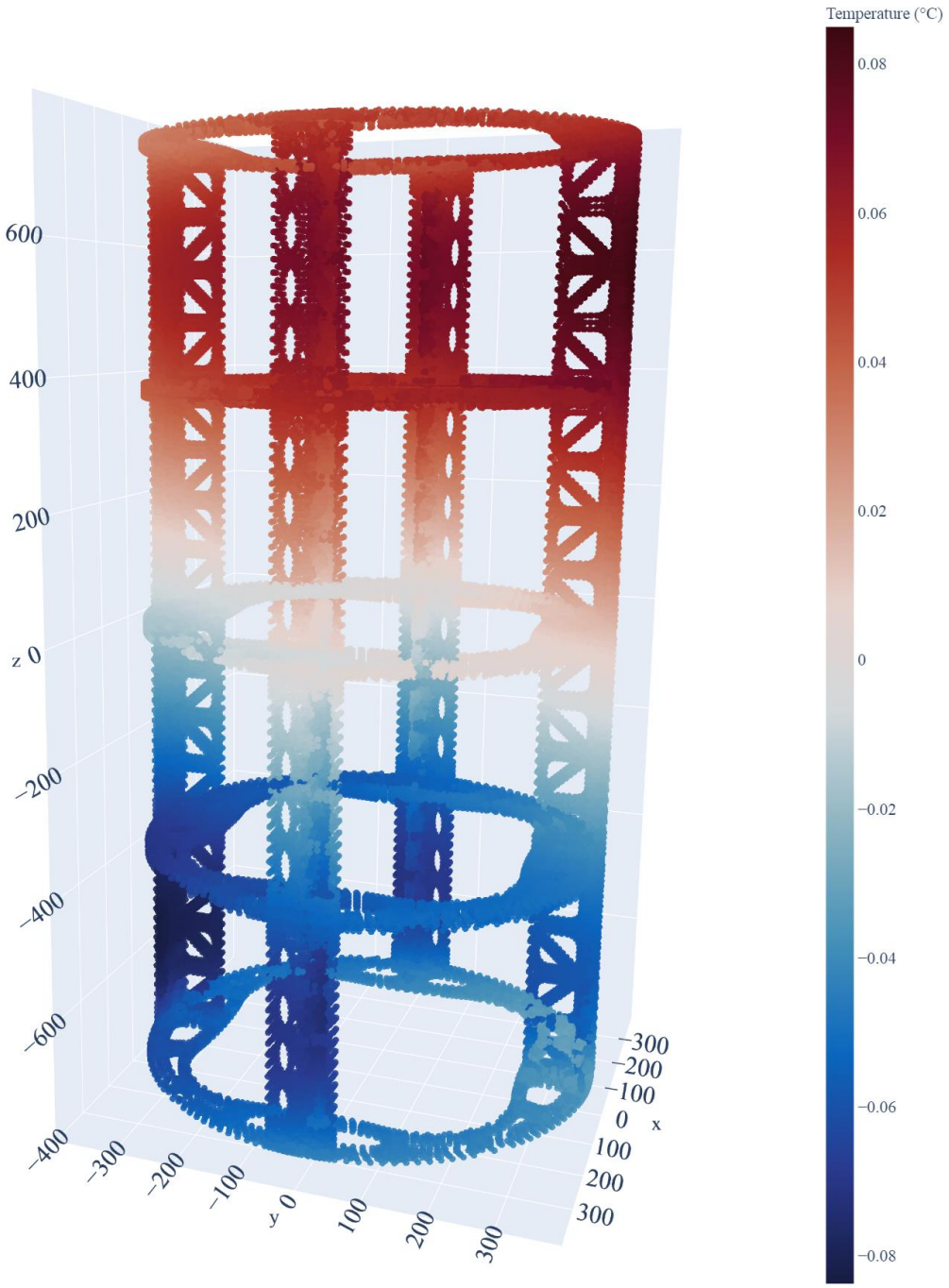

Figure 64. Colour plot showing the temperature distribution reconstruction error across the barrel section assembly for the optimal sensor network

6.5.5 Individual Sensor Influence

In everyday operation there may be times when individual sensors must be removed or fail. The temperature sensor position planning tool facilitates the running of such what-if scenarios against the usual metrics to determine which sensors are most critical in the network. As can be seen in Figure 65, the full sensor network with no sensors removed can provide an RMS error of below 0.04 °C, which increases significantly when individual sensors are removed

from the network. The first 8 sensors – which were fixed during optimisation – appear to be most critical to the network, with RMS rising to around 0.1 °C when they are removed. The other sensors exhibit around half the impact of the fixed sensors and are more variable in their contribution. Here it can be seen that 12 and 15 have the greatest impact of the dynamic sensors when removed. Results for standard deviation are closely correlated to RMS and can be seen in Figure 66.

Figure 65. Column chart comparing the RMS error of the reconstruction when each of the individual sensors are removed (red) to the reference full network performance (green).

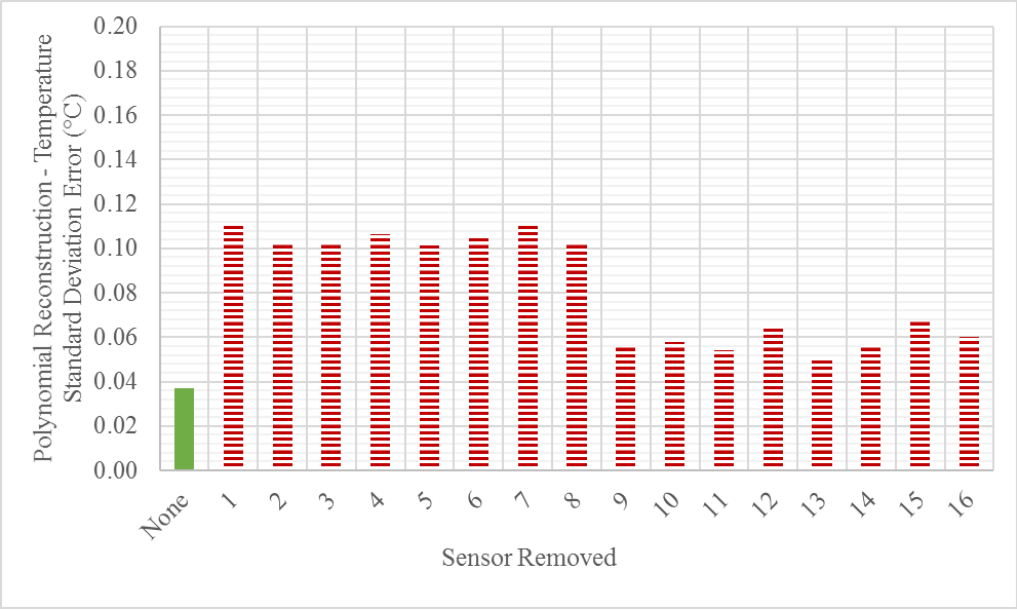

Figure 66. Column chart comparing the standard deviation error of the reconstruction when each of the individual sensors are removed (red) to the reference full network performance (green).

Prescribing a sensor network specification necessarily needs tolerances in order to realise simulated performance, whilst also being achievable in practice. Technically it may be possible to position sensors very accurately within 1 mm, but this would add significant time and cost to the operation. Three temperature sensor positioning errors were tested to determine what might be reasonable positional tolerances for operators to achieve in a production environment:

±10, 25, and 50 mm. As these are intended to be random errors, they are generated using a normal distribution about the original position. The boundaries were limited, so that they cannot go beyond the bounding box, but can approach it. The results of the positioning error experiment can be seen in Figure 67. As would be the case in practice, positioning errors have been applied to all of the sensors in the network, including positions that were fixed for the purposes of the optimisation. The histograms on the left provide a visual comparison to illustrate how the shape of the distribution of results changes with positioning error.

At the lowest positioning error of 10 mm it is clearly the most repeatable of the three tolerances as expected. The interesting result here related back to the fixed points that were shown to make a relatively large impact on the overall sensor network. When these positions were allowed to move, they produced better results than the previous optimal sensor network and returning consistently lower RMS error values. This is useful and actionable knowledge, which in turn will lead to the specification of a sensor network that performs much better than a sensor network that has been specified without testing.

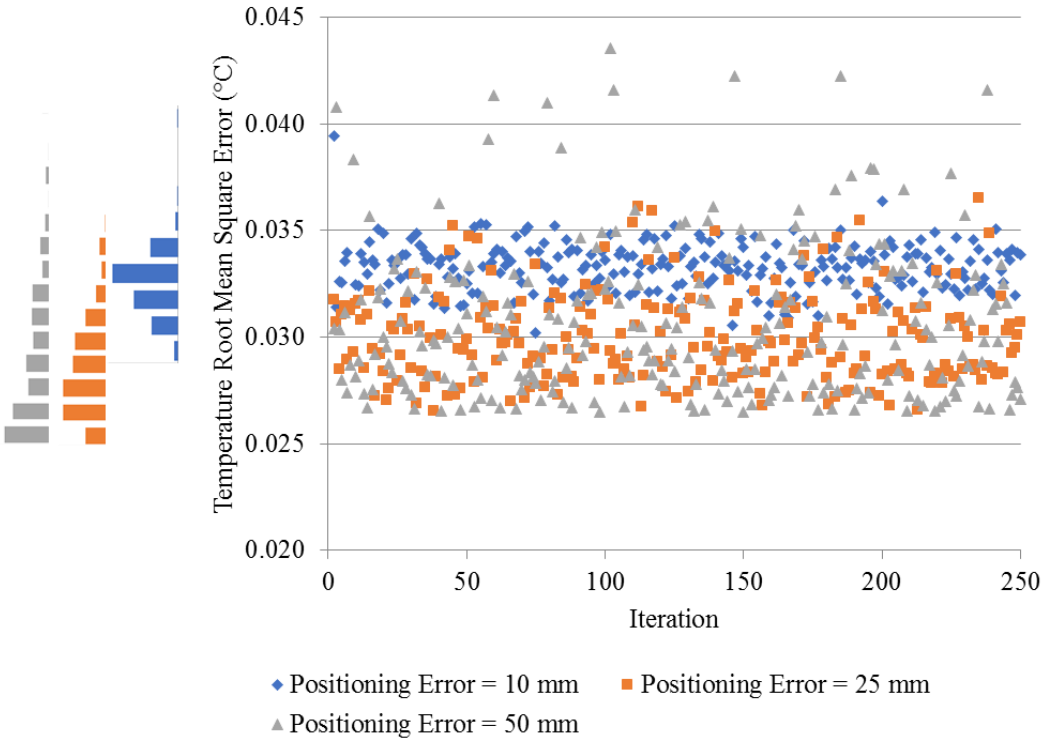

Figure 67. Scatter plot comparing the RMS error of the reconstruction when sensor positioning error is simulated with associated histograms for qualitative comparison.

6.6 Transient Analysis

How can the performance of a given sensor network designed in a steady state condition be predicted for temperature variation over time? Understanding a representative static temperature distribution is the first stage of temperature sensor network design. Many environments will tend to display similar looking temperature distributions in qualitative terms, despite being different absolute temperatures. This is usually because spaces will often

contain the same heat sources and sinks, and the geometry of the volume will remain largely constant.

A large amount of temperature variation occurs over time and can add a significant amount of complexity. In this case, rather than optimising for transience, the optimal temperature sensor network based on a representative static has been tested to see how well it performs over time.

6.6.1 Transient Temperature Distribution

A transient temperature distribution was generated using a cosine wave formula that changed two of the static temperature distribution coefficients over time. The c0 coefficient (during static analysis, c0 = 18) was used to change the constant temperature value over time, and the c1 coefficient (during static analysis, c1 = 1.3) was used to alter the linear vertical gradient over time. Measurements taken over several days of large structures in assembly environments inspired the decision to have oscillating base temperature and changing thermal gradients. Figure 68 shows the temperature distribution over a 24-hour period. The peak temperature occurs around 13:00, and at that time the thermal gradient is also most pronounced. Based on knowledge from previous tests, distributions with larger thermal gradients tend to be more difficult to reproduce.

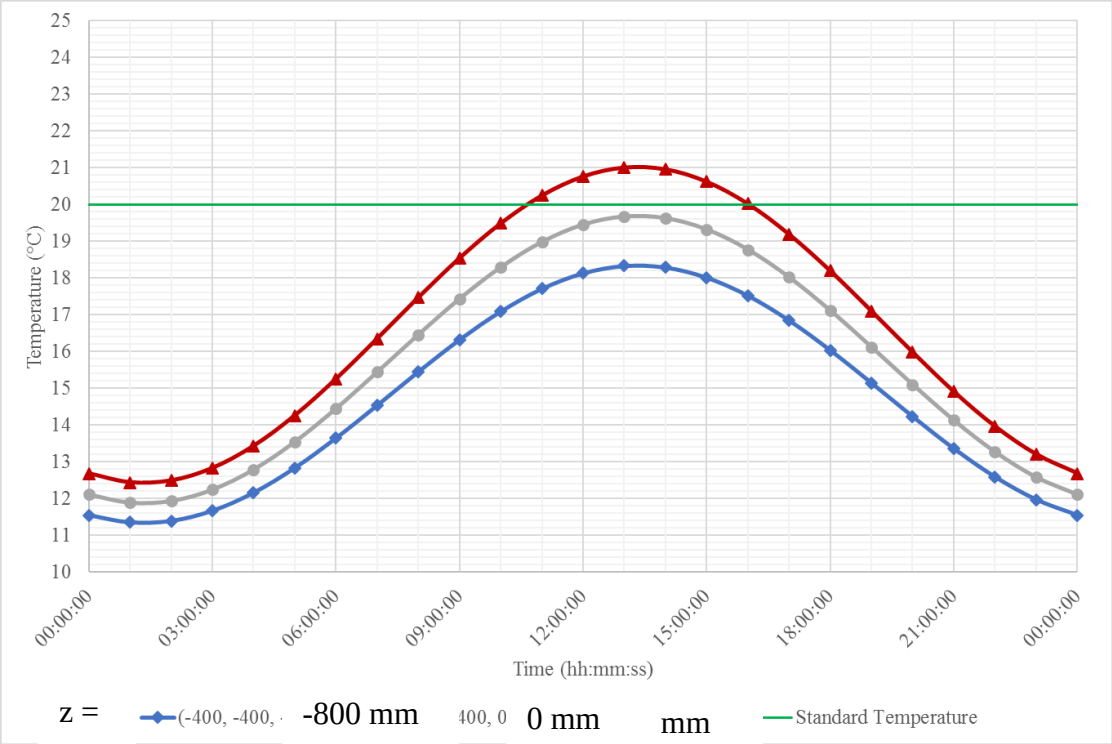

Figure 68. Generated reference temperature distribution over a 24-hour period, showing the temperature at the top, middle, and bottom at x, y = (-400, -400).

6.6.2 Transient Performance Test without Uncertainty

Initial tests were carried out to provide a reference for how well the sensor network performs at each time of day without the presence of temperature sensor uncertainty. Results for the temperature distribution reconstruction can be seen in Figure 69 and Figure 70. The performance of the temperature sensor network is negatively correlated with the complexity of the temperature distribution over time. The effect of complexity is more powerful than the relationship between the conditions for which the temperature sensor network was optimised. Despite the sensor network being optimised in conditions more representative of the morning, which is relatively warm, the network applied to colder conditions with a smaller thermal gradient produce better results, nonetheless. There is again a marked different between the performance of OK reconstruction and linear fitting. The linear polynomial fit has much lower standard deviation and RMS, whilst also being relatively stable over time.

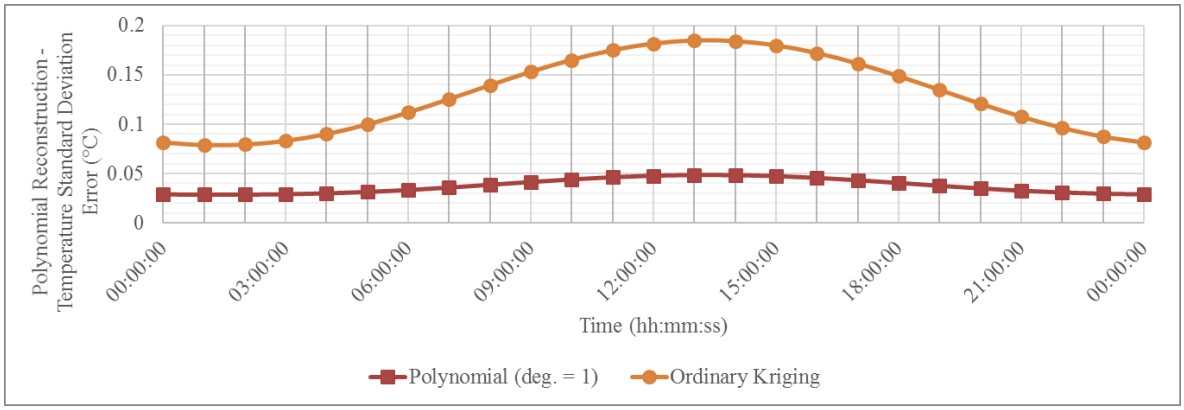

Figure 69. Scatter plot comparing the standard deviation error in temperature of the sensor network with polynomial and kriging reconstruction over 24 hours.

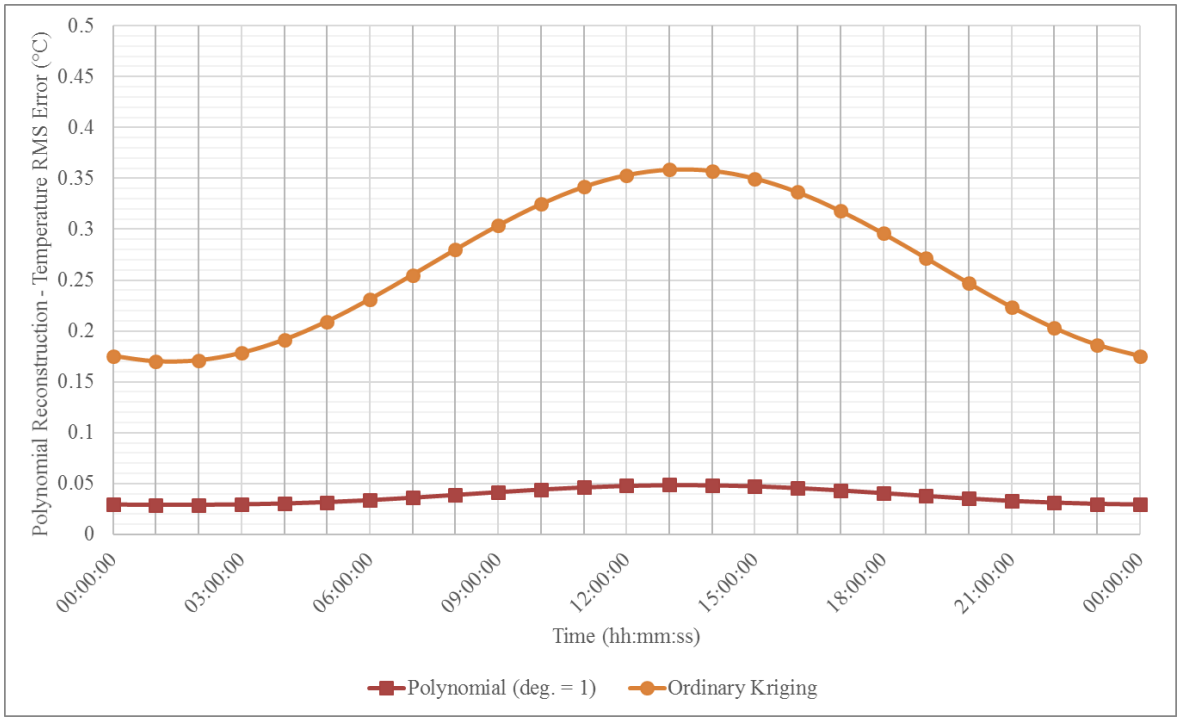

Figure 70. Scatter plot comparing the RMS error in temperature of the sensor network with polynomial and kriging reconstruction over 24 hours.

6.6.3 Transient Performance Test with 0.1 °C Sensor Uncertainty

Sensor uncertainty of 0.1 °C as selected earlier was applied using pseudorandom numbers for a more realistic test. The results of the temperature reproduction can be seen in Figure 71 and Figure 72, and show the same general trends as the reference test without uncertainty. The effect of the applied sensor uncertainty can be seen in the residual error between the points and the fitted curves.

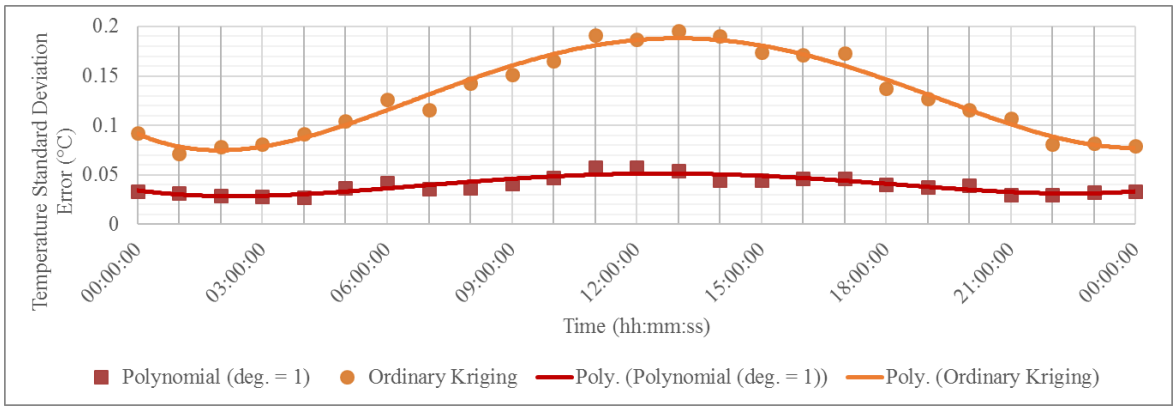

Figure 71. Scatter plot comparing the standard deviation error in temperature of the sensor network with polynomial and kriging reconstruction over 24 hours with 0.1 °C sensor uncertainty.

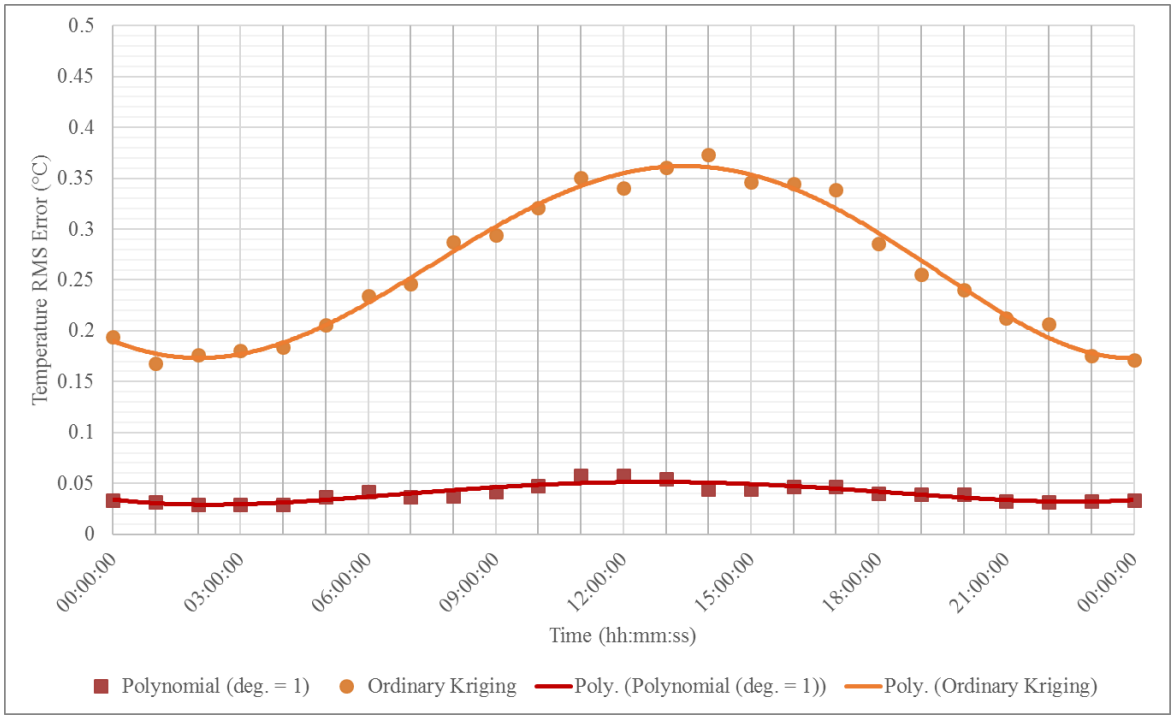

Figure 72. Scatter plot comparing the RMS error in temperature of the sensor network with polynomial and kriging reconstruction over 24 hours with 0.1 °C sensor uncertainty.

Figure 73 provides a better view of the linear fitting reconstruction results. The characteristic 'hump' in performance can be seen more clearly to match the changing temperature distribution.

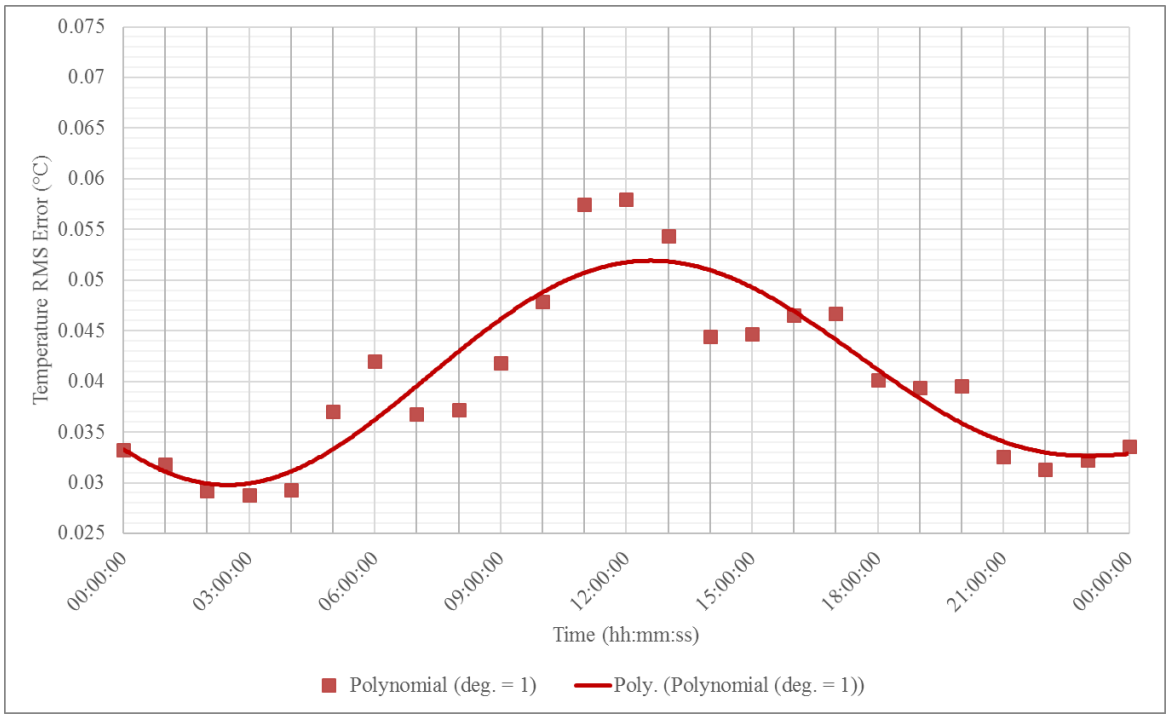

Figure 73. Scatter plot showing the RMS error in temperature of the sensor network with linear polynomial reconstruction over 24 hours with 0.1 °C sensor uncertainty.

Ultimately, his application is all about compensation of thermal effects for dimensional measurement, and the performance must also be considered in terms of how closely it can capture changes in geometry. Results for standard deviation in X, Y, and Z are presented in Figure 74, Figure 75, and Figure 76 respectively. The results for displacement in general following the same trends over time, except the X displacement standard error appears to exhibit some form of drift with performance being slightly worse towards the end of the 24 hours. Figure 77 shows RMS error values of the order of nanometres for both reconstruction methods.

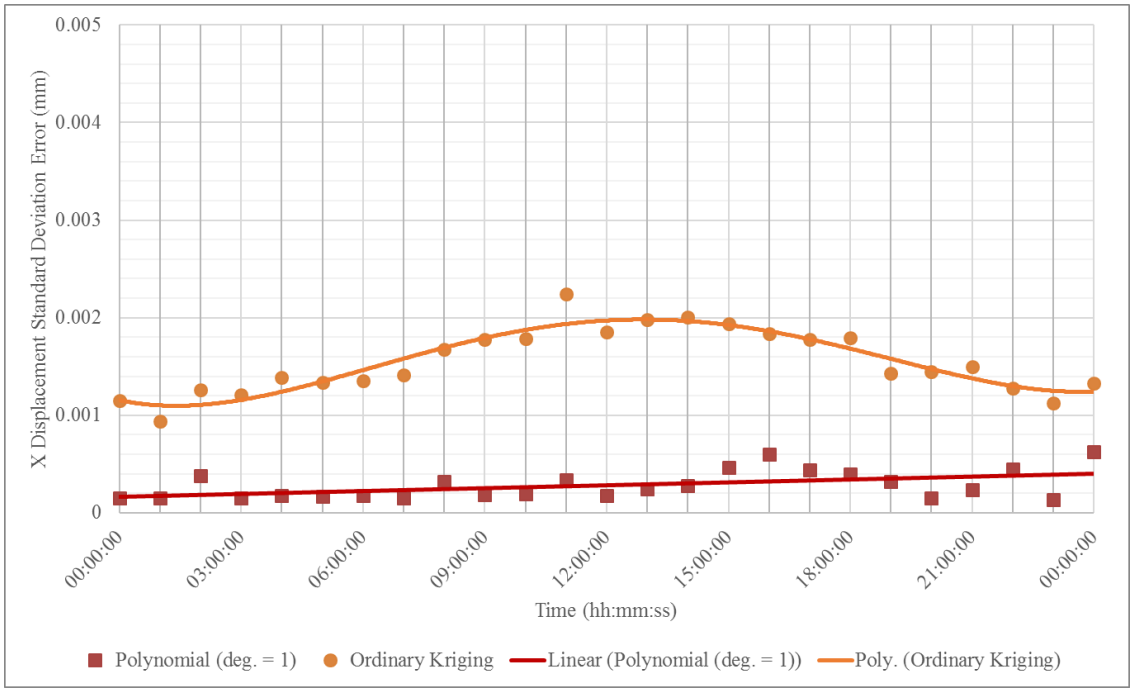

Figure 74. Scatter plot comparing the standard deviation error in X for linear polynomial and OK reconstruction over 24 hours, with 0.1 °C sensor uncertainty.

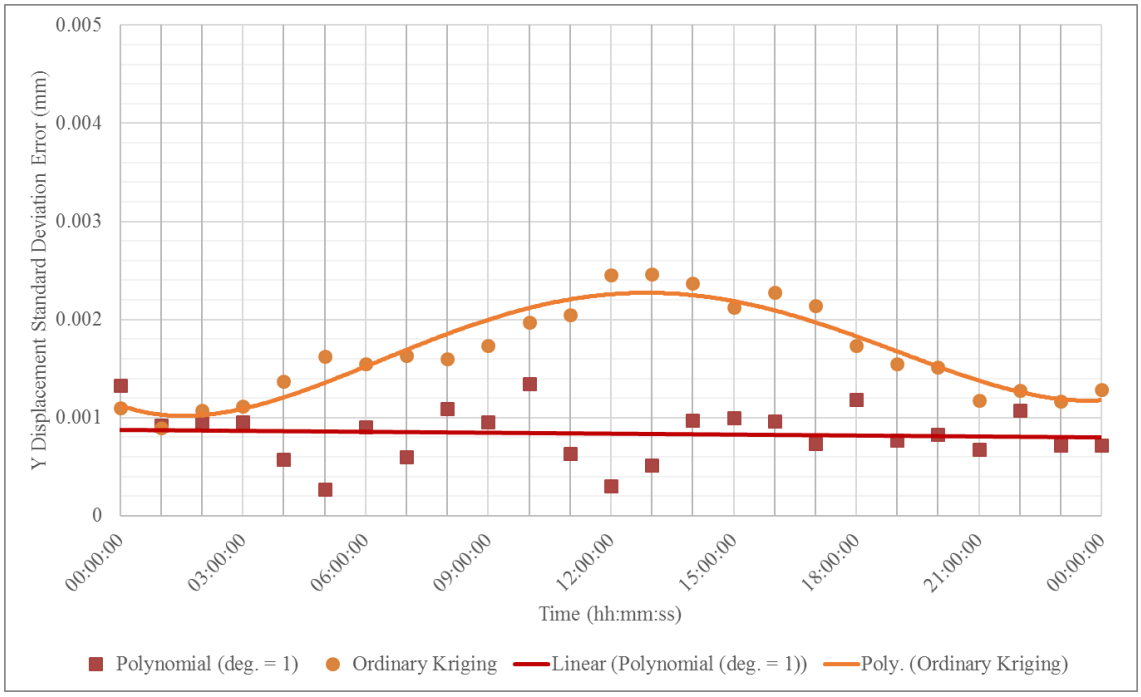

Figure 75. Scatter plot comparing the standard deviation error in Y for linear polynomial and OK reconstruction over 24 hours, with 0.1 °C sensor uncertainty.

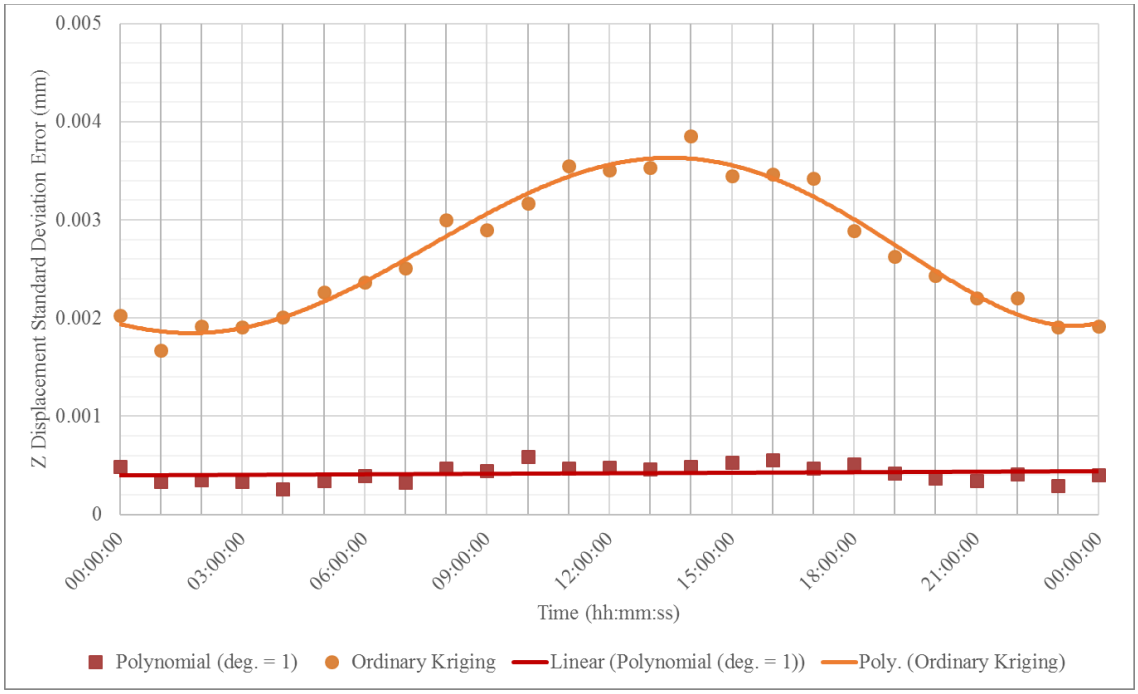

Figure 76. Scatter plot comparing the standard deviation error in Z for linear polynomial and OK reconstruction over 24 hours, with 0.1 °C sensor uncertainty.

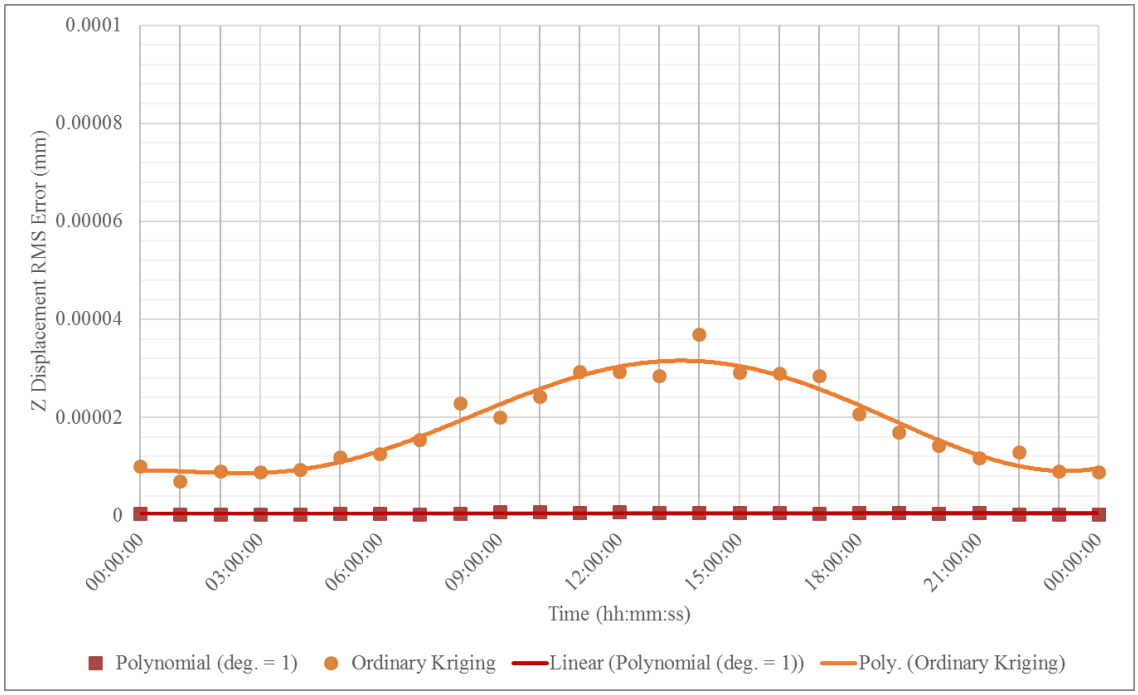

Figure 77. Scatter plot comparing the RMS error in Z for linear polynomial and OK reconstruction over 24 hours, with 0.1 °C sensor uncertainty.

6.7 Major Findings

The results of this case study experiment were encouraging. Provided the sensor network could realise its simulated performance in the physical world, confidence in performing measurements under challenging conditions outside of a metrology laboratory would be high. A reduction in the contribution of thermal effects acting on the object was found to be less than one or two micrometres on a structure that is 1.8 m tall. Taking this approach would provide a far greater level of performance than that which could be achieved using one sensor, uniform scaling, and indiscriminate sensor positioning.

This case study generated some key learning:

1. The positioning of the sensors within the measurement volume and the method of reconstructing the temperature field is often more important for driving improvements than the capability of the individual sensors.
2. There is a need to plan where to place the sensors within the measurement volume so that they provide data to allow the ambient temperature field to be identified.
3. If the placement is to be optimised then some measure of performance is required.
4. Two means of interpolating the ambient field have been investigated: polynomial fitting and Kriging. The selection of a reconstruction method is task-specific and should be tested for proposed applications. Testing out other configurations and scenarios may lead to Kriging in fact performing better.
5. Temperature sensor networks are more sensitive to changes at the spatial boundary and these appear to be most critical for accurate reconstruction.
6. More detailed heuristics can be generated using this approach for intermediate sensors. In the case of the barrel section assembly it was found that asymmetric sensor heights produced better results, for example.

6.8 Chapter 6 – Summary

Chapter 6 provided:

- A specific measurement challenge with representative geometry and temperature distribution.
- Results for how well the temperature sensor network performed.
- Comparison of:
    - Number of sensors;
    - Reconstruction methods;
    - Effect of sensor uncertainty;
    - Effect of removal of individual sensors.
- Results of a random search optimisation to allow the tool to explore which configurations might work best for this specific scenario.
- Results for the temperature sensor network performance when presented with a time-varying temperature distribution.

Contributions:

- Estimation of temperature sensor network performance for a given assembly;
- Estimation of thermal expansion contribution to measurement error for a given assembly;
- Optimisation of temperature sensor networks for a given scenario;
- Time dependent performance testing of temperature sensor networks over full thermal cycle.

The temperature measurement planning tool can be used to estimate temperature sensor network performance on an assembly, including the impact of variation over time.

---

7 Conclusions and Future Work

7.1 Conclusions

At the beginning of the thesis, the question was raised:

How can a temperature measurement planning process be created to produce better outcomes for thermal compensation?

In each of the chapters of this thesis the question of how best to plan temperature measurement has been considered. The problem of thermal effects was explored as this was known to be impactful to dimensional metrology. As a long-standing problem, it needed to be properly broken down in order to identify opportunities for improvement.

The following contributions have been made:

- Definition of a temperature measurement planning methodology;
- Computer-aided temperature measurement planning test bed supported by FEA;
- Estimation of temperature sensor network performance;
- Estimation of thermal expansion contribution to measurement error;
- Optimisation of temperature sensor networks for a given scenario;
- Time dependent performance testing of temperature sensor networks over full thermal cycle.

A review of the literature fulfilled the first objective of the thesis in Chapter 2. This revealed a range of capable temperature measurement technologies with standardisation that focuses primarily on the manufacture of sensors. There were very few consistent approaches to how to use temperature sensors to produce the best results. The problem of modelling thermal effects in large volumes has been considered in a range of fields, for a variety of applications. Planning the measurement of dimensions is well-established in manufacturing, particularly for CMMs, although work has been done at larger scales. There was found to be a clear opportunity to use some of the learning from dimensional measurement planning and apply this to temperature in order to then further support dimensional measurement through modelling thermal expansion.

Experience of thermal expansion was gained in the laboratory and in assembly environments and presented in Chapter 3. The measurement of temperature could have been carried out in a variety of ways and it was thought that how the temperature was measured and interpreted could have lead to significant differences in the simulated thermal expansion. The overall method was promising and highlighted very clearly the limitations of uniform scaling in more complex environments. A more sophisticated approach should be applied to temperature measurement to compensate for thermal expansion in order to provide more traceability of the measurement process.

In Chapter 4, ideas, and considerations were formed into a methodology that forms the primary contribution of this thesis. The core capabilities of the temperature measurement

planning tool, and areas where knowledge was generated are highlighted in Figure 78. This methodology became a computational tool that allowed for the testing of different temperature sensor networks through scripting. Chapters 5 and 6 developed the tool further and showed how it could ultimately be used for specific scenarios. The selection of a reconstruction method is one example of a task-specific consideration and methods should be tested for each proposed application.

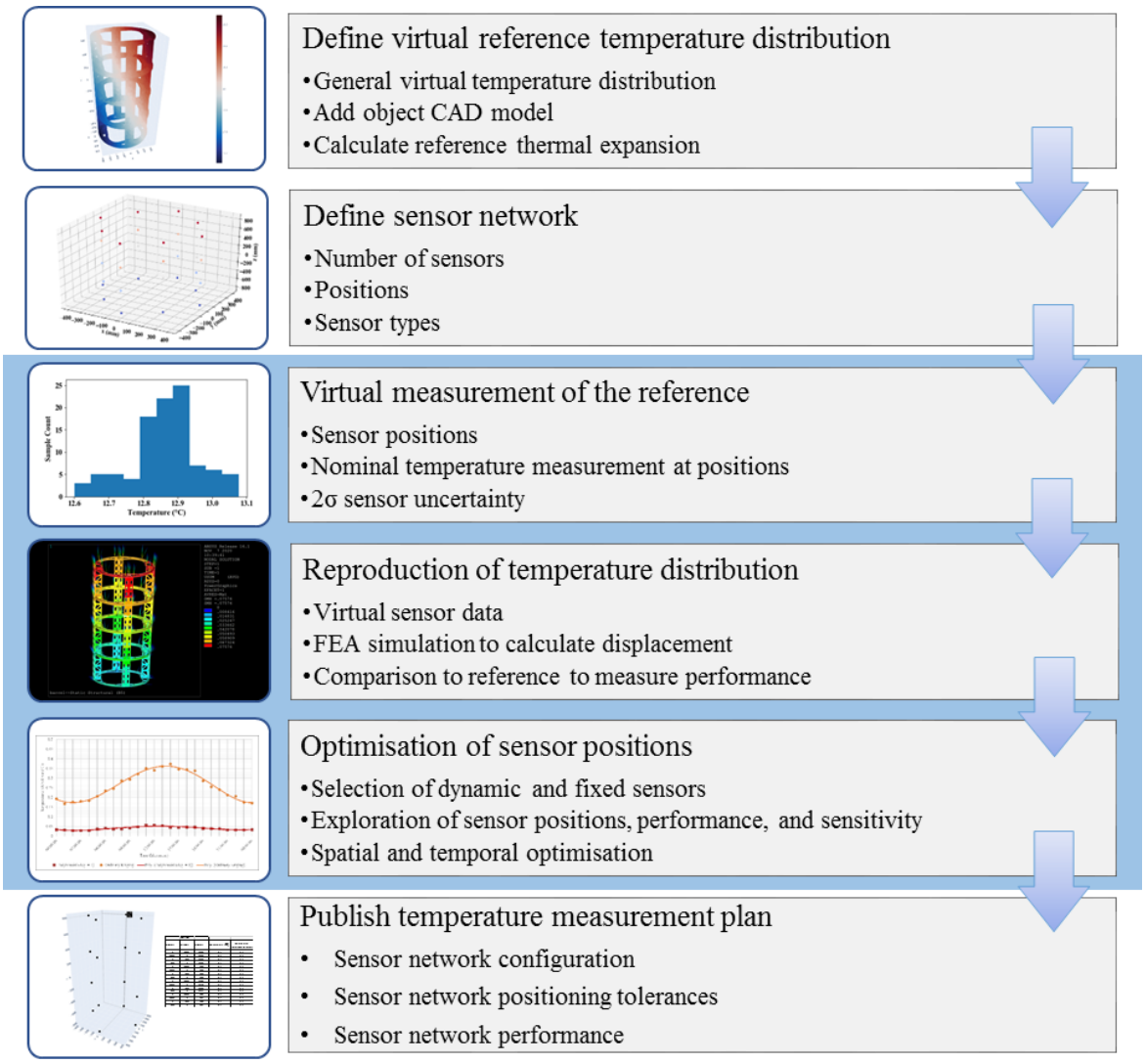

Figure 78. Diagram showing the temperature measurement planning process that has been created, with most significant contributions to knowledge highlighted in blue.

Absolute temperature changes over time, and temperature distribution also often changes in complexity. The positioning of the sensors within the measurement volume and the method of reconstructing the temperature field is often more important for driving improvements than the capability of the individual sensors. There is a need to plan where to place the sensors within the measurement volume so that the temperature field can be reconstructed. Optimisation of sensor positions was considered in Chapter 6. Temperature sensor networks are more sensitive to changes at the spatial boundary and these appear to be most critical for accurate reconstruction.

It is worth noting that beyond thermal effects, several challenges exist which are more related to culture and process: temperature often not being recorded during dimensional

measurement, for example. A large portion of performance improvements come from not making assumptions such as: uniform expansion, and isothermal temperature. With these fundaments in place, there wasn't a test bed for temperature sensor network planning and guidance was hard to find. The temperature measurement planning tool provided a means to quickly test temperature sensor networks and estimate how temperature translates to dimensional error.

Defining a temperature measurement methodology means that there can be some level of agreement. Where there is not total agreement, there is process traceability to justify why decisions were made. Compensation of thermal expansion error in dimensional measurement has its own complexities and sources of uncertainty, so it makes sense to go to the source and focus efforts on reducing temperature measurement error. In an era when sensor networks are increasingly ubiquitous, being able to properly understand the rationale behind their design and characterise their limitations is of real value.

7.2 Future Work

Various avenues could be explored in the future that can make use of the learning from this thesis. The first is that the tool lends itself to extension - modular design means that more sophisticated simulation, reconstruction, and optimisation can be used as new measurement challenges are introduced. Integration with dimensional measurement planning will provide further enhancements. The model-based enterprise technologies that have so far been used to improve inspection planning can eventually include improve temperature measurement planning in much the same way.

Accurate values for CTE would also provide significant improvements in scaling for thermal compensation. Due to the variation between batches, techniques for measuring the CTE of a specific instance of a part in-situ would be preferable.

One of the more practical aspects to consider for this problem in future work would be in the physical sensor network set up. The sensor network integration problem would consider sensor accessibility and wiring around the product, its tooling, and the factory space. This type of planning could be carried out in the process development stage and may have some influence on the final sensor positions. Large volume scanning and immersive technologies have a potential part to play to improve how the computational testing emulates the physical space.

A natural progression of the temperature sensor network optimisation would be to create a cost model so that the sensor network design can be evaluated in terms of costs and benefits. The number of sensors in a temperature sensor network needs to be considered in terms of the value that each sensor adds to the measurement. Whilst temperature sensors off the shelf are relatively inexpensive, particularly compared to the cost of dimensional measurement systems, costs quickly accumulate. Capital costs of individual sensors might be small but will cost significantly more in maintaining up-to-date calibration certificates. Data acquisition systems can carry significant capital costs and will also require some maintenance. One of the use cases of the temperature measurement planning tool is the comparison of sensor networks made up of different sensor types.

Progression through the paradigms of increasingly digital processes will see more tools that make use of multiple physical quantities at different scales and using a range of simulation methods. More and more decisions will be made using these systems, so it is important to keep in mind the methods to quantify the uncertainty of the data being used to make such predictions.

References

[1] D. Sherry, "Thermoscopes, thermometers, and the foundations of measurement," *Studies in History and Philosophy of Science Part A,* vol. 42, pp. 509-524, 2011.

[2] ISO, "ISO 1:2016 Geometrical product specifications (GPS) — Standard reference temperature for the specification of geometrical and dimensional properties," 2016.

[3] J. Hollandt, J. Hartmann, O. Struß, and R. Gärtner, "Chapter 1 - Industrial Applications of Radiation Thermometry," in *Experimental Methods in the Physical Sciences*. vol. 43, Z. M. Zhang, B. K. Tsai, and G. Machin, Academic Press, pp. 1-56, 2010.

[4] K. L. Bevan, M;, *Dimensional Measurement Part 1 - Training Manual,* 1.0, National Physical Laboratory (NPL), 2016.

[5] "BS EN ISO 10360-2:2002: Geometrical product specifications (GPS). Acceptance and reverification tests for coordinate measuring machines (CMM). CMMs used for measuring size," British Standards Institute, 2002.

[6] "BS EN ISO 15530-3:2011: Geometrical product specifications (GPS). Coordinate measuring machines (CMM). Technique for determining the uncertainty of measurement. Use of calibrated workpieces or measurement standards," British Standards Institute, 2011.

[7] *IEEE Sensors Journal,* vol. 8, p. 1145, 2008.

[8] "BS ISO 230-3:2007: Test code for machine tools. Determination of thermal effects," ed: British Standards Institute, 2007.

[9] R. Hou, H. Du, Z. Yan, W. Yu, T. Tao, and X. Mei, "The modeling method on thermal expansion of CNC lathe headstock in vertical direction based on MOGA," *The International Journal of Advanced Manufacturing Technology,* vol. 103, pp. 3629-3641, 2019.

[10] J. Mayr, P. Blaser, A. Ryser, and P. Hernandez-Becerro, "An adaptive self-learning compensation approach for thermal errors on 5-axis machine tools handling an arbitrary set of sample rates," *CIRP Annals,* vol. 67, pp. 551-554, 2018.

[11] K. Takenaka, "Progress of research in negative thermal expansion materials: Paradigm shift in the control of thermal expansion," *Frontiers in chemistry,* vol. 6, pp. 267-267, 2018.

[12] Z.-j. Li, C.-y. Zhao, and Z.-c. Lu, "Thermal error modeling method for ball screw feed system of CNC machine tools in x-axis," *International journal of advanced manufacturing technology,* vol. 106, pp. 5383-5392, 2020.

[13] M. O. dos Santos, G. F. Batalha, E. C. Bordinassi, and G. F. Miori, "Numerical and experimental modeling of thermal errors in a five-axis CNC machining center," *International journal of advanced manufacturing technology,* vol. 96, pp. 2619-2642, 2018.

[14] E. Mirkoohi, J. Ning, P. Bocchini, O. Fergani, K.-N. Chiang, and S. Liang, "Thermal Modeling of Temperature Distribution in Metal Additive Manufacturing Considering Effects of Build Layers, Latent Heat, and Temperature-Sensitivity of Material Properties," *Journal of Manufacturing and Materials Processing,* vol. 2, p. 63, 2018.

[15] X. Song, S. Feih, W. Zhai, C.-N. Sun, F. Li, R. Maiti, *et al.*, "Advances in additive manufacturing process simulation: Residual stresses and distortion predictions in complex metallic components," *Materials & design,* vol. 193, p. 108779, 2020.

[16] D. Ross-Pinnock and P. G. Maropoulos, "Identification of Key Temperature Measurement Technologies for the Enhancement of Product and Equipment Integrity in the Light Controlled Factory," in *Procedia CIRP Special Edition for 8th*

International Conference on Digital Enterprise Technology - DET 2014 – Disruptive Innovation in Manufacturing Engineering towards the 4th Industrial Revolution, DOI: 10.1016/j.procir.2014.10.019, 2014.

[17] D. Ross-Pinnock and P. G. Maropoulos, "Review of industrial temperature measurement technologies and research priorities for the thermal characterisation of the factories of the future," *Proceedings of the Institution of Mechanical Engineers, Part B: Journal of Engineering Manufacture*, February 6, 2015.

[18] P. R. N. Childs, J. R. Greenwood, and C. A. Long, "Review of temperature measurement," *Review of Scientific Instruments*, vol. 71, pp. 2959-2978, 2000.

[19] E. O. Doebelin, *Measurement Systems Application and Design*, Fourth ed. United States: McGraw-Hill, 1990.

[20] H. Ogura, H. Numajiri, M. Izuchi, and M. Arai, "Evaluation of inhomogeneity of Pt/Pd thermocouples," vol. 1, pp. 744-748, 2003.

[21] M. Izuchi, H. Numajiri, H. Ogura, H. Narushima, and M. Arai, "Uncertainty assessment on the calibration of Pt/Pd thermocouples at the freezing point of silver," vol. 1, pp. 753-755, 2003.

[22] A. Ulanovskiy, V. Medvedev, S. Nenashev, Y. Sild, M. Matveyev, A. Pokhodun, *et al.*, "Thermoelectric Characteristic of High-Temperature Thermocouples WRE/WRE," *Journal of Thermophysical Properties and Thermophysics and Its Applications*, vol. 31, pp. 1573-1582, 2010.

[23] J. Ferdouse and B. Mark, "A Study of the Temperature Dependence of Inhomogeneity in Platinum-Based Thermocouples," vol. 684, p. 469, 2003.

[24] T. Hamada and Y. Suyama, "E.M.F. drift and inhomogeneity of type K thermocouples," vol. 2, pp. 989-992, 2004.

[25] Y. A. Abdelaziz and F. Edler, "A method for evaluation of the inhomogeneity of thermoelements," *Meas. Sci. Technol.*, vol. 20, 2009.

[26] M. Holmsten, J. Ivarsson, R. Falk, M. Lidbeck, and L. E. Josefson, "Inhomogeneity measurements of long thermocouples using a short movable heating zone," *Int. J. Thermophys.*, vol. 29, pp. 915-925, 2008.

[27] J. Tamba, K. Yamazawa, S. Masuyama, H. Ogura, and M. Izuchi, "Evaluating the Inhomogeneity of Thermocouples Using a Pressure-Controlled Water Heat Pipe," *Int. J. Thermophys.*, vol. 32, pp. 2436-2451, 2011.

[28] J. V. Pearce, "Quantitative determination of the uncertainty arising from the inhomogeneity of thermocouples," *Meas. Sci. Technol.*, vol. 18, pp. 3489-3495, 2007.

[29] J. C. Y. Yang and D. W. Clarke, "A self-validating thermocouple," *Control Systems Technology, IEEE Transactions on*, vol. 5, pp. 239-253, 1997.

[30] B. Schuh, "Smart thermocouple system for industrial temperature measurement," in *Sensors for Industry, 2001. Proceedings of the First ISA/IEEE Conference*, pp. 8-11, 2001.

[31] A. Mangano and G. Coggiola, "Stability of K-, N- and S-type thermocouples in the temperature range from 0°C to 1060°C," *Measurement*, vol. 12, pp. 171-182, 12// 1993.

[32] F. M. Megahed and Y. A. Abdel-Aziz, "Assessment of Temperature Measurements Using Thermocouples at NIS-Egypt," *International Journal of Thermophysics*, vol. 31, pp. 601-611, 2010.

[33] Y.-G. Kim, K. S. Gam, and K. H. Kang, "An investigation of the thermoelectric properties of type S thermocouples from different manufacturers," *Measurement*, vol. 31, pp. 131-137, 2002.

[34] M. Dalla Palma, N. Pomaro, C. Taliercio, and R. Pasqualotto, "Design and Test of a Thermal Measurement System Prototype for SPIDER Experiment," *Plasma Science, IEEE Transactions on*, vol. 42, pp. 1971-1976, 2014.
[35] B. Samo, B. Jovan, D. Janko, and G. Gregor, "Magnetic effects on thermocouples," *Measurement Science and Technology*, vol. 25, p. 035006, 2014.
[36] M. Genix, P. Vairac, and B. Cretin, "Local temperature surface measurement with intrinsic thermocouple," *International Journal of Thermal Sciences*, vol. 48, pp. 1679-1682, 2009.
[37] F. E. Kennedy, D. Frusescu, and J. Li, "Thin film thermocouple arrays for sliding surface temperature measurement," *Wear*, vol. 207, pp. 46-54, 1997.
[38] T. Jianwen, Z. Yong, T. Xiaojun, and L. Junhua, "Nonlinearity Correction of the Thermocouple Based on Neural Network," in *Intelligent Systems, 2009. GCIS '09. WRI Global Congress on*, pp. 28-32, 2009.
[39] W. Schuh and N. Frost, "Improving Industrial Thermocouple Temperature Measurement," *AIP Conference Proceedings*, vol. 684, pp. 497-502, 2003.
[40] P. R. N. Childs, "6 - Resistance temperature detectors," in *Practical Temperature Measurement*, P. R. N. Childs, Ed., ed Oxford: Butterworth-Heinemann, pp. 145-193, 2001.
[41] L. Crovini, A. Actis, G. Coggiola, and A. Mangano, "Accurate thermometry by means of industrial platinum resistance thermometers," *Measurement*, vol. 10, pp. 31-38, 1992.
[42] Heraeus Sensor Technology. (21/11/2013). *Thin Film vs. Wirewound RTD Elements*., 2013. Available: http://heraeus-sensor-technology-us.com/en/faq/thinfilmvswirewoundrtdelement/thinfilmvswirewoundrtdelement.aspx
[43] C. Bonham, S. J. Thorpe, M. N. Erlund, and R. D. Stevenson, "Stagnation temperature measurement using thin-film platinum resistance sensors," *Measurement Science and Technology*, vol. 25, p. 015101, 2014.
[44] V. Žužek, V. Batagelj, and J. Bojkovski, "Determination of PRT Hysteresis in the Temperature Range from −50 °C to 300 °C," *International Journal of Thermophysics*, vol. 31, pp. 1771-1778, 2010.
[45] D. R. White, C. L. Jongenelen, and P. Saunders, "The Hysteresis Characteristics of Some Industrial PRTs," *International Journal of Thermophysics*, vol. 31, pp. 1676-1684, 2010.
[46] S. Ljungblad, M. Holmsten, L.-E. Josefson, and B. Klevedal, "Long term stability and hysteresis effects in Pt100 sensors used in industry," *AIP Conference Proceedings*, vol. 1552, pp. 421-426, 2013.
[47] J. Valencia-Rodriguez and J. M. Figueroa, "Electromagnetic compatibility in platinum resistance thermometers," pp. 84-85, 2002.
[48] K. Yamazawa, K. Anso, J. V. Widiatmo, J. Tamba, and M. Arai, "Evaluation of Small-Sized Platinum Resistance Thermometers with ITS-90 Characteristics," *International Journal of Thermophysics*, vol. 32, pp. 2397-2408, 2011.
[49] D. Smorgon, V. C. Fernicola, and L. Coslovi, "Low-Cost Ratiometric Front-End for Industrial PRT Applications," *International Journal of Thermophysics*, vol. 32, pp. 2317-2324, 2011.
[50] I. Bajsic and D. Tusar, "Influence of thermal insulation filler on dynamic properties of industrial resistance temperature sensors," *Instrum. Sci. Technol.*, vol. 30, pp. 439-448, 2002.
[51] V. V. Gureyev and A. A. L'Vov, "High Accuracy Semiautomatic Calibration of Industrial RTDs," pp. 1-5, 2007.

[52] K. H. Kang, Y. G. Kim, K. S. Gam, and I. Yang, "Self-testable industrial platinum resistance thermometers integrated with miniature mercury and indium fixed-point cells," *Meas. Sci. Technol.*, vol. 18, pp. 3005-3008, 2007.
[53] D. Ibrahim, "Chapter 5 - Thermistor Temperature Sensors," in *Microcontroller Based Temperature Monitoring and Control*, D. Ibrahim, Ed., ed Oxford: Newnes, pp. 107-127, 2002.
[54] H. G. Schweiger, M. Multerer, and H. J. Gores, "Fast Multichannel Precision Thermometer," *Instrumentation and Measurement, IEEE Transactions on*, vol. 56, pp. 2002-2009, 2007.
[55] J. Kim and J. D. Kim, "Voltage divider resistance for high-resolution of the thermistor temperature measurement," *Measurement*, vol. 44, pp. 2054-2059, 12, 2011.
[56] S. A. Khan, D. T. Shahani, and A. K. Agarwala, "Sensor calibration and compensation using artificial neural network," *ISA Transactions*, vol. 42, pp. 337-352, 7, 2003.
[57] A. U. Keskin, "Comments on the “Sensor calibration and compensation using artificial neural network”, by Khan S.A., Shahani D.T., Agarwala A.K," *ISA Transactions*, vol. 48, pp. 143-144, 2009.
[58] D. Kong, L. T. Le, Y. Li, J. L. Zunino, and W. Lee, "Temperature-Dependent Electrical Properties of Graphene Inkjet-Printed on Flexible Materials," *Langmuir*, vol. 28, pp. 13467-13472, 2012.
[59] A. Hartog, "Distributed fibre-optic temperature sensors: Technology and applications in the power industry," *Power Engineering Journal*, vol. 9, pp. 114-120, 1995.
[60] F. Tanimola and D. Hill, "Distributed fibre optic sensors for pipeline protection," *Journal of Natural Gas Science and Engineering*, vol. 1, pp. 134-143, 2009.
[61] Luna Innovations Incorporated. (13/12/2013). LUNA Technologies DSS™ 4300 Datasheet, 2009. Available: http://www.lambdaphoto.co.uk/pdfs/Lambda_Data_Sheet_DSS.pdf
[62] A. Rogers, "Distributed optical-fibre sensing," vol. 10, ed, 1999, pp. R75-R99.
[63] P. R. Stoddart, P. J. Cadusch, J. B. Pearce, D. Vukovic, C. R. Nagarajah, and D. J. Booth, "Fibre optic distributed temperature sensor with an integrated background correction function," *Measurement Science and Technology*, vol. 16, pp. 1299-1304, 2005.
[64] P. C. Wait, K. De Souza, and T. P. Newson, "A theoretical comparison of spontaneous Raman and Brillouin based fibre optic distributed temperature sensors," *Optics Communications*, vol. 144, pp. 17-23, 1997.
[65] B. Gabriele, A. S. Marcelo, and P. Fabrizio Di, "Simultaneous distributed strain and temperature sensing based on combined Raman–Brillouin scattering using Fabry–Perot lasers," *Measurement Science and Technology*, vol. 21, p. 094025, 2010.
[66] V. Dirk, L. W. A. v. G. Jan, and K. Oswin, "Spatio-temporal noise and drift in fiber optic distributed temperature sensing," *Measurement Science and Technology*, vol. 22, p. 085203, 2011.
[67] I. Hallcrest, *Handbook of Thermochromic Liquid Crystal Technology*, 1991.
[68] I. Sage, "Thermochromic liquid crystals," *Liquid Crystals*, vol. 38, pp. 1551-1561, 2011.
[69] B. K. Reddy and C. Balaji, "Estimation of temperature dependent heat transfer coefficient in a vertical rectangular fin using liquid crystal thermography," *Int. J. Heat Mass Transf.*, vol. 55, pp. 3686-3693, 2012.
[70] J. W. Baughn, "LIQUID-CRYSTAL METHODS FOR STUDYING TURBULENT HEAT-TRANSFER," *Int. J. Heat Fluid Flow*, vol. 16, pp. 365-375, 1995.

[71] A. Tamburini, P. Pitò, A. Cipollina, G. Micale, and M. Ciofalo, "A Thermochromic Liquid Crystals Image Analysis technique to investigate temperature polarization in spacer-filled channels for Membrane Distillation," *Journal of Membrane Science,* vol. 447, pp. 260-273, 2013.
[72] M. Seredyuk, A. B. Gaspar, V. Ksenofontov, S. Reiman, Y. Galyametdinov, W. Haase, *et al.*, "Room temperature operational thermochromic liquid crystals," *Chem. Mat.*, vol. 18, pp. 2513-2519, 2006.
[73] M. Z. Chen, M. T. Du, J. Jiang, D. W. Li, W. Jiang, E. Zhuravlev, *et al.*, "Verifying the symmetry of ultra-fast scanning calorimeters using liquid crystal secondary temperature standards," *Thermochim. Acta,* vol. 526, pp. 58-64, 2011.
[74] N. Fuhrmann, J. Brübach, and A. Dreizler, "Phosphor thermometry: A comparison of the luminescence lifetime and the intensity ratio approach," *Proceedings of the Combustion Institute,* vol. 34, pp. 3611-3618, 2013.
[75] J. Brübach, T. Kissel, M. Frotscher, M. Euler, B. Albert, and A. Dreizler, "A survey of phosphors novel for thermography," *Journal of Luminescence,* vol. 131, pp. 559-564, 2011.
[76] A. L. Heyes, S. Seefeldt, and J. P. Feist, "Two-colour phosphor thermometry for surface temperature measurement," *Optics & Laser Technology,* vol. 38, pp. 257-265, 2006.
[77] J. Ervin, C. Murawski, C. MacArthur, M. Chyu, and D. Bizzak, "Temperature measurement of a curved surface using thermographic phosphors," *Experimental Thermal and Fluid Science,* vol. 11, pp. 387-394, 1995.
[78] S. Someya, M. Uchida, K. Tominaga, H. Terunuma, Y. Li, and K. Okamoto, "Lifetime-based phosphor thermometry of an optical engine using a high-speed CMOS camera," *International Journal of Heat and Mass Transfer,* vol. 54, pp. 3927-3932, 2011.
[79] B. Atakan and D. Roskosch, "Thermographic phosphor thermometry in transient combustion: A theoretical study of heat transfer and accuracy," *Proceedings of the Combustion Institute,* vol. 34, pp. 3603-3610, 2013.
[80] D. G. Walker and S. W. Allison, "Transient measurements using thermographic phosphors," *ISA Transactions,* vol. 46, pp. 15-20, 2007.
[81] M. Aldén, A. Omrane, M. Richter, and G. Särner, "Thermographic phosphors for thermometry: A survey of combustion applications," *Progress in Energy and Combustion Science,* vol. 37, pp. 422-461, 2011.
[82] D. R. Clarke and M. M. Gentleman, "Luminescence sensing of temperatures in thermal barrier coatings," *Surface and Coatings Technology,* vol. 202, pp. 681-687, 2007.
[83] J. Brübach, C. Pflitsch, A. Dreizler, and B. Atakan, "On surface temperature measurements with thermographic phosphors: A review," *Progress in Energy and Combustion Science,* vol. 39, pp. 37-60, 2013.
[84] Raytek Corporation, "MP150 Datasheet," ed. Raytek Website: Raytek Corporation, 2012.
[85] P. Herve, J. Cedelle, and I. Negreanu, "Infrared technique for simultaneous determination of temperature and emissivity," *Infrared Physics & Technology,* vol. 55, pp. 1-10, 2012.
[86] C. D. Wen and I. Mudawar, "Modeling the effects of surface roughness on the emissivity of aluminum alloys," *International Journal of Heat and Mass Transfer,* vol. 49, pp. 4279-4289, 2006.
[87] O. Struß, "Transfer Radiation Thermometer Covering the Temperature Range from −50 °C to 1000 °C," *AIP Conference Proceedings,* vol. 684, pp. 565-570, 2003.

[88] S. Lhospitalier, P. Bourges, A. Bert, J. Quesada, and M. Lambertin, "Temperature measurement inside and near the weld pool during laser welding," *Journal of Laser Applications,* vol. 11, pp. 32-37, 1999.
[89] M. Cotterell, E. Ares, J. Yanes, F. López, P. Hernandez, and G. Peláez, "Temperature and Strain Measurement during Chip Formation in Orthogonal Cutting Conditions Applied to Ti-6Al-4V," *Procedia Engineering,* vol. 63, pp. 922-930, 2013.
[90] S. Vidas and P. Moghadam, "HeatWave: A handheld 3D thermography system for energy auditing," *Energy Build.,* vol. 66, pp. 445-460, 2013.
[91] S. Prakash, L. Pei Yean, and T. Caelli, "3D Mapping of Surface Temperature Using Thermal Stereo," in *Control, Automation, Robotics and Vision, 2006. ICARCV '06. 9th International Conference on Control, Automation, Robotics and Vision*, pp. 1-4, 2006.
[92] J. R. Mahan, W. Conaty, J. Neilsen, P. Payton, and S. B. Cox, "Field performance in agricultural settings of a wireless temperature monitoring system based on a low-cost infrared sensor," *Computers and Electronics in Agriculture,* vol. 71, pp. 176-181, 2010.
[93] S. A. O'Shaughnessy, M. A. Hebel, S. R. Evett, and P. D. Colaizzi, "Evaluation of a wireless infrared thermometer with a narrow field of view," *Computers and Electronics in Agriculture,* vol. 76, pp. 59-68, 2011.
[94] P. R. N. Childs, "5 - Thermocouples," in *Practical Temperature Measurement*, P. R. N. Childs, Ed., ed Oxford: Butterworth-Heinemann, 2001, pp. 98-144.
[95] M. Rezaei-Malek, M. Mohammadi, J.-Y. Dantan, A. Siadat, and R. Tavakkoli-Moghaddam, "A review on optimisation of part quality inspection planning in a multi-stage manufacturing system," *International journal of production research,* vol. 57, pp. 4880-4897, 2018.
[96] Z. Wang, A. Forbes, and P. G. Maropoulos, "Laser tracker position optimization," 2014.
[97] J. E. Muelaner, Z. Wang, P. S. Keogh, J. Brownell, and D. Fisher, "Uncertainty of measurement for large product verification: evaluation of large aero gas turbine engine datums," *Measurement Science and Technology,* vol. 27, p. 115003, 2016.
[98] B. Cai, "Inspection process planning for large volume metrology in digital environment," Thesis (Ph.D.) - University of Bath, 2012., Bath, 2012.
[99] D. Sims-Waterhouse, M. Isa, S. Piano, and R. Leach, "Uncertainty model for a traceable stereo-photogrammetry system," *Precision engineering,* vol. 63, pp. 1-9, 2020.
[100] H. Mahmoud, V. Dhokia, and A. Nassehi, "STEP-based Conceptual Framework for Measurement Planning Integration," *Procedia CIRP,* vol. 43, pp. 315-320, 2016.
[101] P. Saunders, B. Cai, N. Orchard, and P. Maropoulos, "Towards a Definition of PLM-integrated Dimensional Measurement," *Procedia CIRP,* vol. 7, pp. 670-675, 2013.
[102] C. N. Macleod, G. Dobie, S. G. Pierce, R. Summan, and M. Morozov, "Machining-Based Coverage Path Planning for Automated Structural Inspection," *IEEE transactions on automation science and engineering,* vol. 15, pp. 202-213, 2018.
[103] R. Rusby. (Good Practice Guide No. 125 - Introduction to Temperature Measurement, 2016. Available: https://www.npl.co.uk/special-pages/guides/gpg125_intro2tempmeasure
[104] D. Thakur, Y. Kumar, A. Kumar, and P. K. Singh, "Applicability of Wireless Sensor Networks in Precision Agriculture: A Review," *Wireless Personal Communications,* vol. 107, pp. 471-512, 2019.
[105] S. Kim, H. Lee, S. Wi, S.-W. Lee, and I. Seo, *Fluid Dynamics Simulation and Temperature Gradient Validation along a Greenhouse Temperature Gradient*, 2020.

[106] J. P. Abraham, M. Baringer, N. L. Bindoff, T. Boyer, L. J. Cheng, J. A. Church, *et al.*, "A review of global ocean temperature observations: Implications for ocean heat content estimates and climate change," *Reviews of Geophysics,* vol. 51, pp. 450-483, 2013.
[107] C. Zhang, M. Pomianowski, P. K. Heiselberg, and T. Yu, "A review of integrated radiant heating/cooling with ventilation systems- Thermal comfort and indoor air quality," *Energy and Buildings,* vol. 223, p. 110094, 2020.
[108] L. Seduikyte, L. Stasiulienė, T. Prasauskas, D. Martuzevičius, J. Černeckienė, T. Ždankus, *et al.*, "Field Measurements and Numerical Simulation for the Definition of the Thermal Stratification and Ventilation Performance in a Mechanically Ventilated Sports Hall," *Energies,* vol. 12, 2019.
[109] K. Ahmed, E. Sistonen, R. Simson, J. Kurnitski, J. Kesti, and P. Lautso, "Radiant panel and air heating performance in large industrial buildings," *Building Simulation,* vol. 11, 2017.
[110] R. H. Schmitt, M. Peterek, E. Morse, W. Knapp, M. Galetto, F. Härtig, *et al.*, "Advances in Large-Scale Metrology – Review and future trends," *CIRP Annals,* vol. 65, pp. 643-665, 2016.
[111] P. Nath, Z. Hu, and S. Mahadevan, "Sensor placement for calibration of spatially varying model parameters," *Journal of Computational Physics,* vol. 343, pp. 150-169, 2017.
[112] G. M. G. V. Milovanović, "Constructive Elements and Approaches in Approximation Theory," in *Interpolation Processes: Basic Theory and Applications*, ed Berlin, Heidelberg: Springer Berlin Heidelberg, pp. 1-73, 2008.
[113] E. W. Weisstein, *CRC Concise Encyclopedia of Mathematics, Second Edition*: CRC Press, 2002.
[114] J. Li and A. D. Heap, "Spatial interpolation methods applied in the environmental sciences: A review," *Environmental Modelling & Software,* vol. 53, pp. 173-189, 2014.
[115] J. Li and A. D. Heap, "A review of comparative studies of spatial interpolation methods in environmental sciences: Performance and impact factors," *Ecological Informatics,* vol. 6, pp. 228-241, 2011.
[116] J. Kleijnen, "Kriging: Methods and Applications," *SSRN Electronic Journal,* 2017.
[117] G. Bohling. (Kriging. *Resources for C&PE940, Data Analysis in Engineering and Natural Science* [Teaching Material], 2005. Available: http://people.ku.edu/~gbohling/cpe940/Kriging.pdf
[118] P. Goovaerts and D. C. E. E. P. Goovaerts, *Geostatistics for Natural Resources Evaluation*: Oxford University Press, 1997.
[119] Esri. (29/05/18). *ArcMap - What are the different kriging models? 2005.* Available: http://desktop.arcgis.com/en/arcmap/latest/extensions/geostatistical-analyst/what-are-the-different-kriging-models-.htm
[120] G. Machin, K. Anhalt, M. Battuello, F. Bourson, P. Dekker, A. Diril, *et al.*, "The European project on high temperature measurement solutions in industry (HiTeMS) – A summary of achievements," *Measurement,* vol. 78, pp. 168-179, 2016.
[121] J. Yang and E. Bou-Zeid, "Designing sensor networks to resolve spatio-temporal urban temperature variations: fixed, mobile or hybrid?," *Environmental Research Letters,* vol. 14, p. 074022, 2019.
[122] D. Ross-Pinnock and G. Mullineux, "Thermal compensation using the hybrid metrology approach compared to traditional scaling," *DET 2016 Special Edition,* vol. 232, pp. 2364-2374, 11/1 2018.

[123] DeLonghi. (2021, 29/05/2021). *HVA3222 Fan Heater*. Available: https://www.delonghi.com/en-gb/hva3222-fan-heater/p/HVA3222
[124] Aicon. (18/08/2016). *MoveInspect Technology DPA, 2016*. Available: http://aicon3d.com/products/moveinspect-technology/dpa/at-a-glance.html
[125] F. Systems. (18/08/2016). *FLIR® E-Series and E-Series bx — Now with MSX®*, 2016. Available: http://www.flir.co.uk/instruments/display/?id=56911
[126] D. Ross-Pinnock, G. Mullineux, and P. Keogh, "Temperature Sensor Position-Planning," presented at the Proceedings of TMCE 2020, Dublin, Ireland, 2020.
[127] D. Ross-Pinnock, G. Mullineux, and P. Keogh, "Temeprature Sensor Position Planning," *Journal of Integrated Design and Process Science*, 2021.

7.3 Journal Articles

D Ross-Pinnock, G Mullineux, P Keogh, *Temperature Sensor Position-Planning*, Tools and Methods of Competitive Engineering 2020 (TMCE 2020) Special Edition, Journal of Integrated Design and Process Science, (submitted – peer review).

D Ross-Pinnock, G Mullineux. *Thermal compensation using the hybrid metrology approach compared to traditional scaling*, The 9th International Conference on Digital Enterprise Technology (DET 2016) Special Edition, Proceedings of the Institution of Mechanical Engineers, Part B: Journal of Engineering Manufacture. 10. https://doi.org/10.1177/0954405417733766 , 2017.

B Yang, D Ross-Pinnock J, Muelaner, G Mullineux. Thermal compensation for large volume metrology and structures. International Journal of Metrology and Quality Engineering; 8. 21. https://doi.org/10.1051/ijmqe/2017004 , 2017.

D Ross-Pinnock, PG Maropoulos. Review of industrial temperature measurement technologies and research priorities for the thermal characterisation of the factories of the future. Proceedings of the Institution of Mechanical Engineers, Part B: Journal of Engineering Manufacture; 230(5):793-806. https://doi.org/10.1177/0954405414567929 , 2017.

7.4 Conference Papers and Presentations

D Ross-Pinnock, G Mullineux, P Keogh, *Temperature Sensor Position-Planning*, Proceedings of Tools and Methods of Competitive Engineering 2020 (TMCE 2020), Dublin, Ireland, 11-15 May 2020.

JE Muelaner, D Ross-Pinnock, G Mullineux, PS Keogh. *Uncertainties in dimensional measurements due to thermal expansion*, Laser Metrology and Machine Performance XII - 12th International Conference and Exhibition on Laser Metrology, Machine Tool, CMM and Robotic Performance, LAMDAMAP. p. 133-143. 2017.

G Mullineux, D Ross-Pinnock, B Yang. *Point-Based Models for Compensation Of Thermal Effects In Dimensional Metrology*. Tools and Methods of Competitive Engineering. Delft University of Technology. p. 117-128. 2016.

D Ross-Pinnock, G Mullineux. *Thermal Compensation of Photogrammetric Dimensional Measurements in Non-standard Anisothermal Environments*, Procedia CIRP: The 9th International Conference on Digital Enterprise Technology – Intelligent Manufacturing in the Knowledge Economy Era. Vol. 56. Elsevier. p. 416–421 https://doi.org/10.1016/j.procir.2016.10.070 2016.

D Ross-Pinnock, B Yang, P G Maropoulos, *Integration of Thermal and Dimensional Measurement – A Hybrid Computational and Physical Measurement Method*, 38th MATADOR Conference on Advanced Manufacturing, Taiwan, 28-30 March 2015.

D Ross-Pinnock, P G Maropoulos, *Identification of Key Temperature Measurement Technologies for the Enhancement of Product and Equipment Integrity in the Light Controlled Factory*, Procedia CIRP, Volume 25, 8th International Conference on Digital Enterprise Technology - DET 2014 Disruptive Innovation in Manufacturing Engineering towards the 4th Industrial Revolution , p. 114-121, 2014.

7.5 Conference Posters

B Yang, D Ross-Pinnock, G Mullineux, J Muelaner, B Hughes, PS Keogh, PG Maropoulos. *Coping with Poor Thermal Environments and Gravity in Multi-Component Assemblies*, EPMC European Portable Metrology Conference 2015, Manchester, UK, 2015. Best poster award.

B Yang, D Ross-Pinnock, *Integration of Dimensional and Thermal Metrology In the Light Controlled Factory*, Large Volume Metrology Conference, Manchester, UK, 2014.

PG Maropoulos, PS Keogh, J Knight, G Mullineux, W Wadsworth, J Muelaner, D Ross-Pinnock, Z Wang, A Francis, J Huntley, H Dantanarayana, S Robson, J Bohem, S Kyle, L MacDonald, *The Light Controlled Factory*, 3rd Annual EPSRC Manufacturing the Future Conference, Glasgow, UK, 2014.

7.6 Workshop Presentations

D Ross-Pinnock, G Mullineux, *Compensating for thermal and gravitational effects in structures and assemblies*, Large Volume Metrology in Industry - EMRP Project IND53 'LUMINAR' End of Project Workshop, Teddington, UK, 18-19 May 2016.

D Ross-Pinnock, *Integration of Thermal and Dimensional Metrology for Manufacturing Process and Equipment Integrity*, Temperature Measurement Workshop, Glasgow, UK, 2013.

7.7 Public Engagement Activities

D Ross Pinnock, *'Honey, I shrunk the plane!'*, Science Stand-up Charity Event, Bath, UK, 19 April 2016.

Appendix A – Individual AIT Jig Temperatures

7.7.1.1 Jig 1

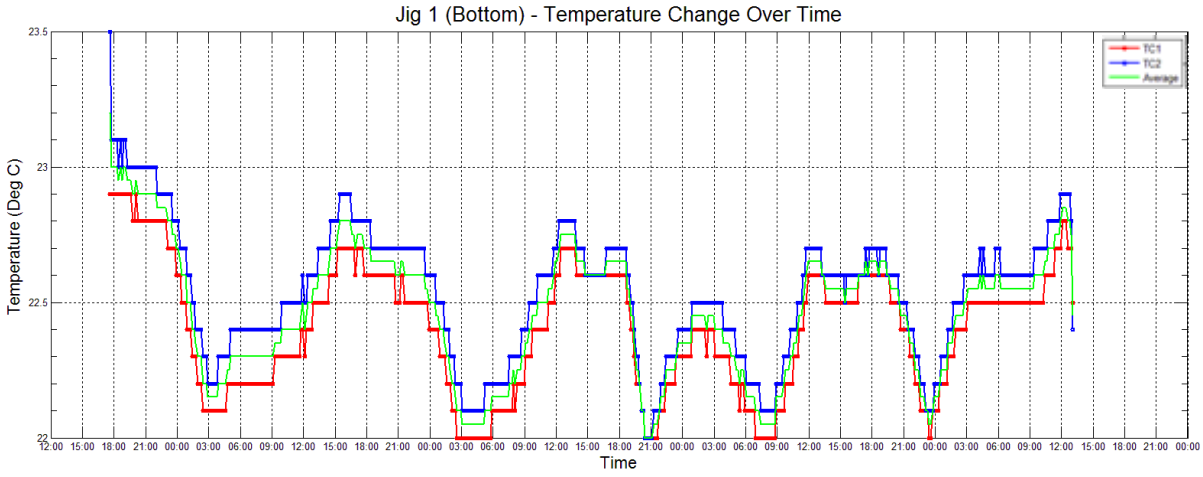

Figure 79 - Graph showing the temperature on Jig 1 (Bottom) over time showing measurements from two thermocouple (K-type) sensors and the mean average

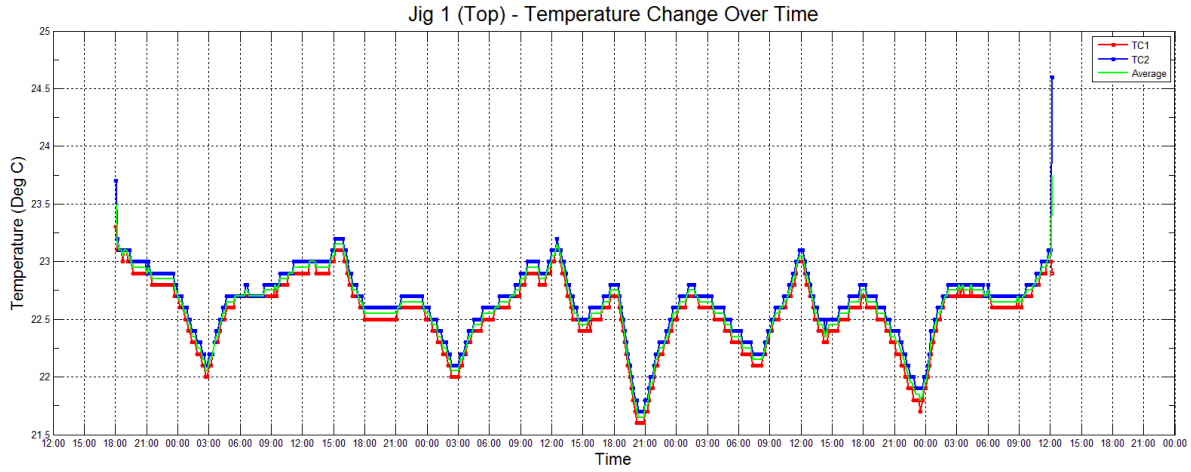

Figure 80 - Graph showing the temperature on Jig 1 (Top) over time showing measurements from two thermocouple (K-type) sensors and the mean average

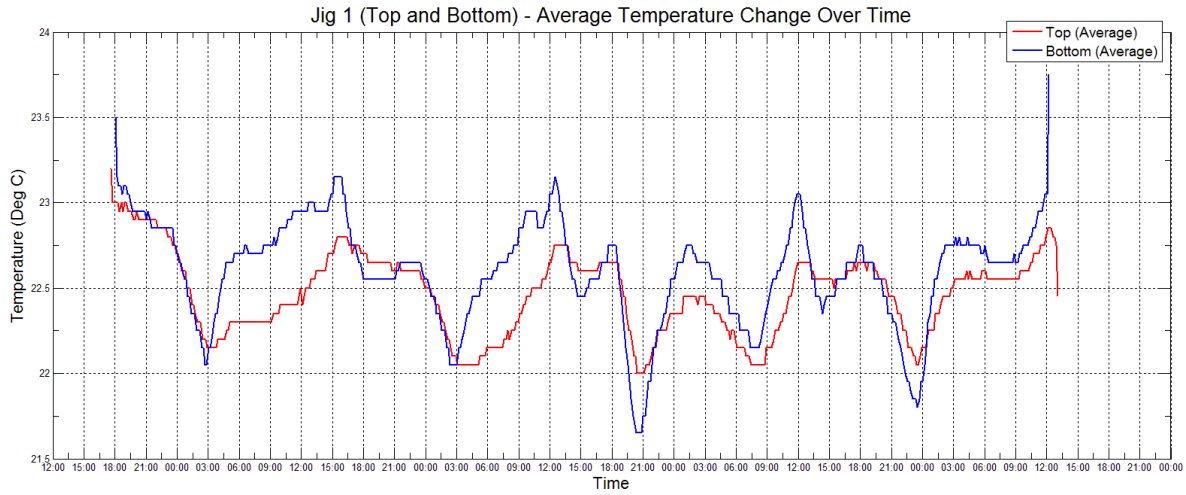

Figure 81 - Graph showing the mean average temperature on Jig 1 over time at the bottom and top of the jig

7.7.1.2 Jig 3

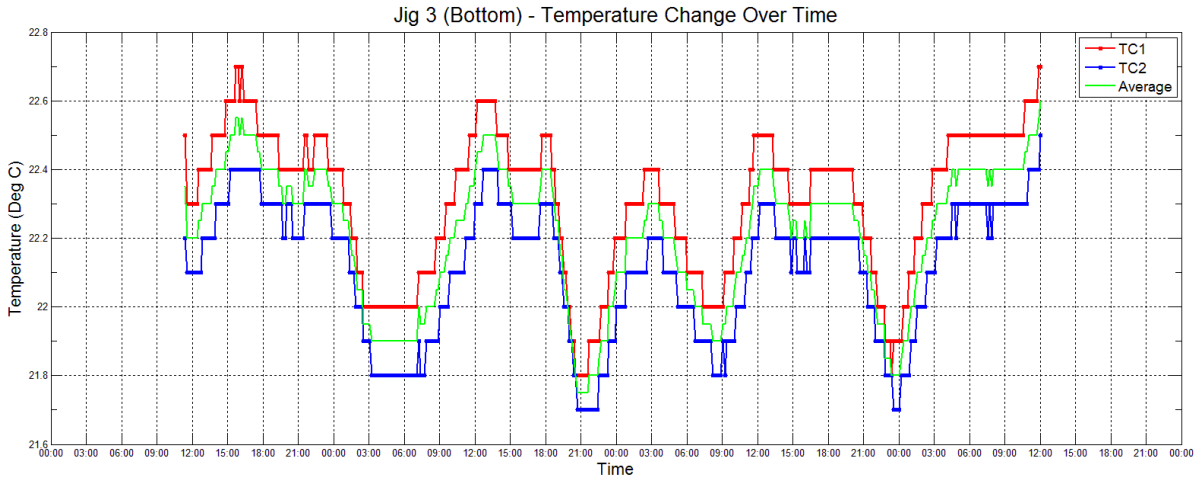

Figure 82 - Graph showing the temperature on Jig 3 (Bottom) over time showing measurements from two thermocouple (K-type) sensors and the mean average

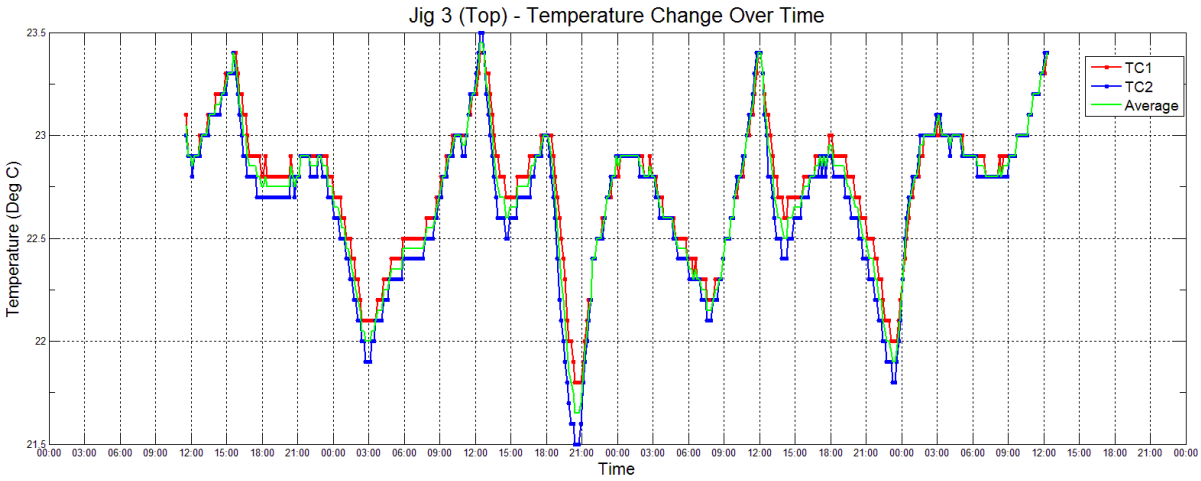

Figure 83 - Graph showing the temperature on Jig 3 (Top) over time showing measurements from two thermocouple (K-type) sensors and the mean average

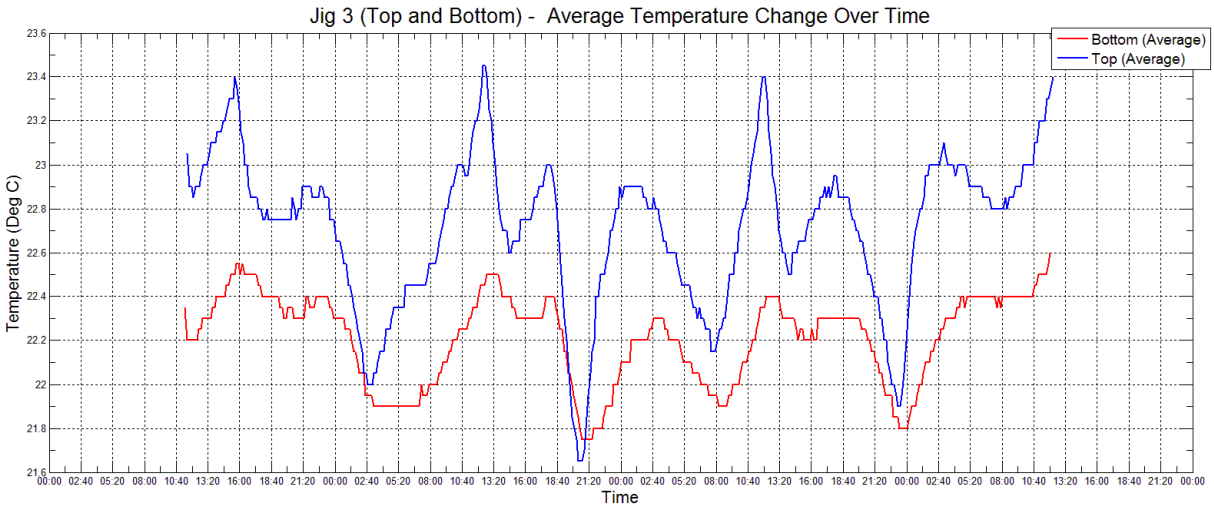

Figure 84 - Graph showing the mean average temperature on Jig 3 over time at the bottom and top of the jig

7.7.1.3 Jig 4

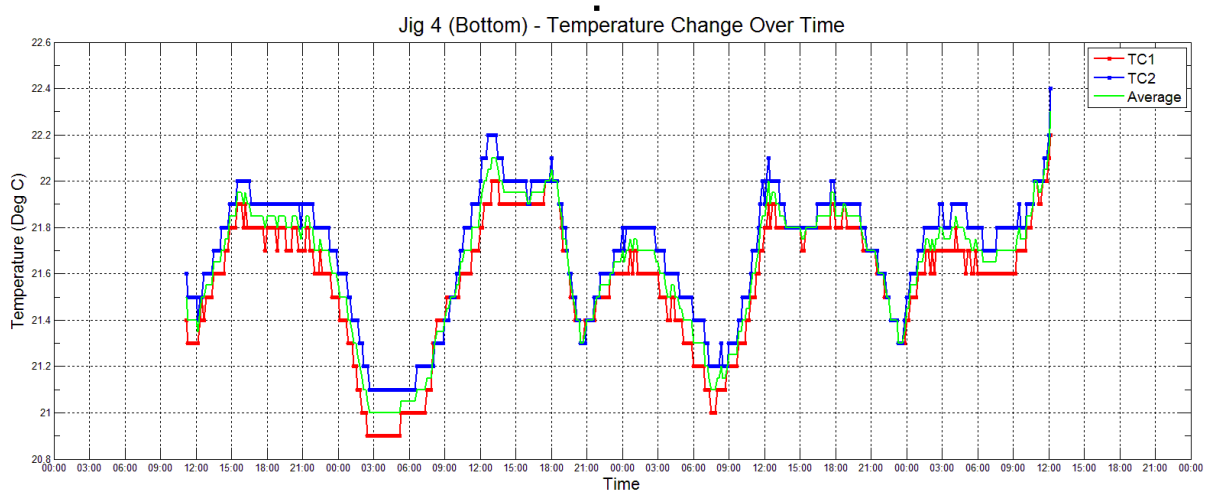

Figure 85 - Graph showing the temperature on Jig 4 (Bottom) over time showing measurements from two thermocouple (K-type) sensors and the mean average

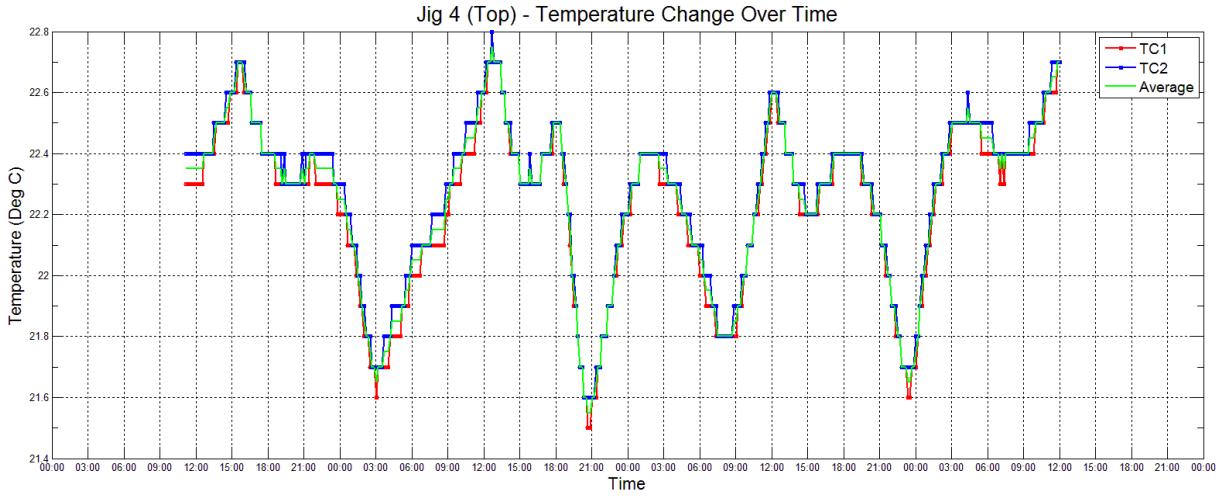

Figure 86 - Graph showing the temperature on Jig 4 (Top) over time showing measurements from two thermocouple (K-type) sensors and the mean average

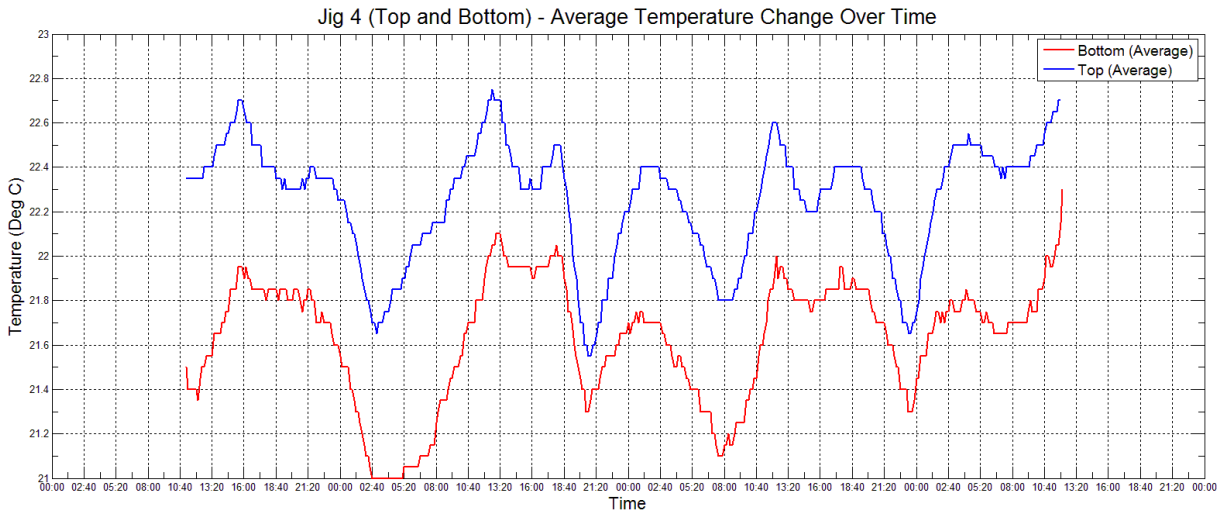

Figure 87 - Graph showing the mean average temperature on Jig 4 over time at the bottom and top of the jig

7.7.1.4 Jig 5

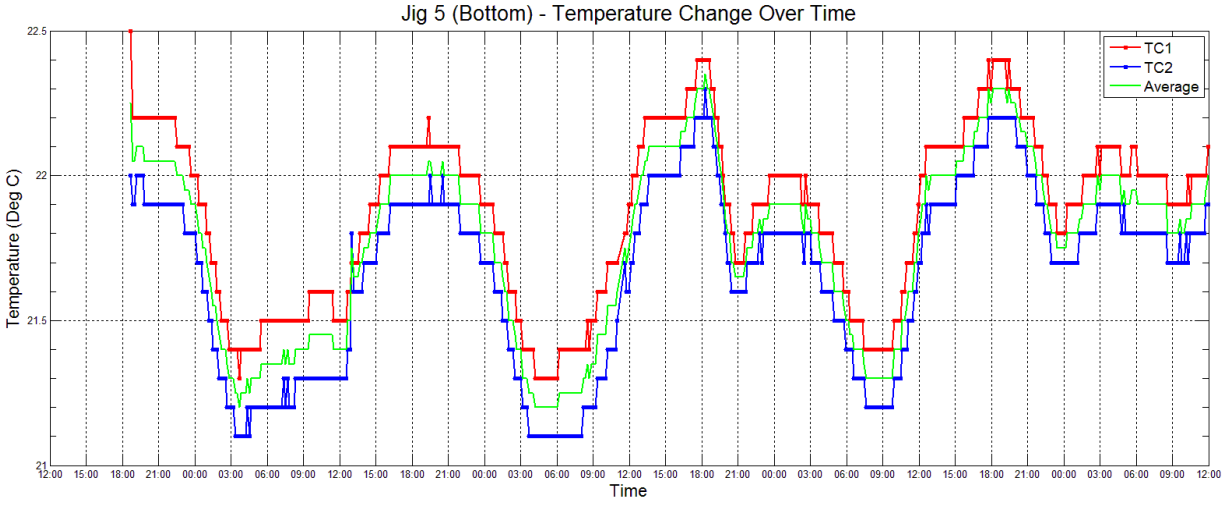

Figure 88 - Graph showing the temperature on Jig 5 (Bottom) over time showing measurements from two thermocouple (K-type) sensors and the mean average

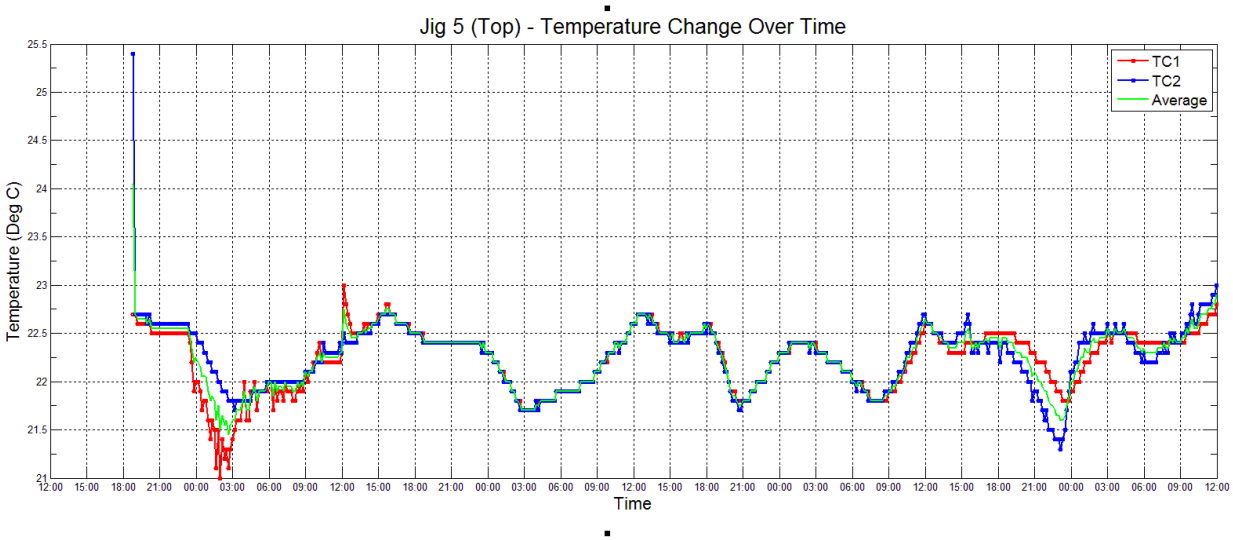

Figure 89 - Graph showing the temperature on Jig 5 (Top) over time showing measurements from two thermocouple (K-type) sensors and the mean average

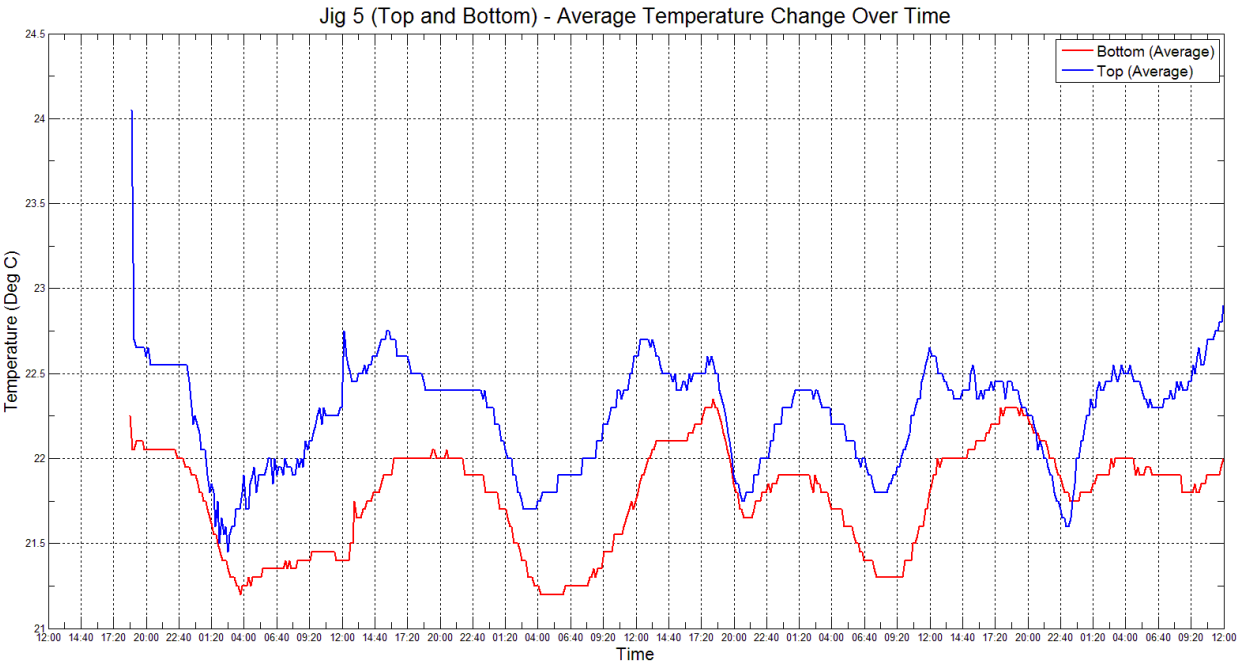

Figure 90 - Graph showing the mean average temperature on Jig 5 over time at the bottom and top of the jig

7.7.1.5 Jig 6

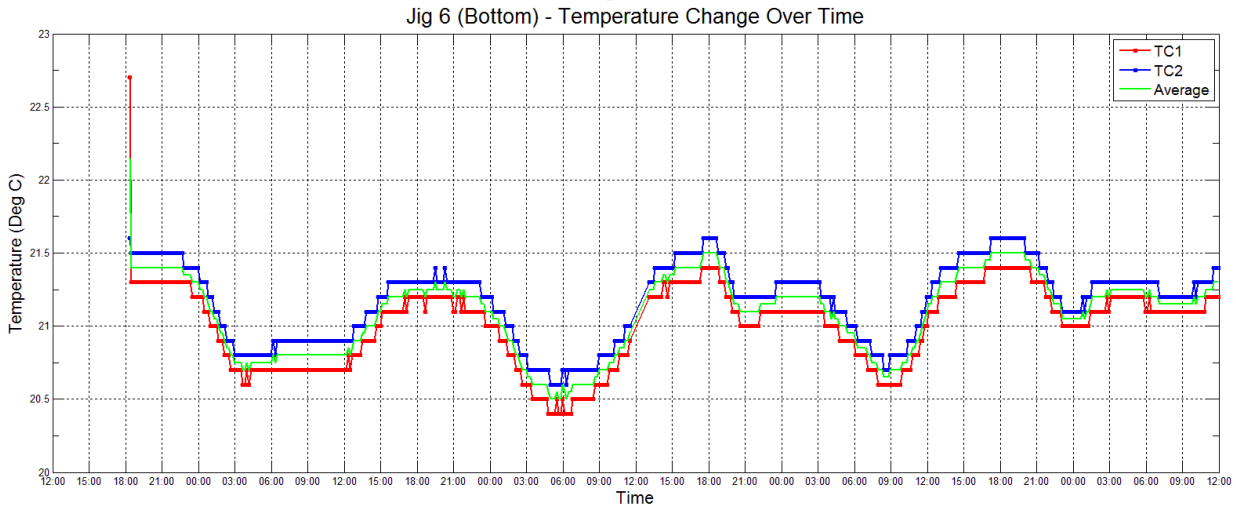

Figure 91 - Graph showing the temperature on Jig 6 (Bottom) over time showing measurements from two thermocouple (K-type) sensors and the mean average

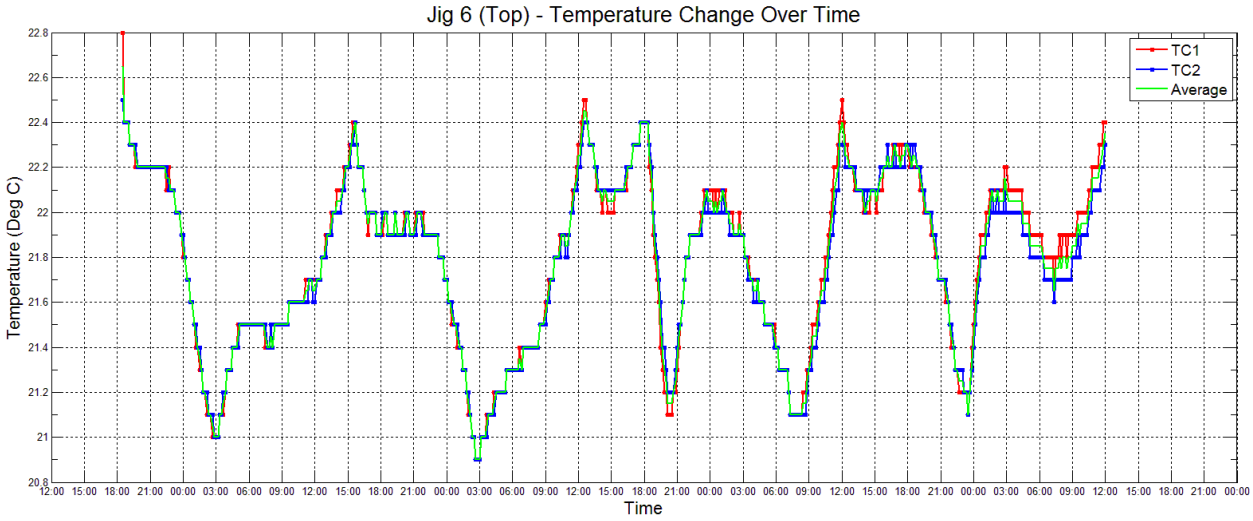

Figure 92 - Graph showing the temperature on Jig 6 (Top) over time showing measurements from two thermocouple (K-type) sensors and the mean average

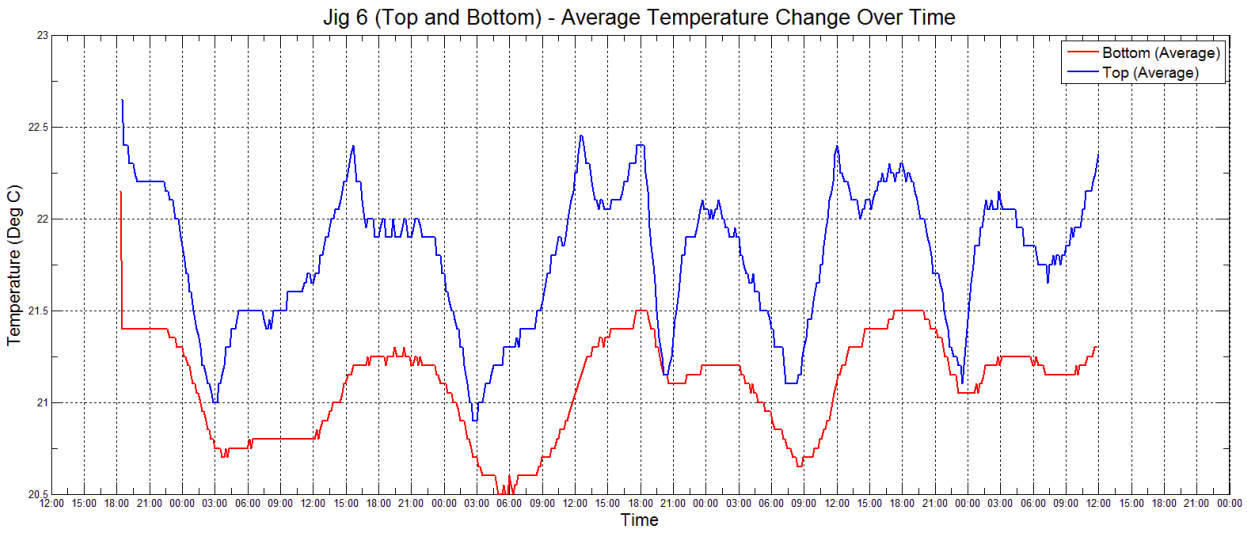

Figure 93 - Graph showing the mean average temperature on Jig 6 over time at the bottom and top of the jig

Appendix B – Naïve Network Test Temperature Distributions

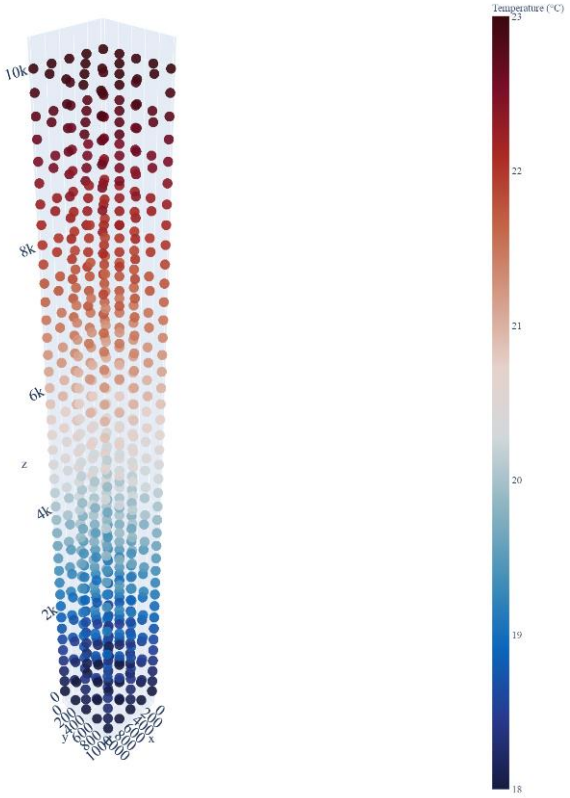

Figure 94 – Naïve network test temperature distribution, ID: 001

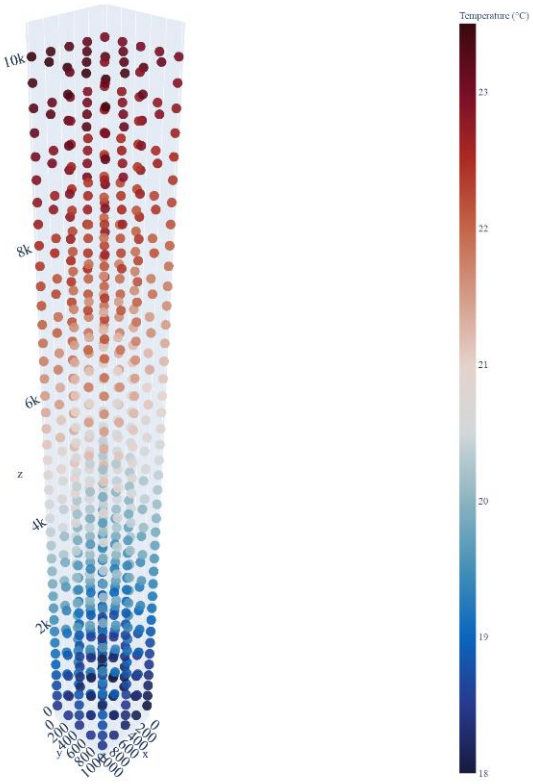

Figure 95 - Naïve network test temperature distribution, ID: 002

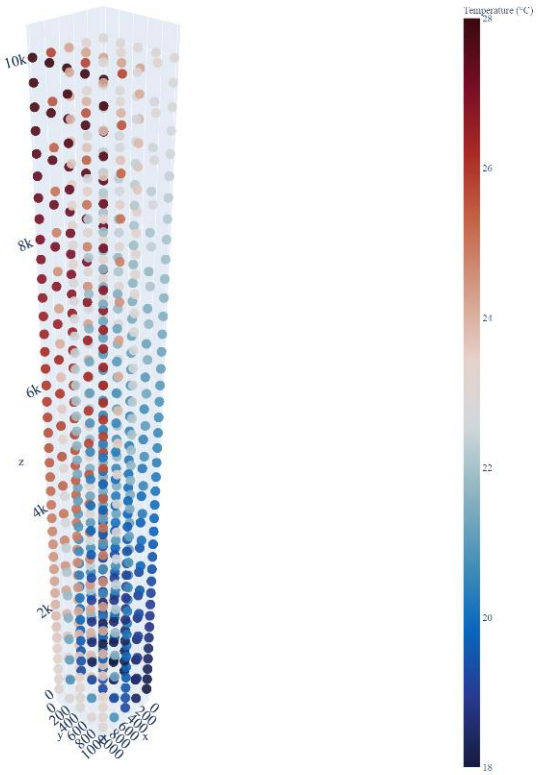

Figure 96 - Naïve network test temperature distribution, ID: 003

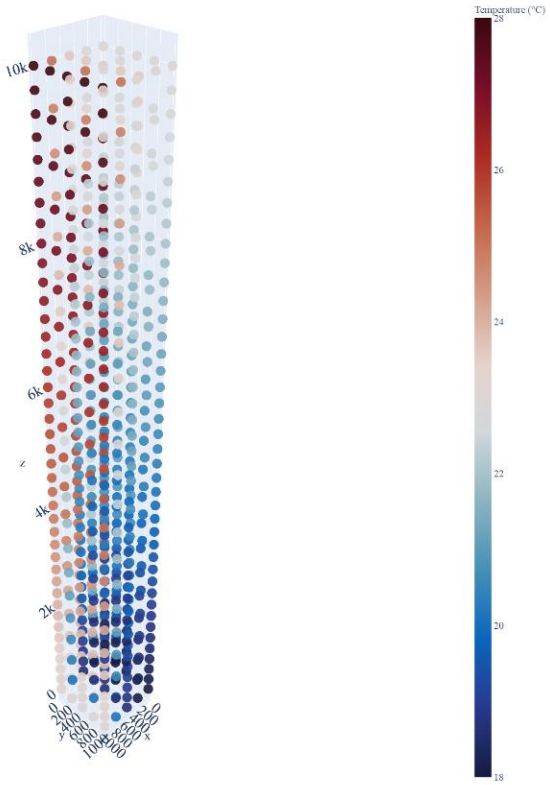

Figure 97 – Naïve network test temperature distribution, ID: 004

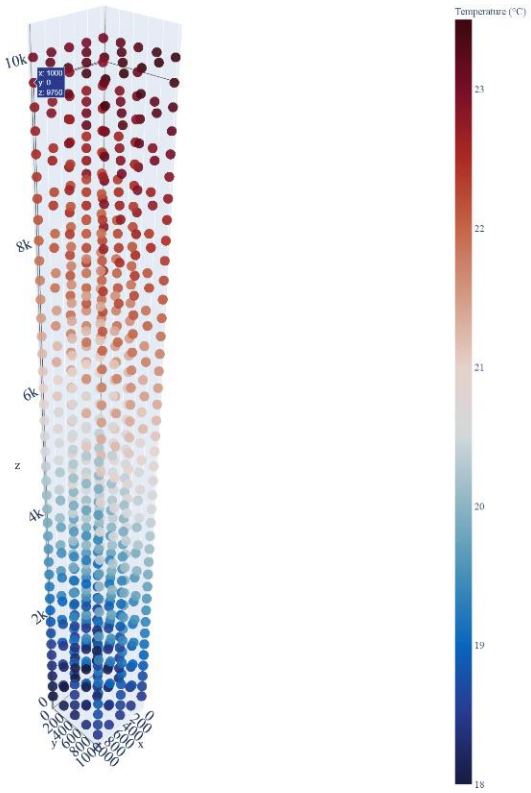

Figure 98 – Naïve network test temperature distribution, ID: 005

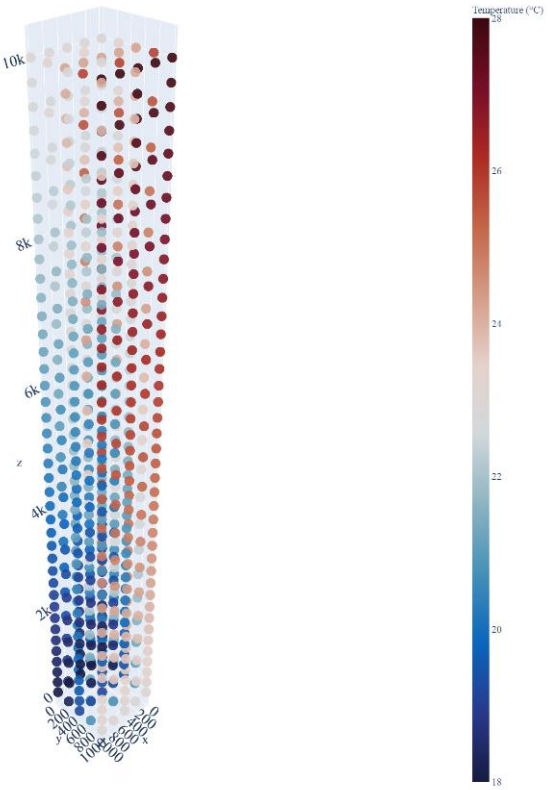

Figure 99 – Naïve network test temperature distribution, ID: 006

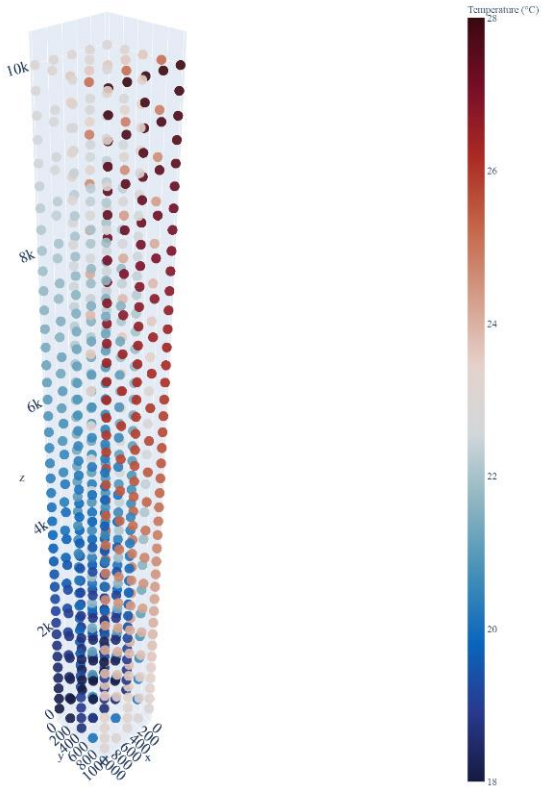

Figure 100 – Naïve network test temperature distribution, ID: 007

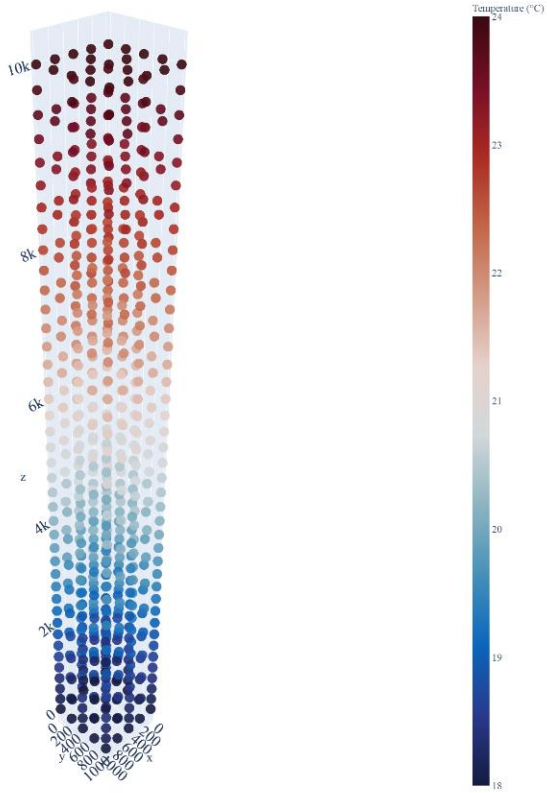

Figure 101 – Naïve network test temperature distribution, ID: 008

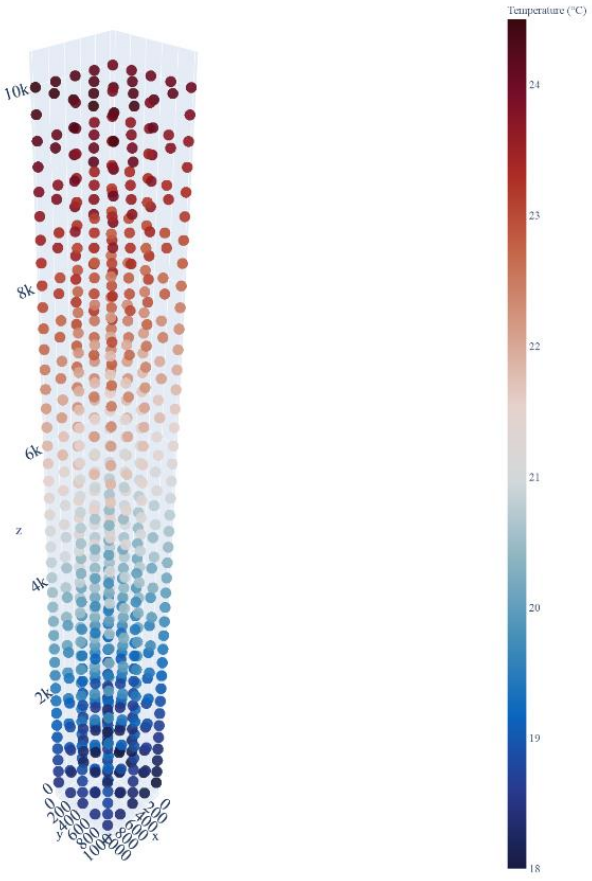

Figure 102 – Naïve network test temperature distribution, ID: 009

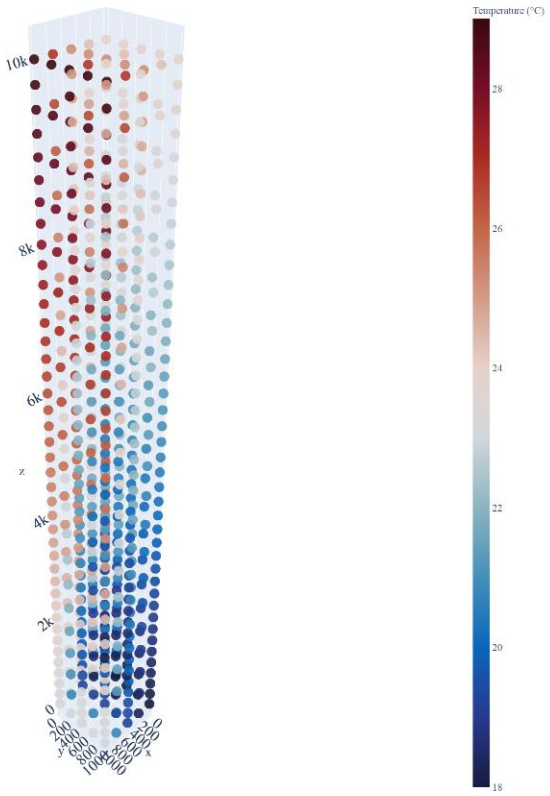

Figure 103 – Naïve network test temperature distribution, ID: 010

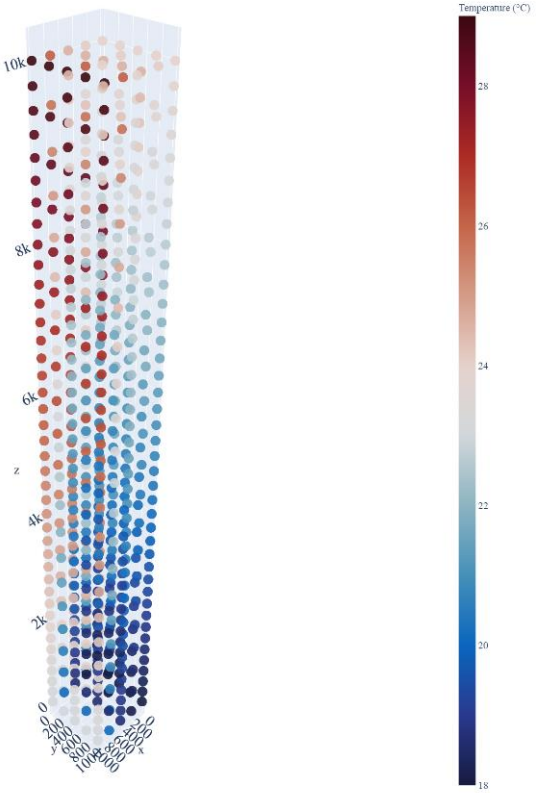

Figure 104 – Naïve network test temperature distribution, ID: 011

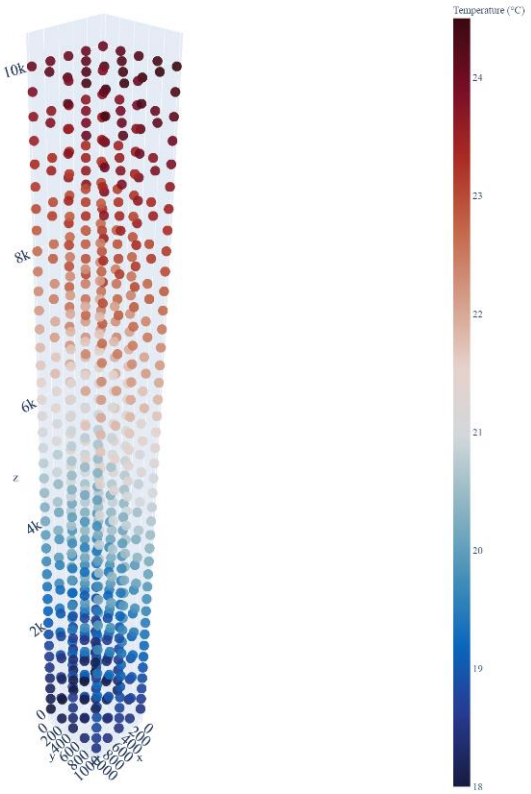

Figure 105 – Naïve network test temperature distribution, ID: 012

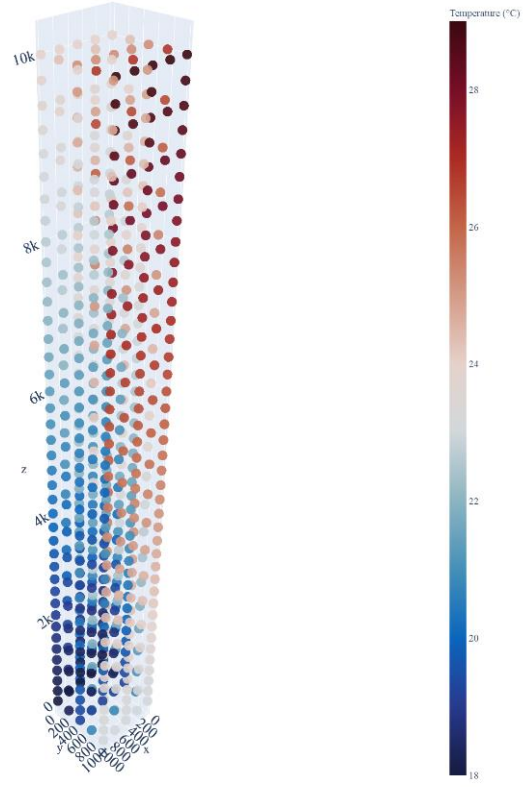

Figure 106 – Naïve network test temperature distribution, ID: 013

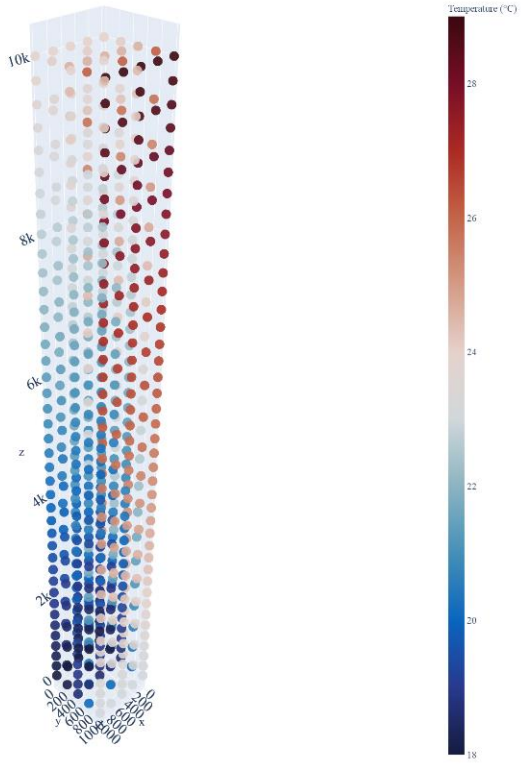

Figure 107 – Naïve network test temperature distribution, ID: 014

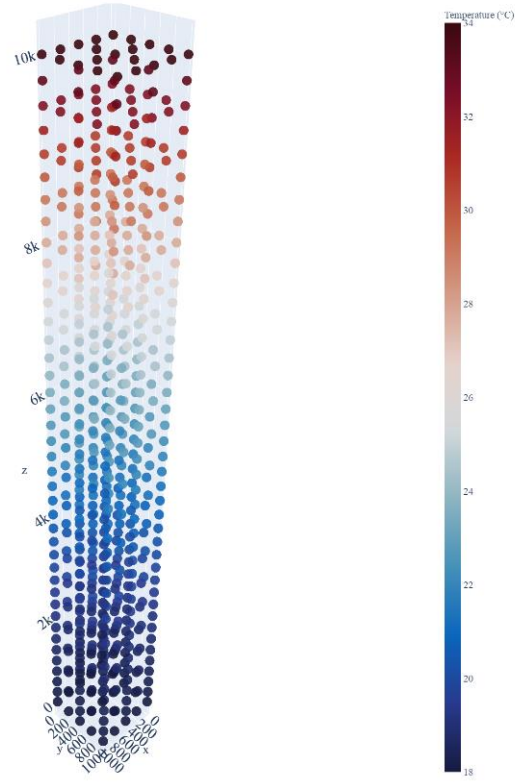

Figure 108 – Naïve network test temperature distribution, ID: 015

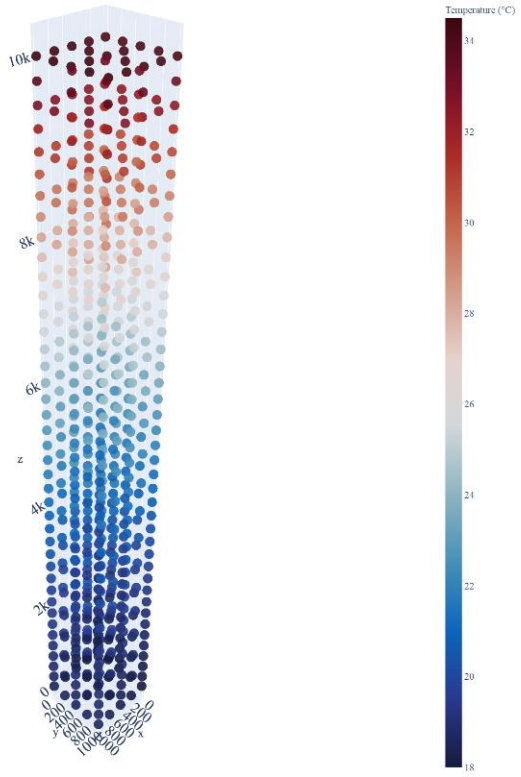

Figure 109 – Naïve network test temperature distribution, ID: 016

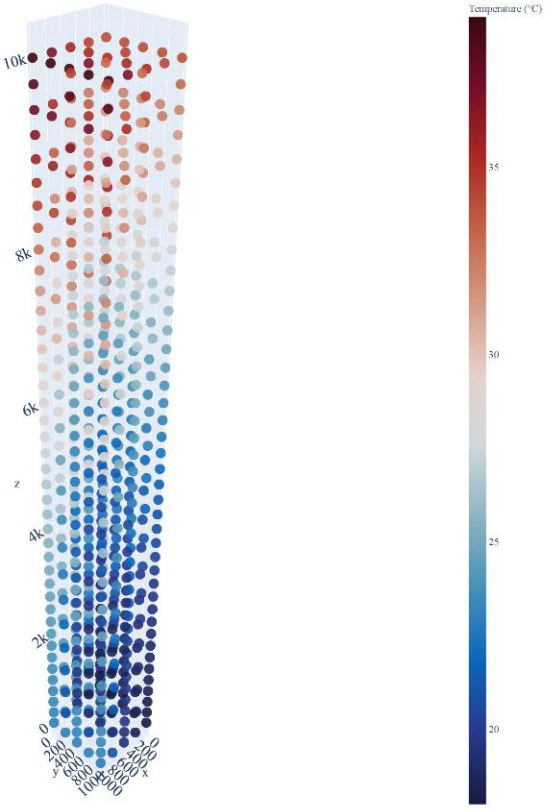

Figure 110 – Naïve network test temperature distribution, ID: 017

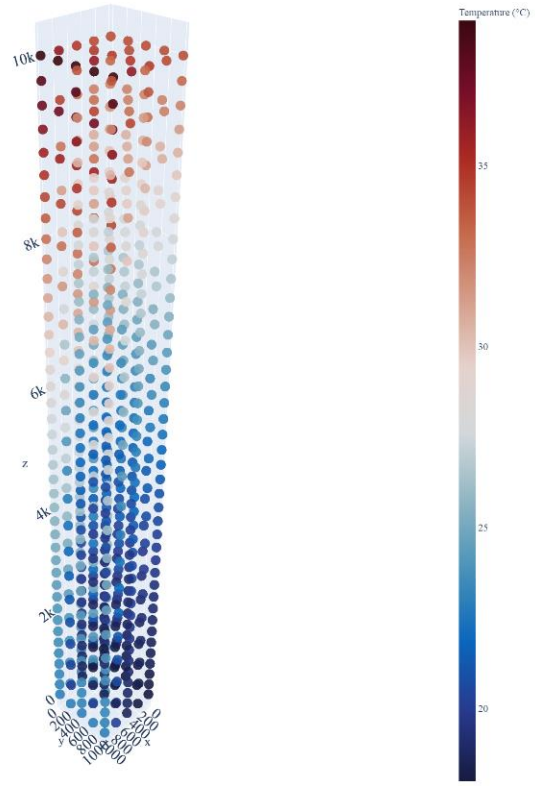

Figure 111 – Naïve network test temperature distribution, ID: 018

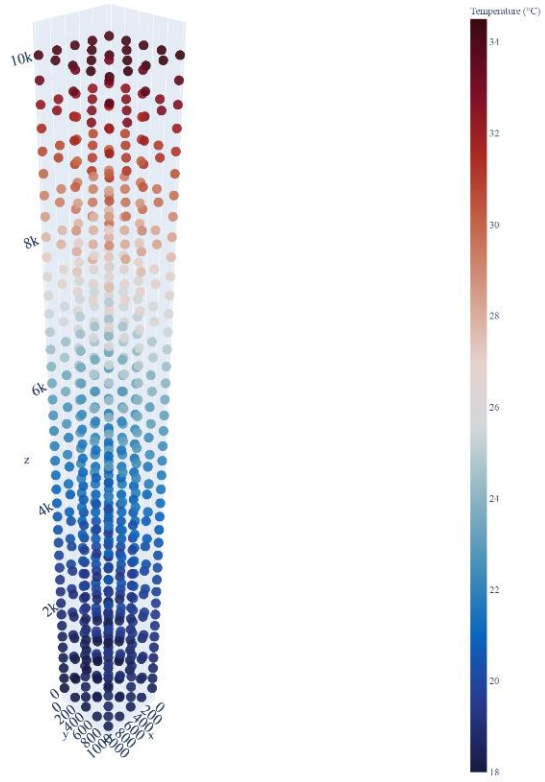

Figure 112 – Naïve network test temperature distribution, ID: 019

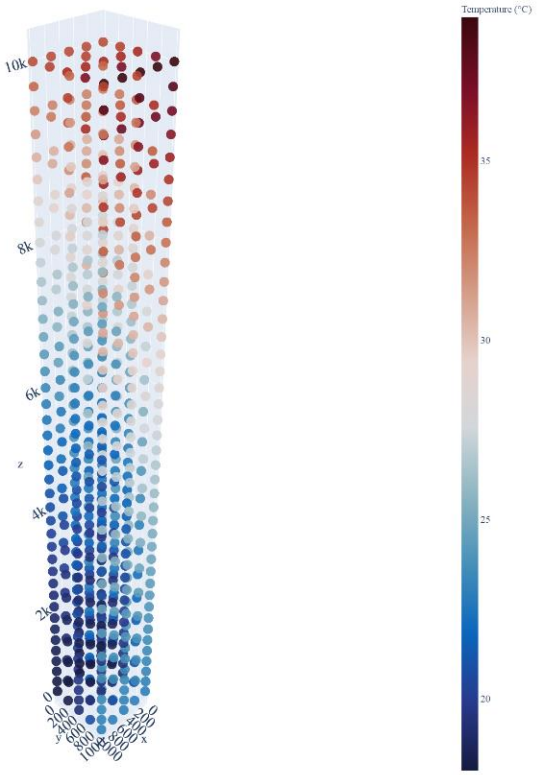

Figure 113 – Naïve network test temperature distribution, ID: 020

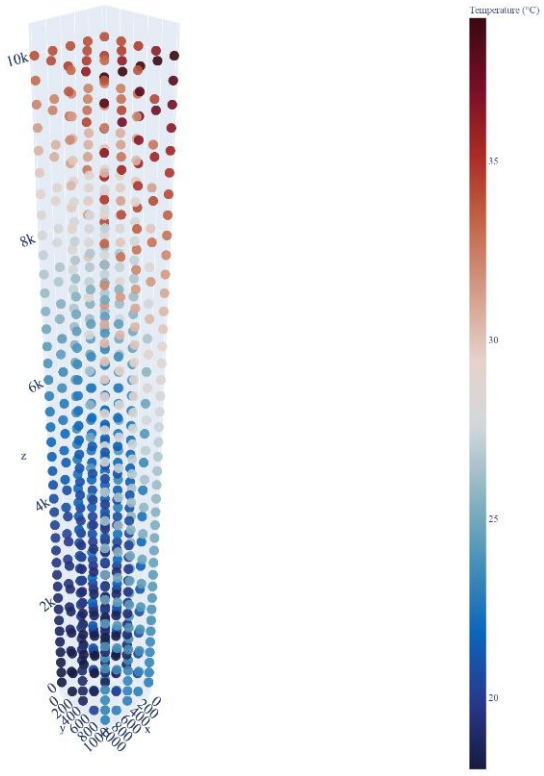

Figure 114 - Naïve network test temperature distribution, ID: 021

Appendix C - Sensor Removal Results Tables

Table 22. Results of naïve 8 sensor network performance as sensors removed with polynomial reconstruction.

	Standard Deviation of Reconstruction Error (mm) Full Network Baseline				Standard Deviation of Reconstruction Error (mm)		
Order	X	Y	Z	Sensor Removed	X	Y	Z
3rd	0.031	0.034	0.239	1	0.342	0.029	0.153
3rd	0.031	0.034	0.239	2	0.344	0.048	0.314
3rd	0.031	0.034	0.239	3	0.186	0.052	0.376
3rd	0.031	0.034	0.239	4	0.183	0.040	0.284
3rd	0.031	0.034	0.239	5	0.182	0.033	0.226
3rd	0.031	0.034	0.239	6	0.184	0.044	0.318
3rd	0.031	0.034	0.239	7	0.343	0.042	0.258
3rd	0.031	0.034	0.239	8	0.342	0.025	0.112

Table 23. Results of naïve 8 sensor network performance as sensors removed with Kriging reconstruction.

Standard Deviation of Reconstruction Error (mm) Full Network Baseline				Standard Deviation of Reconstruction Error (mm)		
X	Y	Z	Sensor Removed	X	Y	Z
0.018	0.023	0.126	1	0.025	0.025	0.136
0.018	0.023	0.126	2	0.022	0.024	0.134
0.018	0.023	0.126	3	0.021	0.024	0.130
0.018	0.023	0.126	4	0.020	0.023	0.128
0.018	0.023	0.126	5	0.022	0.023	0.118
0.018	0.023	0.126	6	0.024	0.023	0.121
0.018	0.023	0.126	7	0.019	0.024	0.126
0.018	0.023	0.126	8	0.020	0.024	0.127

Table 24. Results of naïve 16 sensor network performance as sensors removed with polynomial reconstruction.

	Standard Deviation of Reconstruction Error (mm) Full Network Baseline				Standard Deviation of Reconstruction Error (mm)		
Order	X	Y	Z	Sensor Removed	X	Y	Z
3rd	0.028	0.031	0.206	1	0.124	0.027	0.160
3rd	0.028	0.031	0.206	2	0.126	0.035	0.223
3rd	0.028	0.031	0.206	3	0.108	0.040	0.273
3rd	0.028	0.031	0.206	4	0.106	0.034	0.220
3rd	0.028	0.031	0.206	5	0.060	0.031	0.211
3rd	0.028	0.031	0.206	6	0.061	0.034	0.238
3rd	0.028	0.031	0.206	7	0.173	0.033	0.217
3rd	0.028	0.031	0.206	8	0.172	0.023	0.131
3rd	0.028	0.031	0.206	9	0.097	0.030	0.195
3rd	0.028	0.031	0.206	10	0.098	0.036	0.243
3rd	0.028	0.031	0.206	11	0.036	0.030	0.190
3rd	0.028	0.031	0.206	12	0.037	0.032	0.202
3rd	0.028	0.031	0.206	13	0.040	0.033	0.227
3rd	0.028	0.031	0.206	14	0.041	0.035	0.240
3rd	0.028	0.031	0.206	15	0.052	0.031	0.192
3rd	0.028	0.031	0.206	16	0.050	0.028	0.169

Table 25. Results of naïve 16 sensor network performance as sensors removed with Kriging reconstruction.

Standard Deviation of Reconstruction Error (mm) Full Network Baseline				Standard Deviation of Reconstruction Error (mm)		
X	Y	Z	Sensor Removed	X	Y	Z
0.021	0.025	0.088	1	0.029	0.027	0.087
0.021	0.025	0.088	2	0.026	0.027	0.088
0.021	0.025	0.088	3	0.022	0.025	0.088
0.021	0.025	0.088	4	0.021	0.025	0.088
0.021	0.025	0.088	5	0.023	0.025	0.090
0.021	0.025	0.088	6	0.025	0.025	0.089
0.021	0.025	0.088	7	0.023	0.025	0.086
0.021	0.025	0.088	8	0.024	0.025	0.084
0.021	0.025	0.088	9	0.024	0.025	0.079
0.021	0.025	0.088	10	0.022	0.025	0.080
0.021	0.025	0.088	11	0.025	0.025	0.094
0.021	0.025	0.088	12	0.027	0.025	0.092
0.021	0.025	0.088	13	0.024	0.024	0.083
0.021	0.025	0.088	14	0.022	0.024	0.085
0.021	0.025	0.088	15	0.022	0.026	0.090
0.021	0.025	0.088	16	0.022	0.026	0.090

Table 26. Results of naïve 32 sensor network performance as sensors removed with polynomial reconstruction.

	Standard Deviation of Reconstruction Error (mm) Full Network Baseline				Standard Deviation of Reconstruction Error (mm)		
Order	X	Y	Z	Sensor Removed	X	Y	Z
3rd	0.028	0.025	0.164	1	0.072	0.018	0.091
3rd	0.028	0.025	0.164	2	0.084	0.023	0.143
3rd	0.028	0.025	0.164	3	0.102	0.037	0.260
3rd	0.028	0.025	0.164	4	0.060	0.031	0.209
3rd	0.028	0.025	0.164	5	0.030	0.023	0.152
3rd	0.028	0.025	0.164	6	0.047	0.025	0.172
3rd	0.028	0.025	0.164	7	0.150	0.032	0.223
3rd	0.028	0.025	0.164	8	0.095	0.022	0.140
3rd	0.028	0.025	0.164	9	0.052	0.020	0.119
3rd	0.028	0.025	0.164	10	0.068	0.024	0.158
3rd	0.028	0.025	0.164	11	0.024	0.024	0.150
3rd	0.028	0.025	0.164	12	0.033	0.024	0.156
3rd	0.028	0.025	0.164	13	0.025	0.025	0.169
3rd	0.028	0.025	0.164	14	0.035	0.026	0.177
3rd	0.028	0.025	0.164	15	0.059	0.026	0.171
3rd	0.028	0.025	0.164	16	0.029	0.023	0.147
3rd	0.028	0.025	0.164	17	0.051	0.028	0.191
3rd	0.028	0.025	0.164	18	0.039	0.027	0.193
3rd	0.028	0.025	0.164	19	0.028	0.016	0.071
3rd	0.028	0.025	0.164	20	0.026	0.027	0.168
3rd	0.028	0.025	0.164	21	0.068	0.027	0.168
3rd	0.028	0.025	0.164	22	0.082	0.032	0.215
3rd	0.028	0.025	0.164	23	0.104	0.023	0.147
3rd	0.028	0.025	0.164	24	0.060	0.017	0.092
3rd	0.028	0.025	0.164	25	0.045	0.028	0.195
3rd	0.028	0.025	0.164	26	0.065	0.030	0.204
3rd	0.028	0.025	0.164	27	0.048	0.026	0.169
3rd	0.028	0.025	0.164	28	0.032	0.025	0.166
3rd	0.028	0.025	0.164	29	0.034	0.027	0.188
3rd	0.028	0.025	0.164	30	0.025	0.024	0.162
3rd	0.028	0.025	0.164	31	0.021	0.022	0.130
3rd	0.028	0.025	0.164	32	0.031	0.025	0.166

Table 27. Results of naïve 32 sensor network performance as sensors removed with Kriging reconstruction

Standard Deviation of Reconstruction Error (mm) Full Network Baseline				Standard Deviation of Reconstruction Error (mm)		
X	Y	Z	Sensor Removed	X	Y	Z
0.024	0.028	0.119	1	0.024	0.028	0.119
0.024	0.028	0.119	2	0.024	0.028	0.119
0.024	0.028	0.119	3	0.024	0.028	0.119
0.024	0.028	0.119	4	0.024	0.028	0.119
0.024	0.028	0.119	5	0.025	0.028	0.120
0.024	0.028	0.119	6	0.026	0.028	0.120
0.024	0.028	0.119	7	0.024	0.028	0.119
0.024	0.028	0.119	8	0.025	0.027	0.118
0.024	0.028	0.119	9	0.024	0.027	0.121
0.024	0.028	0.119	10	0.025	0.027	0.120
0.024	0.028	0.119	11	0.026	0.028	0.123
0.024	0.028	0.119	12	0.028	0.028	0.122
0.024	0.028	0.119	13	0.025	0.028	0.121
0.024	0.028	0.119	14	0.025	0.028	0.121
0.024	0.028	0.119	15	0.025	0.028	0.122
0.024	0.028	0.119	16	0.026	0.028	0.121
0.024	0.028	0.119	17	0.024	0.028	0.119
0.024	0.028	0.119	18	0.025	0.028	0.120
0.024	0.028	0.119	19	0.024	0.028	0.119
0.024	0.028	0.119	20	0.024	0.028	0.119
0.024	0.028	0.119	21	0.028	0.028	0.118
0.024	0.028	0.119	22	0.026	0.028	0.119
0.024	0.028	0.119	23	0.024	0.027	0.119
0.024	0.028	0.119	24	0.024	0.028	0.119
0.024	0.028	0.119	25	0.024	0.027	0.121
0.024	0.028	0.119	26	0.030	0.028	0.113
0.024	0.028	0.119	27	0.032	0.028	0.110
0.024	0.028	0.119	28	0.025	0.028	0.122
0.024	0.028	0.119	29	0.025	0.028	0.121
0.024	0.028	0.119	30	0.030	0.026	0.112
0.024	0.028	0.119	31	0.025	0.028	0.121
0.024	0.028	0.119	32	0.028	0.026	0.115